



Engineering *Pseudomonas putida* for the targeted production of new-to-Nature fluorinated compounds

Wirth, Nicolas

Publication date:
2021

Document Version
Publisher's PDF, also known as Version of record

[Link back to DTU Orbit](#)

Citation (APA):
Wirth, N. (2021). *Engineering Pseudomonas putida for the targeted production of new-to-Nature fluorinated compounds*.

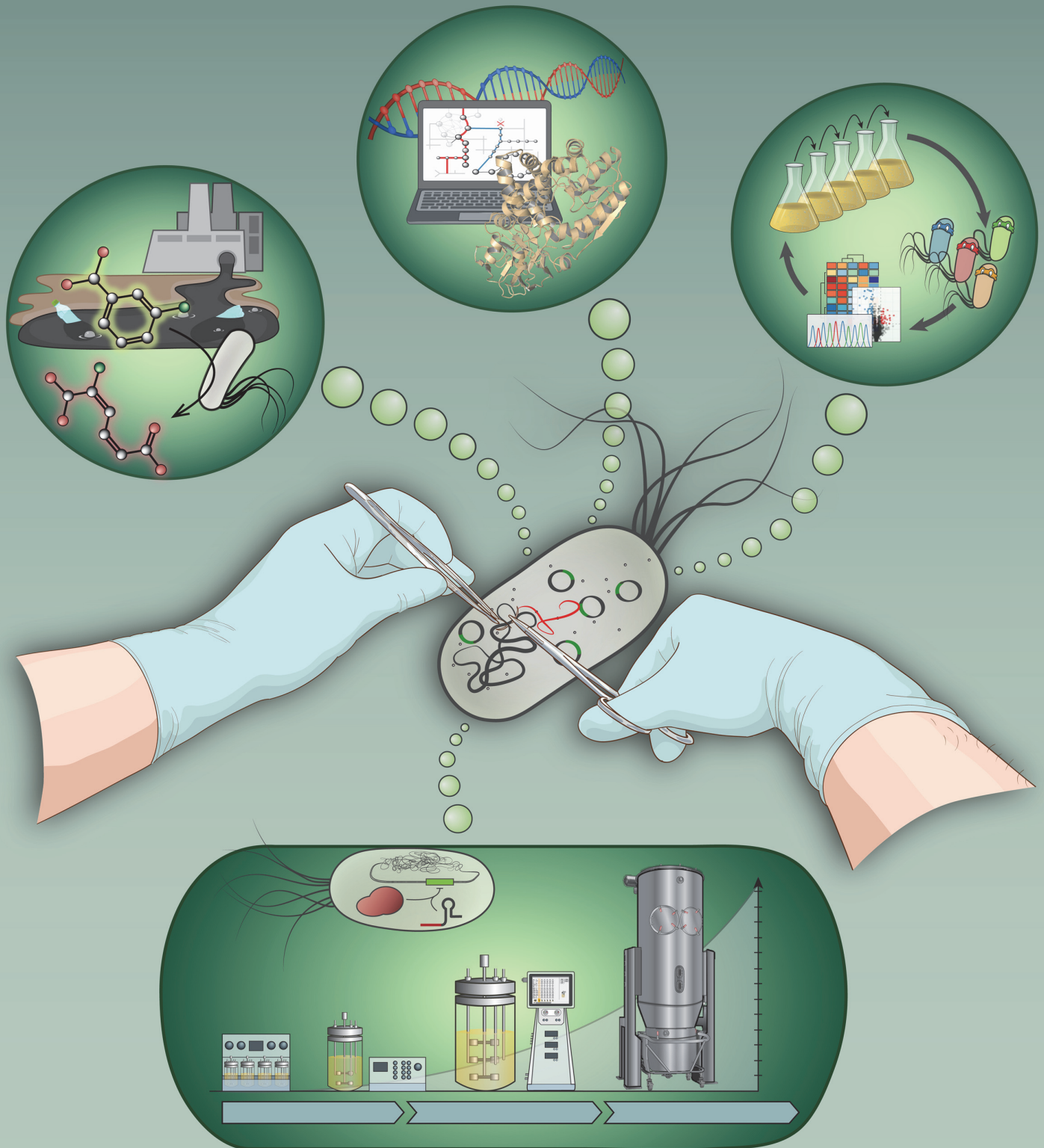
General rights

Copyright and moral rights for the publications made accessible in the public portal are retained by the authors and/or other copyright owners and it is a condition of accessing publications that users recognise and abide by the legal requirements associated with these rights.

- Users may download and print one copy of any publication from the public portal for the purpose of private study or research.
- You may not further distribute the material or use it for any profit-making activity or commercial gain
- You may freely distribute the URL identifying the publication in the public portal

If you believe that this document breaches copyright please contact us providing details, and we will remove access to the work immediately and investigate your claim.

Engineering *Pseudomonas putida* for the targeted production of new-to-Nature fluorinated compounds



Nicolas T. Wirth

**Engineering *Pseudomonas putida* for the targeted
production of new-to-Nature fluorinated compounds**

PhD Thesis

Nicolas Thilo Wirth

Novo Nordisk Foundation Center for Biosustainability
Technical University of Denmark

April 2021



Engineering *Pseudomonas putida* for the targeted production of new-to-Nature fluorinated compounds

PhD thesis written by Nicolas T. Wirth

Supervised by Senior Researcher & Group Leader Pablo I. Nikel

© **PhD Thesis 2021 Nicolas T. Wirth**

Novo Nordisk Foundation Center for Biosustainability

Technical University of Denmark all rights reserved.



The Novo Nordisk Foundation
Center for Biosustainability

*Affectionately dedicated to my son Leon,
may you never stop learning and
pursue your curiosity to explore
the incredible wonders of
our natural world.*

Preface

This thesis is written as a partial fulfilment of the requirements to obtain a PhD degree at the Technical University of Denmark. The work presented in this thesis was carried out between January 2018 and April 2021 at the Novo Nordisk Foundation Center for Biosustainability at the Technical University of Denmark (DTU Biosustain). It was supervised by Senior Researcher & Group Leader Pablo Iván Nikel. Funding was provided by the Novo Nordisk Foundation.

A handwritten signature in blue ink, appearing to read 'N. Wirth', is positioned above a horizontal line.

Nicolas Wirth

Kgs. Lyngby, April 2020

Thesis summary

Fluorine, the most electronegative element in the periodic table, plays a pivotal role in the production of industrial compounds for modern agriculture and medicine, as well as in the manufacture of synthetic materials. The introduction of fluorine atoms into molecular structures substantially modifies their physicochemical properties. Nevertheless, this halogen is rarely found in biological systems, and approaches to integrate fluorometabolites into the biochemistry of living cells are rare. Designing cell factories for the biosynthesis of fluorinated molecules remains a significant challenge in the field of metabolic engineering, requiring not only a deep refactoring of metabolism but also the adoption of a bacterial platform that can host the harsh biochemistries involved. On this background, this thesis exploits *Pseudomonas putida* (*P. putida*) as a powerful cell factory for the production of novel fluorinated products. In order to access the rich metabolic potential of *P. putida*, a streamlined protocol was designed to facilitate genome engineering. Together with a comprehensive molecular toolbox, the developed method significantly reduces the overall workload needed for the genetic modification of Gram-negative bacteria and reduces the time required to introduce specific sequence alterations from up to several weeks down to six days. This toolkit was first put to the test in an applied metabolic engineering setup to establish a synthetic acetyl-coenzyme A auxotrophy in *P. putida* strain KT2440. A family of C2-auxotroph strains was designed to facilitate the direct selection and optimization of biochemical pathways through adaptive laboratory evolution. The functionality of the evolutionary engineering strategy was demonstrated by implementing an alternative, carbon-conserving route for sugar assimilation (i.e., the phosphoketolase shunt from bifidobacteria). Lastly, and building on all these efforts, the rich biochemical capacity of *P. putida* to process aromatic hydrocarbons was leveraged to produce the novel fluorinated platform chemical 2-fluoro-*cis,cis*-muconic acid. In this case, the genome editing toolbox was used for a profound remodeling of the native catabolism in the host to maximize bioconversion yields. Hence, the tools and platform strains developed herein enable a significant expansion of the biocatalytic landscape of *P. putida* through both the implementation of synthetic metabolisms and by refactoring elements of the native biochemical network.

Dansk resumé

Fluor, det mest elektronegative grundstof i det periodiske system, spiller en central rolle i produktionen af industrielle kemiske forbindelser til moderne landbrug og medicin samt i fremstillingen af syntetiske materialer. Indførelsen af fluoratomer i molekyllære strukturer ændrer deres fysisk-kemiske egenskaber betydeligt. Ikke desto mindre findes dette halogen sjældent i biologiske systemer, og der er kun få anvendelser af fluorometabolitter i levende cellers biokemi. Konstruktion af cellefabrikker til biosyntese af fluorholdige molekyler er fortsat en betydelig udfordring inden for metabolisk ingeniørskab, som ikke blot kræver en dybtgående refaktorisering af metabolismen, men også vedtagelse af en bakterieplatform, der kan være vært for de krævede biokemiske processer, der er involveret. På denne baggrund udnytter denne afhandling *Pseudomonas putida* (*P. putida*) som en kraftfuld cellefabrik til fremstilling af nye fluorholdige produkter. For at få adgang til *P. putida*'s rige metaboliske potentiale blev der udviklet en strømlinet protokol, der gør det lettere at lave genmanipulation. Sammen med et omfattende værktøj til genomredigering reducerer den udviklede metode betydeligt den samlede arbejdsbyrde, der er nødvendig for genetisk modifikation af Gram-negative bakterier. Det reducerer desuden tiden, der er nødvendig for at indføre specifikke sekvensændringer, fra op til flere uger ned til seks dage. Denne redskab blev først afprøvet i en anvendt metabolisk ingeniøropsætning for at etablere en syntetisk acetyl-coenzym A auxotrofi i *P. putida* stamme KT2440. En familie af C2-auxotrofe stammer blev designet for at lette den direkte optimering af biokemiske veje gennem adaptiv laboratorieevolution. Funktionaliteten af den evolutionære optimeringsstrategi blev demonstreret ved at implementere en alternativ, kulstofbesparende rute til sukkermetabolisering (dvs. phosphoketolase-shuntet fra bifidobakterier). Til sidst, og på baggrund af alle disse bestræbelser, blev *P. putida*'s rige biokemiske kapacitet til at behandle aromatiske kulbrinter udnyttet til at producere den nye fluorholdige kemiske platform 2-fluoro-*cis,cis*-muconinsyre. I dette tilfælde blev genomredigeringsværktøjet anvendt til en gennemgribende omformning af den oprindelige katabolisme i værten for at maksimere udbyttet af biokonverteringen. De værktøjer og platformstammer, der er udviklet heri, muliggør således en betydelig udvidelse af det biokatalytiske landskab hos *P. putida* både gennem implementering af syntetisk metabolisme og ved at refaktorisere elementer af det oprindelige biokemiske netværk.

Acknowledgement

First and foremost, I would like to express my deepest gratitude to my supervisor and group leader, Pablo I. Nickel. Thank you for giving me the opportunity to do my PhD in this amazing research group. Thank you for enabling me to grow both professionally and personally. Thank you for being an inspiration and that you made it possible for me to pursue any idea that came up—and helped me bring them to fruition. I couldn't have asked for more support during these three years of a roller coaster ride, thank you for always being available.

This brings me to the rest of the Systems Environmental Microbiology team. It is not a given to work with such a great bunch of colleagues. Thank you for sharing all the ups and downs of this journey with me. It was wonderful to deal with such authentic characters every day. A special thanks to Justine Turlin and Ekaterina Kozaeva for your emotional support. Nicolas Krink, you definitely made sure there was never a dull moment in the lab. Thanks for all the stimulating conversations and your extreme curiosity about pretty much every topic—and your dedication! You saved my butt repeatedly in the last weeks by acting as my alter ego in the lab. And Nicolas Gurdo, my alter-alter ego, thank you for assisting me with the final mammoth experiments. It was an absolute pleasure to work with you and benefit from your fermentation expertise. Many thanks to Manu for keeping me grounded from time to time with your lightheartedness. I would also like to thank Àngela Vidal Verdú, the greatest master's student anyone could wish for.

I would also like to express my gratitude to Davinia Salvachua, Christine Singer, and Gregg Beckham for the excellent collaboration and for mentoring me during my external research stay. Thank you for your support, insightful discussions, and expertise! It would have been fantastic if I could have joined you physically as well. Also, a huge thank you to the analytics department at CfB with special thanks to Mette Kristensen for helping me set up a detection method for fluorometabolites and Tune Wulff for prioritizing my proteomics samples time and again. Kasper Enemark-Rasmussen, I am very grateful for all the time you took to help me understand ^{19}F NMR and for the quick delivery of results.

A very special thank you to Karolina for making Denmark my home. I am so grateful to have you around me every day and for everything you do and are for me. For your support, for giving me confidence, for putting up with my constant scientific babble, for every day full of laughter, for dragging me away from work when it was clearly enough, for accepting me just as I am—and for keeping me alive and nourished on this last stretch of the finish line. This PhD would have been so much harder without you by my side. Heartfelt thanks to my mother, who always believes in me and fully supports me in every decision I make.

Lastly, I would like to thank the Novo Nordisk Foundation for funding my PhD position and this research project. The Center for Biosustainability is a wonderful place to do research and all this would not be possible without such great financial support.

List of publications

- 1 Nicolas T. Wirth and Pablo I. Nickel (2020). **Engineering reduced-genome strains of *Pseudomonas putida* for product valorization** In: Lara A., Gosset G. (eds) *Minimal Cells: Design, Construction, Biotechnological Applications* (pp. 69-93). *Springer*. doi: 10.1007/978-3-030-31897-0_3
- 2 Nicolas T. Wirth, Ekaterina Kozaeva, and Pablo I. Nickel (2020). **Accelerated genome engineering of *Pseudomonas putida* by I-SceI-mediated recombination and CRISPR/Cas9 counterselection**. *Microbial Biotechnology* 13(1): 233-249. doi: 10.1111/1751-7915.13396
- 3 Daniel C. Volke , Laura Friis, Nicolas T. Wirth, Justine Turlin, and Pablo I. Nickel (2020). **Synthetic control of plasmid replication enables target- and self-curing of vectors and expedites genome engineering of *Pseudomonas putida***. *Metabolic Engineering Communications* 10: e00126. doi: 10.1016/j.mec.2020.e00126
- 4 Daniel C. Volke, Nicolas T. Wirth, and Pablo I. Nickel (2021). **Rapid genome engineering of *Pseudomonas* assisted by fluorescent markers and tractable curing of plasmids**. *Bio-protocol* 11(4): e3917. doi: 10.21769/BioProtoc.3917.
- 5 Nicolas T. Wirth, Nicolás Gurdo, Lorena Fernández-Cabezón, Tune Wulff, and Pablo I. Nickel (2021). **Establishing a synthetic C2 auxotrophy in *Pseudomonas putida* for evolutionary engineering of alternative catabolic routes**. (Manuscript in preparation)
- 6 Nicolas T. Wirth and Pablo I. Nickel (2021). **Combinatorial pathway balancing enables the production of the novel fluorinated building block 2-fluoromuconate in engineered *P. putida* KT2440**. (Manuscript in preparation)

Patent application:

- 7 Nicolas T. Wirth and Pablo I. Nickel. **Bacterial cells and methods for production of 2-fluoro-*cis,cis*-muconate**. European patent application number 20183692.1 (priority year ending on 02 July 2021).

Publications not included in this thesis:

- 8 Fatemeh Bajoul Kakahi, Dingrong Kang, Daniel C. Volke, Nicolas T. Wirth, Pablo I. Nickel, and Frank Delvigne (2021). **Extracellular DNA (eDNA) enables early detection of the phenotypic switch of *Pseudomonas* sp. during biofilm development**. *bioRxiv*. doi: /10.1101/2021.02.11.430776
- 9 Anh Vu Nguyen, Nicolas T. Wirth, Pablo I. Nickel, Bin Lai, Jens O. Krömer (2021). **Anaerobic glucose uptake pathways cross cytoplasmic membrane of *Pseudomonas putida* KT2440 in bioelectrochemical system**. (Manuscript in preparation)
- 10 Nora Lisa Bitzenhofer, Luzie Kruse, Stephan Thies, Benedikt Wynands, Thorsten Lechtenberg, Jakob Rönitz, Ekaterina Kozaeva, Nicolas T. Wirth, Christian Eberlein, Karl-Erich Jaeger, Pablo I. Nickel, Hermann J. Heipieper, Nick Wierckx, and Anita Loeschcke (2021). **Towards robust *Pseudomonas* cell factories to harbour novel biosynthetic pathways**. *Essays in Biochemistry*. (under revision)

Abbreviations and nomenclature

2KG	2-Ketogluconate	GFP	Green fluorescent protein
5' UTR	5' untranslated region	Gm^R	Gentamicin resistance
AbR	Antibiotic resistance marker	Gnt	Gluconate
AbR	Antibiotic resistance marker	goi	Gene of interest
Abs.	Absorbance	GTP	Guanosine triphosphate
Ac-CoA	Acetyl-coenzyme A	HA	Homologous arm
Ac-P	Acetyl-phosphate	HPLC	High Performance Liquid Chromatography
AI	Artificial intelligence	HR	Homologous recombination
ALE	Adaptive laboratory evolution	Km^R	Kanamycin resistance
Amp^R	Ampicillin resistance	LB	Lysogeny broth
ATP	Adenosine triphosphate	MMR	Mismatch repair system
AU	Arbitrary units	MR	Mutagenesis region
BCD	Bi-cistronic design	mRNA	Messenger RNA
CDS	Coding sequence	msfGFP	Monomeric superfolder green fluorescent protein
CRISPR	Clustered Regularly Interspaced Short Palindromic Repeats	NGS	Next-generation sequencing
DBM	Synthetic Hartman's de Bont minimal medium	NMR	Nuclear magnetic resonance
DBTL cycle	Design-Build-Test-Learn cycle	OD	Optical density
DNA	Deoxyribonucleic acid	ori	Origin of replication
DSB	Double-strand break	oriT	Origin of transfer
ED	Entner-Doudoroff	oriV	Origin of vegetative replication
EMP	Embden-Meyerhof-Parnas	PCR	Polymerase chain reaction
PCR	Polymerase chain reaction	SEVA	Standard European Vector Architecture
PMP	Muconate-producing <i>Pseudomonas</i>	Sm^R	Streptomycin resistance
RBS	Ribosome binding site	Tc^R	Tetracycline resistance
RNA	Ribonucleic acid	TIS	Translation initiation sequence
RNAP	RNA polymerase	tRNA	Transfer ribonucleic acid
SCA	Synthetic C2-auxotroph	USER	Uracil-specific excision reagent
SD sequence	Shine-Dalgarno sequence	UTR	Untranslated region

List of Figures

Figure 1.1. The Design-Build-Test-Learn cycle of Metabolic Engineering.....	7
Figure 2.1. Relevant metabolic characteristics of the Gram-negative environmental bacterium <i>Pseudomonas putida</i> as a chassis For biotechnology.	25
Figure 2.2. Genome engineering of <i>Pseudomonas</i> using suicide plasmids.....	32
Figure 2.3. Genome engineering applications in <i>Pseudomonas</i> species using CRISPR/Cas9 as counterselection system.	35
Figure 3.1. Overview of the genome engineering procedure in <i>Pseudomonas</i>	57
Figure 3.2. Workflow for the construction of suicide vectors for genome engineering.	59
Figure 3.3. Workflow for targeted genomic manipulations in <i>Pseudomonas</i>	69
Figure 3.4. Plasmid curing after successful genome engineering of <i>Pseudomonas</i>	75
Figure 3.5. Deletion of <i>nicX</i> in <i>P. putida</i> KT2440.	77
Figure 3.6. Integration of different fluorescent proteins into a chromosomal landing pad of <i>Pseudomonas putida</i> KT2440.	82
Figure 3.7. Kinetics of the accumulation of fluorescent proteins measured in <i>P. putida</i> KT2440	83
Figure 3.8. Elimination of the <i>ben</i> catabolic activities of <i>P. putida</i> through quick genome engineering using self-curing pQUIRE vectors.	85
Figure 4.1. Key role of Ac-CoA in central carbon metabolism.	114
Figure 4.2. Adaptive laboratory evolution for cell factory optimization.	118
Figure 4.3. In silico flux distribution calculated in wild-type <i>P. putida</i> KT2440 with glucose as carbon source.....	121
Figure 4.4. Flux distribution calculated with iJN1411 after deleting Ac-CoA-producing pathways and introducing the Xfpk reactions.	122
Figure 4.5. Growth of wild-type <i>P. putida</i> KT2440 and synthetic C2-auxotroph strains in a minimal medium	124
Figure 4.6. Acetate-dependent growth of the synthetic C2-auxotroph strains SCA3 and SCA15.....	126
Figure 4.7. Volcano plot of mass spectrometry results showing differentially expressed proteins in strain SCA3 compared to <i>P. putida</i> KT2440.....	128
Figure 4.8. Changes in protein expression within central carbon metabolism for strain SCA3 compared to <i>P. putida</i> KT2440	130
Figure 4.9. Protein abundance of selected central carbon metabolism genes in <i>P. putida</i> KT2440 grown on glucose and glucose + acetate.....	131

Figure 4.10. In vitro assay for the determination of phosphoketolase activity	133
Figure 4.11. The expression of <i>xfpk^{BA}</i> restores growth of a synthetic C2 auxotroph on glucose	135
Figure 4.12. Effect of evolution on the growth physiology of strain SCA3 _{PK-Trn} /pS438· <i>pta^{EC}</i>	137
Figure 4.13. Omics approaches to identify the effects of evolution on SCA3 _{PK-Trn} /pS438· <i>pta^{EC}</i>	138
Figure 4.14. The effect of mutated Tils in strain SCA3 _{PK-Trn} /pS438· <i>pta^{EC}</i>	141
Figure 4.15. Bioreactor fermentations of <i>P. putida</i> KT2440 and SCA3 _{PK-Trn} /pS438· <i>pta^{EC}</i>	143
Figure 4.16. Carbon balance for bioreactor batch fermentations	145
Figure 4.17. Flux distribution predicted by iJN1411 for strain SCA3 _{PK-Trn} /pS438· <i>pta^{EC}</i>	147
Figure 4.18. Analysis of potential tRNA substrates for Tils.....	153
Figure 4.19. Reaction scheme for a biofluorination pathway amenable to evolutionary engineering via a synthetic C2-auxotrophy	159
Figure 5.1. Chemical compounds derived from <i>cis,cis</i> -muconate, and the market share of <i>cc</i> MA-derived products.....	201
Figure 5.2. (Halo-)benzoate degradation in <i>Pseudomonas</i>	204
Figure 5.3. Utilization of chlorobenzoates by <i>P. putida</i> KT2440 and <i>P. knackmussii</i> with glucose as co-substrate	209
Figure 5.4. Inducibility of <i>ortho</i> -cleavage pathway expression systems by chloro- benzoates	210
Figure 5.5. Growth of <i>P. putida</i> KT2440 harboring reporter plasmids in the presence of ClBz	211
Figure 5.6. Physiological response to fluorinated and nonfluorinated <i>ortho</i> - cleavage pathway metabolites	215
Figure 5.7. Coupled ¹⁹ F NMR spectrum of the culture supernatant of <i>P. putida</i> KT2440 during the conversion of 3-FBz.....	217
Figure 5.8. Utilization of fluorobenzoates by <i>P. putida</i> KT2440 and <i>P. knackmussii</i>	219
Figure 5.9. Schematic representation of the nomenclature employed in this study for engineered 2-F- <u>muconate</u> -producing <i>Pseudomonas putida</i> (PMP) strains.....	221
Figure 5.10. Bioconversion performance of first-generation strains in shaken flask fermentations.....	223
Figure 5.11. Quantitative comparison for expression systems used in this study	225
Figure 5.12. Characterization of expression systems used in this study	227

Figure 5.13. Transcriptome analysis of genes forming the <i>ben</i> and <i>cat</i> genes clusters	229
Figure 5.14. Bioconversion performance of second-generation strains	233
Figure 5.15. Bioconversion performance of third-generation strains.....	235
Figure 5.16. Fermentation profiles of fourth-generation bioconversion strains.....	241
Figure 5.17. Toxicity of the bioconversion substrate product for wild-type and engineered <i>P. putida</i>	243

List of Tables

Table 3.1 Plasmids used in Chapter 3.....	55
Table 3.2 Touchdown temperature protocol for Phusion U PCR.....	62
Table 3.3 Touchdown temperature protocol for OneTaq colony PCR	64
Table 3.4 Bacterial strains used in Chapter 3.....	94
Table 4.1 Reactions predicted to contribute to the formation of Ac-CoA on glucose when serially knocked out in iJN1411.	120
Table 4.2 Quantitative physiology parameters of engineered strains in minimal medium with glucose and acetate	127
Table 4.3 Quantitative physiology parameters of glucose-grown PK-shunt strains.....	137
Table 4.4 Bacterial strains used in Chapter 4.....	160
Table 4.5 Plasmids used in Chapter 4.....	161
Table 5.1 Genes encoding enzymes involved in the biodegradation of fluorinated benzoates in <i>P. knackmussii</i> and their homologs in <i>P. putida</i> KT2440 (or in the catabolic pWW0 TOL plasmid of strain mt-2)	207
Table 5.2 Growth rates of selected strains used in Chapter 5	214
Table 5.3 Performance parameters for selected strains used in this study in the bioconversion of 10 mM 3-FBz.....	238
Table 5.4 Bacterial strains used in Chapter 5.....	244
Table 5.5 Plasmids used in Chapter 5.....	255

Table of Contents

PREFACE	I
THESIS SUMMARY.....	II
DANSK RESUMÉ	III
ACKNOWLEDGEMENT	IV
LIST OF PUBLICATIONS.....	VI
ABBREVIATIONS AND NOMENCLATURE.....	VIII
LIST OF FIGURES	IX
LIST OF TABLES	XI
TABLE OF CONTENTS.....	XII
INTRODUCTION AND THESIS OUTLINE.....	1
CHAPTER 1: MODERN BIOTECHNOLOGY AS AN APPLIED ENGINEERING DISCIPLINE	
1.1. Industry 4.0 – biotechnology as a vector of the fourth industrial revolution	5
1.2. The Design-Build-Test-Learn cycle of metabolic engineering	6
References for Chapter 1	12
CHAPTER 2: PSEUDOMONAS PUTIDA AS A CHASSIS FOR METABOLIC ENGINEERING	
2.1. Summary	19
2.1. The potential of <i>P. putida</i> as a chassis for biotechnology	
2.1.1 A historical perspective on microbial <i>chassis</i> for biotechnology applications	20
2.1.2 Bacteria from the genus <i>Pseudomonas</i> as <i>chassis</i>	21
2.1.3 Carbon metabolism in <i>P. putida</i>	23
2.1.4 Domestication of <i>P. putida</i> as a <i>chassis</i>	26
2.2. Strategies for the genetic editing of <i>Pseudomonas</i> species	
2.2.1 Genome engineering of <i>Pseudomonas</i> using suicide plasmids.....	28
2.2.2 CRISPR/Cas9 technologies and recombineering approaches for <i>Pseudomonas</i>	33
References for Chapter 2	38

CHAPTER 3: ACCELERATED GENOME ENGINEERING OF *P. PUTIDA* BY I-SCEI-MEDIATED RECOMBINATION, CRISPR/CAS9 COUNTERSELECTION, AND SELF-CURING PLASMIDS

3.1. Summary	52
3.2. Introduction.....	53
3.3. Technical implementation.....	57
3.4. Application examples	
3.4.1 Deletion of <i>nicX</i> in <i>Pseudomonas putida</i> KT2440	76
3.4.2 Deletion of <i>aceEF</i> in <i>Pseudomonas putida</i> KT2440 using CRISPR/Cas9 counterselection.....	78
3.4.3 Integration of fluorescent protein-encoding genes into a landing pad in <i>Pseudomonas putida</i> KT2440.....	79
3.4.4 Elimination of the <i>ben</i> catabolic activities of <i>Pseudomonas putida</i> KT2440	84
3.5 Discussion.....	86
3.6 Biotechnological applications of reduced-genome variants of <i>Pseudomonas putida</i>	87
3.7 Supplementary material.....	95
References for Chapter 3.....	101

CHAPTER 4: ESTABLISHING A SYNTHETIC C2 AUXOTROPHY IN *P. PUTIDA* FOR EVOLUTIONARY ENGINEERING OF ALTERNATIVE CATABOLIC ROUTES

4.1 Introduction	
4.1.1 The central role of acetyl-coenzyme A in cellular metabolism.....	113
4.1.2 The phosphoketolase reactions shunt the upstream glycolysis to the direct formation of Ac-CoA, bypassing pyruvate decarboxylation.....	116
4.1.3 Evolutionary engineering leverages the vast potential of Darwinian adaptation for the optimization of cell factories.....	117
4.2 Results	
4.2.1 Design of a synthetic C2-auxotroph strain design informed by genome-scale metabolic modeling and analysis of the potential of a phosphoketolase-based glucose utilization pathway.....	119
4.2.2 Experimental validation of acetate auxotrophy and phenotypical characterization of acetate requirements in synthetic C2-auxotroph strains	123
4.2.3 Quantitative proteome analysis exposes the dependency of synthetic C2 auxotrophs on acetate and highlights bottlenecks for a functional phosphoketolase pathway	128

4.2.4	Implementing the phosphoketolase pathway in a synthetic C2 auxotroph restores prototrophy on glucose	132
4.2.5	Adaptive laboratory evolution enabled the integration of the phosphoketolase pathway into the metabolic network of <i>P. putida</i>	136
4.2.6	The PK pathway enables the conservation of carbon during growth on glucose.....	142
4.2.7	FBA-guided reconstruction of metabolic fluxes in strain SCA3 _{PK-Tn} /pS438- <i>pta</i> ^{EC}	146
4.3	Discussion	
4.3.1	A synthetic C2 auxotroph of <i>P. putida</i> provides a tight selection regime for Ac-CoA producing pathways and reveals unknown metabolic connectivities	149
4.3.2	The integration of the phosphoketolase pathway into the metabolic network occurred via stabilization of the total protein content	150
4.3.3	Sequence analysis of potential TisS substrates proposes new functions for previously identified tRNA sequences	152
4.3.4	A flux split between the ED and PK pathways creates a metabolic imbalance in synthetic C2 auxotrophs	154
4.4	Outlook	157
4.5	Materials and Methods	160
4.6	Supplementary Material	171
4.7	References for Chapter 4	186

CHAPTER 5: COMBINATORIAL PATHWAY BALANCING ENABLES THE PRODUCTION OF THE NOVEL FLUORINATED BUILDING BLOCK 2-FLUOROMUCONATE IN ENGINEERED *P. PUTIDA* KT2440

5.1	Introduction	
5.1.1	The central role of acetyl-coenzyme A in cellular metabolism.....	199
5.1.2	The phosphoketolase reactions shunt the upstream glycolysis to the direct formation of Ac-CoA, bypassing pyruvate decarboxylation.....	202
5.2	Results	
5.2.1	Similarities and differences in the enzymatic repertoire of <i>P. putida</i> and <i>P. knackmussii</i> revealed by comparative genome analysis.....	205
5.2.2	An incompatibility of <i>P. putida</i> catechol 1,2-dioxygenases with chlorocatechols prevents the utilization of chlorobenzoates	208

5.2.3	<i>P. putida</i> KT2440 outcompetes <i>P. knackmussii</i> as a whole-cell biocatalyst for conversion of fluoro-substituted benzoates into fluoromuconate	212
5.2.4	Engineering strategies to increase 3-fluorobenzoate bioconversion performance in <i>P. putida</i> KT2440.....	220
5.2.5	Characterization of expression devices to balance bioconversion of 3-fluorobenzoate to 2-fluoro- <i>cis,cis</i> -muconate	224
5.2.6	Implementation of a dynamic catechol 1,2-dioxygenase expression control enabled a balanced, complete conversion of 3-fluorobenzoate into 2-fluoro- <i>cis,cis</i> -muconate	231
5.2.7	Further strain engineering involving genetic "off the beaten path" targets uncovers a vital role of carbon catabolite control	234
5.2.8	Constitutive expression of catechol 1,2-dioxygenase genes enables balanced 2-fluoro- <i>cis,cis</i> -muconate production in plasmid-free strains	239
5.2.9	Engineered <i>P. putida</i> tolerates higher 3-fluorobenzoate concentrations than the parental strain.....	242
5.3	Discussion	248
5.3.1	Divergent metabolic specializations in <i>P. putida</i> and <i>P. knackmussii</i> result in distinct processing of benzoate and its halogenated derivatives.....	248
5.3.2	The overexpression of catechol 1,2-dioxygenase genes simultaneously enhances 3 fluorobenzoate consumption and decreases 3-fluorocatechol conversion.....	249
5.3.3	The targeted replacement of regulatory sequences governing the expression of <i>ortho</i> -cleavage pathway genes reveals hidden control patterns.....	250
5.4	Outlook	253
5.5	Materials and Methods	255
5.6	Supplementary Material	262
5.7	References for Chapter 5	266
CONCLUDING REMARKS AND FUTURE PERSPECTIVES		280

Introduction and thesis outline

Fluorine (F) ranks as the 13th most abundant chemical element in Earth's crust—before carbon, sulfur, chlorine, and many trace elements essential to life. However, Nature has not found any significant biological role for this element, aside from its occurrence within a handful of biogenic compounds that are produced as toxins by a few bacterial and plant species¹. One reason for the virtual absence of fluorinated hydrocarbons in biological systems is that F, the most electronegative of all elements in the periodic table, is extremely reactive and its bonding with carbon (C-F) is highly polarized and exceptionally strong². Furthermore, the free fluoride ion is surrounded by a stable hydration shell in aqueous environments, making it largely inaccessible for chemical reactions^{3,4}. However, the physicochemical properties imparted by F on organic molecules have a prominent role in many commercial products—ranging from pharmaceuticals to synthetic polymers. One in four of all molecules currently licensed as pharmaceutical drugs contain F in order to tweak their pharmacological properties, to increase the hydrophobicity of arenes or to modify the reactivities of target molecules⁵. The chemical reactions used to attach F to organic molecules selectively are often challenging to perform due to the high reactivity and toxicity of the reagents involved, thus limiting the scope of substrates and products⁶. Nevertheless, all current processes for fluorination rely on chemical synthesis.

Biocatalysis offers more than just an alternative for the production of commodity chemicals and fuels. Enzymes are able to perform chemical reactions that cannot be accomplished through means of synthetic chemistry. Thus, biocatalysis allows the synthesis of unique products that create their own markets, not only in the pharmaceutical-medical industry⁷. One of the most critical advantages of enzymes is their ability to catalyze reactions with high specificity (i.e., avoiding by-products on a given substrate). At the same time, most enzymes exhibit some degree of promiscuity with respect to the substrates accepted for their reactions. In the context of this thesis, catalytic (side-)activities on halogen-substituted chemicals are of particular interest.

The chemical potential of enzymes is best exploited when they are used in their natural context of a whole-cell factory that provides for their constant regeneration. For the

production of so-called *contained products* (i.e., those produced in industrial fermentation or other sealed environments such as laboratories or ponds), microbes are the preferred hosts. Bacterial cell factories excel through fast growth, high metabolic rates, low nutrient requirements, and, due to the low complexity of their genomes, high amenability to genetic engineering. In addition, single-celled organisms grow to high densities, which reduces the spatial requirements of production facilities. Since they can be cultivated suspended in liquid media, production processes can be adapted to a large scale. Bacteria have been used for centuries in the food industry for the fermentation of dairy, meat and fish, vegetables, beverages, and the production of organic acids⁸. Modern examples for biotechnological applications using bacteria include the production of industrial enzymes⁹, recombinant biopharmaceuticals¹⁰, transportation fuels¹¹, or polyhydroxyalkanoates (PHAs)¹².

Bacteria can be used not only for the *de novo* production of value-added chemicals from cheap feedstocks via *fermentation*. For chemical conversions that cannot be carried out by currently available synthesis protocols (e.g., where strict stereo- and regioselectivity requirements apply), whole-cell biocatalysts can fill in the gaps. For this purpose, microbial species have been used to perform critical *biochemical* steps for the production of steroids, vitamins, and pesticides¹³ via *biotransformations* (i.e., involving a single biochemical step¹⁴) and *bioconversions* (i.e., involving multiple steps¹⁴). The terms used for these three types of bioprocesses are not precisely defined in the literature and are often used interchangeably. In the context of this thesis, the functional definitions proposed here will be used throughout the chapters.

Bio-based chemical conversions are often performed on complex, aromatic compounds, many of which are toxic to living cells, especially at the concentrations required for an efficient biochemical process^{15,16}. In addition, many of these compounds have low solubility in water, necessitating the use of organic solvents during the process, which are themselves harmful to many organisms¹⁷. A suitable cell factory must therefore not only provide the required biochemical functions but also be able to tolerate such harsh process conditions. The characteristics that qualify a biological host for biotechnological applications are discussed in **Chapter 1**.

Bacteria that are found in the environment constitute ideal cell platforms when toxic chemicals are produced or employed in the biochemical process. Exposed to all kinds of chemical compounds in their natural habitat, species such as members of the *Pseudomonas* group have adapted to deal with the detrimental effects of environmental toxins on the cellular machinery. Due to its versatile and robust metabolic architecture, *Pseudomonas putida* (*P. putida*) was selected as a biotechnological host for the production of fluorinated metabolites in this thesis. The unique properties of this species and past approaches to harness them for biotechnological applications are highlighted in **Chapter 2**.

Due to the high demand for fluorinated molecules that could be used as chemical precursors and the advantages that biocatalytic production processes have over organic-chemical synthesis, biofluorination performed with microbial cell factories harbors an untapped industrial potential. Fluorinase (adenosyl-fluoride synthase), present in some species of the Gram-positive bacterium *Streptomyces*, is the only natural enzyme known to catalyze the formation of a C-F bond. Although actinomycetes are used in numerous applications for the production of secondary metabolites, these species are difficult to cultivate and, with their filamentous phenotype, are relatively slow-growing bacteria¹⁸. Despite recent efforts, the lack of standardized, robust tools for their genetic manipulation further complicates exploiting their biochemical capacities for metabolic engineering¹⁹. On the other hand, a large variety of standardized toolsets has been developed for Gram-negative bacteria and, as will be discussed in **Chapter 2**, many of them have been applied to *Pseudomonas* species. Useful as they are, the pre-existing tools for chromosomal modifications are rather laborious. To facilitate profound restructuring of the metabolic network architecture in a time-efficient fashion, one of the most established genome editing methods was adopted and further refined in **Chapter 3**. By implementing fluorescent markers, each step of the protocol can be monitored with precision without having to resort to time-consuming screening methods. Furthermore, self-curing vectors enable a high throughput in constructing marker-free strains.

With such a highly efficient genome editing tool at hand, *P. putida* strain KT2440 was subjected to in-depth genetic manipulations that rendered it 'auxotrophic' for acetyl-coenzyme A. As outlined in **Chapter 4**, a synthetic C2-auxotrophy enables the optimization of various biochemical pathways (for instance, the fluoroacetate-generating fluorination pathway) through adaptive laboratory evolution. To demonstrate the applicability of such an evolutionary engineering strategy, it was used to establish an alternative, carbon-saving route for sugar assimilation—the phosphoketolase shunt. It will be shown that even fundamental elements of central carbon metabolism can be remodeled to generate valuable production cell platforms with synthetic network architectures.

In **Chapter 5**, a combinatorial approach is pursued to exploit the inherent capacities of *P. putida* for the assimilation of aromatic hydrocarbons for the bioconversion of fluorinated precursors. Applying several iterations of the Design-Build-Test-Learn cycle of metabolic engineering (introduced in the next **Chapter 1**), bottlenecks in the efficient conversion of 3-fluorobenzoate into 2-fluoro-*cis,cis*-muconate were identified and resolved. This novel platform chemical can be produced at maximum theoretical yields with the engineered strains developed herein. The thesis concludes with an outline of future perspectives provided by the presented work.

Chapter 1: Modern biotechnology as an applied engineering discipline

1.1. Industry 4.0 – biotechnology as a vector for the fourth industrial revolution

We are on the brink of a technological revolution. The First Industrial Revolution was the use of water and steam to power *manufacturing*. Enabled by the invention of electricity, the Second Industrial Revolution was characterized by mass production. The advent of electronics and information technology enabled the automation of production processes and led to the Third Industrial Revolution²⁰.

Where we once saw linear progress with occasional technological breakthroughs, we now see new technologies emerging and changing at an exponential pace²¹. The Fourth Industrial Revolution is characterized by a dissolution of barriers between the physical, digital, and biological spheres. In fact, the roots of artificial intelligence (AI), widely regarded as one of the key technologies of our time, lie in biology, as it was directly inspired by and partially modeled after biological neural networks²². Conversely, with the advent of omics technologies and the exponentially decreasing cost of DNA sequencing²³, vast amounts of data are being generated in the biological fields. Bioinformatics increasingly relies on machine-learning algorithms to analyze and interpret data (i.e., *big data*). Combined with robotics and advanced information technologies (ITs), AI accelerates the discovery of new biocatalytic functions and enables combinatorial approaches to build cell factories on a vast scale²⁴.

The new *big data*-driven technologies caused a shift in paradigm in the field of metabolic engineering – the transition from plug-and-play methodology, in which the metabolic capabilities of usually one of the few model host organisms [e.g., *E. coli* (representing Gram-negative bacteria), *B. subtilis* (representing Gram-positive bacteria), or *Saccharomyces cerevisiae* (representing yeasts)] were enriched by bringing in new, characterized genes to a systems-driven approach applicable to a broad range of biological *chassis*²⁵⁻²⁷. The impacts of this technological revolution are reflected in an expansion of each step in the Design-Build-Test-Learn (DBTL) cycle that is used as a framework in metabolic engineering⁷.

1.2. The Design-Build-Test-Learn cycle of metabolic engineering

Microbes provide a promising, sustainable solution for the production of chemicals that has led to the successful production of a growing number of natural products and high-value chemicals. However, scaling up bioproduction processes to industrial levels requires huge resource investments and usually takes many years²⁸. Therefore, great efforts are being deployed to shorten the time from the start of a project to commercial viability²⁹.

Academic and industrial laboratories are increasingly adopting an approach based on the iterative application of the DBTL cycle, which has its origins in traditional engineering disciplines (**Figure 1.1**)³⁰. While each iteration of the cycle still requires months of work, technologies developed in recent years enable to significantly increase throughput and, more importantly, increase the likelihood of success of each individual iteration. The structure of the DBTL cycle, further discussed in the following sections, has been applied extensively in this thesis to guide the metabolic engineering approaches presented in **Chapters 4** and **5**.

The Design phase

After deciding on a target product with a market value, suitable strategies for its production are explored. This involves identifying a potential biochemical route consisting of enzymes that can provide the required catalytic activities. Databases such as Kegg or Biocyc³¹ have compiled a vast collection of identified metabolic routes and enzymes involved. Even previously unidentified reaction pathways can be designed de novo in a process called retrosynthesis using sophisticated algorithms based on known enzyme activities^{32,33}. We are still far from predicting the exact function of a protein based only on its amino acid sequence. However, first success stories provide evidence for the feasibility of an AI-driven bottom-up approach to generate proteins with new, desired functions to fill gaps within a biochemical route.

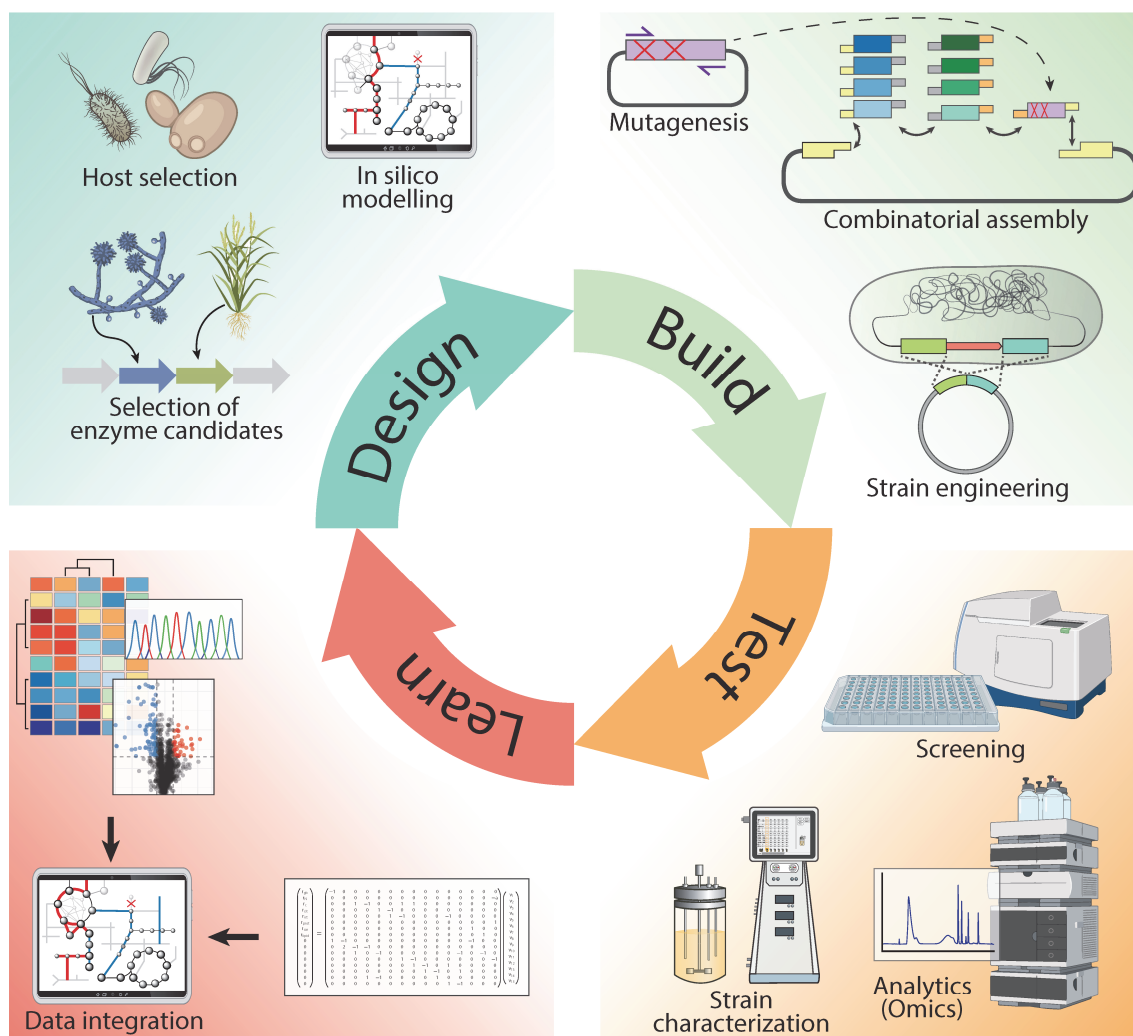


Figure 1.1. The Design-Build-Test-Learn cycle of Metabolic Engineering. A metabolic engineering project starts with the search for suitable enzyme candidates that can form a biochemical route to the desired product. Comprehensive databases have gathered enzymes based on experimentally validated properties, or through automatic computer-aided data mining (e.g., ExplorEnz, ExPASy, BRENDA, KEGG, or MetaCyc) and can help to identify suitable candidates. Once a metabolic pathway has been assembled in silico, an appropriate biological *chassis* must be selected, taking into account aspects of enzyme compatibility, resistance to toxic metabolites, culture conditions, and available knowledge about the system. In addition, the selected cell factory usually needs to be genetically modified to redirect carbon flow from substrates to the product. In the build phase, DNA sequences encoding the required enzymes as well as genomic manipulations are implemented into the host. Subsequently, the generated strain designs are tested for their performance. In this process, omics technologies can provide a comprehensive picture of the observed phenotypes. If available, high-throughput screening methods can be used to find the best performing candidates from a large library of strains. In the final step of the DBTL cycle, the data generated in the *Test* phase are integrated through multivariate data analysis and interpreted to inform the next iteration (adapted from Petzold et al.³⁴).

Significant advances in DNA synthesis technologies and decreasing costs provide unrestricted access to any type of gene and even entire gene clusters, regardless of their origin. Suitable enzyme candidates can be found in comprehensive databases that have collected proteins based on experimentally validated traits or through automated computer-assisted data mining (e.g., ExplorEnz, Expasy, BRENDA, Kegg, MetaCyc). Modern computer software can adjust the sequence pattern to the chosen biological host to facilitate the functional expression of the gene^{35,36}. Combinatorial libraries of identified enzyme candidates can be directly synthesized, reducing the time required for the molecular cloning of constructs in the *Build* phase of the DBTL cycle. Furthermore, modular cloning methodologies can be automated through the use of software tools³⁷.

In the context of choosing suitable enzyme candidates, the right choice of a biological *chassis* is critical. Hosts are usually selected based on several characteristics: (i) their compatibility with the chosen enzymes (e.g., the functional production of eukaryotic enzymes often requires post-translational modifications that a prokaryotic host cannot provide); (ii) accepted feedstocks that allow for an economically feasible process; (iii) required process conditions (e.g., pH, solvents, or temperature); (iv) physiological parameters (e.g., growth rate, stress resistance, or tolerance to substrates and products); (v) their genetic amenability; and (vi) their compatibility with the downstream-processing required to extract the product (e.g., pre-existing secretion mechanisms in the host). Not only since the advent of CRISPR/Cas technologies, the amount of available tools to genetically modify cell factories and express heterologous genes has increased substantially in the past decade, significantly expanding the choice of available species³⁸.

A functional pathway is a fundamental prerequisite for the production of target compounds. However, the provision of precursor metabolites by the cell factory is equally important to enable the highest possible yields. Stoichiometric models, such as genome-scale metabolic models (GSMMs) can help predict metabolic fluxes following genetic interventions³⁹. A range of algorithms has been developed that, in conjunction with GSMMs, can predict appropriate combinations of gene deletions, insertions, and

overexpressions⁴⁰⁻⁴⁵. Most recently, the scope of GSMMs was expanded significantly by implementing regulatory constraints (i.e., resource requirements for the transcription and translation machinery) for metabolic networks⁴⁶⁻⁴⁸. However, due to their complex nature, so-called genome-scale models of metabolism and macromolecular expression (ME-models) are so far available only for a few organisms⁴⁹.

The availability of sophisticated computational tools and an increasing amount of available data enables high throughput in the design phase. The efficiency of implementing the formulated metabolic engineering strategy strongly depends on the selection of appropriate tools for DNA assembly and genome manipulation.

The Build phase

With a price for the synthesis of DNA of as little as \$0.07 per base pair, the manual assembly of DNA fragments is starting to become obsolete⁵⁰. However, most laboratories, especially in academia, still rely on in-house molecular cloning techniques for DNA fragment assembly. A variety of different methods have been developed for this purpose (e.g. Gibson assembly⁵¹, *USER* assembly⁵², restriction digestion and ligation, Golden Gate Cloning⁵³, LIC⁵⁴, or SLIC^{55,56}). All provide equal accuracy and require similar time periods, and each has its own list of advantages and disadvantages^{57a}. With the right cloning strategy, large libraries of genes can be assembled in a randomized fashion that can be screened at high throughput during the *Test* phase^{57b}. An important part of such a combinatorial approach is the right choice of gene expression systems. Gene expression is often a major bottleneck in metabolic engineering, as we are not yet able to reliably model transcription, translation, and protein folding processes. In addition, the relative abundance levels of enzymes in a pathway often need to be balanced to enable efficient performance. The inclusion of different promoters and translation initiation sequences (*TISs*) in a shuffled library increases the chance of constructing a functional pathway.

More relevant than the choice of cloning method is how variation is generated within a library of enzymes for directed evolution applications. Through gene shuffling and

random mutagenesis, the physical and catalytic properties of enzymes can be optimized by a nature-inspired twofold strategy of mutagenesis followed by selection⁵⁸.

After DNA constructs have been assembled, they are introduced into the chosen cell factory either into the chromosome or on autonomously replicating vectors. While plasmids are useful for screening large enzyme libraries or constructing proof-of-principle strains, they tend to be unstable when used in large-scale industrial cultivations. An additional part of the *Build* phase is the rewiring of existing metabolism in host cells through the targeted deletion and expression modulation of genes. An overview of available genetic tools for *P. putida* is provided in the next **Chapter 2**. In **Chapter 3**, a streamlined method for implementing genomic modifications in this bacterial cell factory is presented.

A particular application of the DBTL cycle that overcomes the limitations of rational engineering is adaptive laboratory evolution (ALE)⁵⁹⁻⁶¹. By creating a suitable selection platform, cell factory optimization as part of the *Build* phase is carried out by evolution, exploiting the self-optimizing ability of all living organisms. An applied example of how such an evolutionary approach can be employed for pathway optimization by implementing synthetic metabolisms is discussed in **Chapter 4**. Production of specific recombinant proteins can be enhanced by coupling their translation to functions required for cell survival. By generating a synthetic polycistron of a gene of interest and, for example, an antibiotic resistance determinant, libraries of expression systems and codon compositions can be rapidly screened for the sequence features that ensure optimal protein production based on cell survival at high antibiotic concentrations^{62,63}.

The Test phase

In the *Test* phase, the performance of constructed strains and pathways is evaluated. Our ability to analyze the phenotype of cell factories has improved tremendously with the advent of omics technologies and modern information technology. Next-generation sequencing allows the analysis of the genetic composition of large cell populations. Transcriptomics permits interrogating gene expression changes in response to genetic changes or cultivation conditions. Quantitative analysis of the total protein

content of a strain can help identify bottlenecks in the production of heterologous proteins and characterize expression systems. Liquid and gas chromatography methods can provide a comprehensive picture of the metabolic state of cells and, if combined with isotope-labeled substrates, can even determine the rates of metabolic reactions in the network.

However, although the speed of these technologies has increased significantly in recent years, they often still represent a major bottleneck within the DBTL cycle. More preferable to these analytical approaches are high-throughput screening methods. By coupling biocatalyst performance to an optical output (e.g., fluorescence provided by biosensors responding to product concentrations), the best cell factories can be selected from an extensive library of cells at a significant rate. The most powerful screening can be realized when production is linked to growth (e.g., by implementing synthetic product dependencies), providing both a mechanism for ALE and an easily readable performance parameter.

The Learn phase

Arguably the most essential step of the DBTL cycle is the *Learn* phase. In this phase, the collected observations are put into perspective and used to conclude how modifications introduced into the cell factory impacted strain performance. Sophisticated data analysis tools, including machine learning algorithms, help automate the often arduous task of identifying useful patterns in a vast amount of data. During this process, the interpretability of the results obtained can benefit immensely from a careful *design of experiments* employed in the *Test* phase⁶⁴. Omics data can be integrated into GSM or statistical models that can be interrogated through multivariate data analysis^{65,66}. The conclusions drawn from the *Learn* phase inform the continued *Design* and *Build* process for the next iteration of the DBTL cycle.

References for Chapter 1

- 1 Carvalho, M. F. & Oliveira, R. S. **Natural Production of Fluorinated Compounds and Biotechnological Prospects of the Fluorinase Enzyme.** *Critical Reviews in Biotechnology* **37**, 880-897, doi: 10.1080/07388551.2016.1267109 (2017).
- 2 O'Hagan, D. **Understanding Organofluorine Chemistry. An Introduction to the C-F Bond.** *Chemical Society Reviews* **37**, 308-319, doi: 10.1039/b711844a (2008).
- 3 Yang, Z.-Z. & Li, X. **Ion Solvation in Water from Molecular Dynamics Simulation with the ABEEM/MM Force Field.** *The Journal of Physical Chemistry A* **109**, 3517-3520, doi: 10.1021/jp051106p (2005).
- 4 Vaillancourt, F. H., Yeh, E., Vosburg, D. A., Garneau-Tsodikova, S. & Walsh, C. T. **Nature's Inventory of Halogenation Catalysts: Oxidative Strategies Predominate.** *Chemical Reviews* **106**, 3364-3378, doi: 10.1021/cr050313i (2006).
- 5 Gillis, E. P., Eastman, K. J., Hill, M. D., Donnelly, D. J. & Meanwell, N. A. **Applications of Fluorine in Medicinal Chemistry.** *Journal of Medicinal Chemistry* **58**, 8315-8359, doi: 10.1021/acs.jmedchem.5b00258 (2015).
- 6 Swinson, J. **Fluorine - a Vital Element in the Medicine Chest.** (2005).
- 7 National Academies of Sciences, E., and Medicine; Division on Earth and Life Studies; Board on Life Sciences; Board on Agriculture and Natural Resources; Board on Chemical Sciences and Technology; Committee on Future Biotechnology Products and Opportunities to Enhance Capabilities of the Biotechnology Regulatory System. **Emerging Trends and Products of Biotechnology.** in *Preparing for Future Products of Biotechnology* 230 (The National Academies Press, 2017).
- 8 Lee, B. H. **Bacteria-Based Processes and Products.** in *Fundamentals of Food Biotechnology* 241-312 (2014).
- 9 van Dijk, J. M. & Hecker, M. **Bacillus subtilis: From Soil Bacterium to Super-Secreting Cell Factory.** *Microbial Cell Factories* **12**, 3, doi: 10.1186/1475-2859-12-3 (2013).
- 10 Ferrer-Miralles, N., Domingo-Espín, J., Corchero, J. L., Vázquez, E. & Villaverde, A. **Microbial Factories for Recombinant Pharmaceuticals.** *Microbial Cell Factories* **8**, 17, doi: 10.1186/1475-2859-8-17 (2009).
- 11 Fortman, J. L., Chhabra, S., Mukhopadhyay, A., Chou, H., Lee, T. S., Steen, E. & Keasling, J. D. **Biofuel Alternatives to Ethanol: Pumping the Microbial Well.** *Trends in Biotechnology* **26**, 375-381, doi: 10.1016/j.tibtech.2008.03.008 (2008).

- 12 Surendran, A., Lakshmanan, M., Chee, J. Y., Sulaiman, A. M., Thuoc, D. V. & Sudesh, K. **Can Polyhydroxyalkanoates Be Produced Efficiently from Waste Plant and Animal Oils?** *Frontiers in Bioengineering and Biotechnology* **8**, 169, doi: 10.3389/fbioe.2020.00169 (2020).
- 13 Smitha, M., Singh, S. & Singh, R. **Microbial Bio Transformation: A Process for Chemical Alterations.** *Journal of Bacteriology and Mycology* **4**, doi: 10.15406/jbmoa.2017.04.00085 (2017).
- 14 Berger, R. G. **Biotransformation/Bioconversion.** in *Aroma Biotechnology* (ed Ralf G. Berger) Ch. Chapter 6, 78-91 (Springer Berlin Heidelberg, 1995).
- 15 Singh, R. **Microbial Biotransformation: A Process for Chemical Alterations.** *Journal of Bacteriology and Mycology: Open Access* **4**, doi: 10.15406/jbmoa (2017).
- 16 Mukhopadhyay, A. **Tolerance Engineering in Bacteria for the Production of Advanced Biofuels and Chemicals.** *Trends in Microbiology* **23**, 498-508, doi: 10.1016/j.tim.2015.04.008 (2015).
- 17 Cano-Flores, A., Gómez, J., Escalona-Torres, I. S. & Velasco-Bejarano, B. **Microorganisms as Biocatalysts and Enzyme Sources.** in *Microorganisms* Ch. Chapter 14, (IntechOpen, 2020).
- 18 Shepherd, M. D., Kharel, M. K., Bosserman, M. A. & Rohr, J. **Laboratory Maintenance of *Streptomyces* Species.** *Curr Protoc Microbiol* **Chapter 10**, Unit-10E.11, doi: 10.1002/9780471729259.mc10e01s18 (2010).
- 19 Musiol-Kroll, E. M., Tocchetti, A., Sosio, M. & Stegmann, E. **Challenges and Advances in Genetic Manipulation of Filamentous Actinomycetes-the Remarkable Producers of Specialized Metabolites.** *Natural Product Reports* **36**, 1351-1369, doi: 10.1039/c9np00029a (2019).
- 20 Vermeulen, A. F. **Fourth Industrial Revolution (4ir).** in *Industrial Machine Learning: Using Artificial Intelligence as a Transformational Disruptor* (ed Andreas François Vermeulen) Ch. Chapter 13, 415-532 (Apress, 2020).
- 21 Vandenberg, P. **The Fourth Industrial Revolution.** *Journal of the Asia Pacific Economy* **25**, 194-196, doi: 10.1080/13547860.2019.1686320 (2020).
- 22 Russell, S. J. & Norvig, P. **Artificial Intelligence: A Modern Approach (2nd Ed.).** (Prentice Hall, 2003).
- 23 Wetterstrand, K. A. **DNA Sequencing Costs: Data.**
<<https://www.genome.gov/about-genomics/fact-sheets/DNA-Sequencing-Costs-Data>>.

- 24 Lawson, C. E., Martí, J. M., Radivojevic, T., Jonnalagadda, S. V. R., Gentz, R., Hillson, N. J., Peisert, S., Kim, J., Simmons, B. A., Petzold, C. J., Singer, S. W., Mukhopadhyay, A., Tanjore, D., Dunn, J. G. & Garcia Martin, H. **Machine Learning for Metabolic Engineering: A Review.** *Metabolic Engineering* **63**, 34-60, doi: 10.1016/j.ymben.2020.10.005 (2021).
- 25 Oliveira, A. L. **Biotechnology, Big Data and Artificial Intelligence.** *Biotechnology Journal* **14**, 1800613, doi: 10.1002/biot.201800613 (2019).
- 26 Mukhopadhyay, A., Redding, A. M., Rutherford, B. J. & Keasling, J. D. **Importance of Systems Biology in Engineering Microbes for Biofuel Production.** *Current Opinion in Biotechnology* **19**, 228-234, doi: 10.1016/j.copbio.2008.05.003 (2008).
- 27 Wehrs, M., Tanjore, D., Eng, T., Lievens, J., Pray, T. R. & Mukhopadhyay, A. **Engineering Robust Production Microbes for Large-Scale Cultivation.** *Trends in Microbiology* **27**, 524-537, doi: 10.1016/j.tim.2019.01.006 (2019).
- 28 Nielsen, J. & Keasling, Jay D. **Engineering Cellular Metabolism.** *Cell* **164**, 1185-1197, doi: 10.1016/j.cell.2016.02.004 (2016).
- 29 Chen, Y., Banerjee, D., Mukhopadhyay, A. & Petzold, C. J. **Systems and Synthetic Biology Tools for Advanced Bioproduction Hosts.** *Current Opinion in Biotechnology* **64**, 101-109, doi: 10.1016/j.copbio.2019.12.007 (2020).
- 30 Liu, R., Bassalo, M. C., Zeitoun, R. I. & Gill, R. T. **Genome Scale Engineering Techniques for Metabolic Engineering.** *Metabolic Engineering* **32**, 143-154, doi: 10.1016/j.ymben.2015.09.013 (2015).
- 31 Karp, P. D., Billington, R., Caspi, R., Fulcher, C. A., Latendresse, M., Kothari, A., Keseler, I. M., Krummenacker, M., Midford, P. E., Ong, Q., Ong, W. K., Paley, S. M. & Subhraveti, P. **The Biocyc Collection of Microbial Genomes and Metabolic Pathways.** *Briefings in Bioinformatics* **20**, 1085-1093, doi: 10.1093/bib/bbx085 (2017).
- 32 Prather, K. L. J. & Martin, C. H. **De Novo Biosynthetic Pathways: Rational Design of Microbial Chemical Factories.** *Current Opinion in Biotechnology* **19**, 468-474, doi: 10.1016/j.copbio.2008.07.009 (2008).
- 33 Kumar, A., Wang, L., Ng, C. Y. & Maranas, C. D. **Pathway Design Using De Novo Steps through Uncharted Biochemical Spaces.** *Nature Communications* **9**, 184, doi: 10.1038/s41467-017-02362-x (2018).
- 34 Petzold, C. J., Chan, L. J., Nhan, M. & Adams, P. D. **Analytics for Metabolic Engineering.** *Frontiers in Bioengineering and Biotechnology* **3**, 135, doi: 10.3389/fbioe.2015.00135 (2015).

- 35 Tuller, T., Waldman, Y. Y., Kupiec, M. & Ruppin, E. **Translation Efficiency Is Determined by Both Codon Bias and Folding Energy.** *Proceedings of the National Academy of Sciences USA* **107**, 3645-3650, doi: 10.1073/pnas.0909910107 (2010).
- 36 Athey, J., Alexaki, A., Osipova, E., Rostovtsev, A., Santana-Quintero, L. V., Katneni, U., Simonyan, V. & Kimchi-Sarfaty, C. **A New and Updated Resource for Codon Usage Tables.** *BMC Bioinformatics* **18**, 391, doi: 10.1186/s12859-017-1793-7 (2017).
- 37 Exley, K., Reynolds, C. R., Suckling, L., Chee, S. M., Tsipa, A., Freemont, P. S., McClymont, D. & Kitney, R. I. **Utilising Datasheets for the Informed Automated Design and Build of a Synthetic Metabolic Pathway.** *Journal of Biological Engineering* **13**, 8, doi: 10.1186/s13036-019-0141-z (2019).
- 38 Calero, P. & Nikel, P. I. **Chasing Bacterial Chassis for Metabolic Engineering: A Perspective Review from Classical to Non-Traditional Microorganisms.** *Microbial Biotechnology* **12**, 98-124, doi: 10.1111/1751-7915.13292 (2019).
- 39 Banerjee, D., Eng, T., Lau, A. K., Sasaki, Y., Wang, B., Chen, Y., Prahl, J.-P., Singan, V. R., Herbert, R. A., Liu, Y., Tanjore, D., Petzold, C. J., Keasling, J. D. & Mukhopadhyay, A. **Genome-Scale Metabolic Rewiring Improves Titers Rates and Yields of the Non-Native Product Indigoidine at Scale.** *Nature Communications* **11**, 5385, doi: 10.1038/s41467-020-19171-4 (2020).
- 40 Burgard, A. P., Pharkya, P. & Maranas, C. D. **Optknock: A Bilevel Programming Framework for Identifying Gene Knockout Strategies for Microbial Strain Optimization.** *Biotechnology and Bioengineering* **84**, 647-657, doi: 10.1002/bit.10803 (2003).
- 41 Tepper, N. & Shlomi, T. **Predicting Metabolic Engineering Knockout Strategies for Chemical Production: Accounting for Competing Pathways.** *Bioinformatics* **26**, 536-543, doi: 10.1093/bioinformatics/btp704 (2009).
- 42 Lun, D. S., Rockwell, G., Guido, N. J., Baym, M., Kelner, J. A., Berger, B., Galagan, J. E. & Church, G. M. **Large-Scale Identification of Genetic Design Strategies Using Local Search.** *Molecular Systems Biology* **5**, 296, doi: 10.1038/msb.2009.57 (2009).
- 43 Pharkya, P. & Maranas, C. D. **An Optimization Framework for Identifying Reaction Activation/Inhibition or Elimination Candidates for Overproduction in Microbial Systems.** *Metabolic Engineering* **8**, 1-13, doi: 10.1016/j.ymben.2005.08.003 (2006).

- 44 Pharkya, P., Burgard, A. P. & Maranas, C. D. **Optstrain: A Computational Framework for Redesign of Microbial Production Systems.** *Genome Research* **14**, 2367-2376, doi: 10.1101/gr.2872004 (2004).
- 45 Xu, Z., Zheng, P., Sun, J. & Ma, Y. **Reacknock: Identifying Reaction Deletion Strategies for Microbial Strain Optimization Based on Genome-Scale Metabolic Network.** *PloS One* **8**, e72150, doi: 10.1371/journal.pone.0072150 (2013).
- 46 Yang, L., Ebrahim, A., Lloyd, C. J., Saunders, M. A. & Palsson, B. O. **Dynamicme: Dynamic Simulation and Refinement of Integrated Models of Metabolism and Protein Expression.** *BMC systems biology* **13**, 2, doi: 10.1186/s12918-018-0675-6 (2019).
- 47 O'Brien, E. J. & Palsson, B. O. **Computing the Functional Proteome: Recent Progress and Future Prospects for Genome-Scale Models.** *Current Opinion in Biotechnology* **34**, 125-134, doi: 10.1016/j.copbio.2014.12.017 (2015).
- 48 King, Z. A., O'Brien, E. J., Feist, A. M. & Palsson, B. O. **Literature Mining Supports a Next-Generation Modeling Approach to Predict Cellular Byproduct Secretion.** *Metabolic Engineering* **39**, 220-227, doi: 10.1016/j.ymben.2016.12.004 (2017).
- 49 Lloyd, C. J., Ebrahim, A., Yang, L., King, Z. A., Catoiu, E., O'Brien, E. J., Liu, J. K. & Palsson, B. O. **Cobrame: A Computational Framework for Genome-Scale Models of Metabolism and Gene Expression.** *PLoS computational biology* **14**, e1006302, doi: 10.1371/journal.pcbi.1006302 (2018).
- 50 Bioscience, T. **Pricing for Custom DNA Synthesis**, <<https://www.twistbioscience.com/products/genes>>, accessed on (26-04-2021)
- 51 Gibson, D. G., Young, L., Chuang, R.-Y., Venter, J. C., Hutchison, C. A. & Smith, H. O. **Enzymatic Assembly of DNA Molecules up to Several Hundred Kilobases.** *Nature Methods* **6**, 343-345, doi: 10.1038/nmeth.1318 (2009).
- 52 Bitinaite, J., Rubino, M., Varma, K. H., Schildkraut, I., Vaisvila, R. & Vaiskunaite, R. **USER Friendly DNA Engineering and Cloning Method by Uracil Excision.** *Nucleic Acids Research* **35**, 1992-2002, doi: 10.1093/nar/gkm041 (2007).
- 53 Engler, C., Kandzia, R. & Marillonnet, S. **A One Pot, One Step, Precision Cloning Method with High Throughput Capability.** *PloS One* **3**, e3647, doi: 10.1371/journal.pone.0003647 (2008).
- 54 Horton, R. M., Hunt, H. D., Ho, S. N., Pullen, J. K. & Pease, L. R. **Engineering Hybrid Genes without the Use of Restriction Enzymes: Gene Splicing by Overlap Extension.** *Gene* **77**, 61-68, doi: 10.1016/0378-1119(89)90359-4 (1989).

- 55 Li, M. Z. & Elledge, S. J. **Harnessing Homologous Recombination in Vitro to Generate Recombinant DNA Via Slic.** *Nature Methods* **4**, 251-256, doi: 10.1038/nmeth1010 (2007).
- 56 Li, M. Z. & Elledge, S. J. **Slic: A Method for Sequence- and Ligation-Independent Cloning.** *Methods in Molecular Biology* **852**, 51-59, doi: 10.1007/978-1-61779-564-0_5 (2012).
- 57a Valla, S. & Lale, R. **DNA Cloning and Assembly Methods.** Vol. 1116 (*HUMANA PRESS INC*, 2014).
- 57b Young, R., et al. (2021). **Combinatorial Metabolic Pathway Assembly Approaches and Toolkits for Modular Assembly.** *Metabolic Engineering*. 63: 81-101.
- 58 Nannemann, D. P., Birmingham, W. R., Scism, R. A. & Bachmann, B. O. **Assessing Directed Evolution Methods for the Generation of Biosynthetic Enzymes with Potential in Drug Biosynthesis.** *Future Med Chem* **3**, 809-819, doi: 10.4155/fmc.11.48 (2011).
- 59 Nørholm, M. H. H. **Meta Synthetic Biology: Controlling the Evolution of Engineered Living Systems.** *Microbial Biotechnology* **12**, 35-37, doi: <https://doi.org/10.1111/1751-7915.13350> (2019).
- 60 Sandberg, T. E., Salazar, M. J., Weng, L. L., Palsson, B. O. & Feist, A. M. **The Emergence of Adaptive Laboratory Evolution as an Efficient Tool for Biological Discovery and Industrial Biotechnology.** *Metabolic Engineering* **56**, 1-16, doi: <https://doi.org/10.1016/j.ymben.2019.08.004> (2019).
- 61 Shepelin, D., Hansen, A. S. L., Lennen, R., Luo, H. & Herrgård, M. J. **Selecting the Best: Evolutionary Engineering of Chemical Production in Microbes.** *Genes* **9**, 249, doi: (2018).
- 62 Rennig, M., Martinez, V., Mirzadeh, K., Dunas, F., Röjsäter, B., Daley, D. O. & Nørholm, M. H. H. **Tarsyn: Tunable Antibiotic Resistance Devices Enabling Bacterial Synthetic Evolution and Protein Production.** *ACS Synthetic Biology* **7**, 432-442, doi: 10.1021/acssynbio.7b00200 (2018).
- 63 Rennig, M., Mundhada, H., Wordofa, G. G., Gerngross, D., Wulff, T., Worberg, A., Nielsen, A. T. & Nørholm, M. H. H. **Industrializing a Bacterial Strain for L-Serine Production through Translation Initiation Optimization.** *ACS Synthetic Biology* **8**, 2347-2358, doi: 10.1021/acssynbio.9b00169 (2019).

- 64 Xu, P., Rizzoni, E. A., Sul, S. Y. & Stephanopoulos, G. **Improving Metabolic Pathway Efficiency by Statistical Model-Based Multivariate Regulatory Metabolic Engineering.** *ACS Synthetic Biology* **6**, 148-158, doi: 10.1021/acssynbio.6b00187 (2017).
- 65 Levin, N. **Multivariate Statistics and the Enactment of Metabolic Complexity.** *Social Studies of Science* **44**, 555-578, doi: 10.1177/0306312714524845 (2014).
- 66 Suberu, J., Gromski, P. S., Nordon, A. & Lapkin, A. **Multivariate Data Analysis and Metabolic Profiling of Artemisinin and Related Compounds in High Yielding Varieties of *Artemisia Annu* Field-Grown in Madagascar.** *Journal of Pharmaceutical and Biomedical Analysis* **117**, 522-531, doi: 10.1016/j.jpba.2015.10.003 (2016).

Chapter 2: *Pseudomonas putida* as a chassis for metabolic engineering

The following chapter is based on the book chapter **Engineering reduced-genome strains of *Pseudomonas putida* for product valorization**, published in the context of this thesis in Lara A., Gosset G. (eds) *Minimal Cells: Design, Construction, Biotechnological Applications* (pp 69-93) by Springer.

2.1. Summary

Environmental bacteria, such as strains of the genus *Pseudomonas*, constitute ideal starting points for the design of robust cell factories. These microorganisms are pre-endowed with a number of metabolic and stress-resistance traits that make them optimal for the needs of contemporary biotechnology. Significant technological advances in recent times opened new avenues for metabolic engineering of *Pseudomonas* species. Against this background, this chapter describes current engineering efforts aimed at launching the Gram-negative soil bacterium *P. putida* as a chassis for product valorization and refinement. State-of-the-art synthetic biology approaches for constructing strain variants with improved physiological characteristics or new catalytic capacities are discussed.

2.1. The potential of *Pseudomonas putida* as a chassis for biotechnology

2.1.1 A historical perspective on microbial chassis for biotechnology applications

The microorganisms most frequently used as cell factories in microbial fermentation processes are species that have historically been adopted as model organisms in the laboratory³⁸, such as the Gram-negative bacterium *Escherichia coli* or the archetypal baker's yeast *Saccharomyces cerevisiae* – together with a few other microbial species that had been exploited for their natural capacity to produce a defined set of compounds⁶⁷. Examples of this sort include amino acids (e.g., *Corynebacterium glutamicum*⁶⁸), antibiotics and other antimicrobials (e.g., actinomycetes⁶⁹), or proteins (e.g., *Bacillus subtilis*⁷⁰) and the methylotrophic yeast *Pichia pastoris*^{71,72}. Before the inception of technological advances in biological sciences (and, in particular, genetic and genome engineering approaches), most of the strain engineering efforts were heavily reliant on the limited knowledge (i.e., physiology, genetics, and biochemistry) that had been gathered laboriously over the second half of the 20th century for a modest number of organisms. Success stories of metabolic engineering have thus often focused on the overproduction of natively synthesized metabolites or molecules that are easily accessible from the extant metabolic network (i.e., *cis*-metabolism⁷³) by the addition of simple biochemical pathways.

More recently, the field of metabolic engineering has witnessed a significant increase in the number and nature of the potential microbial chassis that can be used for biotechnological purposes^{74,75}. This occurrence stems from the fact that not only has the knowledge on alternative microbial species expanded enormously, but also the technology bottlenecks for engineering their core properties have been (to a large degree) solved. Achievements within the 'omics' fields enabled us to gain the required knowledge about essentially any microbial platform on a much shorter time scale – and synthetic biology has provided us with tools to manipulate an unprecedented number of living cells at will⁷⁶. When organisms were previously chosen due to the availability of genetic engineering tools or their innate ability to produce the desired compound, we are now experiencing a shift in paradigm: one first tries to establish

the characteristics that an *ideal* biological platform should display for the desired application, e.g., the production of a given target product (including adverse metabolic effects of genetic implants and a suitability for a specific set of production conditions). Then, a suitable *chassis* can be chosen that *naturally* meets the defined criteria in the best possible way, and is then engineered to fulfil its task. This led to an increased interest in species that are true generalists in their nature and that are often found as free-living organisms in diverse environments. Many of such environmental microorganisms are found within the genus *Pseudomonas* and herein, particularly *Pseudomonas putida* has made a name for itself as a promising cell factory.

2.1.2 Bacteria from the genus *Pseudomonas* as *chassis*

Representatives of the species *Pseudomonas putida* are classified as Gram-negative, obligate aerobic γ -proteobacteria with one or several polar flagella that are found in most soil and water habitats where oxygen is available⁷⁷⁻⁷⁹. Members of these bacteria can grow at temperatures between 4 and 40°C (although they grow optimally between 25 and 30°C⁸⁰), and they can form biofilms^{81,82} in a process coordinated by cell-to-cell-communication systems (i.e., quorum sensing) in a cell density-dependent manner⁸³. Due to the ever-changing nature of their natural habitat, *P. putida* is endowed with a versatile metabolic network that provides it with the ability to adapt to many different physicochemical conditions, some of which are of particular interest for industrial fermentation setups (e.g., extreme pH values, temperature gradients, and high concentrations of toxic substances)⁸⁴⁻⁸⁶.

In particular, one of its most remarkable physiological traits was the very reason why its most prominent representative, *P. putida* strain mt-2, was discovered in the first place: the ability to degrade and consume recalcitrant xenobiotic compounds, such as toluene and xylenes⁸⁷ – and this trait goes hand in hand with a remarkably high tolerance to organic solvents⁸⁸. This outstanding trait results from the presence of, *inter alia*, very effective efflux systems, which make *P. putida* an ideal producer of such compounds or a suitable biocatalyst for production processes in two-phase systems⁸⁹⁻⁹¹.

The ability to tolerate high concentrations of organic solvents and aromatic compounds furthermore allows for the use of complex alternative feedstocks that are not accessible for other bacteria⁷³.

An outstanding example in this sense is the wealth of substrates that can be derived from plant biomass, a large fraction of which is represented by lignin. Because bioproduction processes established thus far exploited lignocellulose predominantly as a source of sugars, the lignin fraction remains a largely unused waste product often used for the production of heat and electric energy via combustion. *Pseudomonas*, however, can consume a large variety of the aromatic monomers that are derived from lignin after hydrolysis – even enabling the non-hierarchical co-utilization of these substrates⁹². Moreover, although *P. putida* is not able to efficiently consume the most abundant sugars present in lignocellulose besides glucose, xylose, and arabinose, it can be easily engineered to do so^{93,94}. Consequently, it is now possible to utilize a large proportion of the carbon stored in plant biomass for the production of value-added compounds in fermentation approaches.

Another possibility for the valorization of complex feedstocks containing arenes is to make direct use of the assimilatory pathways that are present within the *cis*-metabolism of *P. putida*. The well-studied *meta*- and *ortho*-cleavage routes to degrade a range of aromatic compounds⁹⁵ converge into the central metabolic intermediate catechol, which is subsequently converted into *cis,cis*-muconic acid [(2*E*,4*E*) 2,4-hexanedioic acid]⁹⁶⁻⁹⁹. The latter molecule has recently gained significant attention in the chemical industry as a platform chemical, representing a precursor for the synthesis of terephthalic acid, 3-hexenedioic acid, 2-hexenedioic acid, 1,6-hexanediol, ϵ -caprolactam, and ϵ -caprolactone; all of which serve as building blocks for value-added commercial polymers [e.g., polyethylene terephthalate (PET) from terephthalic acid or Nylon-6,6 from adipic acid].

Recently, the substrate spectrum that is suitable to produce *cis,cis*-muconic acid from aromatic precursors in *P. putida* was further expanded by introducing heterologous functions that feed the catechol branch with intermediates from degradation routes that produce protocatechuic acid as a central metabolic intermediate. These operations

resulted in a complex converging metabolic network that converts a diverse mix of aromatic substrates into catechol and consequently *cis,cis*-muconic acid¹⁰⁰. As discussed in the next section, engineering the synthesis of this type of compounds (among many others) in *Pseudomonas* species is possible largely due to a specific metabolic wiring characteristic of this species. **Chapter 5** provides an applied example of how the native catabolic capacity for aromatic hydrocarbons in *P. putida* can be exploited to produce specialized halogenated products.

2.1.3 Carbon metabolism in *Pseudomonas putida*

Pseudomonas putida represents a striking example of a bow tie framework¹⁰¹, where a large variety of different substrates are assimilated through a *catabolic funnel* into a core metabolic network to produce activated carriers and precursor metabolites for the synthesis of larger building blocks that constitute biomass (**Figure 2.1B**). The central carbon metabolism of *P. putida* exhibits a rather special architecture when it is exposed to the sugar substrate that is widely preferred in industry, glucose (**Figure 2.1C**). Fructose is the only carbohydrate known to be transported into the cytoplasm through a phosphoenolpyruvate-carbohydrate phosphotransferase system (PTS) system¹⁰². All other sugars use active non-PTS transport systems, often at the costs of higher energy demand. Like many other (aerobic) prokaryotes, most pseudomonads lack a functional 6-phosphofructo-1-kinase (Pfk), a key enzyme of the Embden–Meyerhof–Parnas (EMP) glycolytic pathway, and thus rely on the Entner–Doudoroff (ED) route for the consumption of sugars and sugar acids^{103,104}. The initial steps of glucose consumption occur through a set of three pathways that converge in 6-phosphogluconate (6PG) as a central node and each includes substrate oxidation (generating reduced cofactors) and ATP-dependent phosphorylation steps. The activated intermediate 6PG is then subjected to dehydration (catalyzed by Edd) and aldol cleavage (catalyzed by Eda) that yield the two C3 intermediates pyruvate and glyceraldehyde-3-*P* (G3P). G3P can then be further processed to pyruvate through the lower block of glycolysis (yielding one ATP and one NADH) or be recycled through a cyclic metabolic route termed the *EDEMP cycle* [a metabolic architecture involving enzymes belonging to the ED, EMP, and pentose phosphate (PP) pathways]. This recycling of

metabolites enables *Pseudomonas* to generate additional NADPH reducing power and is a crucial mechanism to counter high levels of oxidative stress¹⁰⁵. A complex regulatory network leads to a sequential uptake of substrates if several carbon sources are present, whereby glucose is taking a subordinate role in favor of some organic acids and amino acids¹⁰⁶.

The successive assimilation of substrates is coordinated by an interplay of global carbon catabolite control (CCR) and function-specific regulatory mechanisms¹⁰⁷. One of the most important of these mechanisms is exerted by the global catabolite repression control protein Crc, which interacts with the protein Hfq to bind to gene transcripts inhibiting their translation¹⁰⁸⁻¹¹³. In fact, regulation of the biochemical activities that constitute central carbon metabolism has been found to occur to a large extent at the post-transcriptional level¹¹⁴. Crc/Hfq inhibits translation of its target messenger RNA (mRNA) upon recognizing a specific sequence motif (AAnAAnAA) near the ribosome-binding site¹¹³. As shown experimentally for the toluene, alkane, and benzoate degradation pathways and proposed for several other catabolic pathways based on the identification of CRC/Hfq-binding motifs, CCR follows a multi-tiered repression strategy that allows dynamic regulation^{115,116}. In this context, CCR influences catabolic activities directly via translational inhibition of enzymes that catalyze the first biochemical reaction of a pathway as well as transport proteins, and indirectly by preventing the production of transcriptional activators¹¹⁶. These regulators in turn activate the expression of pathway-specific genes encoding catabolic enzymes and transporters¹¹⁶. The activity of Crc/Hfq is further modulated by the small regulatory RNAs of the CrcZ family that are produced upon depletion of preferred carbon sources and act as antagonists for the CCR proteins^{117,118}.

Because of the complexity and idiosyncrasies that characterize metabolic regulation in *Pseudomonas* species, a lack of knowledge (particularly about genotype-phenotype relationships) often becomes a bottleneck if one tries to predict the outcome of genetic interventions. As argued below, the inception of a set of dedicated tools for the engineering of *Pseudomonas* has emerged and considerably accelerated the design of whole-cell biocatalysts based on this species.

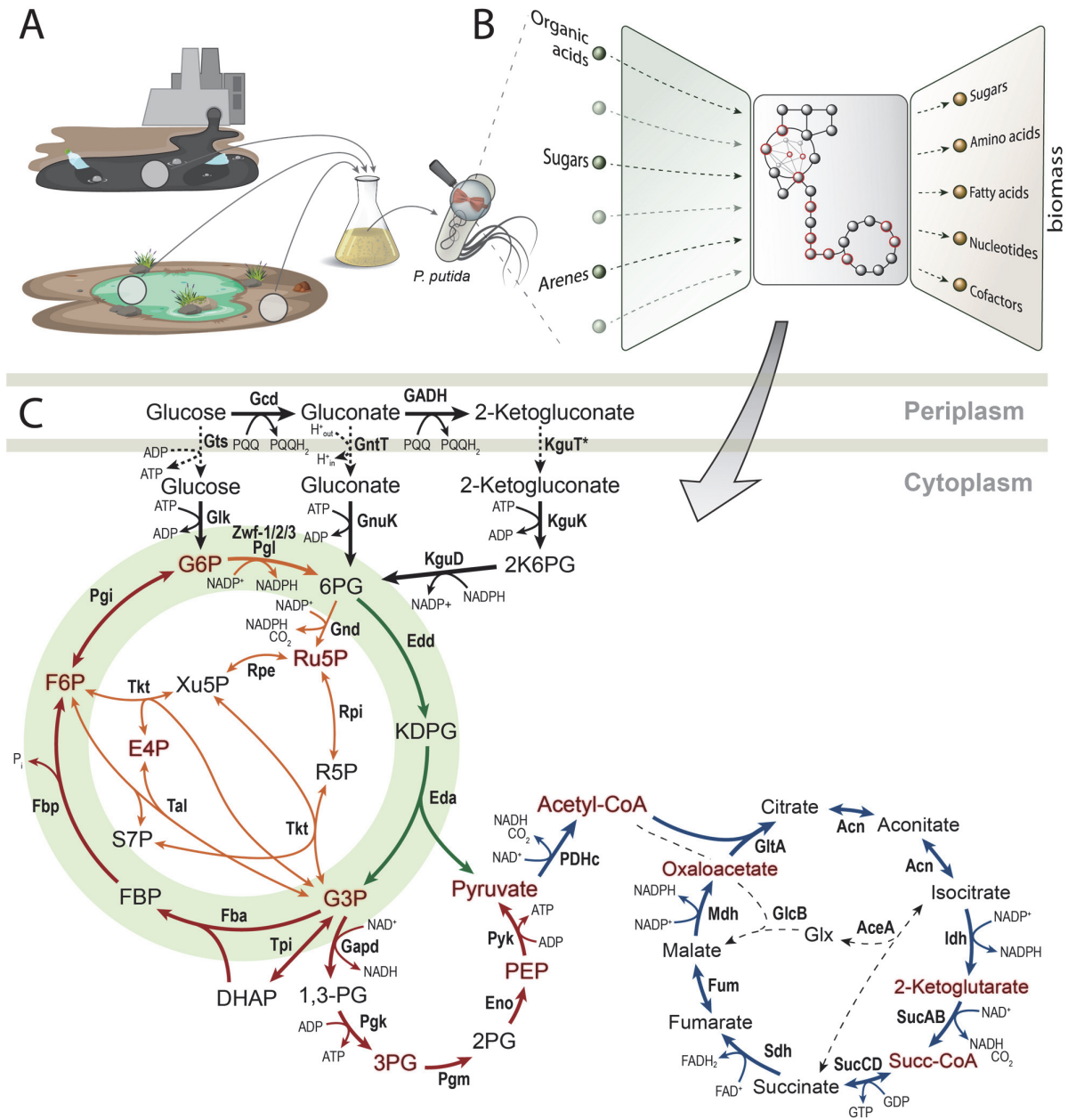


Figure 2.1: Relevant metabolic characteristics of the Gram-negative environmental bacterium *Pseudomonas putida* as a chassis for biotechnology. (A) Strains of *P. putida* can be isolated in most soil and water habitats where oxygen is available, including wastewater reservoirs from chemical plants. **(B)** The metabolic network of *P. putida* KT2440 represents a striking example of a bowtie framework, where a large variety of different substrates are funneled through catabolic pathways into a set of central biochemical reactions that produce activated energy/redox carriers and precursor metabolites (the twelve elemental metabolites in this network¹¹⁹ are highlighted in red) for the formation of biomass. **(C)** Biochemical pathways involved in glucose catabolism in *P. putida* KT2440. The metabolic flux revolves around the EDEMP cycle (highlighted in green) that includes activities from the Entner–Doudoroff pathway (reactions shown in dark green), the pentose phosphate pathway (reactions are shown in orange), and the Embden-Meyerhof-Parnas route (reactions shown in red)¹⁰⁵. Reactions of the tricarboxylic acid (TCA) cycle are indicated in blue. Transport reactions across the plasma membrane are shown with dashed lines. Note that the exact transport mechanism for 2-ketogluconate is unknown (shown

with a dashed arrow). Abbreviations of metabolites are as follows: G6P, glucose-6-P; 6PG, 6-phosphogluconate; F6P, fructose-6-P; 6PG, 6-phosphogluconate; FBP, fructose-1,6-P₂; DHAP, dihydroxyacetone-P; KDPG, 2-keto-3-deoxy-6-phosphogluconate; Ru5P, ribulose-5-P; R5P, ribose-5-P; S7P, sedoheptulose-7-P; E4P, erythrose-4-P; G3P, glyceraldehyde-3-P; 3PG, glycerate-3-P; 2PG, glycerate-2-P; PEP, phosphoenolpyruvate; PQQ, pyrroloquinoline quinone; PQQH₂, pyrroloquinoline quinol; and acetyl-CoA, acetyl-coenzyme A. Enzymes in this scheme are abbreviated as follows: Gcd, glucose dehydrogenase; GADH, gluconate dehydrogenase; GtsABCD, D-glucose ABC-transporter; GntT, gluconate/H⁺ symporter; KguT, putative 2-ketogluconate transporter; Glk, glucose kinase; GnuK, gluconate kinase; KguK, 2-ketogluconate kinase; KguD, 2K6PG reductase; Pgi, phosphohexose isomerase; Zwf, glucose-6-P dehydrogenase; Pgl, phosphogluconolactonase; Edd, 6-phosphogluconate dehydratase; Eda, 2-dehydro-3-deoxy-6-phosphogluconate aldolase; Fba, fructose-1,6-P₂ aldolase; Fbp, fructose-1,6-P₂ phosphatase; Gnd, phosphogluconate dehydrogenase; Rpi, ribose-5-P isomerase; Rpe, ribulose-5-P 3-epimerase; Tkt, transketolase; Tal, transaldolase; Tpi, triosephosphate isomerase; Gapd, glyceraldehyde-3-P dehydrogenase; Pgk, phosphoglycerate kinase; Pgm, phosphoglycerate mutase; Eno, enolase; Pyk, pyruvate kinase; PDHc, pyruvate dehydrogenase complex; GltA, citrate synthase; Acn, aconitase; Idh, isocitrate dehydrogenase; SucAB, 2-ketoglutarate dehydrogenase; SucCD, succinyl-CoA synthetase; Sdh, succinate dehydrogenase; Fum, fumarate hydratase; Mdh, malate dehydrogenase; AceA, isocitrate lyase; and GlcB, malate synthase.

2.1.4 Domestication of *Pseudomonas putida* as a chassis

Since the beginning of the 21st century, various modern techniques that were developed in the field of synthetic as well as systems biology were made available for *P. putida* and contributed to its broad acceptance as a promising and reliable biotechnological platform. The fully sequenced¹²⁰ and extensively annotated¹²¹ genome of *P. putida* KT2440 provided a solid foundation for the integration of several systems biology applications and enabled the defined manipulation of phenotypical traits useful for biotechnological purposes. It furthermore formed the basis for a set of genome-scale metabolic models that were regularly used to guide metabolic engineering strategies and helped to elucidate the physiologic response of *P. putida* to different environments and physicochemical conditions¹²²⁻¹²⁵.

Along the same lines, genetic amenability facilitated the adaptation and development of increasingly sophisticated synthetic biology tools developed for specific gene and genome manipulations^{126,127}. A milestone for establishing a standardized toolbox of well-characterized molecular tools has been the creation of the *Standard European Vector Architecture* (SEVA) platform^{128,129}, containing various genetic elements (e.g., promoters, antibiotic resistance determinants, origins of plasmid replication, and reporter

functions) built in a modular and easily interchangeable fashion. The inducible promoter systems within the SEVA collection were further complemented with synthetic libraries of constitutive promoters that allow for the predictable adjustment of the transcription strength of any desired gene and gene clusters^{130,131}. However, the strength of a promoter alone does not determine the overall expression strength of a gene since translation heavily depends on the sequence context within the mRNA around the ribosome-binding site. This issue can be solved by exploiting the mechanism of translational coupling, which uses standardized, non-coding 5'-untranslated regions and leader sequences that are placed in front of a gene of interest, as firstly established for *E. coli*¹³² and later demonstrated for *P. putida* as well¹³¹. Alternatively, the online RBS calculator 2.1, developed by the Salis laboratory at Penn State University¹³³⁻¹³⁸, allows for the *in silico* prediction of translation initiation rates based on a sequence context or the design of translation initiation sequences (*TIS*) with targeted translation rates, and was successfully applied in *P. putida*¹³⁹⁻¹⁴³.

The plethora of tools and approaches for gene and genome manipulation of this species paved the way towards the genetic domestication of *P. putida* as a *chassis* for biotechnology. However, despite considerable progress in our ability to access genetic manipulations of *Pseudomonas*, this bacterium still shows deficits when it comes to high-throughput genome engineering. This state of affairs can be explained to some extent by present knowledge gaps compared to the microbial forerunners of synthetic biology. More importantly, *P. putida* lacks the high capacity for homologous recombination (HR) displayed by other well-established *chassis*, e.g., *S. cerevisiae* or *B. subtilis*¹⁴⁴, or an inventory of well-characterized bacteriophages, e.g., phages characterized for *E. coli*¹⁴⁵ that, together, provide the molecular tools for an efficient recombineering system. Since the availability of such systems is instrumental for high-throughput genome engineering, several alternatives have emerged over the last years to overcome the technical limitations. In the next section of this chapter, state-of-the-art techniques for genome manipulation in *Pseudomonas* species are reviewed, highlighting the advantages and disadvantages of these procedures.

2.2. Strategies for the genetic editing of *Pseudomonas* species

Driven by the revolution of synthetic biology, different approaches have been designed, attempting to provide reliable, quick, and easy ways to implement defined genetic modifications in *P. putida*. Originally, these methods exclusively relied on native HR functions mediated by RecA, enabling the allelic exchange of a plasmid-encoded sequence with a homologous counterpart on the bacterial chromosome. However, one disadvantage inherent to the HR-mediated mechanism is its impartiality regarding the result of the recombination. In some cases, this occurrence can increase the screening efforts to identify the desired mutant cells in a (sometimes larger) population of wild-type cells with increased fitness. This technical weakness could be overcome with the advent of CRISPR/Cas9 technologies that enable the specific counterselection against the unwanted (i.e., wild-type) sequence.

2.2.1 Genome engineering of *Pseudomonas* using suicide plasmids

In the most established genome engineering methods, the template DNA sequences needed for HR are delivered into *Pseudomonas* encoded on suicide plasmids carrying selectable markers (e.g., antibiotic resistance determinants). These templates include the desired genetic changes flanked on each side by DNA segments (typically ca. 500-1000 bp) that are homologous to the target site of the genome. In this context, a (conditional) suicide vector is a plasmid carrying an origin of vegetative replication (*oriV*), which is natively not functional in its target host. The most prominent and widely used example of a suicide *oriV* in *P. putida* represents that of the plasmid R6K, whose functionality relies on the presence of its cognate replication factor π , encoded by the *pir* gene¹⁴⁶. The advantage of such a vector is that bacterial strains harboring *pir* can be used without limitations for the cloning and propagation of the plasmid. At the same time, survival of *Pseudomonas* under selection pressure depends on integrating the antibiotic resistance determinants into the chromosome. This is mediated by HR between the plasmid-encoded inserts and the target genomic sequence (**Figure 2.3**).

The allelic exchange can be performed within a single step (double crossover), where the two homologous arms (HAs) flanking a mutagenesis region recombine at the same

time or in two consecutive steps (i.e., insertion followed by excision). Hereby, the whole plasmid sequence is co-integrated into the chromosome through a single cross-over event at either of the two individual homologous arms (HA1 and HA2). A second HR leads to the resolution of the plasmid and can leave behind the desired genetic modification. For systems relying on a double-crossover mechanism, a selectable marker is firstly introduced between the two homology regions that can later be removed using the site-specific recombination systems *Flp/FRT* from yeast¹⁴⁷ or *Cre/lox* from phage P1^{148,149}. These systems have the inherent disadvantage of leaving behind scars within the chromosome at the sites of recombination, which, after repeated use of the system for multiple genome interventions, are prone to recombine with each other, potentially leading to the deletion or inversion of large genomic segments.

One predominant problem for two-step-based genome engineering approaches was the low efficiency inherent to the natural HR system of *Pseudomonas*¹²⁶. Consequently, different methods have been exploited to either enforce the resolution of the plasmid or to counter-select against cells, which did not undergo the second HR, respectively. One of the first counterselection strategies adapted to *P. putida* was based on the *sacB* gene derived from *Bacillus subtilis*, encoding for a levansucrase that acts on sucrose to produce levan polysaccharides. These products accumulate in the periplasm of Gram-negative bacteria, where they exert a toxic effect¹⁵⁰. Therefore, the resolution of a suicide plasmid encoding *sacB* can be selected for by growth in a sucrose-containing medium.

A similar approach is based on the *upp* gene, whose natural function in *P. putida* is to phosphoribosylate uracil to yield uridine monophosphate (UMP, 5'-uridylic acid), which is a necessary step in the pyrimidine salvage pathway. Upp also acts on the antimetabolite 5-fluorouracil (5-FU) that is thereby converted into 5-fluoro-UMP. After metabolic transformation of 5-FU into 5-fluoro-UMP, this compound acts as a suicide inhibitor of the essential enzyme thymidylate synthase, resulting in cell death. Cells deficient in the uracil phosphoribosyltransferase function show no physiological response after exposure to 5-FU. After deleting the non-essential *upp* in *P. putida*, the

gene can be used as a counter-selectable marker for molecular tools by merely adding 5-FU to the culture medium¹⁵¹.

Equally working on the biosynthesis of pyrimidine nucleobases is a dual-selection system based on the deletion of the gene *pyrF*, combined with the antimetabolite 5-fluoroorotidine-5'-P¹⁵². The gene product of *pyrF* (orotidine-5'-P decarboxylase) is responsible for the formation of UMP from orotidine-5'-P (OMP), which makes it essential for the *de-novo* biosynthesis of uracil. With a *pyrF* deletion, cells become auxotrophic for uracil and can be 'rescued' via the ectopic expression of *pyrF* from a plasmid (positive selection). At the same time, OMP decarboxylase acts on 5-fluoroorotidine-5'-P (5-FOMP) and converts it into 5-fluoro-UMP with the same toxic effect as described above allowing for a negative selection of genetic elements carrying *pyrF*.

However, all counterselection methods have shown to display shortcomings. The externally added compound for negative selection often does not suppress growth entirely, making it difficult to identify cells that performed the second HR, especially when trying to eliminate (conditionally) essential functions whose deletions result in a growth deficiency. Furthermore, the *upp*/5-FU and *pyrF*/5-FOMP methods require the deletion of relevant metabolic functions in the host, which is not desired in a robust cell factory. Finally, all the counterselection methods based on the action of a single gene are prone to mutate, rendering them ineffective over repeated use of the markers and key genetic elements.

In principle, all these drawbacks could be solved by establishing counterselection techniques based on highly specific endonucleases that are produced endogenously. A widely adopted method uses a suicide plasmid harboring the conditional origin of replication R6K, an antibiotic resistance determinant, and a polylinker region (i.e., multiple cloning site) flanked by two recognition sequences for the homing nuclease *I-SceI* from *S. cerevisiae*. Upon co-integration of the plasmid via homologous recombination, the *SCEI* gene is expressed from an additional helper plasmid, and the meganuclease produced thereof introduces double-strand breaks (DSBs) at both target sites encoded on the integrative plasmid. Cells can escape this lethal cleavage within the chromosome if they eliminate the *I-SceI* recognition sites by a second crossover event

(**Figure 2.2**). The redundancies of the target sequences as well as the *SCEI* gene, which is encoded on plasmids that are maintained at multiple copy numbers, make this system highly efficient and robust. Initially conceptualized by Martínez-García and de Lorenzo¹⁵³, this method was further refined as part of this thesis. A hands-on protocol, new molecular tools complementing the strategy, and application examples for the improved method are presented in **Chapter 3**.

A remaining disadvantage of all counterselection systems discussed in this section is their limited selectiveness regarding the resulting DNA sequence in the chromosome. To introduce a change in the genetic sequence, the modified target region is flanked by two homologous arms (HA1 and HA2, **Figure 2.2**). Either of the two crossover events leading first to the co-integration of the suicide plasmid and then to its resolution can be performed by each of the two HAs. Only if the site of recombination differs between the first and the second crossover, a mutant genotype is created (**Figure 2.2**). If both HR events involve the same HA, the wild-type sequence is restored.

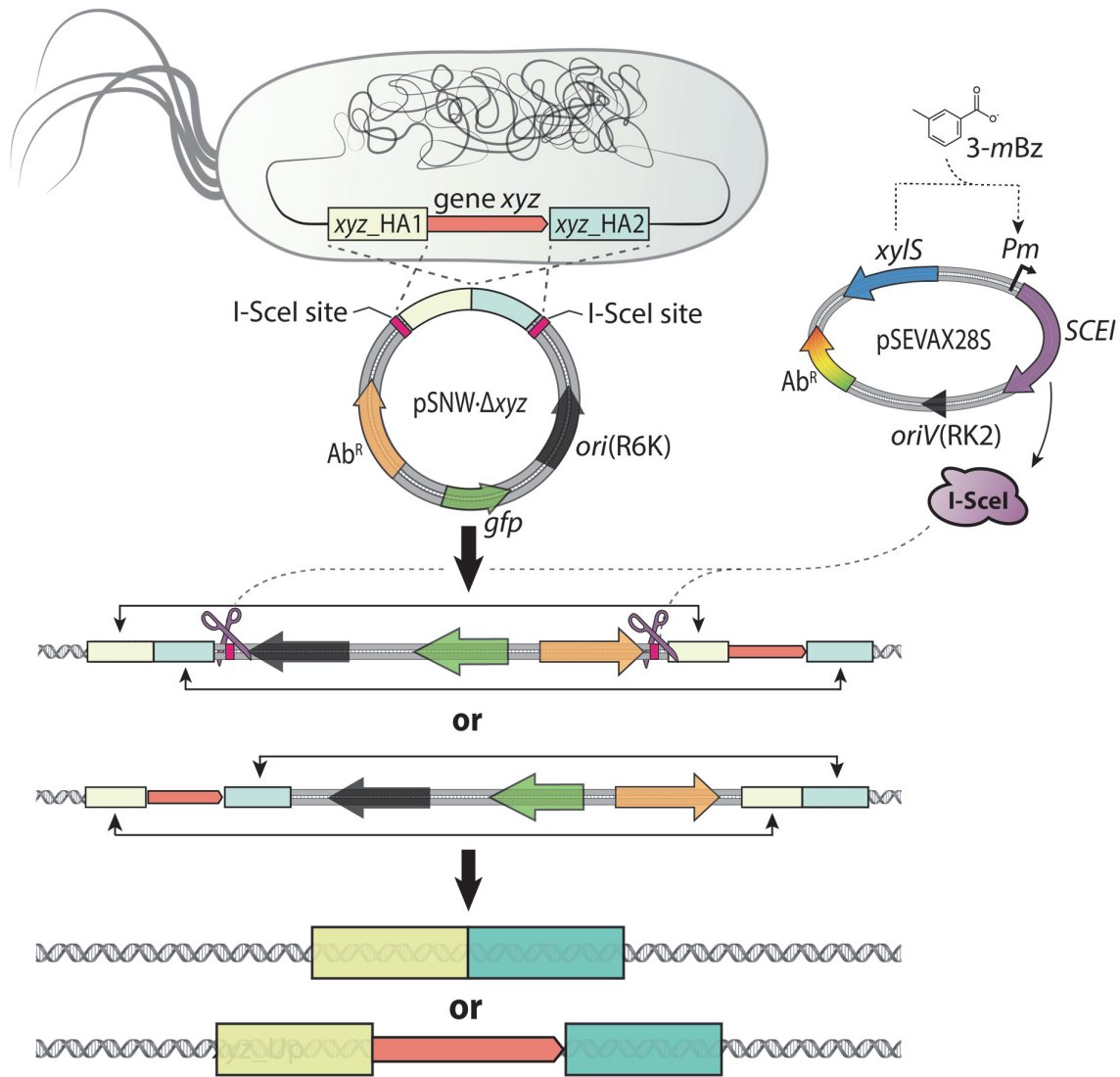


Figure 2.2. Genome engineering of *Pseudomonas* using suicide plasmids. The molecular mechanisms that lead to the desired chromosomal modification are shown for the deletion of gene *xyz* with the method described in detail in **Chapter 3**^{89,154}. Two homology arms (HA) that flank the target mutagenesis site are cloned into the plasmid pSNW, acting as a suicide vector in *P. putida*. The plasmid is co-integrated into the chromosome through RecA-mediated homologous recombination at either of the two HAs, thereby conferring a selectable antibiotic resistance as well as a fluorescence signal to identify transformed cells. Introduction of a replicable plasmid [e.g., vector pSEVA628S, harboring the gene encoding the homing endonuclease I-SceI, the expression of which is inducible upon addition of 3-methylbenzoate (3-mBz)], results in meganuclease-dependent cuts on the two I-SceI target recognition sites located within pGNW by introducing DNA double-strand breaks in the genome. To avoid the lethal cutting mediated by I-SceI, the cells undergo a second homologous recombination, which yields either the desired mutant or a revertant (i.e., wild-type) genotype, depending on which of the two HAs recombine.

2.2.2 CRISPR/Cas9 technologies and recombineering approaches for *Pseudomonas*

Until recently, established genome engineering strategies could not discriminate between mutant and wild-type cells unless a genetic manipulation resulted in a selectable phenotype. On the contrary, the introduction of new biochemical functions or the deletion of genes with a relevant physiological role often results in an evolutionary advantage for the wild-type cells in such a way that often significant screening efforts had to be made for selecting the mutants. This problem has been largely solved when customized CRISPR/Cas9 systems were made accessible after their first introduction in 2012¹⁵⁵⁻¹⁵⁷. Cas9 serves as an endonuclease that can be guided to a specific DNA sequence through its association with a synthetic guide RNA (sgRNA) and is therefore suitable to select *against* particular genotypes. Shortly after its emergence, the new technology was combined with traditional molecular tools for genetic engineering to create new, powerful gene edition systems that further facilitated engineering approaches in several cell factories.

Different approaches for *P. putida* intended to perform chromosomal modifications within a single step (**Figure 2.3**), by using CRISPR/Cas9 counterselection to stimulate the allelic exchange of a sequence from either a plasmid via a double-crossover¹⁵⁸ or with a synthetic DNA fragment (either single or double-stranded) in a process called *recombineering*^{159,160}. It has been established in *E. coli* that one can simply insert modifications into any chromosomal target site using linear, double-stranded (ds) DNA (e.g., PCR products) by flanking fragments with short (typically 40-50 bp) HAs and delivering them into cells that overexpress the three genes of the Red system from phage λ ¹⁶¹. These genes encode (i) a 5' \rightarrow 3' exonuclease (Exo) that digests one of the two strands on the DNA fragment, (ii) a dsDNA binding protein (Gam) that protects the introduced fragment from the attack of endogenous nucleases, and (iii) a single-stranded (ss) DNA-binding protein (Beta) that shields the single-stranded product from degradation and mediates recombination (**Figure 2.3**). Furthermore, it has been shown that recombineering approaches work even more efficiently when using an ssDNA fragment (e.g., a synthesized oligonucleotide) – thereby requiring only the

function of protein Beta¹⁶². This method can generate up to 6% of recombinant cells within a single round of treatment without any means for selection. Traditionally, λ Red recombineering is often used in a two-step approach, similar to strategies based on suicide plasmids, where an antibiotic resistance gene is first introduced at the target site together with a counter-selectable marker. With the second round of recombineering, using a different DNA fragment, the inserted gene cassette is removed, leaving behind only the desired mutation (i.e., markerless modification). Moreover, λ Red recombineering can be combined with CRISPR/Cas9 counterselection, which enabled the introduction of any genetic change within a single step supplying only linear DNA fragments. This technology is particularly powerful when performed multi-cycled and in an automated way, e.g., with the *CRMAGE* method (Crispr/Cas9 and λ Red recombineering based Multiplex Automated Genome Engineering)¹⁶³.

Despite its many advantages, all approaches employing CRISPR/Cas9 technologies suffer from a lack of understanding about the characteristics that qualify an effective sgRNA sequence. Consequently, these methods can have only low efficiency, and extensive screening efforts are often required to identify mutant cells without the introduction of counter-selectable markers. An additional bottleneck for recombineering in *P. putida* strain KT2440 has been identifying recombinase enzymes that function efficiently. In contrast to *E. coli*, *P. putida* KT2440 is missing (or they are yet to be identified) active bacteriophages that could provide DNA-editing enzymes that are specifically tailored to work optimally within its host.

Attempts to render the λ Red system functional in *Pseudomonas* species were reported¹⁶⁴⁻¹⁶⁷, but the information available in the literature would indicate an inferior performance in the absence of selection compared to conventional methods. Recent progress was made by identifying the RecET system in *Pseudomonas syringae*, in which the genes are part of a putative prophage¹⁶⁸. The protein pair resembles the λ Red system in that they share homologies with the Exo and Beta components of the λ Red system, respectively, and thus provide the same functions.

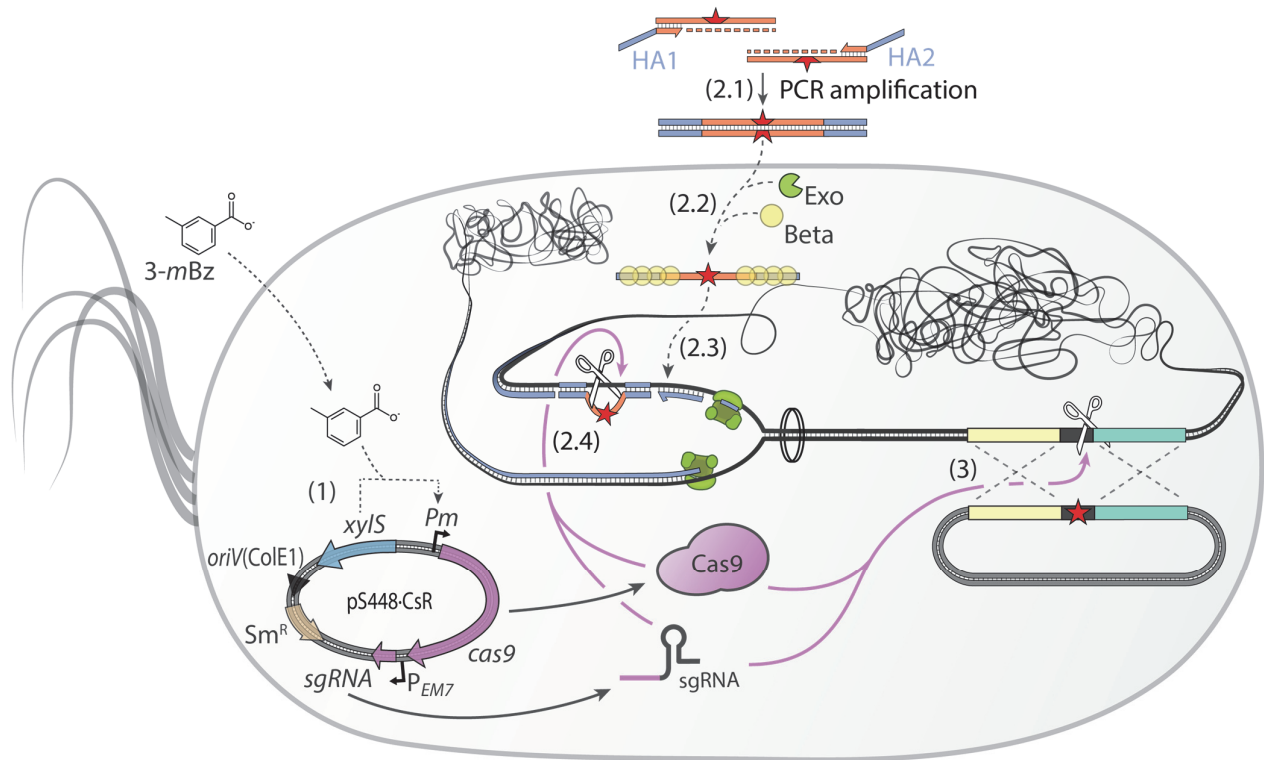


Figure 2.3. Genome engineering applications in *Pseudomonas* species using CRISPR/Cas9 as counterselection system. A plasmid-based CRISPR/Cas9 expression system is shown in the scheme with vector pS448-CsR as an example, as described in **Chapter 3**. This plasmid encodes a streptomycin-resistance gene (Sm^R), the *cas9* gene under the control of the inducible *XylS/Pm* expression system as well as a constitutively-expressed (with the P_{EM7} promoter), customizable cassette including a specific synthetic guide RNA (*sgRNA*). Autonomous replication of this vector is controlled by the ColE1 origin of vegetative replication [*oriV*(ColE1)]. The steps needed for genome engineering of *Pseudomonas* using this system are as follows: (1) upon induction of the system via addition of 3-methylbenzoate (3-mBz), Cas9 is produced, and the protein associates with the *sgRNA* to introduce a double-strand (ds) break in the DNA at the target locus, which is lethal for cells harboring the wild-type sequence. This counterselecting action of CRISPR/Cas9 can be combined with methods of *recombineering* (2). Thereby, a linear DNA fragment [e.g., dsDNA obtained via PCR (2.1) or a chemically-synthesized single-stranded (ss) DNA fragment, both containing homologous arms (HA) to the target locus on each end] is used to introduce genetic modifications (indicated with a red star) at a target site. If dsDNA is used (2.2), one of the two DNA strands can be digested with an exonuclease (e.g., Beta and Exo, from the λ Red system commonly used in *E. coli*), leaving a ssDNA fragment that is protected from further degradation by a ssDNA binding protein (e.g., Beta, SSR, or RecT). The two flanking HAs mediate the introduction of the mutagenic ssDNA fragment into the chromosome via homologous recombination or as an Okazaki fragment during the replication of the bacterial chromosome (2.3). Finally, CRISPR/Cas9 counterselection of the wild-type sequence allows for the allelic exchange of a homologous DNA fragment containing the desired modifications directly from a plasmid via a double-crossover mechanism (3). If the *sgRNA* target is changed during this mutagenesis procedure, only the cells having the allelic exchange can survive in the presence of both Cas9 and the expressed *sgRNA*.

The first reported attempt to employ RecET-based genome engineering in *P. putida* was reported by Choi et al.¹⁵⁹, who used the system to enable recombineering with linear donor dsDNA. However, the reported efficiency of the RecET system was relatively low and was by far outperformed by a suicide plasmid-based approach that the authors combined with the action of RecET as well.

In another approach¹⁶⁹, bioinformatic mining of sequences from known protein families and experimental validation of the most promising enzymes in standardized recombination assays led to the discovery of two new enzymes, *Ssr* from *P. putida* strain DOT-T1E^{160,170} and *Rec2* from *P. putida* CSV86. The *ssr* gene was transplanted into *P. putida* KT2440 and shown to promote recombination with linear ssDNA fragments, although the procedure had lower efficiencies than λ Red-mediated recombineering in *E. coli*. One additional obstacle was identified in the activity of the endogenous mismatch repair (MMR) system, interfering with the implementation of single nucleotide substitutions¹⁷¹. To overcome these restrictions, Aparicio et al.¹⁷² developed a workflow that enables a more efficient recombineering in *P. putida* at mutation frequencies up to 10%, combining the thermo-inducible expression of *Rec2* and *MutLE36K*, a mutated variant of DNA mismatch repair protein¹⁷³⁻¹⁷⁵, transiently repressing the MMR system.

If combined with the conventional two-step mutagenesis approach using suicide plasmids, the sequence-specific counterselection capability that CRISPR/Cas9 systems offer enables the deletion of genes that before could be achieved only with significant efforts – if at all. Directing Cas9 to the wild-type sequence that is intended to be deleted or modified selects for those cells, which resolve the previously co-integrated plasmid in a way that yields the desired mutation. A detailed protocol for this method, conceptualized as part of this thesis, is provided in **Chapter 3**.

Our ability to inactivate targeted genes for physiological characterizations at high speed has recently been upgraded by the emergence of CRISPR/Cas-guided base editing systems¹⁷⁶⁻¹⁷⁸. DNA base editors accurately introduce point mutations without the need for DSBs or donor DNA templates and are HDR-independent. The recently developed tools utilize a catalytically defective Cas nuclease (with one or both of the

DNA-cleaving domains mutated) that is fused to an ssDNA deaminase and, in some applications, is combined with proteins that inhibit DNA repair mechanisms. The developed base editing systems can be categorized into two classes: cytosine base editors (CBEs), which catalyze the conversion of C-G base pairs to T-A, and adenine base editors (ABEs), which catalyze an A-T-to-G-C conversion¹⁷⁸. Combined, BEs and ABEs can generate all four possible single-nucleotide mutations (A→G, C→T, G→A, and T→C). For studies on genotype-phenotype relationships, the introduction of an early *Stop* codon within a gene sequence by mutating any of the codons CGA, CAG, CAA, or TGG into TGA, TAG, or TAA with a CBE-system is a valuable method that has also been applied in *Pseudomonas* species¹⁷⁹.

One way or the other, the constellation of available tools for genome engineering of *Pseudomonas* species and, in particular, of *P. putida* has significantly enabled our ability to interrogate core functions of the cell. The genome manipulation of these species has paved the way to expand the fundamental knowledge on bacterial physiology – and also enabled the design and construction of reduced-genome variants of *P. putida* with enhanced properties for biotechnological applications. Applications for such streamlined strains are further discussed at the end of the following **Chapter 3**.

References for Chapter 2

- 38 Calero, P. & Nikel, P. I. **Chasing Bacterial Chassis for Metabolic Engineering: A Perspective Review from Classical to Non-Traditional Microorganisms.** *Microbial Biotechnology* **12**, 98-124, doi: 10.1111/1751-7915.13292 (2019).
- 67 Beites, T. & Mendes, M. V. **Chassis Optimization as a Cornerstone for the Application of Synthetic Biology Based Strategies in Microbial Secondary Metabolism.** *Frontiers in Microbiology* **6**, 906, doi: 10.3389/fmicb.2015.00906 (2015).
- 68 Baritugo, K. A. G., Kim, H. T., David, Y. C., Choi, J. H., Choi, J. I., Kim, T. W., Park, C., Hong, S. H., Na, J. G., Jeong, K. J., Joo, J. C. & Park, S. J. **Recent Advances in Metabolic Engineering of *Corynebacterium glutamicum* as a Potential Platform Microorganism for Biorefinery.** *Biofuels Bioprod. Biorefining* **12**, 899-925, doi: 10.1002/bbb.1895 (2018).
- 69 Palazzotto, E., Tong, Y., Lee, S. Y. & Weber, T. **Synthetic Biology and Metabolic Engineering of Actinomycetes for Natural Product Discovery.** *Biotechnology Advances* **37**, 107366, doi: 10.1016/j.biotechadv.2019.03.005 (2019).
- 70 Gu, Y., Xu, X., Wu, Y., Niu, T., Liu, Y., Li, J., Du, G. & Liu, L. **Advances and Prospects of *Bacillus subtilis* Cellular Factories: From Rational Design to Industrial Applications.** *Metabolic Engineering* **50**, 109-121, doi: 10.1016/j.ymben.2018.05.006 (2018).
- 71 Yang, Z. & Zhang, Z. **Engineering Strategies for Enhanced Production of Protein and Bio-Products in *Pichia Pastoris*: A Review.** *Biotechnology Advances* **36**, 182-195, doi: 10.1016/j.biotechadv.2017.11.002 (2018).
- 72 Peña, D. A., Gasser, B., Zanghellini, J., Steiger, M. G. & Mattanovich, D. **Metabolic Engineering of *Pichia Pastoris*.** *Metabolic Engineering* **50**, 2-15, doi: 10.1016/j.ymben.2018.04.017 (2018).
- 73 Nikel, P. I. & de Lorenzo, V. ***Pseudomonas putida* as a Functional Chassis for Industrial Biocatalysis: From Native Biochemistry to Trans-Metabolism.** *Metabolic Engineering* **50**, 142-155, doi: 10.1016/j.ymben.2018.05.005 (2018).
- 74 Danchin, A. **Scaling up Synthetic Biology: Do Not Forget the Chassis.** *FEBS Letters* **586**, 2129-2137, doi: 10.1016/j.febslet.2011.12.024 (2012).

- 75 Kim, J., Salvador, M., Saunders, E., González, J., Avignone-Rossa, C. & Jiménez, J. I. **Properties of Alternative Microbial Hosts Used in Synthetic Biology: Towards the Design of a Modular Chassis.** *Essays in Biochemistry* **60**, 303-313, doi: 10.1042/EBC20160015 (2016).
- 76 Abram, K. Z. & Udaondo, Z. **Towards a Better Metabolic Engineering Reference: The Microbial Chassis.** *Microbial Biotechnology* **13**, 17-18, doi: 10.1111/1751-7915.13363 (2019).
- 77 Timmis, K. N. ***Pseudomonas putida*: A Cosmopolitan Opportunist Par Excellence.** *Environmental Microbiology* **4**, 779-781, doi: 10.1046/j.1462-2920.2002.00365.x (2002).
- 78 Palleroni, N. J. **The *Pseudomonas* Story.** *Environmental Microbiology* **12**, 1377-1383, doi: 10.1111/j.1462-2920.2009.02041.x (2010).
- 79 Palleroni, N. J., Kunisawa, R., Contopoulou, R. & Doudoroff, M. **Nucleic Acid Homologies in the Genus *Pseudomonas*.** *International Journal of Systematic and Evolutionary Microbiology* **23**, 333-339, doi: 10.1099/00207713-23-4-333 (1973).
- 80 Poblete-Castro, I., Borrero de Acuña, J. M., Nickel, P. I., Kohlstedt, M. & Wittmann, C. **Host Organism: *Pseudomonas putida*.** in *Industrial Biotechnology: Microorganisms* (eds C. Wittmann & J. C. Liao) 299-326 (Wiley-VCH Verlag GmbH & Co. KGaA, 2017).
- 81 Volke, D. C. & Nickel, P. I. **Getting Bacteria in Shape: Synthetic Morphology Approaches for the Design of Efficient Microbial Cell Factories.** *Advanced Biosystems* **2**, 1800111, doi: 10.1002/adbi.201800111 (2018).
- 82 Benedetti, I., de Lorenzo, V. & Nickel, P. I. **Genetic Programming of Catalytic *Pseudomonas putida* Biofilms for Boosting Biodegradation of Haloalkanes.** *Metabolic Engineering* **33**, 109-118, doi: 10.1016/j.ymben.2015.11.004 (2016).
- 83 Moore, E. R. B., Tindall, B. J., Martins dos Santos, V. A. P., Pieper, D. H., Ramos, J. L. & Palleroni, N. J. **Nonmedical *Pseudomonas*.** in *The Prokaryotes—Volume 6: Proteobacteria · Gamma Subclass* (eds Martin Dworkin *et al.*) 646-703 (Springer New York, 2006).
- 84 Poblete-Castro, I., Becker, J., Dohnt, K., Martins dos Santos, V. A. P. & Wittmann, C. **Industrial Biotechnology of *Pseudomonas putida* and Related Species.** *Applied Microbiology and Biotechnology* **93**, 2279-2290, doi: 10.1007/s00253-012-3928-0 (2012).

- 85 Poblete-Castro, I., Wittmann, C. & Nikel, P. I. **Biochemistry, Genetics and Biotechnology of Glycerol Utilization in *Pseudomonas* Species.** *Microbial Biotechnology* **13**, 32-53, doi: 10.1111/1751-7915.13400 (2019).
- 86 Jiménez, J. I., Miñambres, B., García, J. L. & Díaz, E. **Genomic Analysis of the Aromatic Catabolic Pathways from *Pseudomonas putida* KT2440.** *Environmental Microbiology* **4**, 824-841, doi: 10.1046/j.1462-2920.2002.00370.x (2002).
- 87 Nakazawa, T. **Travels of a *Pseudomonas*, from Japan around the World.** *Environmental Microbiology* **4**, 782-786, doi: 10.1046/j.1462-2920.2002.00310.x (2002).
- 88 Segura, A., Molina, L., Fillet, S., Krell, T., Bernal, P., Muñoz-Rojas, J. & Ramos, J. L. **Solvent Tolerance in Gram-Negative Bacteria.** *Current Opinion in Biotechnology* **23**, 415-421, doi: 10.1016/j.copbio.2011.11.015 (2012).
- 89 Heipieper, H. J., Neumann, G., Cornelissen, S. & Meinhardt, F. **Solvent-Tolerant Bacteria for Biotransformations in Two-Phase Fermentation Systems.** *Applied Microbiology and Biotechnology* **74**, 961-973, doi: 10.1007/s00253-006-0833-4 (2007).
- 90 Simon, O., Klaiber, I., Huber, A. & Pfannstiel, J. **Comprehensive Proteome Analysis of the Response of *Pseudomonas putida* KT2440 to the Flavor Compound Vanillin.** *Journal of proteomics* **109**, 212-227, doi: 10.1016/j.jprot.2014.07.006 (2014).
- 91 Blank, L. M., Ionidis, G., Ebert, B. E., Bühler, B. & Schmid, A. **Metabolic Response of *Pseudomonas putida* During Redox Biocatalysis in the Presence of a Second Octanol Phase.** *FEBS J.* **275**, 5173-5190, doi: 10.1111/j.1742-4658.2008.06648.x (2008).
- 92 Beckham, G. T., Johnson, C. W., Karp, E. M., Salvachúa, D. & Vardon, D. R. **Opportunities and Challenges in Biological Lignin Valorization.** *Current Opinion in Biotechnology* **42**, 40-53, doi: 10.1016/j.copbio.2016.02.030 (2016).
- 93 Wang, Y., Horlamus, F., Henkel, M., Kovacic, F., Schläfle, S., Hausmann, R., Wittgens, A. & Rosenau, F. **Growth of Engineered *Pseudomonas putida* KT2440 on Glucose, Xylose, and Arabinose: Hemicellulose Hydrolysates and Their Major Sugars as Sustainable Carbon Sources.** *GCB Bioenergy* **11**, 249-259, doi: 10.1111/gcbb.12590 (2019).
- 94 Dvořák, P. & de Lorenzo, V. **Refactoring the Upper Sugar Metabolism of *Pseudomonas putida* for Co-Utilization of Cellobiose, Xylose, and Glucose.** *Metabolic Engineering* **48**, 94-108, doi: 10.1016/j.ymben.2018.05.019 (2018).

- 95 Marqués, S. & Ramos, J. L. **Transcriptional Control of the *Pseudomonas putida* TOL Plasmid Catabolic Pathways.** *Molecular Microbiology* **9**, 923-929, doi: 10.1111/j.1365-2958.1993.tb01222.x (1993).
- 96 Chua, J. W. & Hsieh, J. H. **Oxidative Bioconversion of Toluene to 1,3-Butadiene-1,4-Dicarboxylic Acid (*cis,cis*-Muconic Acid).** *World Journal of Microbiology and Biotechnology* **6**, 127-143, doi: 10.1007/BF01200932 (1990).
- 97 Vardon, D. R., Franden, M. A., Johnson, C. W., Karp, E. M., Guarnieri, M. T., Linger, J. G., Salm, M. J., Strathmann, T. J. & Beckham, G. T. **Adipic Acid Production from Lignin.** *Energy & Environmental Science* **8**, 617-628, doi: 10.1039/C4EE03230F (2015).
- 98 Johnson, C. W., Salvachúa, D., Khanna, P., Smith, H., Peterson, D. J. & Beckham, G. T. **Enhancing Muconic Acid Production from Glucose and Lignin-Derived Aromatic Compounds Via Increased Protocatechuate Decarboxylase Activity.** *Metabolic Engineering Communications* **3**, 111-119, doi: 10.1016/j.meteno.2016.04.002 (2016).
- 99 Kohlstedt, M., Starck, S., Barton, N., Stolzenberger, J., Selzer, M., Mehlmann, K., Schneider, R., Pleissner, D., Rinkel, J., Dickschat, J. S., Venus, J., van Duuren, J. N. J. H. & Wittmann, C. **From Lignin to Nylon: Cascaded Chemical and Biochemical Conversion Using Metabolically Engineered *Pseudomonas putida*.** *Metabolic Engineering* **47**, 279-293, doi: 10.1016/j.ymben.2018.03.003 (2018).
- 100 Linger, J. G., Vardon, D. R., Guarnieri, M. T., Karp, E. M., Hunsinger, G. B., Franden, M. A., Johnson, C. W., Chupka, G., Strathmann, T. J., Pienkos, P. T. & Beckham, G. T. **Lignin Valorization through Integrated Biological Funneling and Chemical Catalysis.** *Proceedings of the National Academy of Science USA* **111**, 12013, doi: 10.1073/pnas.1410657111 (2014).
- 101 Sudarsan, S., Dethlefsen, S., Blank, L. M., Siemann-Herzberg, M. & Schmid, A. **The Functional Structure of Central Carbon Metabolism in *Pseudomonas putida* KT2440.** *Appl. Environmental Microbiology* **80**, 5292-5303, doi: 10.1128/AEM.01643-14 (2014).
- 102 Chavarría, M., Goñi-Moreno, A., de Lorenzo, V. & Nikel, P. I. **A Metabolic Widget Adjusts the Phosphoenolpyruvate-Dependent Fructose Influx in *Pseudomonas putida*.** *mSystems* **1**, e00154-00116, doi: 10.1128/mSystems.00154-16 (2016).

- 103 Flamholz, A., Noor, E., Bar-Even, A., Liebermeister, W. & Milo, R. **Glycolytic Strategy as a Tradeoff between Energy Yield and Protein Cost.** *Proceedings of the National Academy of Science USA* **110**, 10039-10044, doi: 10.1073/pnas.1215283110 (2013).
- 104 Conway, T. **The Entner-Doudoroff Pathway: History, Physiology and Molecular Biology.** *FEMS Microbiology Reviews* **9**, 1-27, doi: 10.1111/j.1574-6968.1992.tb05822.x (1992).
- 105 Nickel, P. I., Chavarría, M., Fuhrer, T., Sauer, U. & de Lorenzo, V. ***Pseudomonas putida* KT2440 Strain Metabolizes Glucose through a Cycle Formed by Enzymes of the Entner-Doudoroff, Embden-Meyerhof-Parnas, and Pentose Phosphate Pathways.** *Journal of Biological Chemistry* **290**, 25920-25932, doi: 10.1074/jbc.M115.687749 (2015).
- 106 Molina, L., La Rosa, R., Nogales, J. & Rojo, F. **Influence of the Crc Global Regulator on Substrate Uptake Rates and the Distribution of Metabolic Fluxes in *Pseudomonas putida* KT2440 Growing in a Complete Medium.** *Environmental Microbiology* **21**, 4446-4459, doi: 10.1111/1462-2920.14812 (2019).
- 107 Rojo, F. **Carbon Catabolite Repression in *Pseudomonas*: Optimizing Metabolic Versatility and Interactions with the Environment.** *FEMS Microbiology Reviews* **34**, 658-684, doi: 10.1111/j.1574-6976.2010.00218.x (2010).
- 108 Hester, K. L., Madhusudhan, K. T. & Sokatch, J. R. **Catabolite Repression Control by Crc in 2xYT Medium Is Mediated by Posttranscriptional Regulation of *Bkdr* Expression in *Pseudomonas putida*.** *Journal of Bacteriology* **182**, 1150-1153, doi: 10.1128/jb.182.4.1150-1153.2000 (2000).
- 109 Moreno, R., Ruiz-Manzano, A., Yuste, L. & Rojo, F. **The *Pseudomonas putida* Crc Global Regulator Is an RNA Binding Protein That Inhibits Translation of the Alks Transcriptional Regulator.** *Molecular Microbiology* **64**, 665-675, doi: 10.1111/j.1365-2958.2007.05685.x (2007).
- 110 Moreno, R. & Rojo, F. **The Target for the *Pseudomonas putida* Crc Global Regulator in the Benzoate Degradation Pathway Is the BenR Transcriptional Regulator.** *Journal of Bacteriology* **190**, 1539-1545, doi: 10.1128/JB.01604-07 (2008).
- 111 Putrins, M., Tover, A., Tegova, R., Saks, U. & Kivisaar, M. **Study of Factors Which Negatively Affect Expression of the Phenol Degradation Operon *Pheba* in *Pseudomonas putida*.** *Microbiology* **153**, 1860-1871, doi: 10.1099/mic.0.2006/003681-0 (2007).

- 112 Zimmermann, T., Sorg, T., Siehler, S. Y. & Gerischer, U. **Role of *Acinetobacter Baylyi* Crc in Catabolite Repression of Enzymes for Aromatic Compound Catabolism.** *Journal of Bacteriology* **191**, 2834-2842, doi: 10.1128/JB.00817-08 (2009).
- 113 Moreno, R., Hernández-Arranz, S., La Rosa, R., Yuste, L., Madhushani, A., Shingler, V. & Rojo, F. **The Crc and Hfq Proteins of *Pseudomonas putida* Cooperate in Catabolite Repression and Formation of Ribonucleic Acid Complexes with Specific Target Motifs.** *Environmental Microbiology* **17**, 105-118, doi: 10.1111/1462-2920.12499 (2015).
- 114 Sudarsan, S., Dethlefsen, S., Blank, L. M., Siemann-Herzberg, M. & Schmid, A. **The Functional Structure of Central Carbon Metabolism in *Pseudomonas putida* KT2440.** *Applied Environmental Microbiology* **80**, 5292-5303, doi: 10.1128/AEM.01643-14 (2014).
- 115 Moreno, R., Fonseca, P. & Rojo, F. **The Crc Global Regulator Inhibits the *Pseudomonas putida* pWW0 Toluene/Xylene Assimilation Pathway by Repressing the Translation of Regulatory and Structural Genes.** *Journal of Biological Chemistry* **285**, 24412-24419, doi: 10.1074/jbc.M110.126615 (2010).
- 116 Hernández-Arranz, S., Moreno, R. & Rojo, F. **The Translational Repressor Crc Controls the *Pseudomonas putida* Benzoate and Alkane Catabolic Pathways Using a Multi-Tier Regulation Strategy.** *Environmental Microbiology* **15**, 227-241, doi: 10.1111/j.1462-2920.2012.02863.x (2013).
- 117 Moreno, R., Fonseca, P. & Rojo, F. **Two Small RNAs, Crcy and Crcz, Act in Concert to Sequester the Crc Global Regulator in *Pseudomonas putida*, Modulating Catabolite Repression.** *Molecular Microbiology* **83**, 24-40, doi: 10.1111/j.1365-2958.2011.07912.x (2012).
- 118 Sonnleitner, E., Abdou, L. & Haas, D. **Small RNA as Global Regulator of Carbon Catabolite Repression in *Pseudomonas aeruginosa*.** *Proceedings of the National Academy of Science USA* **106**, 21866-21871, doi: 10.1073/pnas.pnas.0910308106 (2009).
- 119 Noor, E., Eden, E., Milo, R. & Alon, U. **Central Carbon Metabolism as a Minimal Biochemical Walk between Precursors for Biomass and Energy.** *Cell* **39**, 809-820, doi: 10.1016/j.molcel.2010.08.031 (2010).

- 120 Nelson, K. E., Weinel, C., Paulsen, I. T., Dodson, R. J., Hilbert, H., Martins dos Santos, V. A. P., Fouts, D. E., Gill, S. R., Pop, M., Holmes, M., Brinkac, L., Beanan, M., DeBoy, R. T., Daugherty, S., Kolonay, J. et al. **Complete Genome Sequence and Comparative Analysis of the Metabolically Versatile *Pseudomonas putida* KT2440.** *Environmental Microbiology* **4**, 799-808, doi: 10.1046/j.1462-2920.2002.00366.x (2002).
- 121 Belda, E., van Heck, R. G. A., López-Sánchez, M. J., Cruveiller, S., Barbe, V., Fraser, C., Klenk, H. P., Petersen, J., Morgat, A., Nikel, P. I., Vallenet, D., Rouy, Z., Sekowska, A., Martins dos Santos, V. A. P., de Lorenzo, V. et al. **The Revisited Genome of *Pseudomonas putida* KT2440 Enlightens Its Value as a Robust Metabolic Chassis.** *Environmental Microbiology* **18**, 3403-3424, doi: 10.1111/1462-2920.13230 (2016).
- 122 Nogales, J., Palsson, B. Ø. & Thiele, I. **A Genome-Scale Metabolic Reconstruction of *Pseudomonas putida* KT2440: iJN746 as a Cell Factory.** *BMC systems biology* **2**, 79, doi: 10.1186/1752-0509-2-79 (2008).
- 123 Puchałka, J., Oberhardt, M. A., Godinho, M., Bielecka, A., Regenhardt, D., Timmis, K. N., Papin, J. A. & Martins dos Santos, V. A. P. **Genome-Scale Reconstruction and Analysis of the *Pseudomonas putida* KT2440 Metabolic Network Facilitates Applications in Biotechnology.** *PLoS computational biology* **4**, e1000210, doi: 10.1371/journal.pcbi.1000210 (2008).
- 124 Sohn, S. B., Kim, T. Y., Park, J. M. & Lee, S. Y. **In Silico Genome-Scale Metabolic Analysis of *Pseudomonas putida* KT2440 for Polyhydroxyalkanoate Synthesis, Degradation of Aromatics and Anaerobic Survival.** *Biotechnology Journal* **5**, 739-750, doi: 10.1002/biot.201000124 (2010).
- 125 Oberhardt, M. A., Puchałka, J., Martins dos Santos, V. A. P. & Papin, J. A. **Reconciliation of Genome-Scale Metabolic Reconstructions for Comparative Systems Analysis.** *PLoS computational biology* **7**, e1001116, doi: 10.1371/journal.pcbi.1001116 (2011).
- 126 Martínez-García, E. & de Lorenzo, V. **Molecular Tools and Emerging Strategies for Deep Genetic/Genomic Refactoring of *Pseudomonas*.** *Current Opinion in Biotechnology* **47**, 120-132, doi: 10.1016/j.copbio.2017.06.013 (2017).
- 127 Gauttam, R., Mukhopadhyay, A. & Singer, S. W. **Construction of a Novel Dual-Inducible Duet-Expression System for Gene (over)Expression in *Pseudomonas putida*.** *Plasmid* **110**, 102514, doi: 10.1016/j.plasmid.2020.102514 (2020).

- 128 Martínez-García, E., Aparicio, T., Goñi-Moreno, A., Fraile, S. & de Lorenzo, V. **SEVA 2.0: An Update of the Standard European Vector Architecture for De-/Re-Construction of Bacterial Functionalities.** *Nucleic Acids Research* **43**, D1183-D1189, doi: 10.1093/nar/gku1114 (2014).
- 129 Silva-Rocha, R., Martínez-García, E., Calles, B., Chavarría, M., Arce-Rodríguez, A., de las Heras, A., Páez-Espino, A. D., Durante-Rodríguez, G., Kim, J., Nickel, P. I., Platero, R. & de Lorenzo, V. **The Standard European Vector Architecture (SEVA): A Coherent Platform for the Analysis and Deployment of Complex Prokaryotic Phenotypes.** *Nucleic Acids Research* **41**, D666-D675, doi: 10.1093/nar/gks1119 (2013).
- 130 Elmore, J. R., Furches, A., Wolff, G. N., Gorday, K. & Guss, A. M. **Development of a High Efficiency Integration System and Promoter Library for Rapid Modification of *Pseudomonas putida* KT2440.** *Metabolic Engineering Communications* **5**, 1-8, doi: 10.1016/j.meteno.2017.04.001 (2017).
- 131 Zobel, S., Benedetti, I., Eisenbach, L., de Lorenzo, V., Wierckx, N. & Blank, L. M. **Tn7-Based Device for Calibrated Heterologous Gene Expression in *Pseudomonas putida*.** *ACS Synthetic Biology* **4**, 1341-1351, doi: 10.1021/acssynbio.5b00058 (2015).
- 132 Mutalik, V. K., Guimaraes, J. C., Cambray, G., Lam, C., Christoffersen, M. J., Mai, Q. A., Tran, A. B., Paull, M., Keasling, J. D., Arkin, A. P. & Endy, D. **Precise and Reliable Gene Expression Via Standard Transcription and Translation Initiation Elements.** *Nature Methods* **10**, 354–360, doi: 10.1038/nmeth.2404 (2013).
- 133 Salis, H. M., Mirsky, E. A. & Voigt, C. A. **Automated Design of Synthetic Ribosome Binding Sites to Control Protein Expression.** *Nature Biotechnology* **27**, 946-950, doi: 10.1038/nbt.1568 (2009).
- 134 Espah Borujeni, A., Channarasappa, A. S. & Salis, H. M. **Translation Rate Is Controlled by Coupled Trade-Offs between Site Accessibility, Selective RNA Unfolding and Sliding at Upstream Standby Sites.** *Nucleic Acids Research* **42**, 2646-2659, doi: 10.1093/nar/gkt1139 (2013).
- 135 Espah Borujeni, A. & Salis, H. M. **Translation Initiation Is Controlled by RNA Folding Kinetics Via a Ribosome Drafting Mechanism.** *Journal of the American Chemical Society* **138**, 7016-7023, doi: 10.1021/jacs.6b01453 (2016).
- 136 Espah Borujeni, A., Cetnar, D., Farasat, I., Smith, A., Lundgren, N. & Salis, H. M. **Precise Quantification of Translation Inhibition by mRNA Structures That Overlap with the Ribosomal Footprint in N-Terminal Coding Sequences.** *Nucleic Acids Research* **45**, 5437-5448, doi: 10.1093/nar/gkx061 (2017).

- 137 Cetnar, D. P. & Salis, H. M. **Systematic Quantification of Sequence and Structural Determinants Controlling mRNA Stability in Bacterial Operons.** *BioRxiv*, 2020.2007.2022.216051, doi: 10.1101/2020.07.22.216051 (2020).
- 138 Reis, A. C. & Salis, H. M. **An Automated Model Test System for Systematic Development and Improvement of Gene Expression Models.** *ACS Synthetic Biology* **9**, 3145-3156, doi: 10.1021/acssynbio.0c00394 (2020).
- 139 Franden, M. A., Jayakody, L. N., Li, W.-J., Wagner, N. J., Cleveland, N. S., Michener, W. E., Hauer, B., Blank, L. M., Wierckx, N., Klebensberger, J. & Beckham, G. T. **Engineering *Pseudomonas putida* KT2440 for Efficient Ethylene Glycol Utilization.** *Metabolic Engineering* **48**, 197-207, doi: 10.1016/j.ymben.2018.06.003 (2018).
- 140 Meyers, A., Furtmann, C., Gesing, K., Tozakidis, I. E. P. & Jose, J. **Cell Density-Dependent Auto-Inducible Promoters for Expression of Recombinant Proteins in *Pseudomonas putida*.** *Microbial Biotechnology* **12**, 1003-1013, doi: 10.1111/1751-7915.13455 (2019).
- 141 Kushwaha, M. & Salis, H. M. **A Portable Expression Resource for Engineering Cross-Species Genetic Circuits and Pathways.** *Nature Communications* **6**, 7832, doi: 10.1038/ncomms8832 (2015).
- 142 Wang, H., Li, J. & Jewett, M. C. **Development of a *Pseudomonas putida* Cell-Free Protein Synthesis Platform for Rapid Screening of Gene Regulatory Elements.** *Synthetic Biology* **3**, ysy003, doi: 10.1093/synbio/ysy003 (2018).
- 143 Damalas, S. G., Batianis, C., Martin-Pascual, M., de Lorenzo, V. & Martins dos Santos, V. A. P. **SEVA 3.1: Enabling Interoperability of DNA Assembly among the SEVA, Biobricks and Type Iis Restriction Enzyme Standards.** *Microbial Biotechnology* **13**, 1793-1806, doi: 10.1111/1751-7915.13609 (2020).
- 144 Davy, A. M., Kildegaard, H. F. & Andersen, M. R. **Cell Factory Engineering.** *Cell systems* **4**, 262-275, doi: 10.1016/j.cels.2017.02.010 (2017).
- 145 Li, L., Liu, X., Wei, K., Lu, Y. & Jiang, W. **Synthetic Biology Approaches for Chromosomal Integration of Genes and Pathways in Industrial Microbial Systems.** *Biotechnology Advances* **37**, 730-745, doi: 10.1016/j.biotechadv.2019.04.002 (2019).
- 146 Rakowski, S. A. & Filutowicz, M. **Plasmid R6K Replication Control.** *Plasmid* **69**, 231-242, doi: 10.1016/j.plasmid.2013.02.003 (2013).

- 147 Hoang, T. T., Karkhoff-Schweizer, R. R., Kutchma, A. J. & Schweizer, H. P. **A Broad-Host-Range Flp-Frt Recombination System for Site-Specific Excision of Chromosomally-Located DNA Sequences: Application for Isolation of Unmarked *Pseudomonas aeruginosa* Mutants.** *Gene* **212**, 77-86, doi: 10.1016/s0378-1119(98)00130-9 (1998).
- 148 Ayres, E. K., Thomson, V. J., Merino, G., Balderes, D. & Figurski, D. H. **Precise Deletions in Large Bacterial Genomes by Vector-Mediated Excision (Vex)—the *TrfA* Gene of Promiscuous Plasmid RK2 Is Essential for Replication in Several Gram-Negative Hosts.** *Journal of Molecular Biology* **230**, 174-185, doi: 10.1006/jmbi.1993.1134 (1993).
- 149 Marx, C. J. & Lidstrom, M. E. **Broad-Host-Range Cre-Lox System for Antibiotic Marker Recycling in Gram-Negative Bacteria.** *BioTechniques* **33**, 1062-1067, doi: 10.2144/02335rr01 (2002).
- 150 Steinmetz, M., Le Coq, D., Djemia, H. B. & Gay, P. **Genetic Analysis of *SacB*, the Structural Gene of a Secreted Enzyme, Levansucrase of *Bacillus subtilis* Marburg.** *Molecular Genetics and Genomics* **191**, 138-144, doi: 10.1007/BF00330901 (1983).
- 151 Graf, N. & Altenbuchner, J. **Development of a Method for Markerless Gene Deletion in *Pseudomonas putida*.** *Applied Environmental Microbiology* **77**, 5549-5552, doi: 10.1128/AEM.05055-11 (2011).
- 152 Galvao, T. C. & de Lorenzo, V. **Adaptation of the Yeast Ura3 Selection System to Gram-Negative Bacteria and Generation of a $\Delta betCDE$ *Pseudomonas putida* Strain.** *Applied Environmental Microbiology* **71**, 883-892, doi: 10.1128/AEM.71.2.883-892.2005 (2005).
- 153 Martínez-García, E. & de Lorenzo, V. **Engineering Multiple Genomic Deletions in Gram-Negative Bacteria: Analysis of the Multi-Resistant Antibiotic Profile of *Pseudomonas putida* KT2440.** *Environmental Microbiology* **13**, 2702-2716, doi: 10.1111/j.1462-2920.2011.02538.x (2011).
- 154 Wirth, N. T., Kozaeva, E. & Nikel, P. I. **Accelerated Genome Engineering of *Pseudomonas putida* by I-SceI—Mediated Recombination and CRISPR-Cas9 Counterselection.** *Microbial Biotechnology* **13**, In press, DOI: 10.1111/1751-7915.13396, doi: 10.1111/1751-7915.13396 (2019).
- 155 Jinek, M., Chylinski, K., Fonfara, I., Hauer, M., Doudna, J. A. & Charpentier, E. **A Programmable Dual-RNA-Guided DNA Endonuclease in Adaptive Bacterial Immunity.** *Science (New York, N.Y.)* **337**, 816-821, doi: 10.1126/science.1225829 (2012).

- 156 Gasiunas, G., Barrangou, R., Horvath, P. & Siksnys, V. **Cas9-CrRNA Ribonucleoprotein Complex Mediates Specific DNA Cleavage for Adaptive Immunity in Bacteria.** *Proceedings of the National Academy of Science USA* **109**, E2579-2586, doi: 10.1073/pnas.1208507109 (2012).
- 157 Jakočiūnas, T., Jensen, M. K. & Keasling, J. D. **System-Level Perturbations of Cell Metabolism Using CRISPR/Cas9.** *Current Opinion in Biotechnology* **46**, 134-140, doi: 10.1016/j.copbio.2017.03.014 (2017).
- 158 Cook, T. B., Rand, J. M., Nurani, W., Courtney, D. K., Liu, S. A. & Pflieger, B. F. **Genetic Tools for Reliable Gene Expression and Recombineering in *Pseudomonas putida*.** *Journal of Industrial Microbiology and Biotechnology* **45**, 1-11, doi: 10.1007/s10295-017-2001-5 (2018).
- 159 Choi, K. R., Cho, J. S., Cho, I. J., Park, D. & Lee, S. Y. **Markerless Gene Knockout and Integration to Express Heterologous Biosynthetic Gene Clusters in *Pseudomonas putida*.** *Metabolic Engineering* **47**, 463-474, doi: 10.1016/j.ymben.2018.05.003 (2018).
- 160 Aparicio, T., de Lorenzo, V. & Martínez-García, E. **CRISPR/Cas9-Based Counterselection Boosts Recombineering Efficiency in *Pseudomonas putida*.** *Biotechnology Journal* **13**, 1700161, doi: 10.1002/biot.201700161 (2018).
- 161 Murphy, K. C. **Recombination and Recombineering.** in *Ecosal Plus · Domain 7: Genetics and Genetic Tools* (ed J. M. Slauch) DOI: 10.1128/ecosalplus.ESP-0011-2015 (ASM Press, 2016).
- 162 Ellis, H. M., Yu, D., DiTizio, T. & Court, D. L. **High Efficiency Mutagenesis, Repair, and Engineering of Chromosomal DNA Using Single-Stranded Oligonucleotides.** *Proceedings of the National Academy of Science USA* **98**, 6742-6746, doi: 10.1073/pnas.121164898 (2001).
- 163 Ronda, C., Pedersen, L. E., Sommer, M. O. A. & Nielsen, A. T. **CRMAGE: CRISPR Optimized MAGE Recombineering.** *Scientific Reports* **6**, 19452, doi: 10.1038/srep19452 (2016).
- 164 Lesic, B. & Rahme, L. G. **Use of the Λ Red Recombinase System to Rapidly Generate Mutants in *Pseudomonas aeruginosa*.** *BMC molecular biology* **9**, 20, doi: 10.1186/1471-2199-9-20 (2008).
- 165 Liang, R. & Liu, J. **Scarless and Sequential Gene Modification in *Pseudomonas* Using PCR Product Flanked by Short Homology Regions.** *BMC microbiology* **10**, 209, doi: 10.1186/1471-2180-10-209 (2010).

- 166 Luo, X., Yang, Y., Ling, W., Zhuang, H., Li, Q. & Shang, G. ***Pseudomonas putida* KT2440 Markerless Gene Deletion Using a Combination of Lambda Red Recombineering and Cre/LoxP Site-Specific Recombination.** *FEMS Microbiology Letters* **363**, doi: 10.1093/femsle/fnw014 (2016).
- 167 Yin, J., Zheng, W., Gao, Y., Jiang, C., Shi, H., Diao, X., Li, S., Chen, H., Wang, H., Li, R., Li, A., Xia, L., Yin, Y., Stewart, A. F., Zhang, Y. et al. **Single-Stranded DNA-Binding Protein and Exogenous RecBCD Inhibitors Enhance Phage-Derived Homologous Recombination in *Pseudomonas*.** *iScience* **14**, 1-14, doi: 10.1016/j.isci.2019.03.007 (2019).
- 168 Swingle, B., Bao, Z., Markel, E., Chambers, A. & Cartinhour, S. **Recombineering Using Recte from *Pseudomonas syringae*.** *Applied Environmental Microbiology* **76**, 4960-4968, doi: 10.1128/AEM.00911-10 (2010).
- 169 Ricaurte, D. E., Martínez-García, E., Nyerges, A., Pal, C., de Lorenzo, V. & Aparicio, T. **A Standardized Workflow for Surveying Recombinases Expands Bacterial Genome-Editing Capabilities.** *Microbial Biotechnology* **11**, 176-188, doi: 10.1111/1751-7915.12846 (2018).
- 170 Aparicio, T., Jensen, S. I., Nielsen, A. T., de Lorenzo, V. & Martínez-García, E. **The Ssr Protein (T1E_1405) from *Pseudomonas putida* Dot-T1E Enables Oligonucleotide-Based Recombineering in Platform Strain *P. putida* EM42.** *Biotechnology Journal* **11**, 1309-1319, doi: 10.1002/biot.201600317 (2016).
- 171 Aparicio, T., Nyerges, A., Nagy, I., Pal, C., Martínez-García, E. & de Lorenzo, V. **Mismatch Repair Hierarchy of *Pseudomonas putida* Revealed by Mutagenic ssDNA Recombineering of the *pyrf* Gene.** *Environmental Microbiology* **22**, 45-58, doi: 10.1111/1462-2920.14814 (2020).
- 172 Aparicio, T., Nyerges, A., Martínez-García, E. & de Lorenzo, V. **High-Efficiency Multi-Site Genomic Editing (HEMSE) of *Pseudomonas putida* through Thermoinducible SsDNA Recombineering.** *BioRxiv*, 851576, doi: 10.1101/851576 (2019).
- 173 Matson, S. W. & Robertson, A. B. **The UvrD Helicase and Its Modulation by the Mismatch Repair Protein MutI.** *Nucleic Acids Research* **34**, 4089-4097, doi: 10.1093/nar/gkl450 (2006).
- 174 Aparicio, T., Nyerges, A., Nagy, I., Pal, C., Martinez-Garcia, E. & de Lorenzo, V. **Mismatch Repair Hierarchy of *Pseudomonas putida* Revealed by Mutagenic ssDNA Recombineering of the *pyrF* Gene.** *Environmental Microbiology* **22**, 45-58, doi: 10.1111/1462-2920.14814 (2020).

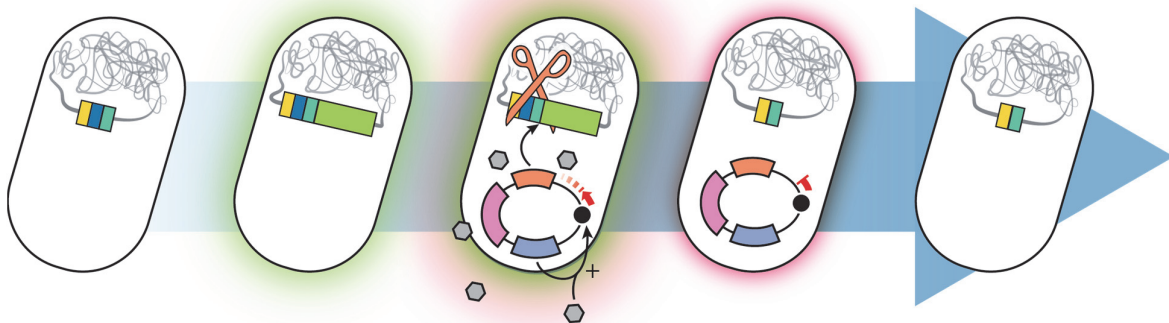
- 175 Aronshtam, A. & Marinus, M. G. **Dominant Negative Mutator Mutations in the *MutI* Gene of *Escherichia coli*.** *Nucleic Acids Research* **24**, 2498-2504, doi: 10.1093/nar/24.13.2498 (1996).
- 176 Komor, A. C., Kim, Y. B., Packer, M. S., Zuris, J. A. & Liu, D. R. **Programmable Editing of a Target Base in Genomic DNA without Double-Stranded DNA Cleavage.** *Nature* **533**, 420-424, doi: 10.1038/nature17946 (2016).
- 177 Gaudelli, N. M., Komor, A. C., Rees, H. A., Packer, M. S., Badran, A. H., Bryson, D. I. & Liu, D. R. **Programmable Base Editing of a •T to G•C in Genomic DNA without DNA Cleavage.** *Nature* **551**, 464-471, doi: 10.1038/nature24644 (2017).
- 178 Yang, B., Yang, L. & Chen, J. **Development and Application of Base Editors.** *CRISPR Journal* **2**, 91-104, doi: 10.1089/crispr.2019.0001 (2019).
- 179 Sun, J., Lu, L.-B., Liang, T.-X., Yang, L.-R. & Wu, J.-P. **CRISPR-Assisted Multiplex Base Editing System in *Pseudomonas putida* KT2440.** *Frontiers in Bioengineering and Biotechnology* **8**, 905, doi: 10.3389/fbioe.2020.00905 (2020).

Chapter 3: Accelerated genome engineering of *Pseudomonas putida* by I-SceI-mediated recombination, CRISPR/Cas9 counterselection, and self-curing plasmids

This chapter is composed of material from the following publications:

1. In Wirth et al. (2019)¹⁵⁴, the genome engineering strategy for I-SceI-mediated counterselection of chromosomally integrated suicide plasmids was refined. The method's scope was extended by implementing additional antibiotic resistance determinants, and the engineering process was streamlined by introducing a green-fluorescent reporter gene into the integrative vectors. Lastly, a molecular tool for CRISPR/Cas9 counterselection in *P. putida* was developed.
2. In Volke et al. (2020)¹⁸⁰, a system for the easy target- and self-curing of plasmids was established. The replication of plasmids carrying the *SCEI* gene was made strictly dependent on the presence of the chemical inducer 3-methylbenzoate (3-*mBz*). By using these plasmids for the genome engineering strategy proposed in publication 1, the curing of auxiliary plasmids after implementing chromosomal modifications could be highly accelerated.
3. The contents of Volke et al. (2021)¹⁸¹ constitute an update to the previously established step-by-step protocol¹⁵⁴ for genome engineering in *P. putida*, combining the toolsets developed in publications 1 and 2.

Graphical abstract



3.1. Summary

Pseudomonas species have become reliable platforms for bioproduction due to their capability to tolerate harsh conditions imposed by large-scale bioprocesses and their remarkable resistance to diverse physicochemical stresses. The last few years have brought forth a variety of synthetic biology tools for the genetic manipulation of pseudomonads, but many of them are either applicable only to obtain certain types of mutations, lack efficiency, or are not easily accessible to be used in different *Pseudomonas* species (e.g., natural isolates).

This chapter describes a versatile, robust, and user-friendly procedure that facilitates any genomic manipulation in *Pseudomonas* species within three to five days. The protocol presented here is based on DNA recombination forced by double-stranded DNA cuts (through the activity of the I-SceI homing meganuclease from yeast) followed by efficient counterselection of mutants (aided by a synthetic CRISPR/Cas9 device). The individual parts of the genome engineering toolbox, tailored for knocking genes in and out, have been standardized to enable portability and easy exchange of functional gene modules as needed. The method was complemented by a newly developed system for conditional, user-controlled plasmid replication that enables the reliable and rapid curing of auxiliary plasmids.

The applicability of the procedure is illustrated both by eliminating selected genomic regions in the platform strain *P. putida* KT2440 (including difficult-to-delete genes) and by integrating different reporter genes (comprising novel variants of fluorescent proteins) into a defined landing site in the target chromosome. At the end of the chapter, perspectives and applications of high-throughput genome editing methods in *P. putida* are discussed.

3.2. Introduction

Supported by the advances in synthetic biology and metabolic engineering made in the last few years, several microbes have emerged from a rather shadowy existence to become suitable biotechnological platforms³⁸. Several members of the genus *Pseudomonas*, for instance, are being adopted by a steadily increasing number of laboratories worldwide as *chassis* for both fundamental and applied studies^{73,182}. *Pseudomonas* species, usually found in natural environments, distinguish themselves from other microorganisms by an unrivaled wealth of biochemical functions that are embedded in robust and flexible metabolisms⁸⁰—allowing bacteria to adapt to a diverse range of stressful conditions¹⁸³. A rich set of synthetic biology tools has been developed to untap the metabolic potential of key representatives of the genus, e.g., *P. putida*, *P. taiwanensis*, and *P. fluorescens*^{126,184-186}. Furthermore, considerable efforts in the scientific *Pseudomonas* community have led to the development of tools to construct clean deletion mutants (**Section 2.2.1**). Among all these efforts, the standardized genome engineering method developed by Martínez-García and de Lorenzo¹⁸⁷, based on the chromosomal integration of a suicide plasmid followed by the action of the homing nuclease I-SceI from *Saccharomyces cerevisiae*, excels for its efficiency and robustness to mediate any kind of genetic modification (e.g., large deletions, point mutations, and allelic exchanges)—and is thus amongst the most intensively used by the scientific *Pseudomonas* community.

The system relies on the plasmid pEMG (**Table 3.1**); this vector contains the conditional origin of replication R6K, which requires the cognate Rep protein π encoded by *pir* for replication. In bacterial strains that lack *pir*, vector pEMG behaves as a suicide plasmid. The vector contains a polylinker region (multiple cloning site) flanked by two I-SceI recognition sites cloned into the *lacZ* α fragment, thus allowing for blue-white screening in *E. coli* cells carrying the *lacZ* Δ M15 mutation. A set of auxiliary SEVA plasmids harbors the gene encoding I-SceI under the control of the 3-methylbenzoate (3-*mBz*)-inducible XylS/*Pm* expression system from strain mt-2¹⁸⁷.

Here, we present a smooth and quick workflow for genome editing of *P. putida* based on the action of I-SceI or CRISPR/Cas9 as a counterselection strategy. The integration

of genes encoding fluorescent proteins (in addition to antibiotic resistance determinants) into the target locus circumvents experimental steps that would be necessary to ensure the presence of the suicide vector. Furthermore, we propose the adoption of the *USER* assembly method¹⁸⁸⁻¹⁹¹ to enable the quick and highly accurate assembling of homology arms (HAs) required for the genome engineering protocol. A new set of helper plasmids for providing *I-SceI* in trans was designed. To avoid the addition of chemical inducers during the genome engineering process, one set of auxiliary plasmids contains *SCEI* under constitutive transcriptional regulation. A second set of helper plasmids was engineered to be conditionally replicated only in the presence of the inducer compound 3-methylbenzoate (*3-mBz*)¹⁹², allowing for the quick curing of the plasmids.

The resulting streamlined protocol enables the introduction of virtually any genomic modification in *P. putida* within 5 days (for a single genetic manipulation including the construction of all necessary plasmids) down to 3 days (time required for each mutagenesis round once the relevant plasmids have been constructed). The subsequent curing of auxiliary plasmids was reduced from several days of continuous culturing down to one day. We demonstrate the potential of the technique by deleting both non-essential and difficult-to-knock-out metabolic genes in the platform strain KT2440. We furthermore show the integration of genes encoding different fluorescent proteins into a suitable landing pad in the *P. putida* chromosome and discuss their application as insertional reporters. The chapter concludes with a discussion of previous approaches towards streamlined, genome-reduced *P. putida* strains and prospects for their application as biotechnological *chassis*.

Table 3.1. Plasmids used in this chapter.

Name^a	Relevant features^b	Source or reference
pEMG	Suicide vector used for deletions in Gram-negative bacteria; <i>oriT</i> , <i>traJ</i> , <i>lacZα</i> , <i>ori</i> (R6K); Km ^R	Martinez-García and de Lorenzo ¹⁸⁷
pRK600	Helper plasmid used for conjugation; <i>oriV</i> (ColE1), <i>mob</i> (RK2), <i>tra</i> (RK2); Cm ^R	Kessler et al. ¹⁹³
pGNW2	Derivative of vector pEMG carrying P _{14g} → <i>msfGFP</i>	Wirth et al. ¹⁵⁴
pGNW4	Derivative of vector pGNW2; Sm ^R	Wirth et al. ¹⁵⁴
pGNW5	Derivative of vector pGNW2; Tc ^R	
pGNW6	Derivative of vector pGNW2; Gm ^R	Wirth et al. ¹⁵⁴
pSNW2	Derivative of vector pGNW carrying P _{14g} (<i>BCD2</i>)→ <i>msfGFP</i>	Volke et al. ¹⁸⁰
pSNW4	Derivative of vector pGNW2; Sm ^R	Volke et al. ¹⁸⁰
pSNW5	Derivative of vector pGNW2; Tc ^R	Volke et al. ¹⁸⁰
pSNW6	Derivative of vector pGNW2; Gm ^R	Volke et al. ¹⁸⁰
pSNW2·Δ <i>benABCD</i>	Derivative of vector pSNW2 carrying HAs to delete <i>benABCD</i> (<i>PP_3161-PP_3164</i>)	Volke et al. ¹⁸⁰
pGNW2·Δ <i>nicX</i>	Derivative of vector pGNW2 carrying HAs to delete <i>nicX</i> (<i>PP_3945</i>) in <i>P. putida</i> KT2440	Wirth et al. ¹⁵⁴
pGNW4·Δ <i>nicX</i>	Derivative of vector pGNW4 carrying HAs to delete <i>nicX</i> (<i>PP_3945</i>) in <i>P. putida</i> KT2440	Wirth et al. ¹⁵⁴
pGNW6·Δ <i>nicX</i>	Derivative of vector pGNW6 carrying HAs to delete <i>nicX</i> (<i>PP_3945</i>) in <i>P. putida</i> KT2440	Wirth et al. ¹⁵⁴
pGNW2·Δ <i>aceEF</i>	Derivative of vector pGNW2 carrying HAs to delete <i>aceEF</i> (<i>PP_0338-PP_0339</i>) in <i>P. putida</i> KT2440	Wirth et al. ¹⁵⁴
pSEVA2313	Expression vector; <i>oriV</i> (pBBR1), P _{EM7} ; Km ^R	Wirth et al. ¹⁵⁴
pS2313-R	Derivative of vector pSEVA2313 carrying P _{EM7} → <i>mRFP1</i> ¹⁹⁴	Wirth et al. ¹⁵⁴
pS2313-B	Derivative of vector pSEVA2313 carrying P _{EM7} → <i>bfp2</i> ¹⁹⁵	Wirth et al. ¹⁵⁴
pS2313-O	Derivative of vector pSEVA2313 carrying P _{EM7} → <i>mOrange2</i> ¹⁹⁶	Wirth et al. ¹⁵⁴
pS2313-T	Derivative of vector pSEVA2313 carrying P _{EM7} → <i>mTurquoise2</i> ¹⁹⁷	Wirth et al. ¹⁵⁴
pGNW2-LP::P _{EM7} - <i>mRFP1</i>	Derivative of vector pGNW2 carrying P _{EM7} → <i>mRFP1</i>	Wirth et al. ¹⁵⁴
pGNW2-LPR	Derivative of vector pGNW2 carrying HAs to insert P _{14g} (<i>BCD2</i>)→ <i>mRFP1</i> into a landing pad in the chromosome of <i>P. putida</i> KT2440	Wirth et al. ¹⁵⁴
pGNW2-LPG	Derivative of vector pGNW2 carrying HAs to insert P _{14g} (<i>BCD2</i>)→ <i>msfGFP</i> into a landing pad in the chromosome of <i>P. putida</i> KT2440	Wirth et al. ¹⁵⁴
pGNW2-LPB	Derivative of vector pGNW2 carrying HAs to insert P _{14g} (<i>BCD2</i>)→ <i>bfp2</i> into a landing pad in the chromosome of <i>P. putida</i> KT2440	Wirth et al. ¹⁵⁴
pGNW4-LPO	Derivative of vector pGNW4 carrying HAs to insert P _{14g} (<i>BCD2</i>)→ <i>mOrange2</i> into a landing pad in the chromosome of <i>P. putida</i> KT2440	Wirth et al. ¹⁵⁴
pGNW6-LPT	Derivative of vector pGNW6 carrying HAs to insert P _{14g} (<i>BCD2</i>)→ <i>mTurquoise2</i> into a landing pad in the chromosome of <i>P. putida</i> KT2440	Wirth et al. ¹⁵⁴
pSEVA128S	Helper plasmid; <i>oriV</i> (RK2), <i>xyIS</i> , <i>Pm</i> → <i>I-SceI</i> ; Amp ^R	Silva-Rocha et al. ¹²⁹
pSEVA228S	Helper plasmid; <i>oriV</i> (RK2), <i>xyIS</i> , <i>Pm</i> → <i>I-SceI</i> ; Km ^R	Silva-Rocha et al. ¹²⁹
pSEVA428S	Helper plasmid; <i>oriV</i> (RK2), <i>xyIS</i> , <i>Pm</i> → <i>I-SceI</i> ; Sm ^R	Silva-Rocha et al. ¹²⁹
pSEVA628S	Helper plasmid; <i>oriV</i> (RK2), <i>xyIS</i> , <i>Pm</i> → <i>I-SceI</i> ; Gm ^R	Silva-Rocha et al. ¹²⁹

pSEVA1213S	Helper plasmid; <i>oriV</i> (RK2), $P_{EM7} \rightarrow I-SceI$; Amp ^R	Wirth et al. ¹⁵⁴
pSEVA6213S	Helper plasmid; <i>oriV</i> (RK2), $P_{EM7} \rightarrow I-SceI$; Gm ^R	Wirth et al. ¹⁵⁴
pSEVA448	Cloning vector; <i>oriV</i> (pRO1600/ColE1), <i>xylS</i> , <i>Pm</i> ; Sm ^R	Silva-Rocha et al. ¹²⁹
pSEVA421-Cas9tr	Cloning vector; <i>oriV</i> (RK2), <i>cas9</i> , <i>tracrRNA</i> ; Sm ^R	Aparicio et al. ¹⁹⁸
pS448-CsR	Derivative of vector pSEVA448 used for CRISPR/Cas9 counterselection; <i>xylS</i> (cured of <i>BsaI</i> -sites), $Pm \rightarrow cas9$, $P_{EM7} \rightarrow sgRNA$; Sm ^R	Wirth et al. ¹⁵⁴
pS448-CsR_aceEF	Derivative of vector pS448-CsR carrying $P_{EM7} \rightarrow aceF$ -specific <i>sgRNA</i> ; Sm ^R	Wirth et al. ¹⁵⁴
pJBSD1	Conditionally-replicating vector; <i>oriV</i> (RK2), $XylS/Pm \rightarrow trfA$; Amp ^R	Karunakaran et al. ¹⁹²
pQURE1-H	Conditionally-replicating vector; derivative of plasmid pJBSD1 carrying $XylS/Pm \rightarrow I-SceI$ and $P_{14g}(BCD2) \rightarrow mRFP$; Amp ^R	Volke et al. ¹⁸⁰
pQURE2-H	Conditionally-replicating vector; derivative of plasmid pJBSD1 carrying $XylS/Pm \rightarrow I-SceI$ and $P_{14g}(BCD2) \rightarrow mRFP$; Km ^R	Volke et al. ¹⁸⁰
pQURE6-L	Conditionally-replicating vector; derivative of plasmid pJBSD1 carrying $XylS/Pm \rightarrow I-SceI$ and $P_{14g} \rightarrow mCherry$; Gm ^R	Volke et al. ¹⁸⁰
pQURE6-M	Conditionally-replicating vector; derivative of plasmid pJBSD1 carrying $XylS/Pm \rightarrow I-SceI$ and $P_{14g} \rightarrow mRFP$; Gm ^R	Volke et al. ¹⁸⁰
pQURE6-H	Conditionally-replicating vector; derivative of plasmid pJBSD1 carrying $XylS/Pm \rightarrow I-SceI$ and $P_{14g}(BCD2) \rightarrow mRFP$; Gm ^R	Volke et al. ¹⁸⁰

-
- a. Plasmids can be obtained from Addgene (www.addgene.org) with the following deposit numbers: pGNW2 (122086), pGNW4 (122088), pGNW6 (122093), pSEVA1213S (122095), pSEVA6213S (122094), and pS448-CsR (122096).
- b. Antibiotic markers: *Amp*, ampicillin; *Cm*, chloramphenicol; *Km*, kanamycin; *Sm*, streptomycin; *Tc*, tetracycline; and *Gm*, gentamicin. HAs, homology arms.

3.3. Technical implementation

The genome-editing procedure begins with the construction of donor DNA that is cloned into the suicide vectors pGNW¹⁵⁴ or pSNW^{180,181} (Figure 3.2). Such donor DNA containing suitable HAs serves as the template for the endogenous homologous DNA recombination machinery. The procedure also includes the cloning of a target-specific synthetic guide RNA (sgRNA) into a dedicated CRISPR/Cas9 plasmid (when applicable), the integration of the donor DNA into the *Pseudomonas* chromosome, and the specific cleavage of chromosomal DNA by endonucleases (i.e., I-SceI or Cas9) for the resolution of co-integrates. The specific steps of the procedure are detailed in the sections below.

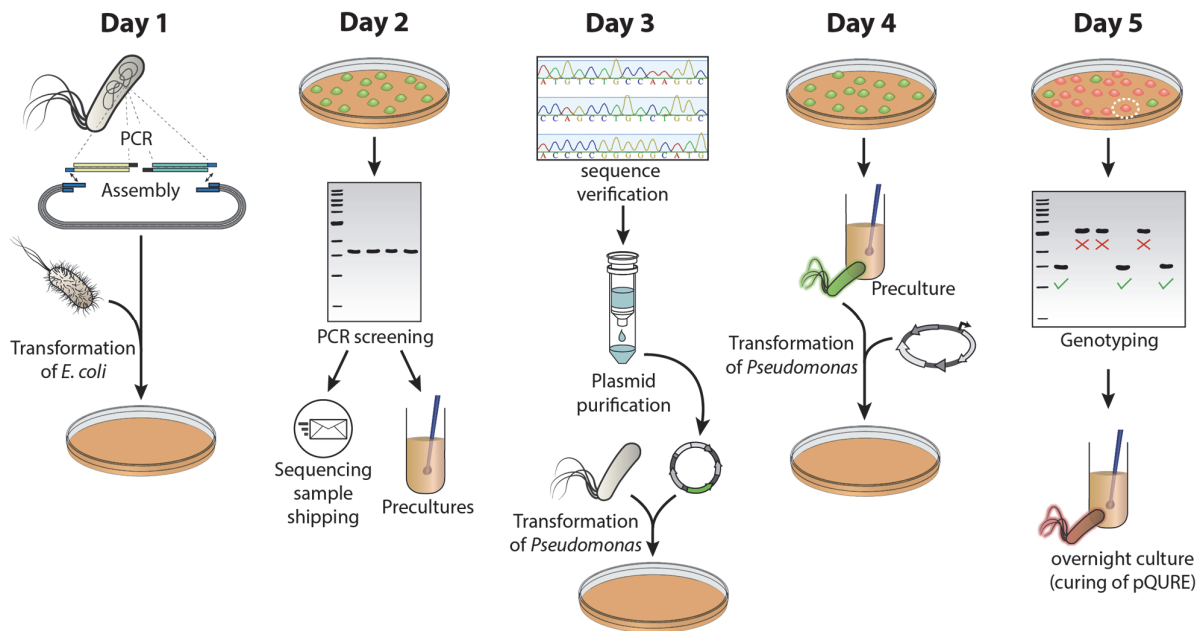


Figure 3.1. Overview of the genome engineering procedure in *Pseudomonas*. On the delivery date of the designed oligonucleotides, homology arms are amplified from the *Pseudomonas* genome and assembled into a suicide vector (pSNW). The resulting plasmid is then delivered into *E. coli* DH5 α *lpir* cells via chemical transformation. Furthermore (optional), a synthetic spacer, completing a synthetic guide RNA (sgRNA), is separately prepared and cloned into the CRISPR/Cas9 vector pS448-CsR. On day 2, *E. coli* transformants are screened for the correct pSNW insert size (and spacer insertion in vector pS448-CsR, if applicable) via colony PCR. The resulting amplicons are sent for sequencing, and the corresponding *E. coli* clones are used to inoculate liquid cultures. Day 3 includes the verification of sequence integrity of the insert in the pSNW vector, the purification of plasmids, and their delivery into *Pseudomonas* via either electroporation or tri-parental mating. The resulting co-integrants are enriched in liquid LB cultures over the course of day 4 and transformed with either an I-SceI—bearing plasmid or plasmid pS448-CsR carrying an appropriate sgRNA. Finally, *Pseudomonas* colonies without (or red, if pQURE^{180,181} was used) fluorescence are tested on day 5 for their genotype via colony PCR. Curing of the auxiliary plasmid pQURE can be performed overnight via outgrowing the cells without 3-methylbenzoate that is required for plasmid propagation.

3.3.1 Design and construction of plasmids

A. Construction of the suicide vector for genetic manipulations

We equipped plasmid pEMG¹⁰⁸ with the gene encoding the monomeric superfolder GFP (msfGFP¹⁹⁹) in the backbone while screening different combinations of promoters and translation initiation sequences (*TISs*) that would give a high fluorescence output when the plasmid is integrated into the target chromosome. The fusion of the strong, constitutive P_{14g} promoter and a variation of the *TIS* preceding *msfGFP*²⁰⁰ allowed for the direct visualization of *Pseudomonas* colonies harboring a single (chromosomal) copy of the novel vector pGNW2 (**Table 3.1**) by inspecting the plates on a blue-light transilluminator. A set of pGNW vectors was constructed by exchanging the kanamycin resistance (Km^R) determinant present in vector pGNW2 by the corresponding SEVA-based^{128,129,201} genes encoding streptomycin (Sm^R), tetracycline (Tc^R), and gentamicin (Gm^R) and resistances, giving rise to vectors pGNW4, pGNW5, and pGNW6, respectively (**Table 3.1**). During the repeated use of this system, we observed a high locus-dependency of msfGFP fluorescence intensity when pGNW was integrated at different chromosomal positions (**Figure 3.S1**). To make the identification of co-integrant cells more reliable, the standard SEVA *TIS* initiating *msfGFP* translation on pGNW was replaced by the bi-cistronic translational coupling sequence *BCD2*¹³². Cells harboring the resulting vectors pSNW2, pSNW4, pSNW5, or pSNW6 demonstrated consistently high fluorescence (**Figure 3.S1** and **Figure 3.S2**). In the following step-by-step protocol, we refer to the set of suicide vectors as pSNW. However, the same procedure is applicable for all created variants.

Construction of plasmids

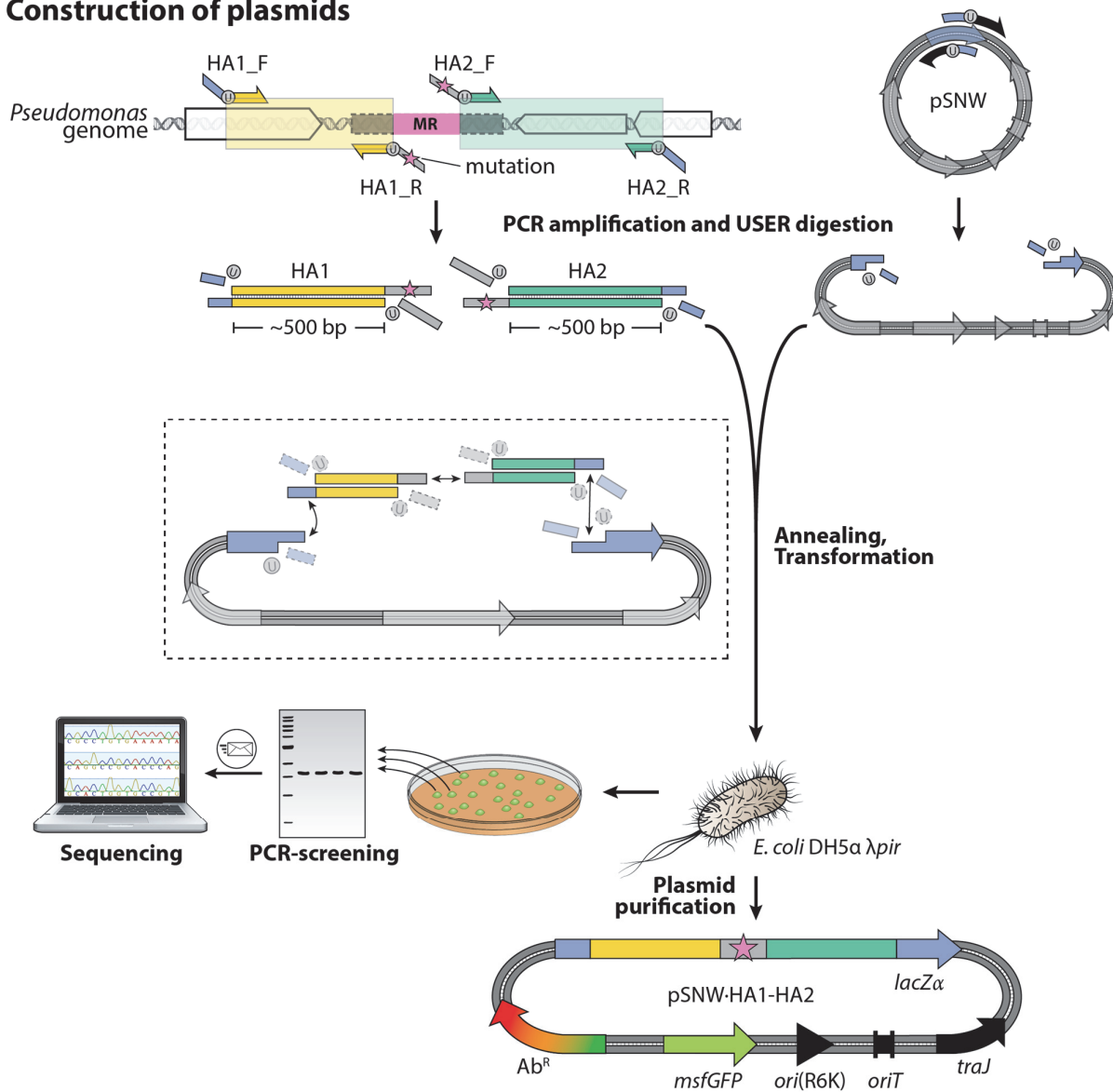


Figure 3.2 Workflow for the construction of suicide vectors for genome engineering. Two homology arms (HA1 and HA2), each spanning 500-1000 bp and located upstream and downstream of the mutagenesis region (MR), are amplified from genomic DNA of *Pseudomonas* via PCR. Modifications (i.e., insertions or substitutions) are introduced between the HAs as overhangs in the oligonucleotides (indicated in the diagram with a red star) or as additional DNA fragments (not shown). For gene deletions, the sequences of the HAs are designed so that they frame the genome sequence to be deleted. HA1 and HA2 are fused and integrated into one of the linearized pSNW vectors via *USER* assembly (shown here) or alternative molecular cloning techniques. The thereby assembled pSNW plasmid is then introduced into *E. coli* DH5α λpir. Individual *E. coli* clones obtained after transformation are examined for green fluorescence on a blue-light transilluminator and checked for the correct pSNW insert size via colony PCR, and the amplicon is sent for sequencing. After the sequence integrity is confirmed, pSNW plasmids are purified from the respective *E. coli* strain and used in the next step.

A pSNW plasmid ready for genome engineering in *Pseudomonas* (**Figure 3.2**) is composed of the vector backbone with an antibiotic-resistance gene, the R6K origin of conditional replication [*ori*(R6K)], the *traJ* gene, a relaxation region (*oriT*) required for bacterial conjugation, and a site-specific DNA insert. This insert is (i) homologous to the target locus [i.e., contains homology arms (HA) upstream and downstream to the region of interest] within the *Pseudomonas* genome, and (ii) contains the desired modification. Such modifications can be as short as a single nucleotide for a point mutation or arbitrarily long for the insertion of whole gene clusters. The insert and the vector backbone are assembled using standard protocols, e.g., traditional cloning by restriction digest and ligation²⁰², Gibson assembly⁵¹, or *USER* assembly²⁰³ that is recommended and further described here.

a. Oligonucleotide design

One primer pair is required to amplify each fragment that constitutes the pSNW derivative via PCR. Depending on the type of modification (see description below), this means that a minimum of three oligonucleotide pairs is required for cloning. A first pair of oligonucleotides (pSNW-*USER*_F: 5'-AGT CGA CCU GCA GGC ATG CAA GCT TCT-3', and pSNW-*USER*_R: 5'-AGG ATC UAG AGG ATC CCC GGG TAC CG-3'; dU residues highlighted in red in the primer sequences) is used to reverse-amplify the pSNW backbone. The resulting linear fragment can be used in a standardized way for every cloning procedure. Two further pairs of primers are required to amplify the homologous regions HA1 and HA2 from the *Pseudomonas* genome, flanking the targeted mutagenesis region (MR). *If applicable*: a fourth (fifth, etc.) primer pair is required to amplify the DNA sequence to be inserted between the two HAs.

- i) Identify the sequence of the two HA regions flanking the target gene or locus on the chromosome of *Pseudomonas*. The upstream homologous arm (HA1, see **Figure 3.2**) spans from 500-1000 bp upstream of the chromosomal target to the first base of the sequence to be deleted or edited, or the integration site. The downstream homologous arm (HA2, see **Figure 3.2**) conversely starts after the last base of the chromosomal target and ends 500-700 bp further downstream. The two HA sequences should have approximately the same size.

Tip for gene deletions: For gene deletions to have minimum polar effects and avoid the potential creation of toxic, truncated polypeptides, we recommend leaving the START and STOP codons of the target gene intact and deleting only the interjacent sequence. Upon deletion, this approach will leave, e.g., 5'-ATG TGA-3' in lieu of the coding sequence, where ATG and TGA are the START and the STOP codons, respectively.

- ii) Open the AMUSER online software. At *STEP 1: Input sequences*, enter the sequence of each fragment comprising the pSNW plasmid insert (HA1, HA2, and, *if applicable*: integration fragment) in FASTA format (including a header preceded by ">" and a DNA sequence). At *STEP 2: Output construct*, select *linear* and click on *Submit query*. The primer sequences from the *AMUSER report* can directly be used to amplify the fragments. Add the motif 5'-AGA TCC U-3' as the primer overhang to the forward primer of HA1, and 5'-AGG TCG ACU-3' as overhang to the reverse primer of HA2. These two overhangs match the ones are used to linearize vector pSNW.
- iii) One standard set of primers can be used to check for the correct insert size after constructing the pSNW derivative in colony PCR and sequence the insert region. The two primers bind within the pSNW backbone immediately upstream (pSNW_seq_F: 5'-TGT AAA ACG ACG GCC AGT-3') and downstream (pSNW_seq_R: 5'-CTT TAC ACT TTA TGC TTC CGG-3') of the insert region, respectively.
- iv) Design one pair of primers for genotyping after the genome manipulation. The primers bind within a range of 50 bp upstream of HA1 and 50 bp downstream of HA2 in the genome, respectively. For small insertions or modifications that do not alter the total length of the sequence comprising both HAs, an additional primer that specifically binds within the insertion/modification is helpful to identify the engineered genotype. For substitutions of only a few base pairs, the mutation-containing region must be amplified and the genotype confirmed by restriction analysis (if applicable) or sequencing.

b. Amplification and assembly of DNA fragments

We recommend using a ‘touchdown’ temperature protocol²⁰⁴ for each PCR amplification, as it circumvents the need for optimizing the annealing temperature and leads to higher yields and specificity²⁰⁵.

- i) Amplify purified vector pSNW using 5 ng of plasmid as template and primers pSNW-*USER_F* and pSNW-*USER_R* using the ThermoScientific™ *Phusion*™ U Hot Start DNA polymerase. Use the temperature protocol illustrated in Table 3.2, with an elongation time of 3 min. Adopt the same temperature protocol to amplify each of the fragments constituting the pSNW insert, only adjusting the duration of the extension steps according to the amplicon lengths. Utilize purified genomic *Pseudomonas* DNA with the appropriate primer pairs to generate the HA1 and HA2 fragments. Perform, if needed, additional PCRs to generate the DNA fragments required for insertions.

Tip: We recommend to gel-purify the linearized pSNW fragment using a gel and PCR clean-up kit according to the manufacturer’s instructions. By using the purified product as a template for further PCRs, digestion with *DpnI* to remove circular plasmids can be omitted. We further recommend generating a large amount of linearized pSNW vector in several parallel PCRs for repeated use in *USER* assembly.

Table 3.2. Touchdown temperature protocol for Phusion U PCR.

Initial denaturation	Touchdown phase			Enrichment phase			Hold
	Denaturation	Annealing	Extension	Denaturation	Annealing	Extension	
98°C	98°C	66°C (-1°C per cycle)	72°C	98°C	56°C	72°C	12°C
30 s	10 s	15 s	20 s/kb	10 s	15 s	20 s/kb	∞
	10 cycles			27 cycles			

- ii) Analyze a 3- to 5- μ l aliquot of each PCR by agarose gel electrophoresis [1% (w v⁻¹) agarose and 1 \times fluorescent nucleic acid gel stain in 1 \times TAE buffer] to verify the correct amplification of the fragments. The concentrations of the fragments can be roughly estimated from the intensities of their bands. If agarose gel electrophoresis reveals the presence of non-specific by-products, the desired bands have to be purified from a gel prior to cloning. If the product appears clean, the PCR reaction can be used directly in the assembly reaction.
- iii) In a PCR tube, combine equimolar amounts of insert fragments in a volume of 7 μ l with 3 μ l of the linearized pSNW vector (~50 ng). Add 1 μ l of 1 U μ l⁻¹ *USER* enzyme (New England BioLabs, Ipswich, MA, USA). Set up a thermocycler and run a reaction program as follows: deoxyuracil excision: 30 min at 37°C; annealing 1: decrease from 28°C to 18°C with -2°C per step of each 3 min; annealing 2: \geq 10 min at 10°C. If a plasmid containing the same antibiotic resistance as the employed pSNW vector was used as template for the amplification of one of the fragments, add 0.5 μ l of FastDigest DpnI (Thermo Fisher Scientific, Waltham, MA, USA) to the reaction mix before incubation at 37°C.
- iv) Transform 50 μ l of chemically-competent *E. coli* DH5 α λ *pir* cells with 5 μ l of the assembly reaction from the previous step. To prepare competent cells and transform them with assembled plasmids, we recommend using the *Mix & Go!* *E. coli* Transformation Buffer Set (Zymo Research, Irvine, CA, USA) and the associated protocol. Plate the cells on LB medium agar supplemented with the respective antibiotic for pSNW.

Tip: If a circular plasmid was used as a template in the PCR for pSNW linearization and if the reaction was directly employed for the assembly reaction (rather than using a gel-purified plasmid), spread the transformed *E. coli* DH5 α λ *pir* cells on plates containing 5-bromo-4-chloro-3-indolyl- β -D-galactopyranoside (XGal) at 40 μ g ml⁻¹. The disruption of the pSNW-borne *lacZ* α sequence then allows for the identification of *E. coli* colonies harbouring “empty” template plasmids via their blue colour in contrast to white colonies, carrying a pSNW with insert.

c. Verification of clones

- i) Inspect plate with transformed *E. coli* DH5 α λ pir on a blue-light transilluminator. Perform a colony PCR with primers pSNW_seq_F and pSNW_seq_R (using OneTaq[®] 2 \times Master Mix; New England BioLabs, Ipswich, MA, USA) on eight to ten colonies that show green fluorescence (and did not develop a blue color in white light if XGal was added to the plate). To this end, prepare 50 μ l of a 1 \times master mix by mixing 25 μ l of OneTaq[®] 2 \times Master Mix with 23 μ l DNase-free water and 1 μ l of each primer (scale up if necessary). Transfer 6 μ l of the 1 \times master mix into PCR tubes and add a small amount of biomass from the *E. coli* colonies grown on the culture plate. Run a PCR with the following temperature protocol (**Table 3.3**, adjust the elongation time according to the expected insert size).

Table 3.3. Touchdown temperature protocol for OneTaq colony PCR.

Initial denaturation	Touchdown phase			Enrichment phase			Hold
	Denaturation	Annealing	Extension	Denaturation	Annealing	Extension	
94°C	94°C	62°C (-1°C per cycle)	68°C	94°C	52°C	68°C	12°C
2 min	20 s	30 s	1 min/kb	20 s	30 s	1 min/kb	∞
	10 cycles			27 cycles			

- ii) Analyze a 3- μ l aliquot of each PCR by agarose gel electrophoresis to verify the correct insert size.

TIP: For *E. coli*, *P. putida*, and many other bacteria, small amounts of biomass from colonies can be directly transferred with a pipette tip or inoculation loop to the reaction mix (avoid transferring agar from the plate to the reaction mixture, as it will inhibit the amplification). For some bacteria, it might be necessary to boil biomass in water and dilute before colony PCR for good amplification results.

- iii) If no band other than that of the expected size is visible in the agarose gel, the reaction sample can directly be sent for sequencing to verify sequence integrity.

For this, mix 0.5 μ l of the PCR reaction with 13.5 μ l of DNase-free water, 1 μ l of DMSO, and 2 μ l of the primer pSNW_seq_F or pSNW_seq_R (one sequencing sample for each primer and each *E. coli* clone) in a sequencing tube and send the tubes for sequencing.

- iv) Inoculate 3-5 ml LB cultures in 50-ml centrifuge tubes (add the corresponding antibiotic) with three individual clones tested for a correct insert size. Incubate the culture at 37°C for 12-18 h in a shaking incubator at 180-250 rpm (depending on the type of incubator). To continue with the genome engineering procedure in *Pseudomonas* on the subsequent day (**Section 3.3.2**), launch a pre-culture of strain KT2440 as well, and incubate with shaking (180-250 rpm) at 30°C.
- v) Purify plasmid DNA from the *E. coli* cultures that tested positive by colony PCR, and send the purified plasmid DNA for sequencing in addition to (or instead of) *step iii*. Use a sequence-verified plasmid for the subsequent procedure in *Pseudomonas*.

B. Cloning of sgRNAs into vector pS448-CsR for counterselection of mutants

To adopt CRISPR/Cas9 as a counterselection tool, the vector pS448-CsR was constructed by *USER* assembly. To this end, pSEVA448 was linearized by reverse-amplification with primers pS448_F and pS448_R (**Table 3.S1**) and assembled with (i) *cas9*, amplified from plasmid pSEVA421-Cas9tr with primers Cas9_F and Cas9_R and (ii) a $P_{EM7} \rightarrow$ sgRNA module (synthesized by Integrated DNA Technologies, Leuven, Belgium; and amplified with primers sgRNA_F and sgRNA_R). This module contains a single guide RNA construct fused to a *trans*-activating CRISPR RNA (*tracrRNA*)-sequence and two *BsaI* recognition sites for the insertion of a spacer. The two *BsaI* recognition sites are placed in inverse orientation immediately upstream of the *tracrRNA* part to enable the creation of incompatible, single-stranded overhangs during linearization by *BsaI*. This step allows for the insertion of a double-stranded DNA (dsDNA) fragment with suitable overhangs. If CRISPR/Cas9 is to be used as a counterselection

tool, vector pS448·CsR must be equipped with an adequate spacer²⁰⁶, which targets the original sequence that becomes modified, as described below.

a. Spacer design

For the use of CRISPR/Cas9 as a counterselection tool, a spacer is inserted into vector pS448·CsR to target the original sequence disrupted during genome engineering. The spacer represents the CRISPR RNA (crRNA)-part of the sgRNA and is defined by the 20-nt sequence upstream of a spacer adjacent motif (PAM, 5'-NGG-3') on either of both DNA strands within a target DNA region. Strand specificity is not relevant when CRISPR/Cas9 is employed for counterselection. The most efficiency-determining parameter of this system is the sgRNA's specificity for its target. To choose a suitable spacer sequence for counterselection, we recommend using the online tool *CRISPy-web*²⁰⁷, as indicated below.

- i) Upload a GenBank file with the complete genomic sequence of the *Pseudomonas* species used into CRISPy-web.
- ii) Specify either the gene that is to be deleted or exchanged.
- iii) Choose a suitable 20-nt spacer candidate sequence from the top entries in the list provided by the CRISPy-web application.
- iv) Design and order two oligonucleotides that are complementary to each other. The first oligonucleotide represents the 20 nt of the spacer sequence obtained in the previous step. The second oligonucleotide is the reverse complement of the first oligonucleotide. Add a 5'-GCGCG-3' overhang to the 5'-end of the first oligonucleotide. Add a 5'-AAAC-3' overhang to the 5'-end of the second oligonucleotide and a single C residue to its 3'-end. For example, if *aceF* (*PP_0338*) is to be targeted, the sequences would be oligonucleotide 1, 5'- GCGCG CTC ATT CGC GTA CCT GAC AT -3'; and oligonucleotide 2, 5'- AAAC ATG TCA GGT ACG CGA ATG AG C -3' (oligonucleotides *aceEF_F* and *aceEF_R* in **Table 3.S1**; additions are underlined). For ligation into pS448·CsR, the oligonucleotides need to be phosphorylated at the 5'-OH terminus. The oligonucleotides can either be purchased with

terminal phosphorylation or phosphorylated in situ using T4 polynucleotide kinase (PNK, see below).

b. DNA preparation and construction of derivatives of vector pS448·CsR

- i) Digest vector pS448·CsR with *Bsa*I or *Eco*31I (Thermo Fisher Scientific) according to the manufacturer's recommendations. Use agarose gel electrophoresis and gel purification to isolate the linearized plasmid (9.9 kb) from the non-restricted fraction.
- ii) Dissolve the two spacer oligonucleotides at 100 μ M. Phosphorylate and anneal the oligonucleotides in a thermocycler^{208,209}. This can be performed in a single 10- μ l reaction containing 6 μ l of water, 1 μ l of each oligonucleotide, 1 μ l of T4 ligase buffer and 1 μ l of T4 PNK (New England BioLabs, Ipswich, MA, USA). Use the following temperature protocol: 30 min at 37°C, 4 min at 95°C, followed by 70 cycles consisting of 12 s each, starting at 95°C and decreasing the temperature by 1°C in each cycle.
- iii) Dilute the annealed and phosphorylated oligonucleotides 1:200 with water, i.e., to a final dsDNA concentration of 50 nM.
- iv) Ligate the dsDNA encoding the sgRNA-spacer into the linearized pS448·CsR vector in a 10- μ l reaction containing 3 μ l of the diluted insert from the previous step, 30 ng of *Bsa*I-digested pS448·CsR vector, 1 μ l of T4 ligase buffer, 1 μ l of T4 DNA ligase (New England BioLabs) and water, if needed, to reach the final volume.
- v) Ligate 30 min at room temperature and transform a 50- μ l aliquot of chemically-competent *E. coli* DH5 α cells with 5 μ l of the ligation mixture. Plate on LB medium agar supplemented with streptomycin (100 μ g ml⁻¹).
- vi) Purify plasmid DNA from three individual *E. coli* transformants, and verify the sequence integrity by sequencing with primer SEVA-T0_F (5'-GAA CGC TCG GTT GCC GCC-3').

c. Efficiency test for the sgRNA for counterselection

This step is optional and is meant to provide an estimation of the efficiency of the sgRNA in targeting the locus targeted during the procedure (thus providing an estimate of the success rate of the whole counterselection procedure).

- i) Inoculate 10 ml of LB medium with *P. putida* KT2440 and grow the cells overnight at 30°C with agitation.
- ii) Prepare the cells for electroporation. To this end, we adopted the procedure by Choi et al.²¹⁰. These steps can be performed at room temperature. In brief, distribute the cell suspension into four microcentrifuge tubes and harvest it in a microcentrifuge at 11,000 g for 1 min. Wash the cells twice with 1 ml of 300 mM sucrose (filter-sterilized) for each pellet and finally resuspend and combine them in a total of 400 μ l 300 mM sucrose in a single tube. Transfer 100 μ l of cells suspended in sucrose into an electroporation cuvette with 2 mm gap width.
- iii) Individually electroporate 100- μ l cell aliquots with 100 ng of the empty pS448-CsR and 100 ng of the sgRNA-harboring with a voltage of 2.5 kV, 25 μ F capacitance, and 200 Ω resistance (e.g., in a Gene Pulser Xcell™ Electroporation System, Bio-Rad Laboratories, Hercules, California, USA).
- iv) Let the cells recover for 2 h at 30°C and plate them onto the LB medium agar supplemented with streptomycin (100 μ g ml⁻¹). Incubate the plates for overnight at 30°C.
- v) Inspect the plates. Those with cells harboring pS448-CsR with a specific sgRNA should have considerably fewer colonies (if any). We typically see a number of CRISPR/Cas9 escapers in the low double-digit range (i.e. 10–20 colonies) while *P. putida* transformed with an empty pS448-CsR vector will form several hundred colonies within 16 h.

3.3.2 Genome editing in *Pseudomonas putida*

To introduce mutations into the *P. putida* genome, the suicide plasmid pSNW (constructed in the previous section) is integrated into the chromosome at the target location employing the native homologous recombination mechanism (Figure 3.3). After selecting for pSNW co-integration, the meganuclease I-SceI or the CRISPR/Cas9 system is delivered into the cells on a replicative plasmid. The expression of the DNA modifying enzymes—and thus restriction of pSNW within the chromosome—enforces second homologous recombination that can yield either the mutant genotype or a revertant genotype (i.e., wild-type sequence).

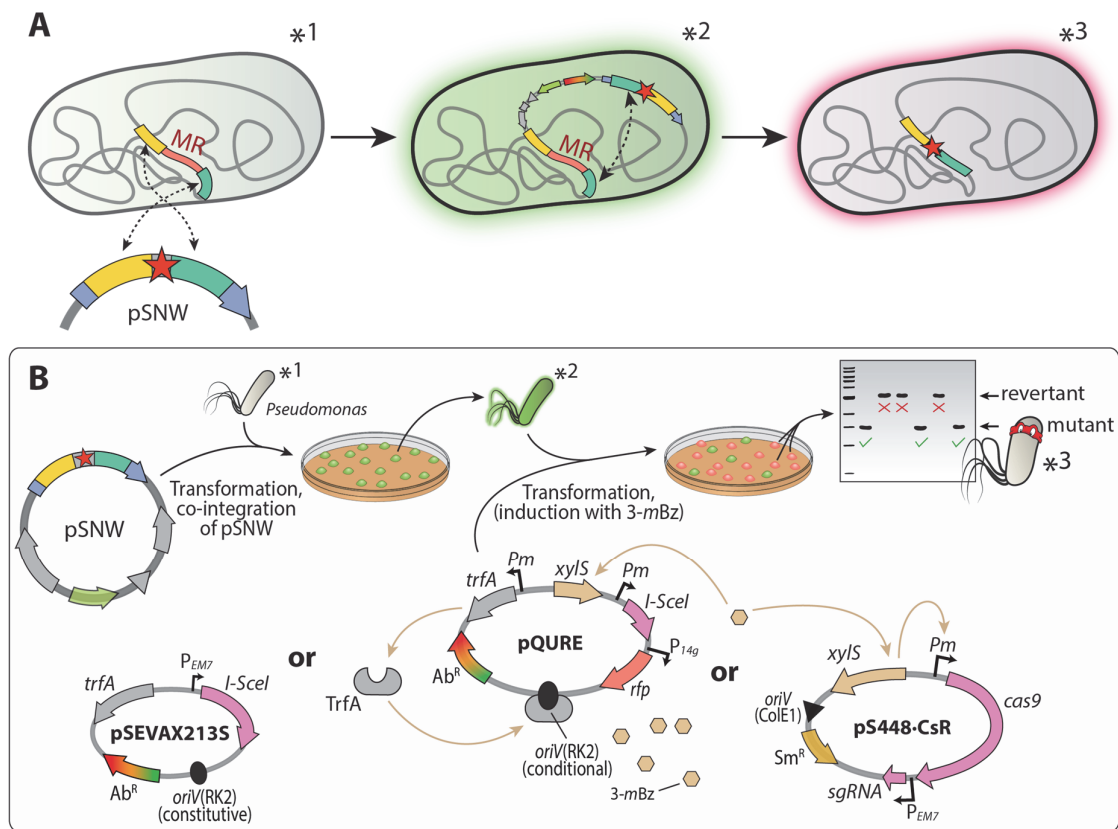


Figure 3.3. Workflow for targeted genomic manipulations in *Pseudomonas*. *Pseudomonas* cells are transformed with pSNW via electroporation or tri-parental mating. One to five individual green fluorescent colonies are combined and enriched in liquid LB medium cultures. The cells are transformed either with a pQURE plasmid, pSEVAX213S, or a derivative of vector pS448-CsR carrying an appropriate sgRNA. Expression of the gene encoding the I-SceI meganuclease or Cas9 mediates resolving of the pSNW sequence from the chromosome. Strains that resolved pSNW show either only red fluorescence (with pQURE) or no fluorescence (with pS448-CsR or pSEVAX213S) under blue-light exposure. These clones are tested via colony PCR and sequencing for a revertant (i.e., wild-type) or mutant genotype. Asterisks indicate the relevant genotypes and the molecular events happening in the *Pseudomonas* chromosome (A) during the corresponding steps of the genome engineering protocol (B).

A. Integration of pSNW derivatives into the chromosome

The suicide vector pSNW carrying appropriate HAs has to be delivered into the cells to enable its chromosomal integration via HR. This step can be achieved either by electroporation or by tri-parental mating. The latter procedure is recommended if working with significantly growth-restricted strains. Furthermore, the co-integration efficiency is strongly dependent on the targeted chromosomal locus. If no clones are obtained after electroporation, the much more efficient plasmid delivery achieved by tri-parental mating provides a fallback method to achieve co-integration.

d. Plasmid delivery by electroporation

- i) Grow an overnight culture of *P. putida* KT2440 in 5-10 ml of LB medium. The *Pseudomonas* culture can be started at the same time that the overnight cultures of *E. coli* DH5 α λ pir with pSNW are initiated (page 65).
- ii) Prepare the culture for electroporation as described (page 68).
- iii) Add 500-1000 ng of pSNW to a 100- μ l cell aliquot in a an electroporation cuvette. Thereby, the volume of pSNW should not exceed 10 μ l. Perform electroporation as described (page 68).
- iv) Transfer the cell suspension into a sterile test or centrifuge tube (5-50 ml) and recover the cells with shaking at 30°C for 2 h.
- v) Harvest the cells by centrifugation (11,000 g; 1 min) at room temperature, and plate the whole suspension onto LB medium agar supplemented with the respective antibiotic for the pSNW vector used (50 μ g ml⁻¹ Km for pSNW2, 100 μ g ml⁻¹ Sm for pSNW4, 10 μ g ml⁻¹ Tc for pSNW5, or 10 μ g ml⁻¹ Gm for pSNW6). Incubate the cells overnight at 30°C.
- vi) Inspect the plate on a blue-light transilluminator. Transformants should show green fluorescence (usually all colonies).

e. Plasmid delivery by tri-parental mating

- i) Grow overnight cultures of *Pseudomonas*, *E. coli* DH5 α λ pir/pSNW, and *E. coli* HB101/pRK600 in at least 1 ml of LB medium (supplemented with the appropriate antibiotic) each. Incubate at 30°C for *Pseudomonas* or 37°C for *E. coli*, respectively.
- ii) Dry an LB medium agar plate without added antibiotics by placing it opened on a clean bench for 1 h.
- iii) Combine 100 μ l of each pre-culture into a reaction tube and pellet the cells in a microcentrifuge at 10,000 g for 1 min at room temperature. Wash the cells with 1 ml of fresh LB medium and finally resuspend them in 20-30 μ l of LB medium. Pipette the whole suspension onto the pre-dried LB medium agar plate. For bacterial conjugation to work, the cells have to be brought into close proximity within a non-planktonic state. A dried agar plate will absorb a small volume of media, allowing the bacterial cells to form a biofilm-like structure on the agar surface.
- iv) Incubate the cells at 30°C for 3-5 h.
- v) Use an inoculation loop to take the biomass up from the agar surface and resuspend it in 1 ml of LB medium. Spread 100 μ l of this suspension directly onto a cetrimide agar plate supplemented with the antibiotic to select for the used pSNW vector, as well as 50 μ g ml⁻¹ ampicillin. Concentrate the remaining cells to about 100 μ l by centrifugation. Resuspend and spread them onto a second plate. The chosen concentration of Amp was found not to affect the growth of *P. putida* KT2440 that is naturally resistant to β -lactam antibiotics, while completely suppressing the growth of most *E. coli* strains, which may show some residual growth in the presence of cetrimide.
- vi) Incubate the plates at 30°C for 16-24 h until colonies have formed that show green fluorescence under blue-light exposure.

B. Introduction of endonucleases

In the context of the publications forming the basis of this chapter^{154,180,181}, three new molecular tools to resolve co-integrated suicide plasmids were developed (**Figure 3.3B**). The first set of vectors, comprising pSEVA1213S and pSEVA6213S, harbors I-SceI under the transcriptional control of the constitutive P_{EM7} promoter, enabling highly efficient selection against co-integrants without the addition of inducer compounds¹⁵⁴. The second set of auxiliary plasmids belong to the pQURE toolset¹⁸⁰, in which the *oriV*(RK2)-replication initiator protein TrfA was set under the control of the XylS/*Pm* promoter system¹⁹². Consequently, plasmid replication is dependent on the induction by 3-*mBz*. Simultaneously, the addition of the inducer triggers the expression of the *Pm*-controlled *SCEI*. Furthermore, pQURE plasmids harbor a constitutively expressed, red fluorescent reporter construct of varying intensity (**Table 3.1**), allowing for an easy identification of cells harboring the vectors. Lastly, CRISPR/Cas9 counterselection is enabled by using the designed pS448·CsR vector¹⁵⁴.

- i) Combine 1-5 individual *Pseudomonas* colonies with a co-integrated pSNW vector into 5-10 ml of LB medium (supplemented with antibiotic to select for pSNW) in a test or centrifuge tube (5-50 ml) and incubate with shaking at 30°C for at least 5 h (see next step). Using several individual colonies increases the chances of having cells with both the two possible genetic configurations after pSNW co-integration (**Figure 3.5**), and reduces the impact of unspecific insertion of the suicide plasmid at untargeted chromosomal sites. Furthermore, the more biomass is used to inoculate the LB medium culture, the quicker the cell density required for the next step is reached so that the protocol can be continued on the same day.
- ii) After the cells have reached an optical density at 600 nm (OD_{600 nm}) of at least 0.3, use 20-100 ng of an I-SceI-bearing plasmid (i.e., pSEVAX213S or pQURE, see **Table 3.1**) or 100-200 ng of plasmid pS448·CsR to transform *Pseudomonas* by electroporation as described (**Section 3.3.1.B.c**; page 68). Transfer the cell suspension into a sterile test or centrifuge tube and recover the cells shaking at 30°C for 1 h. If a plasmid containing the XylS/*Pm* expression system (i.e., pQURE or pS448·CsR) is

used, add 3-*mBz* to a final concentration of 3 mM to the LB medium used for cell recovery.

TIP: The co-transformation of both an *I-SceI* harboring plasmids and pS448·CsR can significantly reduce the occurrence of cells escaping CRISPR/Cas9 counterselection. In this case, both plasmids should be employed in the electroporation at concentrations of 250 ng.

- iii) Plate 70 µl of cell suspension on LB medium agar supplemented with the respective antibiotic to select for pQURE, pSEVAX213S, or pS448·CsR selection. Incubate the cells overnight at 30°C. If a plasmid containing the *XylS/Pm* expression system (i.e., pQURE or pS448·CsR) is used, add 3-*mBz* to a final concentration of 1 mM to the LB medium plates to ensure proper induction of the system.
- iv) Inspect the plate on a blue-light table. *Pseudomonas* clones that have lost vector pSNW through homologous recombination will show no green fluorescence.
- v) Test ≥ 8 individual colonies without green fluorescence via colony PCR using the genotyping primers to distinguish mutant from revertant genotypes. The fraction of clones that have maintained fluorescence after counterselection is expected to be significantly higher when using CRISPR/Cas9 as compared to *I-SceI*, due to a higher probability of escaping restriction by mutating the sgRNA recognition sequence.

TIP: When using an *I-SceI*-mediated counterselection, it is common to find a fairly even distribution of revertant and mutant genotypes. However, the proportions can also be strongly skewed towards one of the two outcomes, depending on the targeted chromosomal locus. If no mutants are identified in the first colony PCR, the screening can be extended to several dozen clones to find clones with the desired genotype.

3.3.3 Curing of auxiliary plasmids

Once the mutation has been confirmed, the last step in the procedure is to cure the mutant cells from the plasmid(s) used during genome editing (**Figure 3.4**).

- i) Use a single colony of mutant *Pseudomonas* to inoculate 3-10 ml of LB medium in a test or centrifuge tube.
- ii) Culture the cells shaking at 30°C.
- iii) *For pSEVAX213S or pS448-CsR*: Every 4-16 h, transfer 1 µl of the culture into 3-10 ml of fresh LB medium (without any additives). Continue the culturing process for 2-3 days, and pass the cells into fresh medium even if the formation of biomass in the tubes cannot be seen. This procedure ensures that the cells are kept in a state of maximum division rate. If the mutant cells have severe growth deficiencies due to the deletion of important genes or the introduction of DNA that could impair growth, the curing of a plasmid can require continuous cultivation for an extended period. *For pQURE*: One overnight culture is usually sufficient to get plasmid-free clones.
- iv) Dilution-streak the culture on an LB medium agar plate without added antibiotics or 3-*mBz*.
- v) *For pSEVAX213S or pS448-CsR*: Test individual colonies for the loss of the plasmid by re-streaking on LB medium agar with the respective antibiotic. *For pQURE*: Inspect the plate on a blue-light transilluminator. Plasmid-free clones can be distinguished from pQURE-harboring cells via the absence of fluorescence (**Figure 3.4**).

TIP: After incubating the plates at 30°C until colonies have formed, the extended incubation at 4°C for several days allows the RFP produced from pQURE to mature and significantly enhances the red fluorescence of plasmid-harboring cells.

Plasmid curing

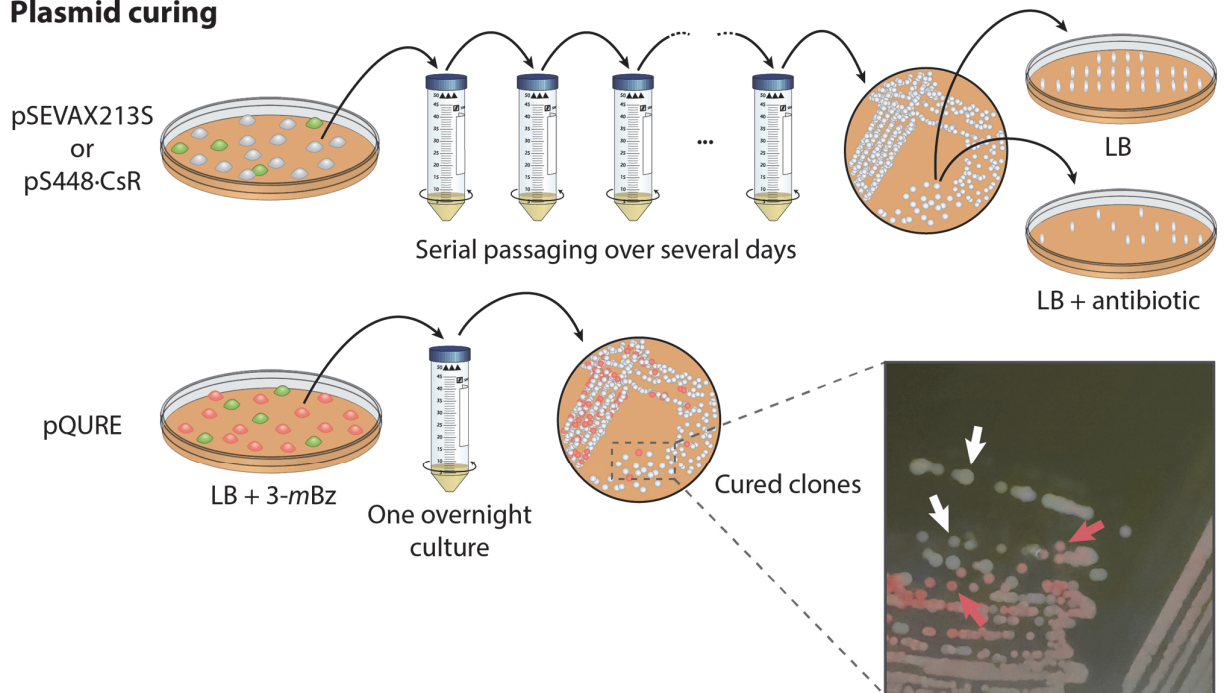


Figure 3.4. Plasmid curing after successful genome engineering of *Pseudomonas*. The biomass from a single mutant *Pseudomonas* colony is used to inoculate 5–10 ml of LB medium, and the suspension is incubated at 30°C with shaking. To cure pSEVAX213S or pS448-CsR: Two to three times per day, a small volume of this culture is transferred into fresh LB medium. After 2–3 days (i.e., at least six passages), the cells are isolated on LB medium agar plates and tested for the loss of plasmids based on their antibiotic resistance profile. To cure pQURE: after one overnight culture in LB medium (without the addition of 3-mBz), the cells are isolated on LB medium agar plates. Plasmid-free cells (white arrows) can be identified by the absence of red fluorescence, in contrast to colonies that still carry pQURE (red arrows).

3.4. Application examples

3.4.1 Deletion of *nicX* in *Pseudomonas putida* KT2440

P. putida KT2440 can grow on nicotinic acid as the sole carbon source¹²¹. The degradation pathway, encoded in the *nic* gene cluster, involves the hydroxylation of nicotinate to 6-hydroxynicotinate, its further reduction to 2,5-dihydroxypyridine (**Figure 3.5A**), and the deoxygenation to *N*-formylmaleamic acid, which can be further converted into fumarate²¹¹. An interruption of the metabolic route at the level of 2,5-dihydroxypyridine via the deletion of *nicX* (encoding a 2,5-dihydroxypyridine 5,6-dioxygenase) leads to the formation of a dark-green colored compound with green fluorescence that is accumulated inside the cells and secreted into the medium²¹². After autoxidation, the metabolite forms brown polymers. Since it allows for the direct identification of mutant clones with the addition of nicotinic acid to the culture medium, deletion of *nicX* in strain KT2440 was chosen to optimize the genome engineering protocol.

The primer pairs *nicX*_HA1_F/*nicX*_HA1_R and *nicX*_HA2_F/*nicX*_HA2_R (**Table 3.S1**) were used to amplify the two homology regions that flank *nicX*. The PCR products were assembled into vectors pGNW2, pGNW4, and pGNW6 via *USER* assembly, yielding pGNW2· Δ *nicX*, pGNW4· Δ *nicX*, and pGNW6· Δ *nicX*, respectively (**Figure 3.5B**). After their purification from *E. coli* DH5 α λ pir, the suicide plasmids were integrated into the chromosome of strain KT2440 by electroporation. The co-integrand clones were transformed with either plasmid pSEVA6213S (in clones where either vector pGNW2· Δ *nicX* or pGNW4· Δ *nicX* was used for the integration) or plasmid pSEVA1213S (in clones where vector pGNW6· Δ *nicX* was used for the integration step). The cells were plated on LB medium agar containing Gm or Amp. **Figure 3.5C** shows a photograph of an LB medium agar plate supplemented with Gm and 5 mM nicotinic acid, taken one day after transforming *P. putida* KT2440·pGNW2· Δ *nicX* with plasmid pSEVA6213S.

Thirty randomly picked colonies from the plates obtained after each deletion procedure were tested for their genotype via colony PCR using primers *nicX*_g-check_F/*nicX*-g-check_R (**Table 3.S1**). The different colorations of mutant and revertant colonies (matching the results obtained by PCR) allowed for their direct identification. With all three plasmid combinations, the fraction of mutant colonies was close to 50% (53%, 46%, and 48%, respectively). However, this equal distribution of

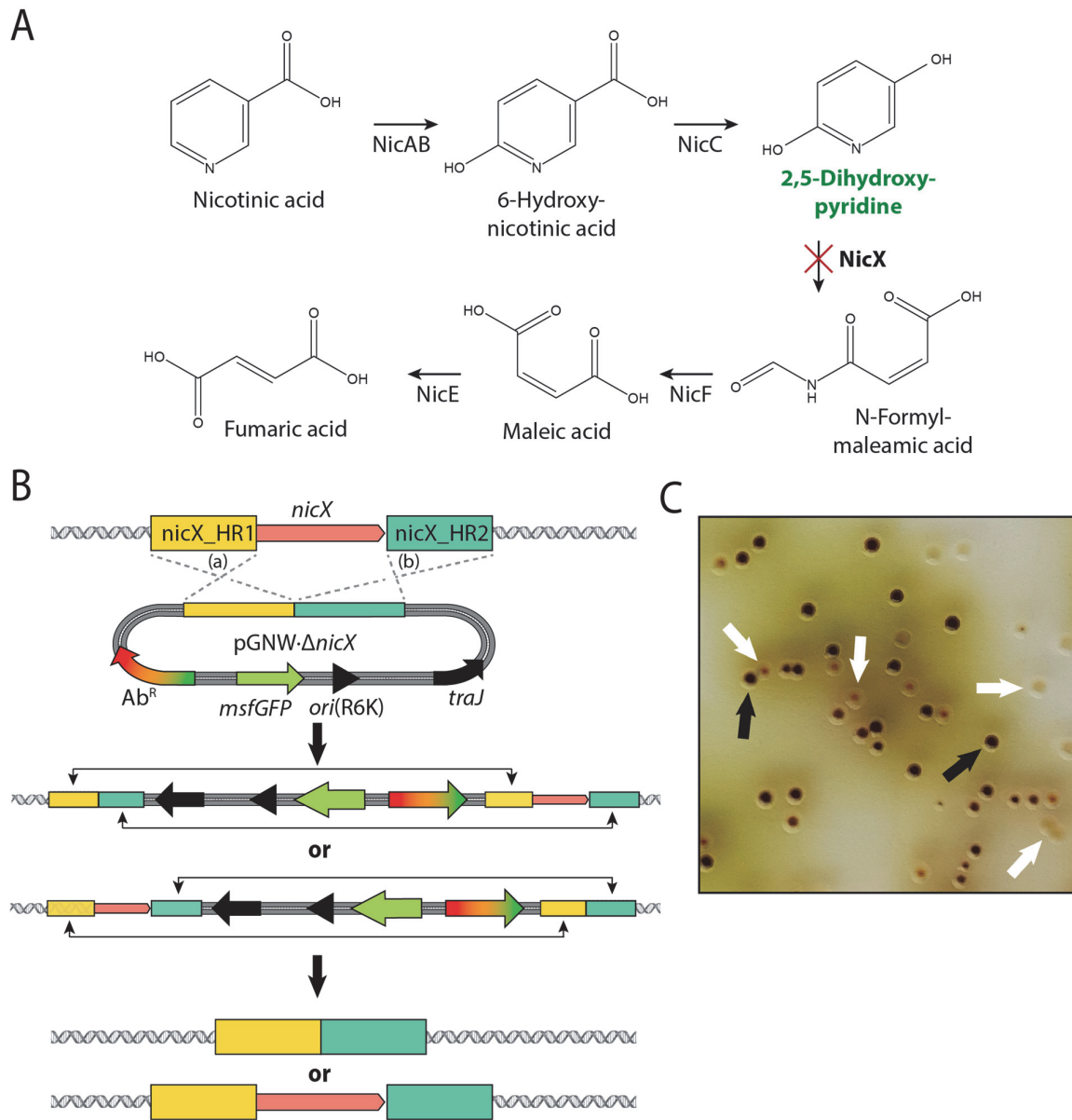


Figure 3.5. Deletion of *nicX* in *P. putida* KT2440. (A) Proposed degradation pathway of nicotinic acid in *P. putida*. The key metabolic intermediate accumulating upon elimination of *nicX* (encoding 2,5-dihydroxypyridine-5,6-dioxygenase) is highlighted in green. The targeted, in-frame deletion of *nicX* is indicated by a red cross. (B) Schematic representation of the molecular mechanism for the integration of the suicide plasmid pGNW- Δ *nicX* in the chromosome of strain KT2440 as well as the second recombination leading to either a revertant or a mutant genotype. (C) Representative picture of a section of an LB medium agar plate (containing 10 $\mu\text{g mL}^{-1}$ Gm and 5 mM nicotinic acid) seeded with an isolate of strain KT2440 that was previously co-integrated with the suicide plasmid pGNW2- Δ *nicX* and transformed with the helper plasmid pSEVA6213S. The accumulation of 2,5-dihydroxypyridine (green-to-brown pigmented colonies) can be easily detected by visual inspection of the plates. The picture was taken after incubation for 16 h at 30°C followed by 24 h at 4°C. The black arrows indicate colonies formed by *P. putida* Δ *nicX* cells; the white arrows identify colonies displaying a revertant (i.e., wild-type) genotype.

mutant and revertant genotypes is not always the norm. Depending on the chromosomal locus, almost exclusively clones carrying the intended gene deletion can be found in some cases. In other cases, increased screening effort is required to find mutants within a majority of revertants. The outcome of the second crossover event is not necessarily related to phenotypic effects but can likely be caused by molecular effects at the involved sequence region (e.g., occupancy of the involved segments by DNA-binding proteins).

3.4.2 Deletion of *aceEF* in *Pseudomonas putida* KT2440 using CRISPR/Cas9 counterselection

As an obligate aerobic bacterium, *P. putida* strongly relies on an active tricarboxylic acid cycle for the generation of reducing equivalents that are used, inter alia, to generate ATP through oxidative phosphorylation²¹³. The pyruvate dehydrogenase complex (PDHc), which catalyzes the entry reaction to the tricarboxylic acid cycle, plays a vital role in the central carbon metabolism of *Pseudomonas*^{101,105}. The PDHc is a multimeric system composed of three different proteins, AceE, AceF, and Lpd^{214,215}. In *P. putida*, the genes encoding AceE (*PP_0339*) and AceF (*PP_0338*) form an operon¹²¹. The deletion of the PDHc played a critical role in this thesis for creating a synthetic C2-auxotroph platform for evolutionary engineering (**Chapter 4**). However, considering its central contribution to sugar catabolism, genes encoding the PDHc were found to be a difficult knock-out to achieve if relying on an untargeted selection strategy. The resulting mutant would become bradytroph (or auxotroph, depending on the carbon source) for C2 units as the reaction converting pyruvate into acetyl-coenzyme A is blocked.

Thus, we have used CRISPR/Cas9 for the counterselection of the correct mutants. The homology arms to delete *aceE* and *aceF* were amplified from chromosomal DNA of *P. putida* KT2440 using the primers *aceEF_HA1_F/ aceEF_HA1_R* and *aceEF_HA2_F/aceEF_HA2_R* (**Table 3.S1**) and cloned into vector pGNW2. *Pseudomonas* co-integrants were then transformed with 200 ng of plasmid pS448-CsR_aceF (**Table 3.S1**) and selected on LB medium agar supplemented with Sm, 3-*mBz*, and 10 mM

acetate to enhance the growth of bradytrophic mutant cells. After 2 days, 10 out of 39 colonies of standard size and a majority (29 out of 39) of very small colonies could be identified on the plate (**Figure 3.S3**).

Inspection under blue-light exposure revealed that all larger colonies had kept green fluorescence and thus had escaped CRISPR/Cas9-mediated restriction. All non-fluorescent colonies were tested by colony PCR with primers *aceEF_g-check_F/aceEF_g-check_R* (**Table 3.S1**) and were found to have *aceEF* deleted. In a separate experiment, co-integrant cells were transformed with both pSEVA6213S and pS448-CsR_aceF (250 ng of each plasmid). Selection on LB medium agar plates containing Gm, Sm, 3-*mBz*, and acetate (as a direct source of acetyl-coenzyme A) led to the formation of only three colonies, all of which had *aceEF* deleted.

3.4.3 Integration of fluorescent protein-encoding genes into a landing pad in *Pseudomonas putida* KT2440

To evaluate the system's suitability for the insertion of DNA at a defined position, a landing pad was chosen within the intergenic region between *PP_0013* (*gyrB*) and *PP_5421*, close to the chromosomal origin of replication of *P. putida* KT2440^{120,121,216}. First, plasmid pGNW2-LP::P_{EM7}-mRFP was assembled from four fragments in a *USER* assembly reaction. To this end, vector pGNW2 was amplified with pGNW-*USER_F* and pGNW-*USER_R* (**Table 3.S1**). The two HAs framing the landing pad were amplified from genomic DNA with the primer pairs LP_HA1_F/LP_HA1_R and LP_HA2_F/LP_HA2_R (**Table 3.S1**). A fourth fragment containing the gene encoding the monomeric red fluorescent protein mRFP1¹⁹⁴ and the *rrnB*-T1 terminator element was amplified with RFP4LP_F and RFP4LP_R (**Table 3.S1**) from vector pS2313-R. The primers RFP4LP_F and LP_HA1_R furthermore contained extended overhangs to introduce the constitutive P_{EM7} promoter upstream of the *mRFP1* coding sequence. However, this promoter was found to give a too low expression for visualization (data not shown). Thus, its sequence was exchanged with the P_{14g} promoter²⁰⁰ and the translational coupler *BCD2*²¹⁷ by amplifying pGNW2-LP::P_{EM7}-mRFP with oligonucleotides [P_{14g}(*BCD2*)_F]/[P_{14g}(*BCD2*)_R] and a *BCD2*-fragment from a gBlock containing this

regulatory element (purchased from Integrated DNA Technologies, Leuven, Belgium) with [BCD2-P_{14g}_F]/[BCD2-P_{14g}_R]. The resulting plasmid was termed pGNW2·LPR (**Table 3.1**).

To exchange *mRFP1* in the landing pad with different fluorescent proteins and transfer the landing pad to vectors pGNW4 or pGNW6, two- or four-fragment *USER* reactions were performed with interchangeable modules. These modules were amplified and assembled as indicated in **Table 3.S2**. The *msfGFP* gene was amplified from vector pGNW4. The genes encoding the other fluorescent proteins were amplified from the plasmids pS2313·B, pS2313·O, and pS2313·T that had been constructed as follows: The sequences of the genes *bfp2*, *mOrange2*, and *mTurquoise2* were extracted from their original publications (**Table 3.1**), cured of protein tags and restriction sites to make them SEVA-compatible and purchased as custom genes (Integrated DNA Technologies, Leuven, Belgium). The synthetic DNA fragments were then cloned into the expression vector pSEVA2313 via *USER* assembly, using the primer pairs pS2313_F/pS2313_R (for pSEVA2313), pS_BFP2_F/pS_BFP2_R (for *bfp2*), and pS_Ora_Tq_F/pS_Ora_Tq_F (for *mOrange2* and *mTurquoise2*; **Table 3.S1**), yielding plasmids pS2313·B, pS2313·O, and pS2313·T, respectively.

The resulting plasmids pGNW2·LPR, pGNW2·LPG, pGNW2·LPB, pGNW4·LPO, and pGNW6·LPT (**Table 3.1**) were individually integrated into the chromosome of *P. putida* KT2440 as indicated in the protocol. The backbones were removed from the co-integrants by the delivery and induction of plasmid pSEVA128S (for pGNW2·LPR), pSEVA628S (for pGNW2·LPG and pGNW2·LPB), pSEVA228S (for pGNW4·LPO), and pSEVA428S (for pGNW6·LPT), respectively (**Figure 3.6A**). On the following day, the plates with the resulting strains (*P. putida* KT·LPR, KT·LPG, KT·LPB, and KT·LPO, **Table 3.4**) were placed at 4°C to let the fluorescent proteins mature since none of them showed any visible coloration under blue-light exposure. After 7 days, photographs of the plates were taken on a blue-light transilluminator (**Figure 3.6B**). *Pseudomonas* colonies with integrated mBFP2 (strain KT·LPB) showed not visible fluorescence even after further prolonged incubation (data not shown). To determine the kinetics of the

fluorescent proteins in *P. putida* KT2440, at least three biological replicates of the mutant strains (verified by colony PCR with primers Seq-LP_F and Seq-LP_R, **Table 3.S1**) and the wild-type strain were grown at 30°C in 96-well plates (Greiner CELLSTAR™; Sigma-Aldrich, St. Louis, MO, USA; polystyrene, round bottom) with 200 µl of de Bont minimal medium²¹⁸ per well, supplemented with 30 mM citrate, and covered with a sealing membrane (Diversified Biotech Breathe-Easy™; VWR, Radnor, PA, USA). The kinetics of bacterial growth and fluorescence were acquired by measuring the OD₆₃₀ as well as the excitation/emission values of mRFP1 at 582 nm/609 nm, mBFP2 at 385 nm/450 nm, mOrange2 at 541 nm/567 nm, and mTurquoise2 at 451 nm/477 nm (**Figure 3.7**). Although under the transcriptional control of the same regulatory elements, the five fluorescent proteins differed in both the intensity of their signal as well as their expression pattern. The fluorescence intensity of only msfGFP increased steadily for the whole cultivation time of 50 h; the signal of the remaining four reporter proteins reached stagnation after 15 h (mOrange2), 8 h (mRFP1 and mBFP2) and 25 h (mTurquoise2). Since all cultured strains continued to grow until the end of the experiment, the biomass-specific fluorescence (not shown) decreased continuously. The prolonged growth of *P. putida* can be attributed to a limited oxygen transfer through the sealing membrane used to cover the microtiter plates.

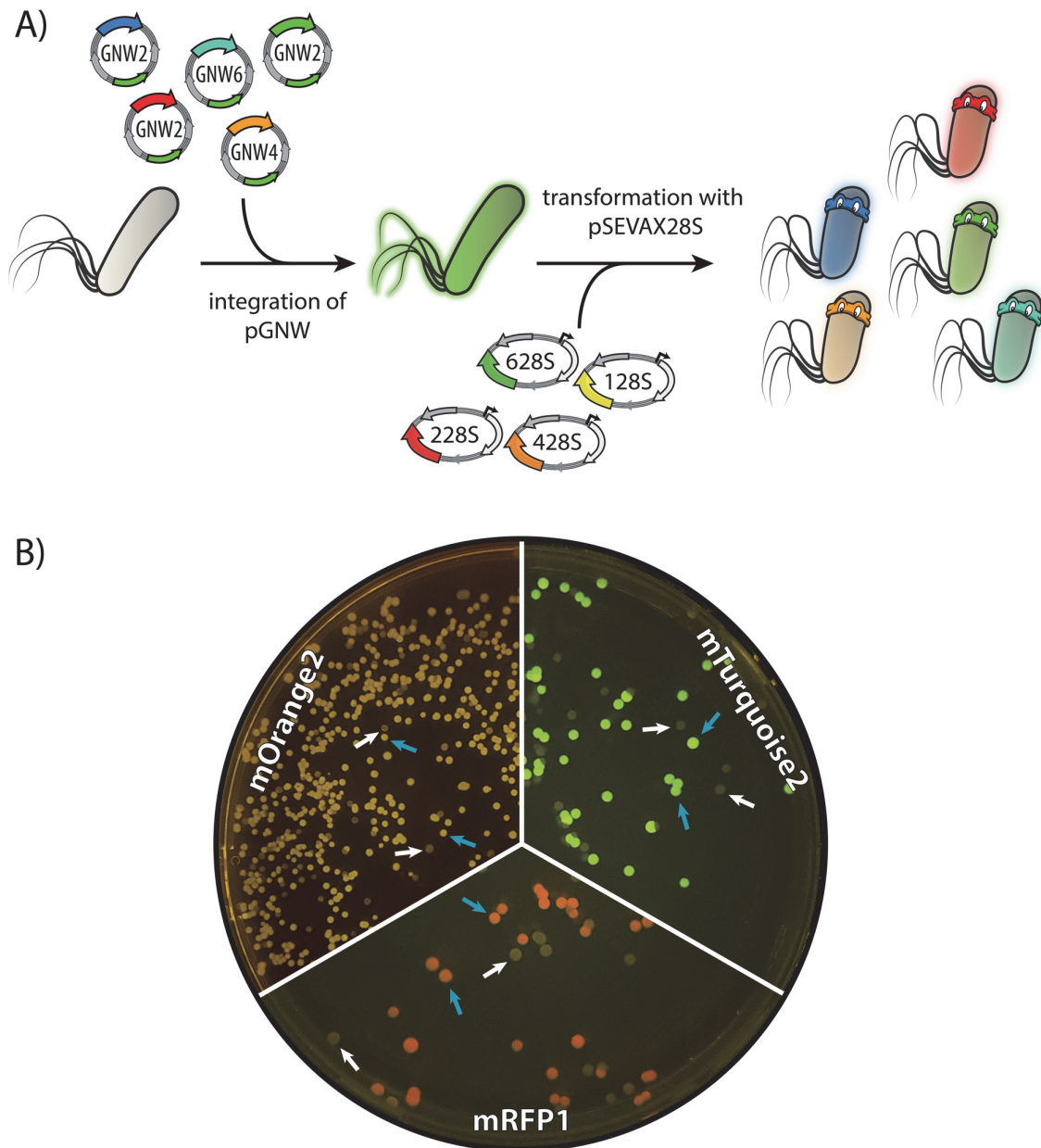


Figure 3.6. Integration of different fluorescent proteins into a chromosomal landing pad of *Pseudomonas putida* KT2440. (A) Genes encoding the fluorescent proteins mRFP1, mOrange2, mTurquoise2, msfGFP, and mBFP2 [placed under transcriptional control of a $P_{14g}(BCD2)$ regulatory element], were integrated into a chosen landing site in the chromosome of *P. putida* KT2440 using the insertional vectors pGNW2, pGNW4, or pGNW6. After the selection of co-integrants, the second homologous recombination was mediated by the inducible expression of the gene encoding the I-SceI meganuclease from pSEVAX28S vectors. (B) Images of the plates were taken after incubation for 16 h at 30°C followed by 7 days at 4°C to allow for proper fluorescent protein maturation. mBFP2-integrated colonies showed no visible fluorescence under blue-light exposure (not shown). The blue arrows indicate colonies of mutated strains displaying different integrated fluorescent proteins; white arrows identify colonies of cells displaying a revertant genotype (i.e., wild-type) without fluorescence.

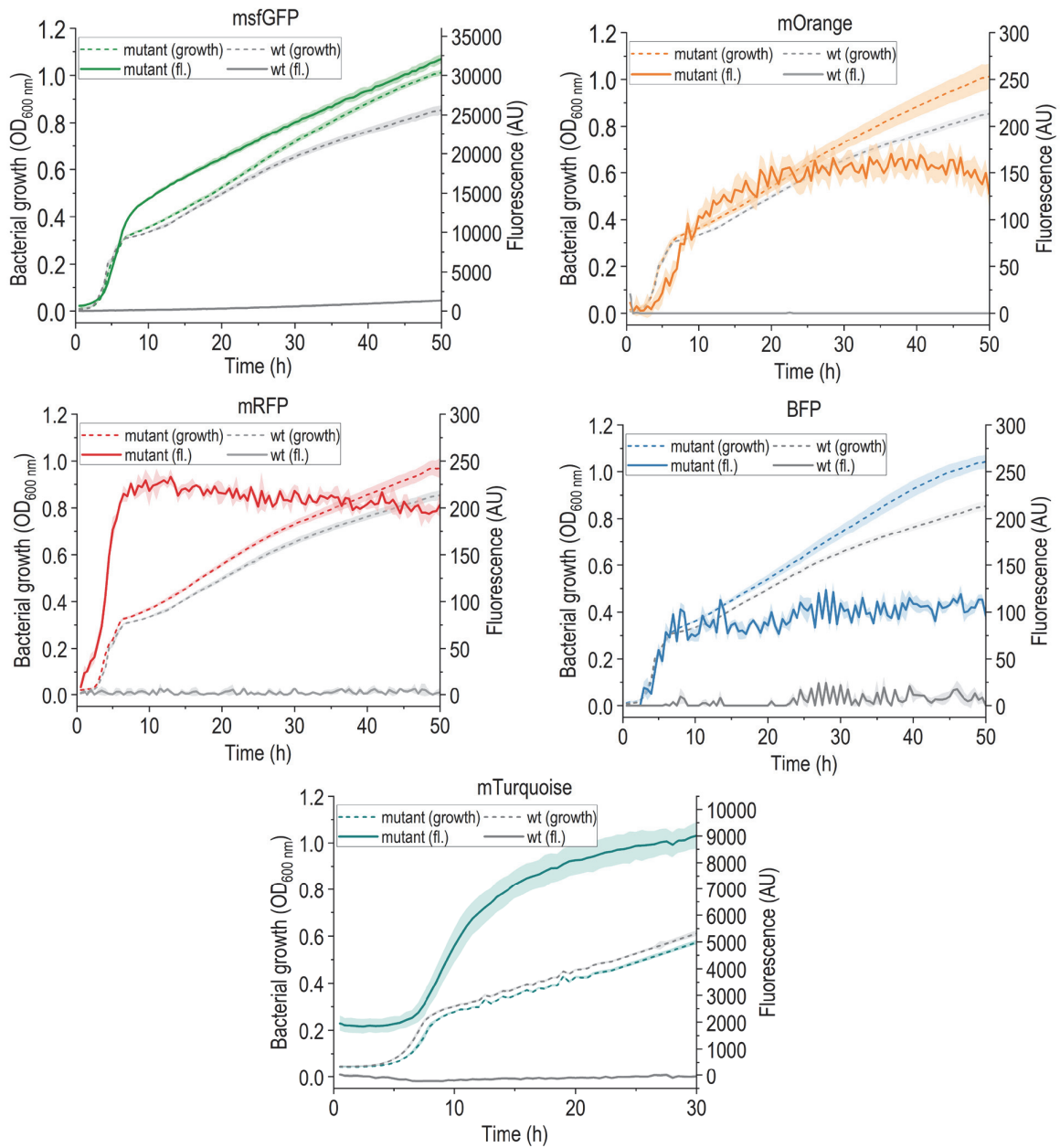


Figure 3.7 Kinetics of the accumulation of fluorescent proteins measured in *P. putida* KT2440. Mutant and wild-type cells were grown in 96-well plates, covered with sealing membranes, in DBM medium supplemented with 30 mM citrate as the sole carbon source. Growth and fluorescence kinetics were acquired by measuring the culture optical density at 630 nm ($OD_{630\text{ nm}}$) as well as the excitation/emission values of fluorescent proteins as follows: msfGFP at 485 nm/528 nm, mRFP1 at 582 nm/609 nm, mBFP2 at 385 nm/450 nm, mOrange2 at 541 nm/567 nm, and mTurquoise2 at 451 nm/477 nm. Error bars indicate standard deviations from three biological replicates.

3.4.4 Elimination of the *ben* catabolic activities of *Pseudomonas putida* KT2440

P. putida strain mt-2 carries the catabolic plasmid pWW0, which allows the cells to assimilate toluene, xylene, and ethylbenzene via the TOL degradation pathway²¹⁹. The involved biochemical reactions can be divided into two functional segments, the *upper* TOL pathway and the *meta*-cleavage route, and the respective enzymes are encoded in two separate gene clusters²²⁰. Through the action of the *upper* pathway enzymes, the methyl group attached to the aromatic substrates is sequentially oxidized to yield the respective carboxylic acid. These metabolites are further processed into the corresponding catechol, which is then cleaved in the *meta* position to yield a semialdehyde²²¹. The aldehyde can be further assimilated into the central carbon metabolites pyruvate and acetyl coenzyme A. The mt-2 strain as well as its descendant KT2440 also harbor an *ortho*-cleavage pathway for the degradation of benzoate(s), chromosomally encoded in the *ben* gene cluster⁸⁶. While specialized on its native substrate benzoate (discussed in detail in **Chapter 5**), the Ben enzymes also show some activity on the methyl-substituted derivative 3-*mBz*²²², leading to 3-methylcatechol (**Figure 3.8A**). The spontaneous oxidation and polymerization of 3-methylcatechol results in the formation of brown-colored polymers²²³, which interfere with colorimetric and fluorimetric determinations (e.g., bacterial growth assessed by optical density measurements). This interference is a common nuisance when utilizing the *XylS/Pm* expression system induced by 3-*mBz* in *P. putida*.

We set out to eliminate the *ben* gene cluster of *P. putida* KT2440 using the described genome engineering procedure with self-curing auxiliary vectors. To this end, we equipped the suicide plasmid pSNW2 with HAs to remove a chromosomal 3.8-kb DNA fragment comprising *benA*, *benB*, *benC*, and *benD* (**Figure 3.8B**). The resulting vector pSNW2- Δ *benABCD* was integrated into the chromosome. Resolving of the suicide plasmid was induced by the self-curing vector pQUIRE6-H. Three successive cultivation steps (firstly, selecting for msfGFP-positive cells after pSNW2- Δ *benABCD* co-integration; secondly, selecting for msfGFP-negative/mRFP-positive colonies after transformation with pQUIRE6-H; thirdly, picking clones that have lost all fluorescent

markers) sufficed to generate plasmid-free *P. putida* $\Delta benABCD$ clones in < 3.5 days. Colonies grown on LB medium plates supplemented with 3-*mBz* did not show any pigmentation, providing evidence for the Ben⁻ phenotype (**Figure 3.8**).

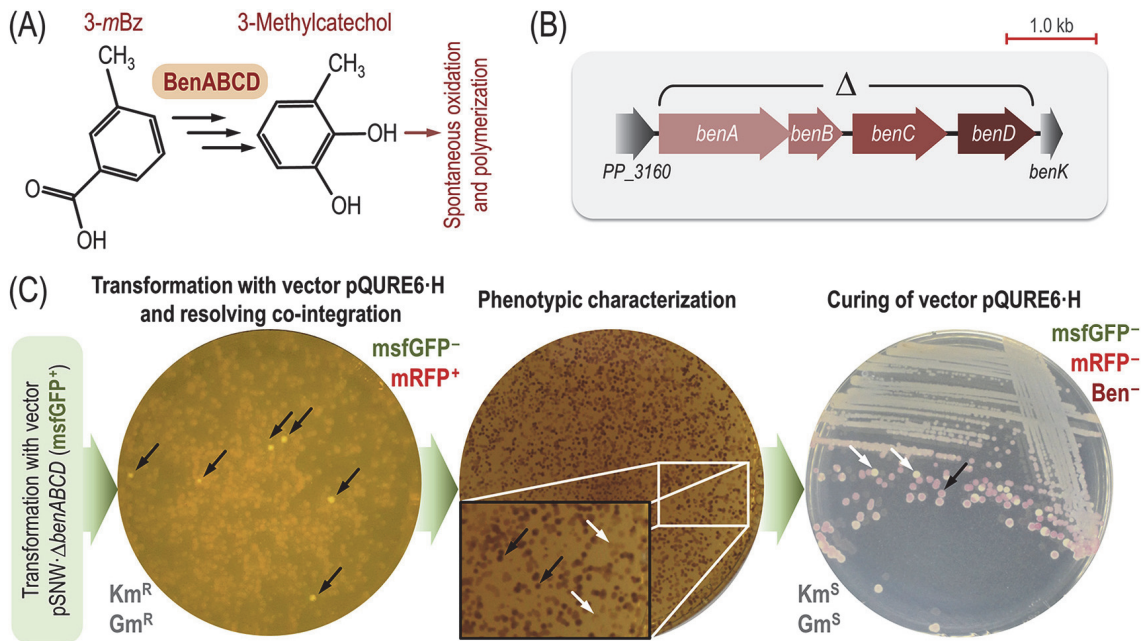


Figure 3.8. Elimination of the Ben catabolic activities of *P. putida* through quick genome engineering using self-curing pQURE vectors. (A) The Ben activities mediate the conversion of 3-methylbenzoate (3-*mBz*) into 3-methylcatechol, which undergoes spontaneous oxidation and polymerization into brown-coloured aggregates. (B) Genomic structure of the *ben* locus in *P. putida* KT2440. The individual genes within the cluster encode BenA, subunit α of benzoate 1,2-dioxygenase; BenB, subunit β of benzoate 1,2-dioxygenase; BenC, electron transfer component of benzoate 1,2-dioxygenase; and BenD, 1,2-dihydroxybenzoate dehydrogenase. The Δ symbol identifies the genomic region targeted for deletion. (C) Overview of the engineering process to delete *benABCD* in *P. putida* KT2440. Co-integration of the suicide plasmid pSNW- $\Delta benABCD$ (**Table 3.1**) into the chromosome can be screened for by selecting clones that display a Km^R and msfGFP⁺ phenotype. After confirming the genotype of the co-integrants by colony PCR, they were transformed with vector pQURE6-H (*XylS/Pm*→*trfA*, Gm^R). This strain was grown for 5 h in the presence of 3 mM 3-*mBz* and plated onto solid LB medium (with 1 mM 3-*mBz*) to recover msfGFP⁻ and mRFP⁺ colonies. The very few colonies still displaying msfGFP fluorescence (indicated with black arrows) were discarded. The deletion of *benABCD* results in a Ben⁻ phenotype, characterized by the absence of brown pigmentation of $\Delta benABCD$ -colonies in the presence of 3-*mBz*. To assess this phenotype, colonies were plated onto solid LB medium containing 2 mM 3-*mBz* and incubated at 30°C for 24 h. The Ben⁺ (black arrows) or Ben⁻ (white arrows) phenotypes were clearly spotted after storing the plates at 4°C for one additional day. The final step of the procedure was the self-curing of vector pQURE6-H, accomplished by streaking a Ben⁻ colony onto a non-selective medium plate (i.e., neither 3-*mBz* nor any antibiotic are added). After a 24-h incubation at 30°C, msfGFP⁻ and mRFP⁻ colonies were easily spotted (white arrows) and could be distinguished from mRFP⁺ clones (still retaining vector pQURE6-H, black arrow) even in white light. Relevant genotypes were confirmed by PCR amplification of the corresponding genomic regions with specific oligonucleotides and DNA sequencing.

3.5. Discussion

The present genome engineering protocol reduces the hands-on work of the original procedure by Martínez-García and de Lorenzo¹⁸⁷. We further streamlined the protocol with (i) the adoption of the *USER* assembly method that enables a standardized workflow¹⁹¹, (ii) a reporter function (i.e., fluorescence) for the donor plasmid that allows for its direct visualization within host cells²²⁴, (iii) additional antibiotic resistances to broaden the host spectrum, and (iv) CRISPR/Cas9 counterselection, particularly relevant for the construction of difficult knock-outs. The protocol described herein yields reliable results for targeted mutagenesis in *Pseudomonas* species within a standard workweek.

The plasmid-curing step during genome engineering typically consumed several days during the routine loss-by-dilution protocol. With the use of the self-curing auxiliary plasmids, this procedure has been brought down to a mere overnight cultivation in a simple culture medium (omitting 3-*mBz* in its formulation). Owing to the presence of red fluorescent markers in pQURE vectors (the output level of which can be selected according to the application), laborious sensitivity screenings are entirely circumvented. Furthermore, for applications where achieving a vector loss efficiency of 100% is crucial, plasmid-free bacteria can be isolated by fluorescence-activated cell sorting. The self-curing vectors are of particular value for curing plasmid DNA from cells that are severely impaired in growth (as some of the strains discussed in **Chapter 4**) and are thus less prone to lose plasmids during proliferation.

We have illustrated the flexibility of this system by combining different molecular elements of the toolbox to delete genomic regions in *P. putida* KT2440 and demonstrated the functionality of four new fluorescent proteins (mRFP1, BFP2, mOrange2, and mTurquoise2) in this host via their targeted integration into a landing site in the chromosome. While the synthetic biology toolbox for *Pseudomonas* is subjected to continuous improvement, the protocol discussed herein represents the fastest extant procedure for genome editing of *P. putida* and related species.

Because of the ease with which it can be used to achieve gene deletions and insertions, this protocol formed the basis for realizing the various strain designs discussed in the following chapters of this thesis (**Chapter 4** and **5**). Furthermore, the method is currently being employed for continued genome-reduction efforts in *P. putida* KT2440¹⁸⁰. In the following section, previous efforts to generate genome-reduced strains and their potential for biotechnological applications are discussed.

3.6. Biotechnological applications of reduced-genome variants of *Pseudomonas putida*

With efficient molecular tools at hand that are compatible with *P. putida*, very extensive chromosome editing projects are possible. Since the genetic engineering process itself constitutes no longer a significant bottleneck, scientists can take up the search for functions within the genome that are of no use or even undesired for a robust microbial cell factory. A wide variety of experimental approaches has been used within the last decade to identify and study essential genes, e.g., in *E. coli*, *Bacillus subtilis*, or *Pseudomonas aeruginosa*. These methods comprise targeted gene deletions, the generation of conditional knockout mutants, genome-wide RNA interference screens, and libraries acquired through saturation transposon mutagenesis²²⁵⁻²³¹.

In *E. coli*, the list of genes considered essential consists of 300 open reading frames (ORFs) out of a number of 4288²³⁰. These ORFs encode functions required for protein synthesis and quality control, cell wall biosynthesis, cell division, DNA replication and chromosome maintenance, RNA synthesis, and degradation, as well as core metabolic functions²³¹. However, while we understand more and more about the genes that allow a biological cell to survive and sustain growth, we still lack knowledge about functions that become essential in conditions different from those defined to study gene essentiality. Moreover, within the category of genes considered non-essential, there can be found some that ensure cell robustness and resistance to different types of stress, and many genes still encode for functions that thus far have not been identified^{232,233}. Because of these deficits in our understanding of complex biological systems, the idea of designing a “minimal cell” from its roots is currently less auspicious than identifying a suitable biological *chassis* that already displays desired characteristics and remove unnecessary and unwanted properties—while adding others.

Being a ubiquitous bacterium that can be found in a large variety of different habitats, *P. putida* is adapted to survive and thrive under very diverse conditions and using a wealth of different substrates. Therefore, it has acquired many functions that are not essential for survival under the controlled conditions of a bio-fermentation setup. Although a set of “essential” genes depends on the given application, one can identify

certain gene sets that encode functions generally classified as having adverse effects. First, these functions can be related to metabolic regulations and biochemical processes that affect the consumption of a chosen substrate and its conversion into a desired product⁷³. When adopting synthetic devices or systems to produce heterologous enzymes in order to access new metabolic routes or to produce such proteins themselves, the accompanying biochemical functions should not interfere with the extant metabolism. Consequently, they should be largely metabolically inert or entirely decoupled from the host biochemistry²³⁴. Molecular devices should furthermore not interfere with the native regulation patterns—which in some cases are poorly understood.

A suitable approach to designing a microbial platform for the production of certain aromatic compounds could be to first remove the comprehensive collection of functions related to their metabolism and implement completely orthogonal systems for their production²³⁵. When adopting the widely used *XylS/P_m* regulator/promoter system for the inducible expression of genes²³⁶, for instance, the native regulation system in *P. putida* was shown to respond by activating a range of different metabolic and regulatory genes upon exposure to one of the system's diverse effectors (benzoic acid and derivatives thereof)^{237,238}. In addition, a well-known nuisance when using *P. putida* for the production of biofuels (and structurally related molecules) is its remarkable capacity to degrade the final products and intermediate metabolites by the action of many different and promiscuous oxidoreductases and other catabolic activities²³⁹. Thus, getting rid of such metabolic activities while at the same time taking advantage of the other metabolic and stress endurance traits that the *chassis* provides is a key step toward creating an ideal whole-cell biocatalyst.

A variety of cellular processes affect the internal supply of metabolic currencies that are needed within a myriad of biochemical processes [e.g., NAD(P)H and ATP, reflected in the energy charge and redox ratios] without providing a benefit in a production setup. Besides being used to facilitate biochemical reactions that would otherwise be unfavorable, ATP is required in large quantities to ensure the proper folding of polypeptides, mediated by the essential chaperon complex GroEL/ES. In fact,

GroEL/ES is one of the cellular processes with the highest demand for ATP, especially when the proteome is compromised by physical and chemical stresses²⁴⁰. Thus, it seems evident that one limiting factor for the quantitative production of foreign proteins is the supply of ATP.

One example of an energy-wasting process is the flagellar motion that many bacteria use to move from a location of nutrient scarcity to one that provides substrates that are needed for growth as well as oxygen—a process that appears redundant in a stirred fermentation tank. In 2014, Martínez-García et al.²⁴¹ reported the removal of a large stretch of DNA (~70 kb, corresponding to ~1.1% of the genome) from the chromosome of *P. putida* KT2440, including 69 relevant structural and regulatory genes for the assembly and export of flagella as well as several chemotaxis functions. This operation resulted in a diverse set of physiological changes in the reduced-genome strain. Most obviously, a complete absence of cell motility was observed, resulting in higher sedimentation rates. The loss of the outer membrane-associated flagella furthermore decreased surface hydrophobicity, a property that is of advantage for mixed planktonic culture systems because it reduces the formation of biofilms that complicate purification processes and impairs fermentation equipment. Indeed, non-flagellated cells demonstrated substantially decreased biofilm formation in an early phase of the cultivation. However, after 24 h of prolonged cultivation, the formation of biofilms was increased compared to the wild-type strain due to an elevated production of exopolysaccharides, possibly triggered by incipient nutrient starvation and oxygen limitation. It will have to be determined which effect is dominant in a large-scale production setup or if the long-term response can be countered by further strain engineering.

Most significant were, however, the changes that could be observed within the mutant metabolism. The lag phase after exposure to various carbon sources was reduced, and the maximum growth rate was significantly altered (i.e., decreased for growth in complex medium and in minimal medium with glucose and succinate as sole carbon sources, increased for growth on fructose). This was accompanied by a change in the ATP/ADP ratio (i.e., the energy charge of the cell) by a factor of ~1.3. Concurrently,

the non-flagellated mutant had a 1.2-fold higher NADPH/NADP⁺ ratio than the wild-type strain while the catabolic charge (i.e., the NADH/NAD⁺ ratio) remained essentially constant. An increased availability of NADPH does not only enhance the anabolic capacity of the cell for biosynthesis but also increases its tolerance toward oxidative stress and UV exposure^{242,243}—a trait that is useful for most industrially relevant fermentation and biotransformation applications.

An essential property of a cell factory in large-scale production scenarios is its genetic stability²⁴⁴. Unless countered via the implementation of some sort of product-addiction mechanism that ensures that cells maintain a producing phenotype, genetically modified cell factories tend to escape the metabolic burden that was imposed on them through evolutionary mechanisms. These processes result in mutations that lead to a loss of function within the overexpressed genes or pathways. Genetic diversity within a population of bacterial cells is favorable in a natural context because it enables the adaptation of the organism to changing environments, but it is detrimental for a robust cell factory²⁴⁵.

In nature, mutations in the genome can be caused through errors made by DNA polymerases during replication, by error-prone DNA repair mechanisms, or because of external stress factors, e.g., UV irradiation or mutagenic chemicals. Yet another source of genetic instability lies dormant within the chromosome of many bacteria in the form of viral DNA and transposing elements, where these elements can constitute up to 20% of the chromosome²⁴⁶. Lysogenic phages can be found within the genomic sequence of many bacteria. They usually become inactive until cells encounter certain stresses such as DNA damage or nutrient starvation or because of stochastic events that trigger their excision and resumption of a lytic cycle^{246,247}. Although subject to continuous decay while resting within the bacterial chromosome, they often retain some of their gene functions if they provide a benefit for the host. For example, prophages can express immunity and exclusion systems that provide a barrier for the superinfection with a related phage. The prophage could have introduced fitness-enhancing genes that it had acquired horizontally from different sources (e.g., antibiotic or stress resistance determinants^{248,249}). Another function that is regularly retained is that of

transposition within the genome. While mobile genetic elements might contain beneficial functions under certain (selective) conditions, thus being selected for in a positive way, they also represent a disruptive mutagenic force by randomly inserting into gene clusters that are crucial for a producing phenotype.

In *P. putida* KT2440, 2.6% of the genome was found to encode phage-related functions, distributed about four prophage elements, each containing up to 72 ORFs²⁴¹. Intensive studies on their functionality revealed that none of the prophages was able to re-initiate a lytic cycle despite having the ability to be excised under specific environmental conditions. However, deletion of all prophage regions led to enhanced tolerance to a diverse set of stress factors. Prophage-less *P. putida* showed increased survival in stationary phase and lower sensitivity to UV-irradiation and to various types of chemical mutagens. Moreover, the removal of the proviral load led to an increase in fitness in a set of different culture media compositions²⁴¹.

Extensive analysis of the annotated genome of *P. putida* KT2440 further revealed the presence of 54 transposable elements, one of which (Tn4652) has been reported to become particularly active in vivo under carbon starvation²⁴⁷. As will be discussed in **Chapter 4**, the excision of a chromosomal segment of 95 kb located 1 kb downstream of Tn4652 could have contributed to restoring prototrophy on glucose for a synthetic C2-auxotroph *P. putida* in this thesis. In a study published in 2014, Martínez-García et al.²⁴¹ removed all of these mobile genetic elements together with the previously established targets for genome reduction in *P. putida* (i.e., the flagellar system and proviral elements) as well as dsDNA-degrading systems that are likely to interfere with the introduction of foreign DNA during genetic engineering efforts. The deleted regions comprised a total number of 299 genes corresponding to ~4.3% of the genome in *P. putida* KT2440 and resulted in the cell-factory strain *P. putida* EM42. This strain was subjected to extensive physiological and genetic characterization.

As already described for a flagella-less strain, lag phases were consistently decreased on various carbon sources, likely due to an increased NADPH/NADP⁺ ratio that enabled the cells to overcome oxidative stress during starvation^{242,243}. The growth performance of such a genome-reduced variant in complex medium was slightly decreased,

while growth in defined media was not affected for any of the various carbon sources tested. However, the genome-reduced strain was able to form significantly more biomass from the same amount of substrate, suggesting that the multiple deletions reduced the maintenance requirements during the cultivation. This experimental observation is in line with an elevated energy charge in strain EM42 (likely due to the absence of flagella, as described above), as well to as an increased intracellular concentration of the central metabolite acetyl-CoA—thereby indicating a better availability of resources for the synthesis of biomass components. The altered maintenance requirements of genome-reduced *P. putida* strains were later confirmed quantitatively²⁵⁰. Because of the ATP-dependency that is inherent to the expression of heterologous proteins, an increased energy availability resulted in a more efficient production of foreign polypeptides by *P. putida* EM42, as shown within the same study as well as in further experiments^{242,250}. Finally, the surplus of ATP allows strain EM42 to survive and even grow at elevated temperatures (42°C) that are usually lethal for wild-type strain *P. putida* KT2440²⁵¹.

Recently, strain EM42 was subjected to further genome reductions removing functions that can be disadvantageous in a laboratory setting¹⁸⁰. Specifically, we sought to remove key chromosomal elements encoding functions that might (i) confer resistance to β -lactam antibiotics, (ii) interfere with the use of fluorescent markers, and (iii) interfere with the use of 3-*mBz* as an inducer of the *XylS/Pm* expression system. Examination of the genome of strain EM42 identified ten chromosomal targets to achieve these goals: eight β -lactamase and β -lactamase-like genes, the siderophore gene *pvdD*, and the *benABCD* gene cluster.

P. putida exhibits naturally high resistance to ampicillin (Amp), limiting the use of β -lactams for selection purposes. Both efflux pumps and β -lactamases are responsible for this resistance. Removal of the efflux pumps in strain KT2440 increased susceptibility to these antibiotics but simultaneously undermined solvent resistance²⁵². Therefore, the deletions were restricted to the eight genes putatively encoding for β -lactamases or metallo- β -lactamase family proteins to reduce resistance to Amp without affecting solvent tolerance. In addition, *pvdD* was deleted, encoding for a large non-

ribosomal peptide synthase involved in siderophore formation²⁵³. Siderophores are high-affinity iron-chelating molecules essential for capturing metal from the environment²⁵⁴. Not only is the energy- and resource-intensive biosynthesis of these secondary metabolites unnecessary in the presence of sufficient iron (as under laboratory conditions), but siderophores also exhibit fluorescent properties^{255,256} that can interfere with the measurement of introduced reporter functions. Finally, the catabolic activities of the *ortho*-cleavage pathway were targeted to facilitate the use of the XylS/*Pm* expression system (**Section 3.4.4**). The genes encoding these functions are distributed throughout the bacterial chromosome.

The deletion of all genes resulted in a reduction of approximately 23 kb in the genome of strain EM42, resulting in the streamlined *P. putida* strain SEM10. This strain showed increased sensitivity to β -lactam antibiotics, allowing ampicillin resistance determinants (Amp^R) to be used as selection markers at similar antibiotic concentrations as for *E. coli*¹⁸⁰. In *P. putida* SEM10 cultures grown in the presence of 3-*mBz*, the removal of *benABCD* prevented the development of 3-methylcatechol-derived pigments (**Section 3.4.4**). The removal of *pvdD* significantly reduced the autofluorescence of the genome-reduced strain. On the other hand, no change in the strain's growth phenotype was observed in a complete medium or defined medium with citrate as a carbon source compared to *P. putida* EM42, suggesting that the introduced deletions are irrelevant for the cells' fitness under controlled laboratory conditions¹⁸⁰.

Further genome reduction of strain SEM10 towards a reference *chassis* is currently underway in our laboratory—an overarching objective that profits from the rapid genome engineering strategies presented here. These tools furthermore facilitated the intricate metabolic engineering projects presented in the following two chapters.

Table 3.4. Bacterial strains used in this chapter.

Strain	Relevant characteristics ^a	Reference or source
<i>Escherichia coli</i>		
DH5 α	Cloning host; F- λ^- <i>endA1 glnX44(AS) thiE1 recA1 relA1 spoT1 gyrA96(Nal^R) rfbC1 deoR nupG Φ80(lacZΔM15) Δ(argF-lac)U169 hsdR17(<i>r_K⁻ m_K⁺</i>)</i>	Hanahan and Meselson ²⁵⁷
DH5 α λ <i>pir</i>	Cloning host; same as DH5 α but λ <i>pir</i> lysogen	Platt et al. ²⁵⁸
HB101	Helper strain used for triparental mating; F- <i>thi-1 hsdS20(r_B⁻, m_B⁻) supE44 recA13 ara-14 leuB6 proA2 lacY1 galk2 rpsL20(Sm^R) xyl-5 mtl-1</i>	Boyer and Roulland-Dussoix ²⁵⁹
<i>Pseudomonas putida</i>		
KT2440	Wild-type strain, derived from <i>P. putida</i> mt-2 ²⁶⁰ cured of the TOL plasmid pWW0	Bagdasarian et al. ²⁶¹
KT2440 Δ <i>aceEF</i>	Same as KT2440, but with an in-frame deletion of the <i>aceEF</i> genes (<i>PP_0038-PP_0339</i>)	This work
KT2440 Δ <i>nicX</i>	Same as KT2440, but with an in-frame deletion of the <i>nicX</i> gene (<i>PP_0395</i>)	This work
KT2440 Δ <i>benABCD</i>	Same as KT2440, but with an in-frame deletion of the <i>ben</i> gene cluster (<i>PP_3161-PP_3164</i>)	
KT-LPR	Same as KT2440, but carrying a P _{14g} (<i>BCD2</i>) \rightarrow <i>mRFP1</i> element integrated between <i>PP_0013</i> (<i>gyrB</i>) and <i>PP_5421</i>	This work
KT-LPG	Same as KT2440, but carrying a P _{14g} (<i>BCD2</i>) \rightarrow <i>msfGFP</i> element integrated between <i>PP_0013</i> (<i>gyrB</i>) and <i>PP_5421</i>	This work
KT-LPB	Same as KT2440, but carrying a P _{14g} (<i>BCD2</i>) \rightarrow <i>bfp2</i> element integrated between <i>PP_0013</i> (<i>gyrB</i>) and <i>PP_5421</i>	This work
KT-LPO	Same as KT2440, but carrying a P _{14g} (<i>BCD2</i>) \rightarrow <i>mOrange2</i> element integrated between <i>PP_0013</i> (<i>gyrB</i>) and <i>PP_5421</i>	This work
KT-LPT	Same as KT2440, but carrying a P _{14g} (<i>BCD2</i>) \rightarrow <i>mTurquoise2</i> element integrated between <i>PP_0013</i> (<i>gyrB</i>) and <i>PP_5421</i>	This work

a. Antibiotic markers: *Nal*, nalidixic acid; and *Sm*, streptomycin.

3.7. Supplementary material

Table 3.S1. Oligonucleotides used in this chapter.

Name	Sequence (5'→3')	T _m (°C) ^a
pSNW-USER_F	AGTCGACCUGCAGGCATGCAAGCTTCT	71.8
pSNW- USER_R	AGGATCUAGAGGATCCCCGGGTACCG	66.1
Seq-pSNW_F	TGAAAACGACGGCCAGT	54.2
Seq-pSNW_R	ATGACCATGATTACGCCGG	55.2
SEVA-T0_F	GAACGCTCGGTTGCCGCC	64.4
nicX_HA1_F	AGATCCUCATGCGGCGGAAGATTTTC	59.1
nicX_HA1_R	ACCCCTACAUCGGGGTTCTCCTGGG	62.7
nicX_HA2_F	ATGTAGGGGUTATACTGGCCGG	59.9
nicX_HA2_R	AGGTCGACUGCAGCAGGTACAAAATGGC	59.1
nicX_g-check_F	GCCTGACGATTTAGAGCG	53.7
nicX_g-check_R	AAGAAGCAGGCCAGAGATG	54.9
LP_HA1_F	AGATCCUTCATCGAAAGTAACGCGC	58.9
LP_HA1_R	ATGCCGAUATACTATGCCGATGATTAATTGTCAACAGAT CAGGTCTGAAGCTCTCG	58.9
LP_HA2_F	ACCAAUTGCTCCAGCGATCAC	59.1
LP_HA2_R	AGGTCGACUGAACACGTTCTCACTGGG	59.6
pS448_F	AGTCGGUGCAATTCGAGCTCGGTACCCG	57.4
pS448_R	ATATGTUTTTCTCTAACC GCGGC	58.3
Cas9_F	AACATAUGGATAAGAAATACTCAATAGGCT	52.2
Cas9_R	AGATCAGUCACCTCCTAGCTGACTCA	55.1
sgRNA_F	ACTGATCUAGAGTGCACCTGCAGGCA	57.7
sgRNA_R	ACCGACUCGGTGCCACTTTTTCAAGTTG	57.3
pS2313_F	ACTAGTCTUGGACTCCTGTTGATAGAT	56.0
pS2313_R	ATGTTTUTCCTCCTAAGCTTGCATG	55.8
pS_BFP2_F	ACATATGGUGTCTAAGGGCGAAGAGCTGAT	58.3
pS_BFP2_R	AGTTTAAUTAAGTTTGTGCCCCAGTTTGCT	59.0
pS_Ora_Tq_F	AAAACAUATGGTGAGCAAGGGCGA	57.8
pS_Ora_Tq_R	AAGACTAGUTTACTTGTACAGCTCGTCCAT	58.9
RFP4LP_F	ATCGGCAUAGTATAATACGACAAGGTGAGGAACTAAACC ACTGAGCACTACTAGAGAAAG	55.6
RFP4LP_R	ATTTGGUAGAGAGCGTTCACCGAC	59.5
P _{14g} (BCD2)_F	AATGGCTUCCTCCGAAGACG	61.2
P _{14g} (BCD2)_R	AGAGCCUTGTCAATGGGCGATCAGGTCTGAAGCTCTCG	58.9
BCD2-P _{14g} _F	AGGCTCUCGCGGCCAGGTATAATTGCACGAGGGCCCAA GTTCACTTAAAAAG	60.9
BCD2-P _{14g} _R	AAGCCATUAGAAAACCTCCTTAGCATGA	58.1
BCD2_R	AGAAAACCUCCTTAGCATGATTAAG	58.4
pGNW_LP_F	AAGTAAUACGCTGATAGTGCTAGTG	57.8
BFP2_F	AGGTTTTCUAATGGTGTCTAAGGGCGAAGAG	61.1
BFP2_R	ATTACTUAATTAAGTTTGTGCCCCAGTTTGC	62.3
GFP_F	AGGTTTTCUAATGCGTAAAGGTGAAGAACTGTTC	60.9
GFP_R	ATTACTUATTTGTAGAGTTCATCCATGCCG	64.0
Ora_Tq_F	AGGTTTTCUAATGGTGAGCAAGGGCGAG	61.7
Ora_Tq_R	ATTACTUGTACAGCTCGTCCATGC	62.1

<i>aceEF_HA1_F</i>	AGATCCUCGAAGACTCGCTTGAAGAGG	59.7
<i>aceEF_HA1_R</i>	AGCCATGUAAGCCAGCACACTGC	55.9
<i>aceEF_HA2_F</i>	ACATGGCUTGCTCCAGGG	58.3
<i>aceEF_HA2_R</i>	AGGTCGACUCGATGAACTGCTGGTTGCG	59.6
<i>Seq-LP_F</i>	ACCAACTTTTCCGCTTTGCAC	57.2
<i>Seq-LP_R</i>	CGAAAGACTGGGCCTTTTCGT	58.4
<i>aceEF_g-check_F</i>	GTTTGGCTGGAGATTTTGGG	54.8
<i>aceEF_g-check_R</i>	CCTTGATCGGCGTGAAATAG	53.8
<i>aceEF_F</i>	GCGCGCTCATTGCGGTACCTGACAT	N.A.
<i>aceEF_R</i>	AAACATGTCAGGTACGCGAATGAGC	N.A.
<i>benABCD_HA1_F</i>	AGATCCUGGTTTATTTACCAAGCGATGGGGA	66.0
<i>benABCD_HA1_R</i>	ATGGCCAGGGUCTCCCTTGTTATTGTTTAG	69.0
<i>benABCD_HA2_F</i>	ACCCTGGCCAUGTGAACCGCAACCTCAAGGCAAA	69.0
<i>benABCD_HA2_R</i>	AGGTCGACUCGTTTCATCAGTGCCACGGC	66.8

- a. The melting temperatures (T_m) were calculated using the online T_m calculator by Thermo Fisher Scientific (only the annealing parts of the primers were included in the analysis). For primers used for PCR amplification with Phusion U polymerase, 'Phusion DNA polymerase' was chosen as the setting, with a primer concentration of 0.5 μ M. For primers used for colony PCR, 'Taq-based DNA polymerase' was chosen as the setting, with a primer concentration of 0.2 μ M. N.A., not applicable (i.e., not used in PCR).

Table 3.S2 Assembly of pGNW plasmids with genes encoding fluorescent proteins within a chromosomal landing pad. Listed are the respective plasmid backbones used for each fluorescent protein, as well as the primers used to amplify these plasmids and the additional fragments to assemble the corresponding DNA fragments. The sequences of the primers are presented in **Table 3.S1**.

Fluorescent protein	Plasmid backbone (oligonucleotide)	Primers for HA1	Primers for gene insert	Primers for HA2
msfGFP	pGNW2 (pGNW_LP_F/ BCD2_R)	–	GFP_F/ GFP_R	–
mBFP2	pGNW2 (pGNW_LP_F/ BCD2_R)	–	BFP2_F/ BFP2_R	–
mOrange2	pGNW4 (pGNW-USER_F/ pGNW-USER_R)	LP_HA1_F/ BCD2_R	Ora_Tq_F/ Ora_Tq_R	pGNW_LP_F/ LP_HA2_R
mTurquoise2	pGNW6 (pGNW-USER_F/ pGNW-USER_R)	LP_HA1_F/ BCD2_R	Ora_Tq_F/ Ora_Tq_R	pGNW_LP_F/ LP_HA2_R

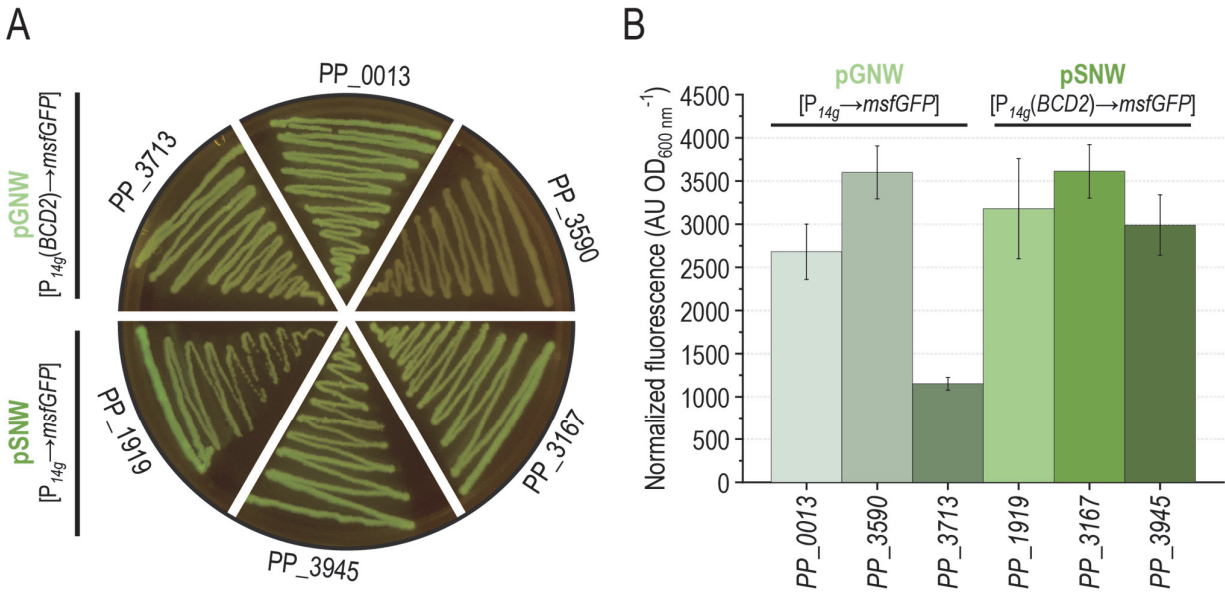


Figure 3.S1. Locus dependency of msfGFP fluorescence expressed from co-integrated suicide vectors. The plasmids pGNW (carrying homology arms for the deletion of *PP_0013*, *PP_3590*, or *PP_3713*) or pSNW (carrying homology arms for the deletion of *PP_1919*, *PP_3167*, or *PP_3945*) were co-integrated into *P. putida* KT2440. The only difference between plasmids of the same type is the insertion locus. **(A)** An individual colony of each co-integrate was streaked onto an LB medium plate containing Km, and incubated overnight (18 h) at 30°C. The plates were photographed under blue-light exposure. **(B)** Normalized green fluorescence (fluorescence intensity divided by the optical density at 600 nm) in *P. putida* KT2440 carrying the vectors co-integrated in the chromosome. Cells were cultured in minimal de Bont medium supplemented with 30 mM glucose in microtiter plates. Data represent the mean value of each parameter \pm standard deviation of three biological replicates.

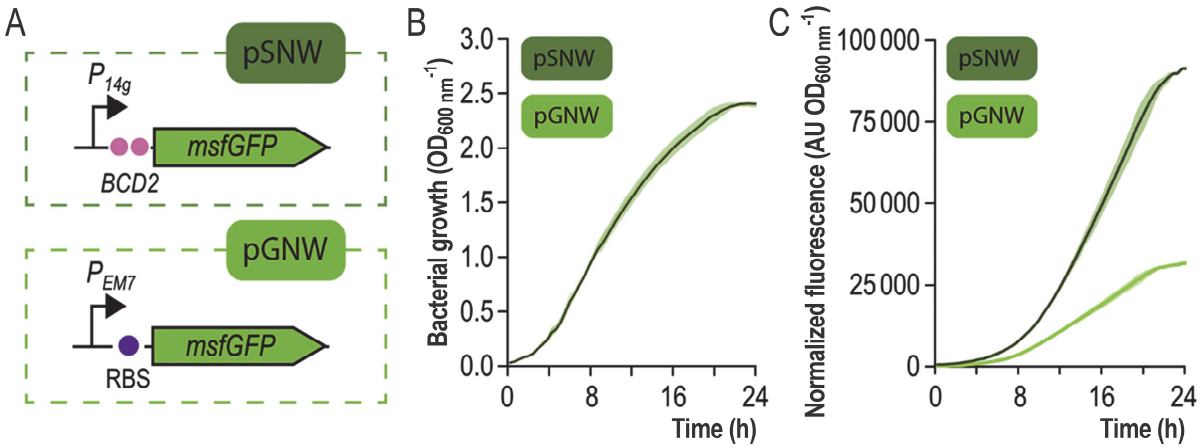


Figure 3.S2 Genetic upgrading of suicide vector pGNW into pSNW. (A) The fluorescence brought about by *msfGFP* in the insertional suicide vector pGNW was enhanced by addition of a bicistronic translational coupler (*BCD2*) in front of the gene. Bacterial growth (B) and green fluorescence levels normalized to the optical density measured at 600 nm ($OD_{600\text{ nm}}$) (C) in *P. putida* KT2440 carrying either pGNW2- $\Delta benABCD$ or pSNW2- $\Delta benABCD$ (which only differ in the genetic architecture of the fluorescent marker added to the backbone) integrated as a single copy into the target chromosomal locus. Cells were grown in LB medium. Error bars indicate standard deviations from at five biological replicates.

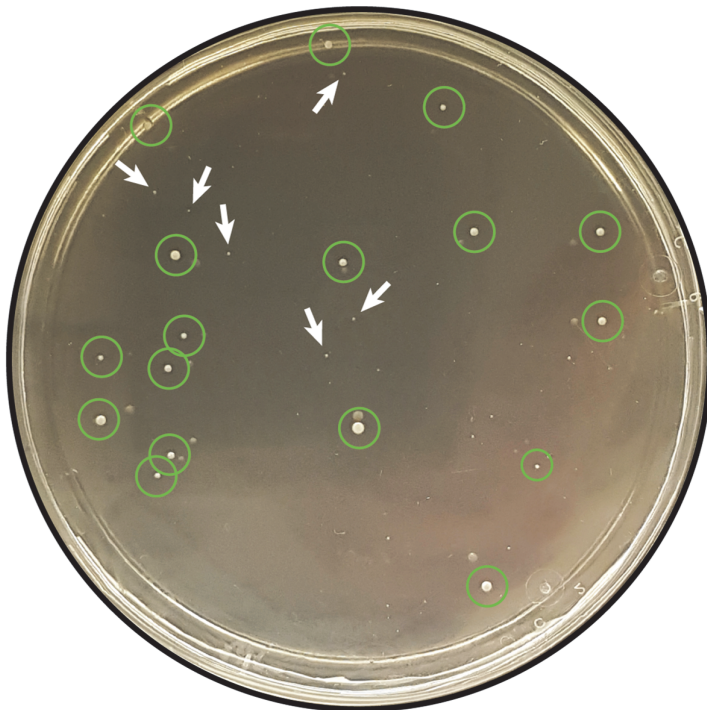
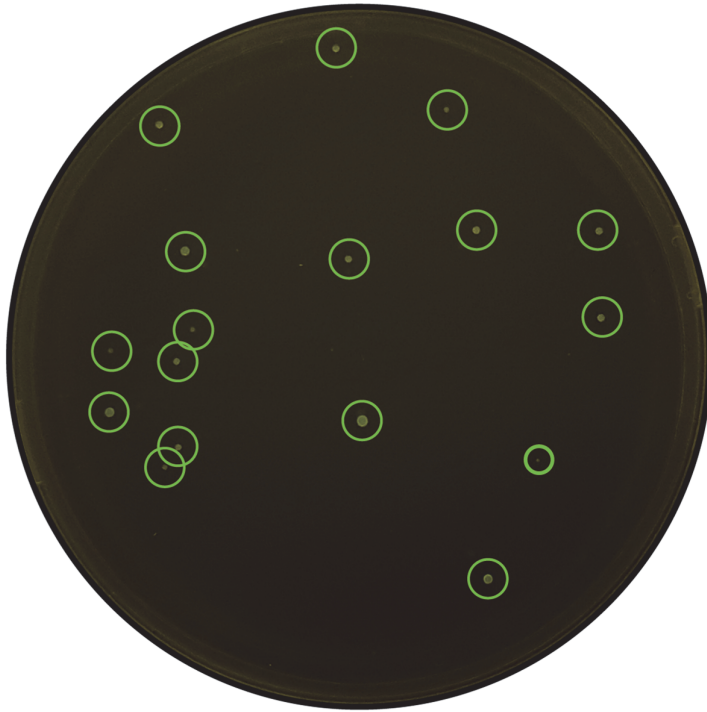


Figure 3.S3 Deletion of *aceEF* in *P. putida* KT2440 using a synthetic CRISPR/Cas9 device for counterselection. Green circles indicate fluorescent colonies that escaped restriction by Cas9; white arrows indicate examples of identified colonies arising from *P. putida* $\Delta aceEF$ cells.

References for Chapter 3

- 38 Calero, P. & Nikel, P. I. **Chasing Bacterial Chassis for Metabolic Engineering: A Perspective Review from Classical to Non-Traditional Microorganisms.** *Microbial Biotechnology* **12**, 98-124, doi: 10.1111/1751-7915.13292 (2019).
- 51 Gibson, D. G., Young, L., Chuang, R.-Y., Venter, J. C., Hutchison, C. A. & Smith, H. O. **Enzymatic Assembly of DNA Molecules up to Several Hundred Kilobases.** *Nature Methods* **6**, 343-345, doi: 10.1038/nmeth.1318 (2009).
- 73 Nikel, P. I. & de Lorenzo, V. ***Pseudomonas putida* as a Functional Chassis for Industrial Biocatalysis: From Native Biochemistry to Trans-Metabolism.** *Metabolic Engineering* **50**, 142-155, doi: 10.1016/j.ymben.2018.05.005 (2018).
- 80 Poblete-Castro, I., Borrero de Acuña, J. M., Nikel, P. I., Kohlstedt, M. & Wittmann, C. **Host Organism: *Pseudomonas putida*.** in *Industrial Biotechnology: Microorganisms* (eds C. Wittmann & J. C. Liao) 299-326 (Wiley-VCH Verlag GmbH & Co. KGaA, 2017).
- 86 Jiménez, J. I., Miñambres, B., García, J. L. & Díaz, E. **Genomic Analysis of the Aromatic Catabolic Pathways from *Pseudomonas putida* KT2440.** *Environmental Microbiology* **4**, 824-841, doi: 10.1046/j.1462-2920.2002.00370.x (2002).
- 101 Sudarsan, S., Dethlefsen, S., Blank, L. M., Siemann-Herzberg, M. & Schmid, A. **The Functional Structure of Central Carbon Metabolism in *Pseudomonas putida* KT2440.** *Appl. Environmental Microbiology* **80**, 5292-5303, doi: 10.1128/AEM.01643-14 (2014).
- 105 Nikel, P. I., Chavarría, M., Fuhrer, T., Sauer, U. & de Lorenzo, V. ***Pseudomonas putida* KT2440 Strain Metabolizes Glucose through a Cycle Formed by Enzymes of the Entner-Doudoroff, Embden-Meyerhof-Parnas, and Pentose Phosphate Pathways.** *Journal of Biological Chemistry* **290**, 25920-25932, doi: 10.1074/jbc.M115.687749 (2015).
- 120 Nelson, K. E., Weinel, C., Paulsen, I. T., Dodson, R. J., Hilbert, H., Martins dos Santos, V. A. P., Fouts, D. E., Gill, S. R., Pop, M., Holmes, M., Brinkac, L., Beanan, M., DeBoy, R. T., Daugherty, S., Kolonay, J. et al. **Complete Genome Sequence and Comparative Analysis of the Metabolically Versatile *Pseudomonas putida* KT2440.** *Environmental Microbiology* **4**, 799-808, doi: 10.1046/j.1462-2920.2002.00366.x (2002).

- 121 Belda, E., van Heck, R. G. A., López-Sánchez, M. J., Cruveiller, S., Barbe, V., Fraser, C., Klenk, H. P., Petersen, J., Morgat, A., Nickel, P. I., Vallenet, D., Rouy, Z., Sekowska, A., Martins dos Santos, V. A. P., de Lorenzo, V. et al. **The Revisited Genome of *Pseudomonas putida* KT2440 Enlightens Its Value as a Robust Metabolic Chassis.** *Environmental Microbiology* **18**, 3403-3424, doi: 10.1111/1462-2920.13230 (2016).
- 126 Martínez-García, E. & de Lorenzo, V. **Molecular Tools and Emerging Strategies for Deep Genetic/Genomic Refactoring of *Pseudomonas*.** *Current Opinion in Biotechnology* **47**, 120-132, doi: 10.1016/j.copbio.2017.06.013 (2017).
- 128 Martínez-García, E., Aparicio, T., Goñi-Moreno, A., Fraile, S. & de Lorenzo, V. **SEVA 2.0: An Update of the Standard European Vector Architecture for De-/Re-Construction of Bacterial Functionalities.** *Nucleic Acids Research* **43**, D1183-D1189, doi: 10.1093/nar/gku1114 (2014).
- 129 Silva-Rocha, R., Martínez-García, E., Calles, B., Chavarría, M., Arce-Rodríguez, A., de las Heras, A., Páez-Espino, A. D., Durante-Rodríguez, G., Kim, J., Nickel, P. I., Platero, R. & de Lorenzo, V. **The Standard European Vector Architecture (SEVA): A Coherent Platform for the Analysis and Deployment of Complex Prokaryotic Phenotypes.** *Nucleic Acids Research* **41**, D666-D675, doi: 10.1093/nar/gks1119 (2013).
- 132 Mutalik, V. K., Guimaraes, J. C., Cambray, G., Lam, C., Christoffersen, M. J., Mai, Q. A., Tran, A. B., Paull, M., Keasling, J. D., Arkin, A. P. & Endy, D. **Precise and Reliable Gene Expression Via Standard Transcription and Translation Initiation Elements.** *Nature Methods* **10**, 354–360, doi: 10.1038/nmeth.2404 (2013).
- 154 Wirth, N. T., Kozaeva, E. & Nickel, P. I. **Accelerated Genome Engineering of *Pseudomonas putida* by I-SceI—Mediated Recombination and CRISPR-Cas9 Counterselection.** *Microbial Biotechnology* **13**, In press, DOI: 10.1111/1751-7915.13396, doi: 10.1111/1751-7915.13396 (2019).
- 180 Volke, D. C., Friis, L., Wirth, N. T., Turlin, J. & Nickel, P. I. **Synthetic Control of Plasmid Replication Enables Target- and Self-Curing of Vectors and Expedites Genome Engineering of *Pseudomonas putida*.** *Metabolic Engineering Communications* **10**, e00126, doi: 10.1016/j.mec.2020.e00126 (2020).
- 181 Volke, D. C., Wirth, N. T. & Nickel, P. I. **Rapid Genome Engineering of *Pseudomonas* Assisted by Fluorescent Markers and Tractable Curing of Plasmids.** *Bio-protocol* **11**, e3917, doi: 10.21769/BioProtoc.3917 (2021).
- 182 Loeschcke, A. & Thies, S. ***Pseudomonas putida*-a Versatile Host for the Production of Natural Products.** *Applied Microbiology and Biotechnology* **99**, 6197-6214, doi: 10.1007/s00253-015-6745-4 (2015).

- 183 Nikel, P. I., Chavarría, M., Danchin, A. & de Lorenzo, V. **From Dirt to Industrial Applications: *Pseudomonas putida* as a Synthetic Biology Chassis for Hosting Harsh Biochemical Reactions.** *Current Opinion in Biotechnology* **34**, 20-29, doi: 10.1016/j.cbpa.2016.05.011 (2016).
- 184 Domröse, A., Weihmann, R., Thies, S., Jaeger, K. E., Drepper, T. & Loeschcke, A. **Rapid Generation of Recombinant *Pseudomonas putida* Secondary Metabolite Producers Using *Ytrex*.** *Synthetic and Systems Biotechnology* **2**, 310-319, doi: 10.1016/j.synbio.2017.11.001 (2017).
- 185 Cook, T. B., Rand, J. M., Nurani, W., Courtney, D. K., Liu, S. A. & Pfleger, B. F. **Genetic Tools for Reliable Gene Expression and Recombineering in *Pseudomonas putida*.** *Journal of Industrial Microbiology and Biotechnology* **45**, 517-527, doi: 10.1007/s10295-017-2001-5 (2018).
- 186 Wynands, B., Lenzen, C., Otto, M., Koch, F., Blank, L. M. & Wierckx, N. J. P. **Metabolic Engineering of *Pseudomonas Taiwanensis* Vlb120 with Minimal Genomic Modifications for High-Yield Phenol Production.** *Metabolic Engineering* **47**, 121-133, doi: 10.1016/j.ymben.2018.03.011 (2018).
- 187 Martínez-García, E. & de Lorenzo, V. **Engineering Multiple Genomic Deletions in Gram-Negative Bacteria: Analysis of the Multi-Resistant Antibiotic Profile of *Pseudomonas putida* KT2440.** *Environmental Microbiology* **13**, 2702-2716, doi: 10.1111/j.1462-2920.2011.02538.x (2011).
- 188 Smith, C., Day, P. J. & Walker, M. R. **Generation of Cohesive Ends on PCR Products by Udg-Mediated Excision of Du, and Application for Cloning into Restriction Digest-Linearized Vectors.** *PCR Methods and Applications* **2**, 328-332, doi: 10.1101/gr.2.4.328 (1993).
- 189 Bitinaite, J. & Nichols, N. M. **DNA Cloning and Engineering by Uracil Excision.** *Current Protocols in Molecular Biology* **3**, 3.21, doi: 10.1002/0471142727.mb0321s86 (2009).
- 190 Nour-Eldin, H. H., Geu-Flores, F. & Halkier, B. A. **USER Cloning and USER Fusion: The Ideal Cloning Techniques for Small and Big Laboratories.** *Methods in Molecular Biology* **643**, 185-200, doi: 10.1007/978-1-60761-723-5_13 (2010).
- 191 Cavaleiro, A. M., Kim, S. H., Seppälä, S., Nielsen, M. T. & Nørholm, M. H. **Accurate DNA Assembly and Genome Engineering with Optimized Uracil Excision Cloning.** *ACS Synthetic Biology* **4**, 1042-1046, doi: 10.1021/acssynbio.5b00113 (2015).

- 192 Karunakaran, P., Endresen, D. T., Ertesvåg, H., Blatny, J. M. & Valla, S. **A Small Derivative of the Broad-Host-Range Plasmid RK2 Which Can Be Switched from a Replicating to a Non-Replicating State as a Response to an Externally Added Inducer.** *FEMS Microbiology Letters* **180**, 221-227, doi: 10.1111/j.1574-6968.1999.tb08799.x (1999).
- 193 Kessler, B., de Lorenzo, V. & Timmis, K. N. **A General System to Integrate *lacZ* Fusions into the Chromosomes of Gram-Negative Eubacteria: Regulation of the *P_m* Promoter of the TOL Plasmid Studied with All Controlling Elements in Monocopy.** *Molecular Genetics and Genomics* **233**, 293-301, doi: 10.1007/BF00587591 (1992).
- 194 Campbell, R. E., Tour, O., Palmer, A. E., Steinbach, P. A., Baird, G. S., Zacharias, D. A. & Tsien, R. Y. **A Monomeric Red Fluorescent Protein.** *Proceedings of the National Academy of Science USA* **99**, 7877-7882, doi: 10.1073/pnas.082243699 (2002).
- 195 Subach, O. M., Cranfill, P. J., Davidson, M. W. & Verkhusha, V. V. **An Enhanced Monomeric Blue Fluorescent Protein with the High Chemical Stability of the Chromophore.** *PloS One* **6**, e28674, doi: 10.1371/journal.pone.0028674 (2011).
- 196 Shaner, N. C., Lin, M. Z., McKeown, M. R., Steinbach, P. A., Hazelwood, K. L., Davidson, M. W. & Tsien, R. Y. **Improving the Photostability of Bright Monomeric Orange and Red Fluorescent Proteins.** *Nature Methods* **5**, 545-551, doi: 10.1038/nmeth.1209 (2008).
- 197 Goedhart, J., von Stetten, D., Noirclerc-Savoye, M., Lelimosin, M., Joosen, L., Hink, M. A., van Weeren, L., Gadella, T. W. & Royant, A. **Structure-Guided Evolution of Cyan Fluorescent Proteins Towards a Quantum Yield of 93%.** *Nature Communications* **3**, 751, doi: 10.1038/ncomms1738 (2012).
- 198 Aparicio, T., de Lorenzo, V. & Martínez-García, E. **CRISPR/Cas9-Based Counterselection Boosts Recombineering Efficiency in *Pseudomonas putida*.** *Biotechnol. J.* **13**, e1700161, doi: 10.1002/biot.201700161 (2018).
- 199 Landgraf, D. **Quantifying Localizations and Dynamics in Single Bacterial Cells** Ph.D. thesis, Harvard University, (2012).
- 200 Zobel, S., Benedetti, I., Eisenbach, L., de Lorenzo, V., Wierckx, N. & Blank, L. M. **Tn7-Based Device for Calibrated Heterologous Gene Expression in *Pseudomonas putida*.** *ACS Synthetic Biology* **4**, 1341-1351, doi: 10.1021/acssynbio.5b00058 (2015).

- 201 Martínez-García, E., Goñi-Moreno, A., Bartley, B., McLaughlin, J., Sánchez-Sampedro, L., Pascual del Pozo, H., Prieto Hernández, C., Marletta, A. S., De Lucrezia, D., Sánchez-Fernández, G., Fraile, S. & de Lorenzo, V. **SEVA 3.0: An Update of the Standard European Vector Architecture for Enabling Portability of Genetic Constructs among Diverse Bacterial Hosts.** *Nucleic Acids Research* **48**, D1164-D1170, doi: 10.1093/nar/gkz1024 (2019).
- 202 Sambrook, J., Russell, D. W., Sambrook, J. & Russell, D. W. **Molecular Cloning: A Laboratory Manual.** (Cold Spring Harbor Laboratory Press {a}, 2001).
- 203 Cavaleiro, A. M., Kim, S. H., Seppala, S., Nielsen, M. T. & Norholm, M. H. **Accurate DNA Assembly and Genome Engineering with Optimized Uracil Excision Cloning.** *ACS Synthetic Biology* **4**, 1042-1046, doi: 10.1021/acssynbio.5b00113 (2015).
- 204 Don, R. H., Cox, P. T., Wainwright, B. J., Baker, K. & Mattick, J. S. **'Touchdown' PCR to Circumvent Spurious Priming During Gene Amplification.** *Nucleic Acids Research* **19**, 4008, doi: 10.1093/nar/19.14.4008 (1991).
- 205 Korbie, D. J. & Mattick, J. S. **Touchdown PCR for Increased Specificity and Sensitivity in PCR Amplification.** *Nature Protocols* **3**, 1452-1456, doi: 10.1038/nprot.2008.133 (2008).
- 206 Bhaya, D., Davison, M. & Barrangou, R. **CRISPR-Cas Systems in Bacteria and Archaea: Versatile Small RNAs for Adaptive Defense and Regulation.** *Annual Review of Genetics* **45**, 273-297, doi: 10.1146/annurev-genet-110410-132430 (2011).
- 207 Blin, K., Pedersen, L. E., Weber, T. & Lee, S. Y. **Crispy-web: An Online Resource to Design sgRNAs for CRISPR Applications.** *Synthetic and Systems Biotechnology* **1**, 118-121, doi: 10.1016/j.synbio.2016.01.003 (2016).
- 208 Ruiz, J. A., Fernández, R. O., Nikel, P. I., Méndez, B. S. & Pettinari, M. J. **Dye(Arc)Mutants: Insights into an Unexplained Phenotype and Its Suppression by the Synthesis of Poly (3-Hydroxybutyrate) in Escherichia coli Recombinants.** *FEMS Microbiology Letters* **258**, 55-60, doi: 10.1111/j.1574-6968.2006.00196.x (2006).
- 209 Jiang, W., Bikard, D., Cox, D., Zhang, F. & Marraffini, L. A. **RNA-Guided Editing of Bacterial Genomes Using CRISPR-Cas Systems.** *Nature Biotechnology* **31**, 233-239, doi: 10.1038/nbt.2508 (2013).
- 210 Choi, K. H., Kumar, A. & Schweizer, H. P. **A 10-Min Method for Preparation of Highly Electrocompetent Pseudomonas aeruginosa Cells: Application for DNA Fragment Transfer between Chromosomes and Plasmid Transformation.** *Journal of Microbiological Methods* **64**, 391-397, doi: 10.1016/j.mimet.2005.06.001 (2006).

- 211 Jiménez, J. I., Canales, Á., Jiménez-Barbero, J., Ginalska, K., Rychlewski, L., García, J. L. & Díaz, E. **Deciphering the Genetic Determinants for Aerobic Nicotinic Acid Degradation: The *Nic* Cluster from *Pseudomonas putida* KT2440.** *Proceedings of the National Academy of Science USA* **105**, 11329-11334, doi: 10.1073/pnas.0802273105 (2008).
- 212 Jiménez, J. I., Fraile, S., Zafra, O. & de Lorenzo, V. **Phenotypic Knockouts of Selected Metabolic Pathways by Targeting Enzymes with Camel-Derived Nanobodies (VHHs).** *Metabolic Engineering* **30**, 40-48, doi: 10.1016/j.ymben.2015.04.002 (2015).
- 213 Nikel, P. I., Martínez-García, E. & de Lorenzo, V. **Biotechnological Domestication of Pseudomonads Using Synthetic Biology.** *Nature Reviews Microbiology* **12**, 368-379, doi: 10.1038/nrmicro3253 (2014).
- 214 Reed, L. J., Pettit, F. H., Eley, M. H., Hamilton, L., Collins, J. H. & Oliver, R. M. **Reconstitution of the *Escherichia coli* Pyruvate Dehydrogenase Complex.** *Proceedings of the National Academy of Science USA* **72**, 3068-3072, doi: 10.1073/pnas.72.8.3068 (1975).
- 215 Angelides, K. J., Akiyama, S. K. & Hammes, G. G. **Subunit Stoichiometry and Molecular Weight of the Pyruvate Dehydrogenase Multienzyme Complex from *Escherichia coli*.** *Proceedings of the National Academy of Science USA* **76**, 3279-3283, doi: 10.1073/pnas.76.7.3279 (1979).
- 216 Reynolds, T. S. & Gill, R. T. **Quantifying Impact of Chromosome Copy Number on Recombination in *Escherichia coli*.** *ACS Synthetic Biology* **4**, 776-780, doi: 10.1021/sb500338g (2015).
- 217 Mutalik, V. K., Guimaraes, J. C., Cambray, G., Lam, C., Christoffersen, M. J., Mai, Q.-A., Tran, A. B., Paull, M., Keasling, J. D., Arkin, A. P. & Endy, D. **Precise and Reliable Gene Expression Via Standard Transcription and Translation Initiation Elements.** *Nature Methods* **10**, 354, doi: 10.1038/nmeth.2404
- 218 Hartmans, S., Smits, J. P., van der Werf, M. J., Volkering, F. & de Bont, J. A. **Metabolism of Styrene Oxide and 2-Phenylethanol in the Styrene-Degrading *Xanthobacter* Strain 124x.** *Applied Environmental Microbiology* **55**, 2850-2855, doi: 10.1128/AEM.55.11.2850-2855.1989 (1989).
- 219 de Lorenzo, V. & Joshi, H. **Genomic Responses of *Pseudomonas putida* to Aromatic Hydrocarbons.** in *Consequences of Microbial Interactions with Hydrocarbons, Oils, and Lipids: Biodegradation and Bioremediation* (ed Robert Steffan) Ch. Chapter 25-1, 1-15 (Springer International Publishing, 2019).

- 220 Ramos, J. L., Marques, S. & Timmis, K. N. **Transcriptional Control of the *Pseudomonas* TOL Plasmid Catabolic Operons Is Achieved through an Interplay of Host Factors and Plasmid-Encoded Regulators.** *Annual Review of Microbiology* **51**, 341-373, doi: 10.1146/annurev.micro.51.1.341 (1997).
- 221 Abril, M. A., Michan, C., Timmis, K. N. & Ramos, J. L. **Regulator and Enzyme Specificities of the TOL Plasmid-Encoded Upper Pathway for Degradation of Aromatic Hydrocarbons and Expansion of the Substrate Range of the Pathway.** *Journal of Bacteriology* **171**, 6782-6790, doi: 10.1128/jb.171.12.6782-6790.1989 (1989).
- 222 Wolfe, M. D., Altier, D. J., Stubna, A., Popescu, C. V., Münck, E. & Lipscomb, J. D. **Benzoate 1,2-Dioxygenase from *Pseudomonas putida*: Single Turnover Kinetics and Regulation of a Two-Component Rieske Dioxygenase.** *Biochemistry* **41**, 9611-9626, doi: 10.1021/bi025912n (2002).
- 223 Jiménez, J. I., Pérez-Pantoja, D., Chavarría, M., Díaz, E. & de Lorenzo, V. **A Second Chromosomal Copy of the *Cata* Gene Endows *Pseudomonas putida* mt-2 with an Enzymatic Safety Valve for Excess of Catechol.** *Environmental Microbiology* **16**, 1767-1778, doi: 10.1111/1462-2920.12361 (2014).
- 224 Calero, P., Jensen, S. I. & Nielsen, A. T. **Broad-Host-Range Prouser Vectors Enable Fast Characterization of Inducible Promoters and Optimization of p-Coumaric Acid Production in *Pseudomonas putida* KT2440.** *ACS Synthetic Biology* **5**, 741-753, doi: 10.1021/acssynbio.6b00081 (2016).
- 225 Yu, B. J., Sung, B. H., Koob, M. D., Lee, C. H., Lee, J. H., Lee, W. S., Kim, M. S. & Kim, S. C. **Minimization of the *Escherichia coli* Genome Using a Tn5-Targeted Cre/Loxp Excision System.** *Nature Biotechnology* **20**, 1018-1023, doi: 10.1038/nbt740 (2002).
- 226 Kobayashi, K., Ehrlich, S. D., Albertini, A., Amati, G., Andersen, K. K., Arnaud, M., Asai, K., Ashikaga, S., Aymerich, S., Bessieres, P., Boland, F., Brignell, S. C., Bron, S., Bunai, K., Chapuis, J. et al. **Essential *Bacillus subtilis* Genes.** *Proceedings of the National Academy of Sciences USA* **100**, 4678-4683, doi: 10.1073/pnas.0730515100 (2003).
- 227 Baba, T., Ara, T., Hasegawa, M., Takai, Y., Okumura, Y., Baba, M., Datsenko, K. A., Tomita, M., Wanner, B. L. & Mori, H. **Construction of *Escherichia coli* K-12 in-Frame, Single-Gene Knockout Mutants: The Keio Collection.** *Molecular Systems Biology* **2**, 2006.0008, doi: 10.1038/msb4100050 (2006).
- 228 Kato, J. & Hashimoto, M. **Construction of Consecutive Deletions of the *Escherichia coli* Chromosome.** *Molecular Systems Biology* **3**, 132, doi: 10.1038/msb4100174 (2007).

- 229 Liberati, N. T., Urbach, J. M., Miyata, S., Lee, D. G., Drenkard, E., Wu, G., Villanueva, J., Wei, T. & Ausubel, F. M. **An Ordered, Nonredundant Library of *Pseudomonas aeruginosa* Strain PA14 Transposon Insertion Mutants.** *Proceedings of the National Academy of Sciences USA* **103**, 2833-2838, doi: 10.1073/pnas.0511100103 (2006).
- 230 Goodall, E. C. A., Robinson, A., Johnston, I. G., Jabbari, S., Turner, K. A., Cunningham, A. F., Lund, P. A., Cole, J. A. & Henderson, I. R. **The Essential Genome of *Escherichia coli* K-12.** *mBio* **9**, e02096-02017, doi: 10.1128/mBio.02096-17 (2018).
- 231 Juhas, M., Reuss, D. R., Zhu, B. & Commichau, F. M. ***Bacillus subtilis* and *Escherichia coli* Essential Genes and Minimal Cell Factories after One Decade of Genome Engineering.** *Microbiology* **160**, 2341-2351, doi: 10.1099/mic.0.079376-0 (2014).
- 232 Acevedo-Rocha, C. G., Fang, G., Schmidt, M., Ussery, D. W. & Danchin, A. **From Essential to Persistent Genes: A Functional Approach to Constructing Synthetic Life.** *Trends in Genetics* **29**, 273-279, doi: 10.1016/j.tig.2012.11.001 (2013).
- 233 Danchin, A. & Fang, G. **Unknown Unknowns: Essential Genes in Quest for Function.** *Microbial Biotechnology* **9**, 530-540, doi: 10.1111/1751-7915.12384 (2016).
- 234 Durante-Rodriguez, G., de Lorenzo, V. & Nikel, P. I. **A Post-Translational Metabolic Switch Enables Complete Decoupling of Bacterial Growth from Biopolymer Production in Engineered *Escherichia coli*.** *ACS Synthetic Biology* **7**, 2686-2697, doi: 10.1021/acssynbio.8b00345 (2018).
- 235 Yu, L. P., Wu, F. Q. & Chen, G. Q. **Next-Generation Industrial Biotechnology-Transforming the Current Industrial Biotechnology into Competitive Processes.** *Biotechnology Journal* **14**, e1800437, doi: 10.1002/biot.201800437 (2019).
- 236 Gawin, A., Valla, S. & Brautaset, T. **The XylS/*P_m* Regulator/Promoter System and Its Use in Fundamental Studies of Bacterial Gene Expression, Recombinant Protein Production and Metabolic Engineering.** *Microbial Biotechnology* **10**, 702-718, doi: 10.1111/1751-7915.12701 (2017).
- 237 Pérez-Pantoja, D., Kim, J., Silva-Rocha, R. & de Lorenzo, V. **The Differential Response of the *P_{ben}* Promoter of *Pseudomonas putida* mt-2 to BenR and XylS Prevents Metabolic Conflicts in M-Xylene Biodegradation.** *Environmental Microbiology* **17**, 64-75, doi: 10.1111/1462-2920.12443 (2015).

- 238 Volke, D. C., Turlin, J., Mol, V. & Nikel, P. I. **Physical Decoupling of XylS/Pm Regulatory Elements and Conditional Proteolysis Enable Precise Control of Gene Expression in *Pseudomonas putida***. *Microbial Biotechnology* **13**, 222-232, doi: 10.1111/1751-7915.13383 (2020).
- 239 Vallon, T., Simon, O., Rendgen-Heugle, B., Frana, S., Mückschel, B., Broicher, A., Siemann-Herzberg, M., Pfannenstiel, J., Hauer, B., Huber, A., Breuer, M. & Takors, R. **Applying Systems Biology Tools to Study n-Butanol Degradation in *Pseudomonas putida* KT2440**. *Eng Life Sci* **15**, 760-771, doi: 10.1002/elsc.201400051 (2015).
- 240 Billerbeck, S., Calles, B., Müller, C. L., de Lorenzo, V. & Panke, S. **Towards Functional Orthogonalisation of Protein Complexes: Individualisation of Groel Monomers Leads to Distinct Quasihomogeneous Single Rings**. *ChemBioChem* **14**, 2310-2321, doi: 10.1002/cbic.201300332 (2013).
- 241 Martínez-García, E., Jatsenko, T., Kivisaar, M. & de Lorenzo, V. **Freeing *Pseudomonas putida* KT2440 of Its Proviral Load Strengthens Endurance to Environmental Stresses**. *Environmental Microbiology* **17**, 76-90, doi: 10.1111/1462-2920.12492 (2015).
- 242 Martínez-García, E., Nikel, P. I., Chavarria, M. & de Lorenzo, V. **The Metabolic Cost of Flagellar Motion in *Pseudomonas putida* KT2440**. *Environmental Microbiology* **16**, 291-303, doi: 10.1111/1462-2920.12309 (2014).
- 243 Rolfe, M. D., Rice, C. J., Lucchini, S., Pin, C., Thompson, A., Cameron, A. D., Alston, M., Stringer, M. F., Betts, R. P., Baranyi, J., Peck, M. W. & Hinton, J. C. **Lag Phase Is a Distinct Growth Phase That Prepares Bacteria for Exponential Growth and Involves Transient Metal Accumulation**. *Journal of Bacteriology* **194**, 686-701, doi: 10.1128/jb.06112-11 (2012).
- 244 de Lorenzo, V. & Couto, J. **The Important Versus the Exciting: Reining Contradictions in Contemporary Biotechnology**. *Microbial Biotechnology* **12**, 32-34, doi: 10.1111/1751-7915.13348 (2019).
- 245 Fernández-Cabezón, L., Cros, A. & Nikel, P. I. **Evolutionary Approaches for Engineering Industrially-Relevant Phenotypes in Bacterial Cell Factories**. *Biotechnology Journal* **14**, In press, DOI: 10.1002/biot.201800439, doi: 10.1002/biot.201800439 (2019).
- 246 Casjens, S. **Prophages and Bacterial Genomics: What Have We Learned So Far?** *Molecular Microbiology* **49**, 277-300, doi: 10.1046/j.1365-2958.2003.03580.x (2003).

- 247 Ilves, H., Horak, R. & Kivisaar, M. **Involvement of Sigma(S) in Starvation-Induced Transposition of *Pseudomonas putida* Transposon Tn4652.** *Journal of Bacteriology* **183**, 5445-5448, doi: 10.1128/jb.183.18.5445-5448.2001 (2001).
- 248 Winstanley, C., Langille, M. G., Fothergill, J. L., Kukavica-Ibrulj, I., Paradis-Bleau, C., Sanschagrin, F., Thomson, N. R., Winsor, G. L., Quail, M. A., Lennard, N., Bignell, A., Clarke, L., Seeger, K., Saunders, D., Harris, D. et al. **Newly Introduced Genomic Prophage Islands Are Critical Determinants of in Vivo Competitiveness in the Liverpool Epidemic Strain of *Pseudomonas aeruginosa*.** *Genome Research* **19**, 12-23, doi: 10.1101/gr.086082.108 (2009).
- 249 Wang, X., Kim, Y., Ma, Q., Hong, S. H., Pokusaeva, K., Sturino, J. M. & Wood, T. K. **Cryptic Prophages Help Bacteria Cope with Adverse Environments.** *Nature Communications* **1**, 147, doi: 10.1038/ncomms1146 (2010).
- 250 Lieder, S., Nikel, P. I., de Lorenzo, V. & Takors, R. **Genome Reduction Boosts Heterologous Gene Expression in *Pseudomonas putida*.** *Microbial Cell Factories* **14**, 23, doi: 10.1186/s12934-015-0207-7 (2015).
- 251 Aparicio, T., de Lorenzo, V. & Martínez-García, E. **Improved Thermotolerance of Genome-Reduced *Pseudomonas putida* EM42 Enables Effective Functioning of the PL/CI857 System.** *Biotechnology Journal* **14**, e1800483, doi: 10.1002/biot.201800483 (2019).
- 252 Martinez-Garcia, E. & de Lorenzo, V. **Engineering Multiple Genomic Deletions in Gram-Negative Bacteria: Analysis of the Multi-Resistant Antibiotic Profile of *Pseudomonas putida* KT2440.** *Environmental Microbiology* **13**, 2702-2716, doi: 10.1111/j.1462-2920.2011.02538.x (2011).
- 253 Matilla, M. A., Ramos, J. L., Duque, E., de Dios Alche, J., Espinosa-Urgel, M. & Ramos-Gonzalez, M. I. **Temperature and Pyoverdine-Mediated Iron Acquisition Control Surface Motility of *Pseudomonas putida*.** *Environmental Microbiology* **9**, 1842-1850, doi: 10.1111/j.1462-2920.2007.01286.x (2007).
- 254 Cornelis, P. **Iron Uptake and Metabolism in Pseudomonads.** *Applied Microbiology and Biotechnology* **86**, 1637-1645, doi: 10.1007/s00253-010-2550-2 (2010).
- 255 Meyer, J.-M., Geoffroy, V. A., Baida, N., Gardan, L., Izard, D., Lemanceau, P., Achouak, W. & Palleroni, N. J. **Siderophore Typing, a Powerful Tool for the Identification of Fluorescent and Nonfluorescent Pseudomonads.** *Applied and Environmental Microbiology* **68**, 2745-2753, doi: 10.1128/aem.68.6.2745-2753.2002 (2002).

- 256 Schalk, I. J., Rigouin, C. & Godet, J. **An Overview of Siderophore Biosynthesis among Fluorescent Pseudomonads and New Insights into Their Complex Cellular Organization.** *Environmental Microbiology* **22**, 1447-1466, doi: 10.1111/1462-2920.14937 (2020).
- 257 Hanahan, D. & Meselson, M. **Plasmid Screening at High Colony Density.** *Methods in Enzymology* **100**, 333-342, doi: 10.1016/0378-1119(80)90144-4 (1983).
- 258 Platt, R., Drescher, C., Park, S. K. & Phillips, G. J. **Genetic System for Reversible Integration of DNA Constructs and LacZ Gene Fusions into the *Escherichia coli* Chromosome.** *Plasmid* **43**, 12-23, doi: 10.1006/plas.1999.1433 (2000).
- 259 Boyer, H. W. & Roulland-Dussoix, D. **A Complementation Analysis of the Restriction and Modification of DNA in *Escherichia coli*.** *Journal of Molecular Biology* **41**, 459-472, doi: 10.1016/0022-2836(69)90288-5 (1969).
- 260 Worsley, M. J. & Williams, P. A. **Metabolism of Toluene and Xylenes by *Pseudomonas putida (arvilla)* mt-2: Evidence for a New Function of the TOL Plasmid.** *Journal of Bacteriology* **124**, 7-13, doi: 10.1128/JB.124.1.7-13.1975 (1975).
- 261 Bagdasarian, M., Lurz, R., Rückert, B., Franklin, F. C. H., Bagdasarian, M. M., Frey, J. & Timmis, K. N. **Specific Purpose Plasmid Cloning Vectors. Ii. Broad Host Range, High Copy Number, RSF1010-Derived Vectors, and a Host-Vector System for Gene Cloning in *Pseudomonas*.** *Gene* **16**, 237-247, doi: 10.1016/0378-1119(81)90080-9 (1981).

Chapter 4: Establishing a synthetic C2 auxotrophy in *Pseudomonas putida* for evolutionary engineering of alternative catabolic routes

Summary

Acetyl-coenzyme A (Ac-CoA) is a metabolic hub in the central carbon metabolism of all living cells. Besides connecting glycolytic routes to the tricarboxylic acid (TCA) cycle, Ac-CoA is a key precursor of essential biomass components, e.g., amino acids, lipids, and building blocks of the bacterial cell wall. Conversely, the thioester acts as a metabolic sink for catabolic pathways of a large variety of molecules, thereby feeding the central biochemical network. This dual role of Ac-CoA as an essential precursor metabolite, on the one hand, and as the end-degradation product of many industrially relevant compounds, on the other, allows production to be tightly coupled to cell growth. To this end, a synthetic “auxotrophy” for two-carbon compounds (SCA) was established in *Pseudomonas putida* following an in silico-guided metabolic engineering approach. The applicability of the evolutionary engineering strategy driven by Ac-CoA demand was demonstrated by implementing an alternative route for sugar assimilation—the phosphoketolase (PK) shunt from bifidobacteria, representing a direct link of sugar-phosphates to Ac-CoA without CO₂ release. Such synthetic metabolism would enable the conservation of substrate-derived carbon, resulting in increased maximum product yields on sugar feedstocks. During adaptive laboratory evolution, the engineered SCA strain integrated the PK shunt into the metabolic network to restore C2 prototrophy. Changes in the protein translation process due to the mutation of *tilS*, encoding a rare isoleucine-tRNA synthetase, were identified as a possible mechanism for adjusting the network-wide proteome profile resulting in an improved growth phenotype. The co-occurrence of the Entner-Doudoroff (ED) and the PK pathways resulted in significant pyruvate and 2-ketogluconate secretion as overflow metabolites. The results presented in this chapter demonstrate that the central metabolism of *P. putida* can be radically rewired to incorporate heterologous Ac-CoA-producing pathways and novel metabolic connectivities. Approaches to address the observed metabolic imbalances through continued strain engineering are discussed.

4.1. Introduction

4.1.1. The central role of acetyl-coenzyme A in cellular metabolism

The progress made in synthetic biology and metabolic engineering is driving ever-accelerating technological developments in bioproduction. Sophisticated computational methods facilitate the discovery of new enzymes and provide increasingly reliable roadmaps to produce relevant compounds from inexpensive feedstocks in biological systems. Simultaneously, a steadily increasing set of molecular tools allows for the transfer and functional implementation of biochemical functions in any desired host organism. Once a suitable pathway has been functionally implemented, one commonly encountered obstacle for the efficient production of the desired compound is a sufficient supply of precursor metabolites. Every biochemical pathway starts with metabolites from central carbon metabolism. However, biological systems have evolved to efficiently utilize growth substrates by balancing biochemical fluxes to avoid metabolite accumulation²⁶².

Acetyl-coenzyme A (Ac-CoA) is a central metabolite, identified as a key node in the metabolism of all living organisms^{263,264}. This thioester represents a *metabolite hub* and the entry point to the tricarboxylic acid (TCA) cycle, in which essential biomass precursors and most of the energy-generating reducing equivalents for respiring organisms are produced. Ac-CoA also plays a central role as (co-)substrate in biochemical pathways leading to essential biomass constituents like amino acids, cell wall components (acetylated amino sugars), and fatty acids. Moreover, many secondary metabolites of industrial interest (polyketides, isoprenoids, sterols, alcohols, and polyhydroxyalkanoates) can be produced through biochemical pathways with Ac-CoA as the precursor. Conversely, various catabolic pathways for a broad spectrum of compounds form a catabolic 'funnel' converging in Ac-CoA (**Figure 4.1A**). Importantly, and due to its central role as a biomass precursor, Ac-CoA can serve as a pivotal node for creating metabolic networks where the production and simultaneous degradation of a product is tightly coupled to growth, provided that this product is the organism's only source of Ac-CoA (**Figure 4.1B**).

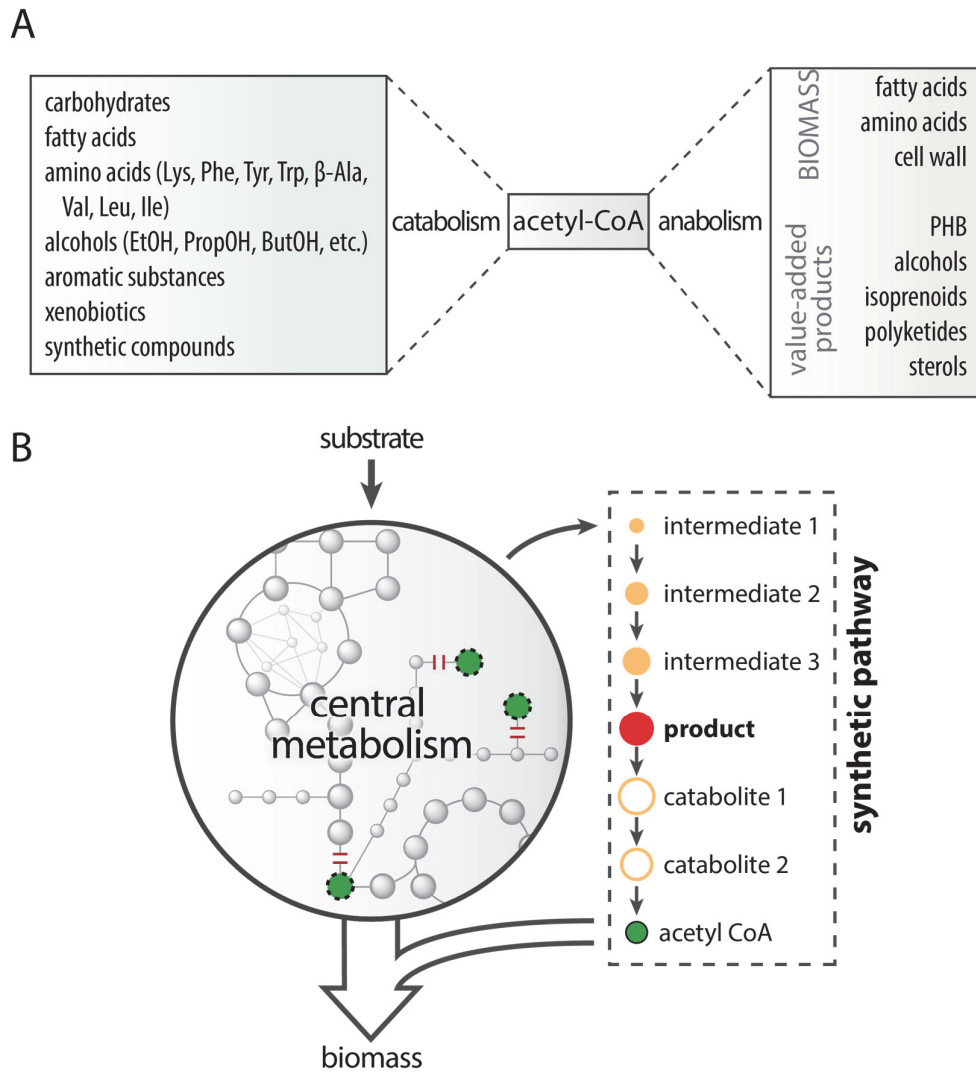


Figure 4.1. Key role of Ac-CoA in central carbon metabolism. (A) A large fraction of cellular metabolism can be illustrated as a bowtie structure in which various carbon compounds are funneled through a multitude of catabolic pathways with Ac-CoA as the end- or side-product. Conversely, Ac-CoA serves as the starting point (or co-substrate) for the biosynthesis of many essential biomass constituents or secondary metabolites of industrial interest. **(B)** Schematic representation of an evolutionary engineering selection scheme in which native sources of Ac-CoA (green circles with dashed contours) are deleted (red lines). Cell growth becomes only possible in the presence of externally supplied acetate or via the use of a new metabolic route, which couples the production of a compound of interest to the formation of the essential Ac-CoA.

When faced with the choice of a suitable microbiological *chassis*, a diverse list of properties needs to be considered. In typical laboratory microorganisms such as *Escherichia coli*, new metabolic pathways can be easily implemented or existing ones redirected. However, some applications can profit from a more robust metabolic architecture dis-

played by many environmental organisms. Exposed to ever-changing habitat conditions, including alternating availability of various substrates, exposure to toxic chemicals, as well as chemical and physical stressors, soil generalists like *Pseudomonas putida* can excel under harsh biofermentation conditions or when toxic compounds are being produced. An overview of the metabolic architecture of *P. putida* is provided in **Section 2.1.3**. Having adapted to frequent periods of starvation (e.g., in soil environments), the metabolism of *P. putida* is optimized for the utilization of a wide variety of substrates without the production of overflow metabolites to ensure high carbon efficiencies^{265,266}. In addition, *P. putida* has low energy demands for cell maintenance^{265,267}. Rather than reacting to changing metabolic conditions by adjusting the expression of genes in central metabolism, *P. putida* exerts control on biochemical activities predominantly through post-transcriptional mechanisms or metabolic regulation¹¹⁴. One prerequisite for a metabolite-based regulation is that compound concentrations are accurately controlled to allow for a dynamic response changing conditions.

The intracellular Ac-CoA concentration and its relative levels compared to nonesterified CoA is maintained at low values in *P. putida* regardless of the metabolic status, in contrast to facultatively anaerobic bacteria²⁶⁸. Despite lacking an acetate kinase for the activation of acetate (hence, Ac-CoA synthetase is used for acetate assimilation), *P. putida* harbors a functional phosphate acetyltransferase (Pta)²⁶⁹. Like in *E. coli*, acetyl phosphate (Ac-P) was shown to be involved in the post-translational modification of proteins (e.g., the transcriptional activator NtrC activated under nitrogen-limited conditions) to control their activity^{270,271}.

In the two most prevalent glycolytic routes in bacteria, the Embden-Meyerhof-Parnas (EMP) pathway, and the Entner-Doudoroff (ED) pathway, Ac-CoA is almost exclusively formed through pyruvate oxidation. This reaction, catalyzed by the pyruvate dehydrogenase complex (PDHc), involves the substrate's decarboxylation, leading to a loss of carbon within the metabolite pool. An alternative glycolytic route that can provide Ac-CoA without releasing CO₂, the phosphoketolase pathway²⁷², was first described in heterolactic fermentative bacteria.

4.1.2. The phosphoketolase reactions shunt the upstream glycolysis to the direct formation of Ac-CoA, bypassing pyruvate decarboxylation

Phosphoketolases (PKs) form a unique class of enzymes closely related to the enzyme transketolase (EC 2.2.1.1) that is part of the pentose phosphate pathway. They require thiamine diphosphate (ThDP) and a divalent metal ion as essential cofactors and catalyze the cleavage of xylulose 5-phosphate (Xu5P) or fructose 6-phosphate (F6P) to Ac-P and glyceraldehyde 3-phosphate (G3P) or erythrose 4-phosphate (E4P), respectively. The enzymatic reaction involves ketol cleavage, dehydration, and phosphorolysis in a single biochemical step²⁷³. PKs are naturally found in obligate anaerobic and heterofermentative bacteria, some fungal species, cyanobacteria, and microalgae as part of an alternative route for the degradation of sugars²⁷⁴. Depending on their substrate specificity, one can distinguish two subfamilies: members of the EC 4.1.2.9 (XPK) group act only on Xu5P, while PKs belonging to EC 4.1.2.22 (XFPK) accept both Xu5P and F6P as substrates²⁷⁵, with varying preferences in different organisms²⁷⁶. The produced Ac-P can be converted into Ac-CoA via Pta, thereby allowing direct conversion of sugar phosphates into Ac-CoA without the loss of carbon accompanying the oxidative decarboxylation performed by the PDHc. Streamlining sugar utilization through the use of this carbon-conserving pathway has the potential of increasing maximum theoretical yields for Ac-CoA-derived products in biotechnological applications²⁷⁷. The introduction of PKs into microbial model organisms has been successfully used in the past to enhance titers for acetate^{278,279}, poly(3-hydroxybutyrate)²⁸⁰, fatty acid ethyl esters²⁸¹, and 3-hydroxypropionic acid²⁸². In a recent application, *Corynebacterium glutamicum* was used in an evolutionary engineering approach to improve the specific PK activity via disruption of the host's linear glycolysis, thereby boosting the production of L-glutamate²⁸³.

4.1.3. Evolutionary engineering leverages the vast potential of Darwinian adaptation for the optimization of cell factories

Microbial organisms play an essential role in the sustainable production of a wide range of industrial products, including biofuels²⁸⁴, food additives, pharmaceuticals, surfactants²⁸⁵, and polymers^{286,287}. Despite an increasing body of knowledge about the biochemistry of microbes and the rules that govern their regulation, and a rapid acceleration of technologies available in bioengineering, the inherent complexity of biological systems still poses an obstacle when deliberately trying to alter certain traits. Traditional engineering approaches are often hampered by a lack of comprehensive understanding of the host organism and the inability to predict the system's response reliably, especially after introducing several genetic changes at once.

This barrier notwithstanding, nature itself offers the possibility of refactoring even the most complex structures: the process of evolution. Since the middle of the 19th century, adaptive laboratory evolution (ALE) has been increasingly used to gain insights into evolutionary mechanisms and improve beneficial traits under specified selection conditions^{59,288,289} (**Figure 4.2**). Classically used to enhance general host properties like the resistance to chemicals, growth characteristics under industrially relevant conditions, or the ability to utilize alternative feedstocks, ALE can also be employed to improve the performance of a whole-cell biocatalyst for specific biochemical tasks²⁹⁰. The only prerequisite for such an evolutionary engineering approach is that the desired trait can be subject to a selection pressure that couples an improved catalytic performance to a fitness gain. This can be achieved via the creation of interdependencies within the host metabolism (e.g., product additions), through the right choice of selection conditions (e.g., by using antimetabolites), or by a combination of both^{288,291}.

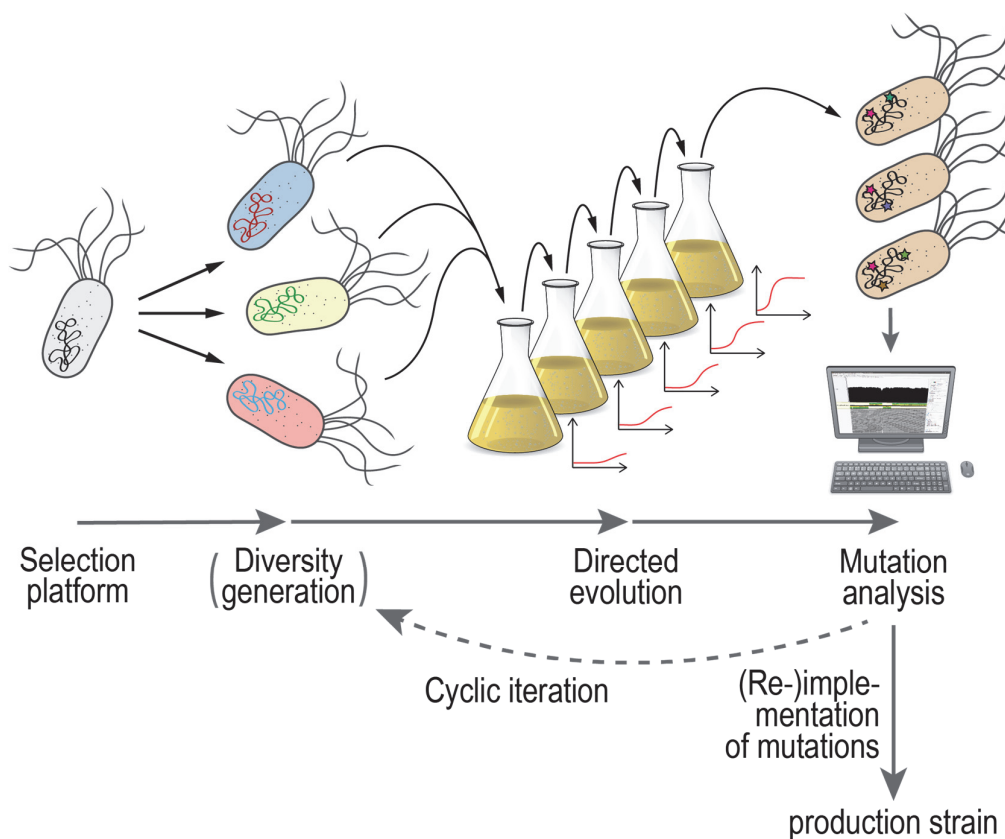


Figure 4.2. Adaptive laboratory evolution for cell factory optimization. A suitable selection strain is subjected to repeated cultivation under restrictive conditions (e.g., toxic compounds, limited substrate availability, or antimetabolites). During extended exposure to the stressor, the individual cells in the population acquire mutations that promote and enhanced growth physiology. Through Darwinian mechanisms, beneficial mutations are established within the population. Once the phenotype has improved, the respective clones can be analyzed regarding the acquired mutations. Beneficial mutations can be retro-engineered in a production host, or the cells can be used directly to exploit the optimized phenotype. The ALE process can be accelerated if the genetic variability in the population is artificially enhanced (i.e., by mutagenesis methods, genome shuffling, or implementation of libraries for gene variants and expression systems) before selection.

In this study, *in silico* modeling was used to identify pathways consuming and producing Ac-CoA in *Pseudomonas putida* KT2440. Building on these results, a synthetic C2 auxotrophy was introduced by eliminating all Ac-CoA-producing reactions. Next, the resulting strains were used to implement the carbon-conserving phosphoketolase pathway to demonstrate the utility of the C2-based selection scheme. By limiting the essential Ac-CoA supply exclusively to the introduced biochemical shunt in synthetic C2-auxotroph (SCA) strains, we show that heterologous pathways yielding Ac-CoA can be optimized through evolutionary engineering.

4.2. Results

4.2.1. Design of a synthetic C2-auxotroph strain design informed by genome-scale metabolic modeling and analysis of the potential of a phosphoketolase-based glucose utilization pathway

The pyruvate dehydrogenase complex (PDHc) serves as the link between glycolysis and the TCA cycle in *P. putida* and represents the primary source of Ac-CoA for most heterotrophs. To generate a robust C2 auxotroph platform strain on glucose for evolutionary engineering applications, we employed an in silico-guided approach to identify native pathways that could supply acetyl-CoA in the absence of PDHc under stringent selection conditions. To this end, we performed flux-balance analyses (FBA) using the genome-scale *P. putida* KT2440 model iJN1411 with glucose as the carbon source (**Figure 4.3**). The identified reactions, their corresponding genes, and the associated catabolic pathways are listed in **Table 4.1**. Furthermore, the flux towards the compound that contributes to biomass formation and represents the start of the catabolic pathway was computed for each reaction identified via FBA. The reactions were ranked according to their absolute flux value. With these reactions 'knocked-out' in iJN1411, the two possible PK reactions on fructose 6-phosphate (FPK) and xylulose 5-phosphate (XPK) were introduced into the synthetic C2-auxotroph (SCA) model.

The flux distribution after optimizing for the biomass reaction on glucose is shown in **Figure 4.4**. Provided that the model does not consider thermodynamic constraints, the maximum growth rate achievable with an alternative, PK-based upper central metabolism (0.61 h^{-1}) is close to that of the wildtype model (0.62 h^{-1} , **Figure 4.3**). The ED pathway (flux through Edd and Eda) is completely inactive. Therefore, the PK pathway constitutes a feasible alternative to the ED pathway in the obligate aerobic organism. All metabolic flux is channeled into the pentose phosphate pathway (PPP), with a 7-fold increased phosphogluconate dehydrogenase (Gnd) activity compared to wildtype model iJN1411. The ribulose 5-phosphate 3-epimerase (Rpe) reaction is also greatly enhanced (69-fold) to provide F6P and Xu5P for the PK reactions.

Table 4.1. Reactions predicted to contribute to the formation of Ac-CoA on glucose when serially knocked out in iJN1411. Genes in bold were deleted in strain SCA3. Genes in parentheses were not removed, as being part of a multi-enzyme complex in which at least one protein was deleted. The indicated fluxes represent the predicted rate of the first reaction leading into the respective pathway in wild-type iJN1411.

Gene	iJN1411 reaction ID	Associated pathway	Flux towards pathway precursor (mmol g _{CDW} ⁻¹ h ⁻¹)
ace , aceF , (<i>lpdA</i>)	PDH PDHbr	Pyruvate dehydrogenase complex	5.76
bkdAA , (<i>bkdAB</i> , <i>bkdB</i> , <i>lpdV</i>)	OIVD2 OIVD3 OIVD1r	Branched chain keto acid dehydrogenase	0.63 0.15 0.39
ItaE	THRAr, THRA2r	L-threonine aldolase	0.31
<i>pcaB</i> , <i>pcaC</i> , <i>pcaD</i>	MUCCY_kt, 4CMLCL_kt, OXOAEI	3-Dehydroshikimate degradation	0.25
<i>paaK</i>	PACCOAL	L-Phe degradation	0.12
<i>davB</i>	LYSMO	L-Lys degradation	0.11
<i>gabT</i>	APT NAT, ABTA	L-Lys degradation	0.11
<i>hmgA</i> , <i>hmgB</i> , <i>hmgC</i>	HGNTOR, FUMAC, MACACI	L-Tyr degradation	0.084
<i>eutB</i> , <i>eutC</i>	ETHAAL	Ethanolamine degradation	0.05 *1
<i>mmsA-l</i>	MMSAD3	β-Alanine metabolism	0.0004
<i>glcB</i>	MALS	Malate synthase*2	-
<i>acoA</i> , <i>acoB</i> , <i>acoC</i>		Acetoin dehydrogenase complex*3	0

*1 The calculated flux towards ethanolamine was only 0.047 mmol g_{CDW}⁻¹ h⁻¹. However, phosphatidylethanolamine was shown to be the most abundant membrane component in *P. putida* KT2440, constituting about two-thirds of the total glycerophospholipid fraction²⁹². The relatively high abundance of ethanolamine made its degradation appear a plausible potential source of Ac-CoA.

*2 According to calculated flux distributions, the glyoxylate shunt should be inactive to allow for optimal growth with the alternative PK-glycolysis (preventing the use of C2 units as energy source).

*3 The acetoin cleavage system (acetoin dehydrogenase complex) was shown to be functional in *P. putida*, producing acetyl-CoA with a mechanism analogous to that of the PDHC²⁹³.

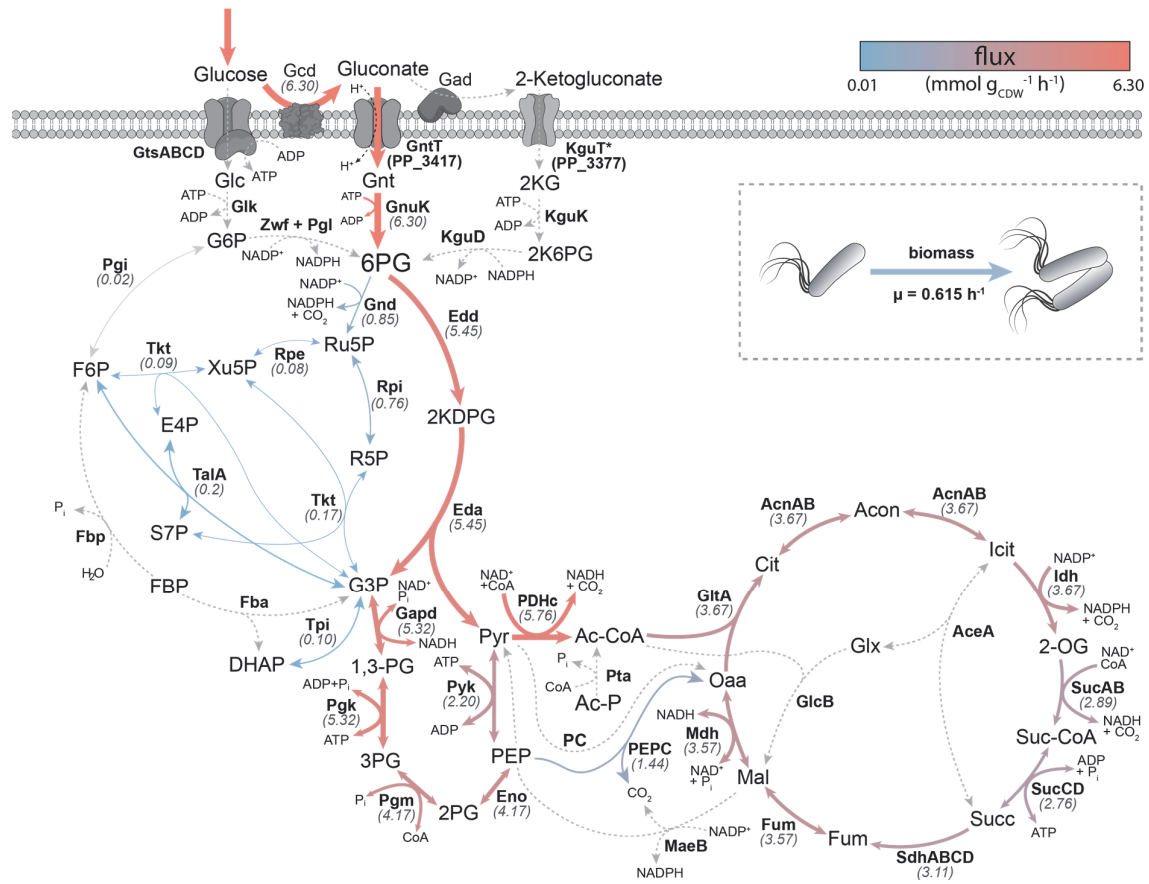


Figure 4.3. In silico flux distribution calculated in wild-type *P. putida* KT2440 with glucose as carbon source. The thickness of reaction arrows are drawn in scale reflecting their flux value (from 0.01 to 6.30 mmol g_{CDW}⁻¹ h⁻¹). Colors also encode the flux values from blue (0.01 mmol g_{CDW}⁻¹ h⁻¹) to red (6.30 mmol g_{CDW}⁻¹ h⁻¹). Reactions with no flux are drawn as grey, dashed lines. Only organic cofactors, CO₂ and phosphate (P) are shown as co-substrates. Abbreviations for metabolites: 2K6PG, 2-keto-gluconate-6-P; 2PG, glycerate-2-P; 3PG, glycerate-3-P; 6PG, 6-phosphogluconate; 2KG, 2-ketogluconate; Ac-P, acetyl-P; CoA, coenzyme A; DHAP, dihydroxyacetone-P; E4P, erythrose-4-P; F6P, fructose-6-P; FBP, fructose-1; G3P, glyceraldehyde-3-P; G6P, glucose-6-P; Glc, glucose; Gnt, gluconate; KDPG, 2-keto-3-deoxy-6-phosphogluconate; PEP, phosphoenolpyruvate; R5P, ribose-5-P; Ru5P, ribulose-5-P; S7P, sedoheptulose-7-P; 2-OG, 2-oxogluconate; acon, aconitate; Ac-P, acetyl-P; Cit, citrate; Fum, fumarate; Glx, glyoxylate; Icit, isocitrate; Mal, malate; Oaa, oxaloacetate; P_i, phosphate; Pyr, pyruvate; Succ, succinate; Suc-Coa, succinyl-CoA; Xu5P, xylulose-5-P; Abbreviations for enzymes: AceA, isocitrate lyase; Acn, aconitase; Eda, 2-dehydro-3-deoxy-phosphogluconate aldolase; Edd, phosphogluconate dehydratase; Eno, enolase; Fba, fructose-1; FPK, fructose-6-P phosphoketolase; Fbp, Fructose-1; Fum, fumarate hydratase; GADH, gluconate dehydrogenase; Gap, glyceraldehyde-3-P dehydrogenase; Gcd, glucose dehydrogenase; GlcB, malate synthase.; Glk, glucose kinase; GltA, citrate synthase; Gnd, phosphogluconate dehydrogenase; GntT, gluconate/H⁺ symporter; GnuK, gluconate kinase; GtsABCD, D-glucose ABC-transporter; MaeB, malic enzyme; Idh, isocitrate dehydrogenase; KguD, 2K6PG reductase; KguK, 2-ketogluconate kinase; KguT, putative 2-ketogluconate transporter; Mdh, malate dehydrogenase; PEPC, PEP carboxylase; PC, pyruvate carboxylase; PDHc, pyruvate dehydrogenase complex; Pgi, phosphohexose-isomerase; Pgl, phosphogluconolactonase; Pgm, phosphoglycerate mutase; Pta, phosphotransacetylase; Pyk, pyruvate kinase; Rpe, ribulose-5-P 3-epimerase; Rpi, ribose-5-P isomerase; Sdh, succinate dehydrogenase; SucAB, 2-oxoglutarate dehydrogenase; SucCD, succinyl-CoA synthetase; Tal, transaldolase; Tkt, transketolase; Tpi, triosephosphate isomerase; XPK, xylulose-5-P phosphoketolase; Zwf, glucose-6-P dehydrogenase. Reactions catalyzed by multiple isoenzymes, some with different cosubstrate specificities (e.g., Pgi, Zwf, or Gapd), were lumped together for the sake of simplicity.

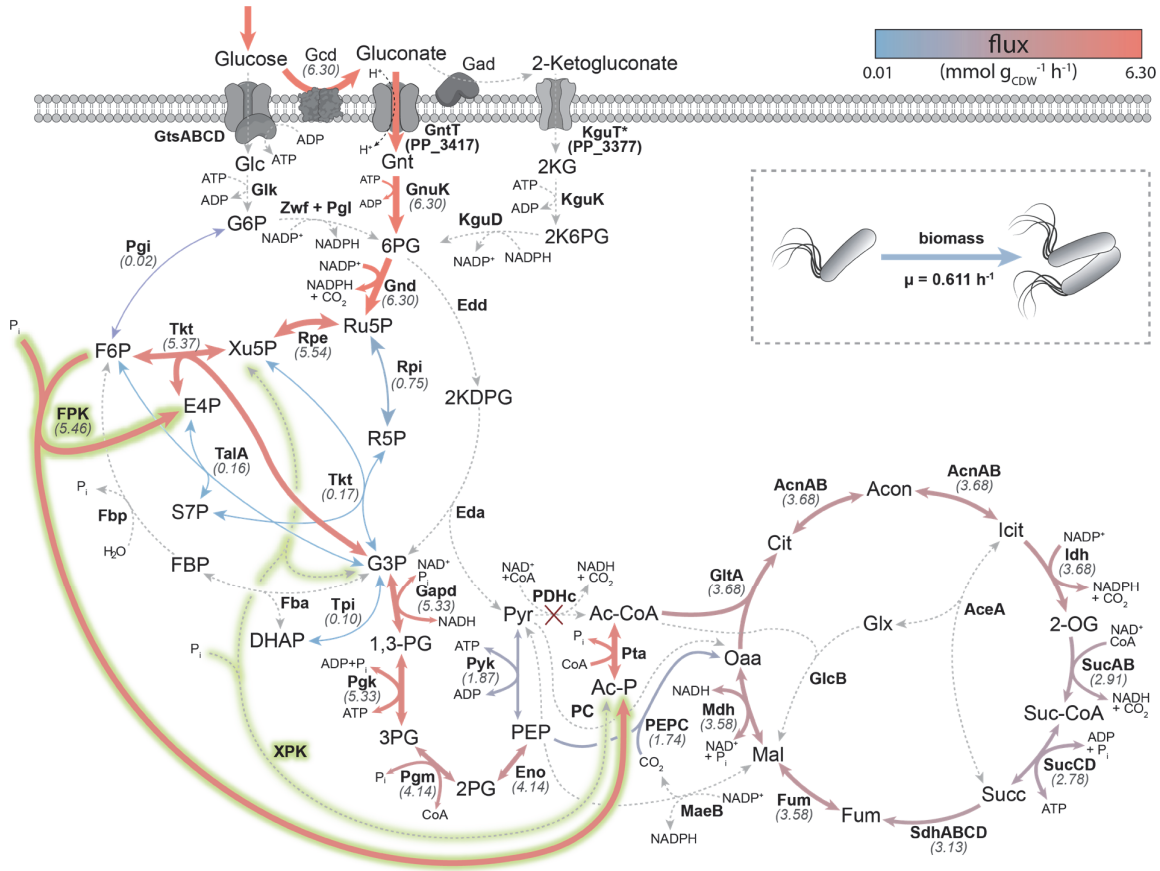


Figure 4.4. Flux distribution calculated with iJN1411 after deleting Ac-CoA-producing pathways and introducing the Xfpk reactions. The reactions and enzymes of the heterologous PK pathway are highlighted by a green shading. Note that the enzyme can use either F6P or Xu5P as the substrate. A description of color schemes and abbreviations is given in **Figure 4.4**.

The flux distribution shown in **Figure 4.4** represents only one possible FBA solution in which the PK acts exclusively on F6P. However, there is an infinite number of possible flux distributions in which the total flux of 5.46 is distributed between FPK and XPK, providing equal amounts of Ac-P and G3P. PPP metabolite levels are balanced in each solution by the transaldolase (TalA) and transketolase (Tkt) reactions. In both distributions, glucose is exclusively fed into central metabolism through the 6-phosphogluconate (6PG) route, contrasting with experimentally determined metabolic flux distributions, in which only 78% of the consumed glucose enters the cells in the form of gluconate, 10% as glucose, and 12% as 2-ketogluconate (2KG, Nickel et al.²⁹⁴). The equilibrating effect of the PPP enzymes potentially allows for a balanced flux through the PK pathway and downstream glycolysis. Hence, no significant increase of anapleurotic reactions is observed.

4.2.2. Experimental validation of acetate auxotrophy and phenotypical characterization of acetate requirements in synthetic C2-auxotroph strains

Informed by the in silico prediction with iJN1411, a whole family of synthetic C2-auxotroph (SCA) strains was created with an increasing number of deletions of genes involved in the potential formation of Ac-CoA (**Table 4.4**). The auxotrophy was confirmed by testing their growth in synthetic de Bont minimal (DBM) medium with various carbon sources. All strains deficient in PDHc (strains SCA1, SCA3, SCA9, SCA15, and SCA18) could not grow within 120 h after inoculation with glucose as the carbon source (**Figure 4.5**) as well as on fructose and gluconate (data not shown). Strains with an intact PDHc (strains SCA8_{PD} and SCA14_{PD}) demonstrated growth comparable to wild-type strain KT2440. Thus, the deletion of *aceE* and *aceF* suffices to establish auxotrophy for C2-carbon compounds on glycolytic substrates in wild-type *P. putida*. Cells that had only the PDHc inactivated were not impaired in their ability to utilize acetate as the only carbon source (**Figure 4.S1, Table 4.2**). The 14 implemented gene deletions did not affect the phenotype of SCA14 when grown glycolytic substrates or the TCA cycle metabolite citrate. However, the removal of several genes involved in the assimilation of amino acids (**Table 4.4**), among other targets, resulted in decreased biomass yields and more pronounced diauxic shifts (**Figure 4.S2**) when grown in a rich medium (LB).

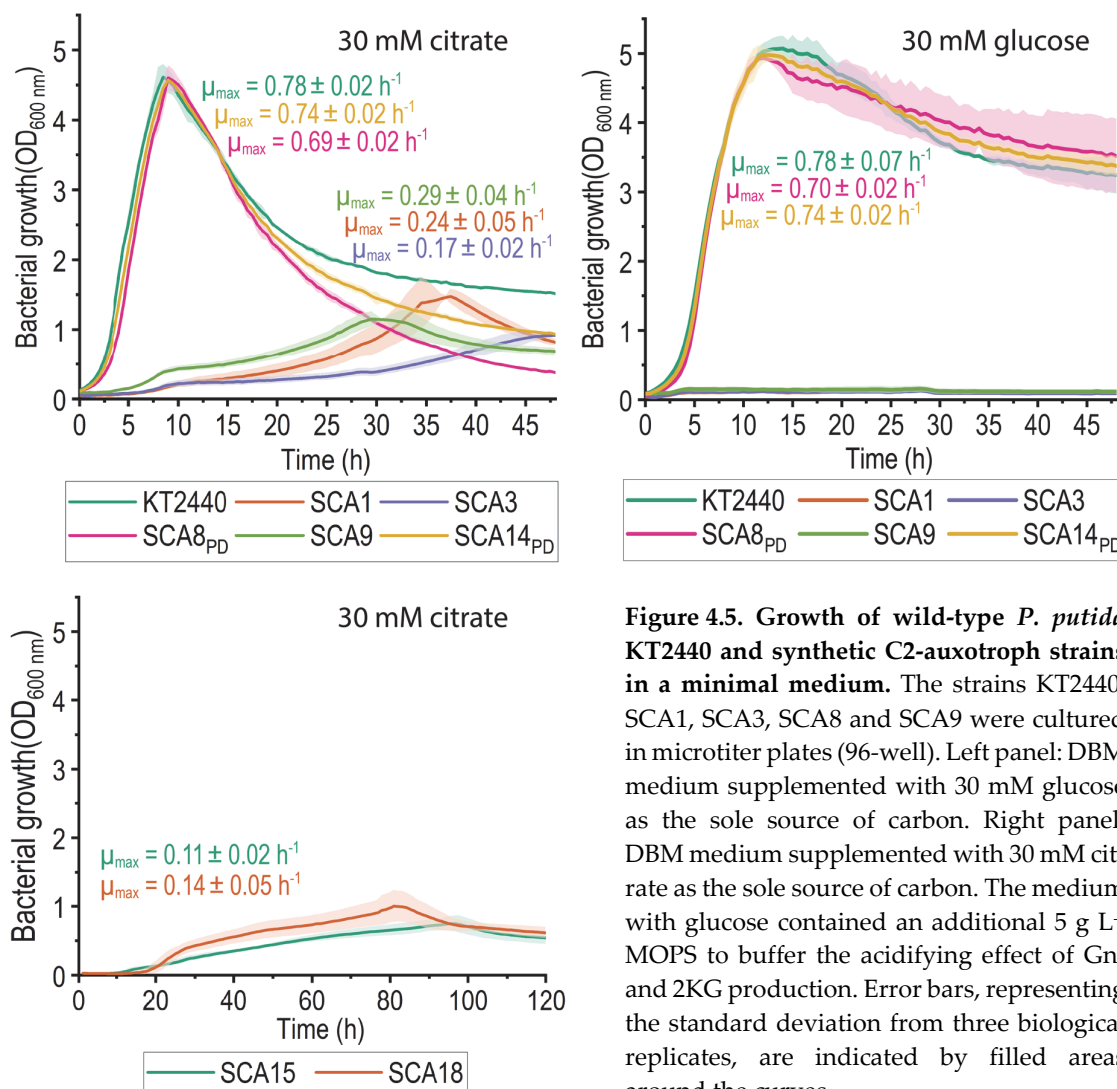


Figure 4.5. Growth of wild-type *P. putida* KT2440 and synthetic C2-auxotroph strains in a minimal medium. The strains KT2440, SCA1, SCA3, SCA8 and SCA9 were cultured in microtiter plates (96-well). Left panel: DBM medium supplemented with 30 mM glucose as the sole source of carbon. Right panel: DBM medium supplemented with 30 mM citrate as the sole source of carbon. The medium with glucose contained an additional 5 g L⁻¹ MOPS to buffer the acidifying effect of Gnt and 2KG production. Error bars, representing the standard deviation from three biological replicates, are indicated by filled areas around the curves.

Glucose (C6) and acetate (C2) are co-consumed in *P. putida* KT2440 (Figure 4.S3). Thereby, glucose is used as an energy source as long as acetate is assimilated. After the depletion of acetate, the carbon skeleton of glucose is utilized for the formation of biomass. With their co-utilization, it seemed possible to restore growth in SCA strains via the co-feeding of acetate in addition to glucose. To gain insights into the requirements for acetate as co-substrate, SCA3 and SCA15 were cultured in minimal medium with 30 mM glucose as well as varying concentrations of potassium acetate (K-Ac; Figure 4.6). There was a linear dependency of the maximum biomass concentration reached by the strains and acetate when supplied up to 1.8 g L⁻¹ (30 mM). At higher cell concentrations, oxygen limitation becomes a limiting factor in microtiter plates

due to low oxygen transfer rates, leading to a disproportional rise in cell densities at increasing substrate concentrations. The maximum specific growth rate (μ_{\max}) of SCA3 was equal to that of wild-type *P. putida* on glucose and acetate (**Table 4.2**). However, the cumulative effects of twelve additional deletions in SCA15 led to a μ_{\max} reduction by about one-half while lowering the acetate-specific biomass yield (Y_{XS}) by about one-fourth.

The reduced μ_{\max} and Y_{XS} in SCA15 were likely the result of inactivation of the glyoxylate shunt via deletion of *glcB*, causing all carbon introduced into the TCA cycle by acetate-derived Ac-CoA to be converted into CO₂. Thus, essential TCA cycle intermediates need to be replenished from glycolytic end-metabolites (pyruvate and PEP) exclusively. However, the required anaplerotic reactions might not be active under the given regulatory regime with both glucose and acetate as substrates. The inactivation of the glyoxylate shunt also prevented the utilization of acetate as the only carbon source for SCA15 (**Figure 4.S1**).

All SCA strains, including SCA15, were still able to grow on citrate as the sole source of carbon (**Figure 4.5**). To rule out any side-activity of the citrate synthase in the reverse direction (further addressed in *Discussion*), its encoding gene *gltA* was deleted alongside genes involved in carbon catabolite repression. However, the resulting strain, SCA18, was still able to grow on citrate as the sole carbon source, with no apparent growth deficiencies compared to SCA15 (**Figure 4.5**).

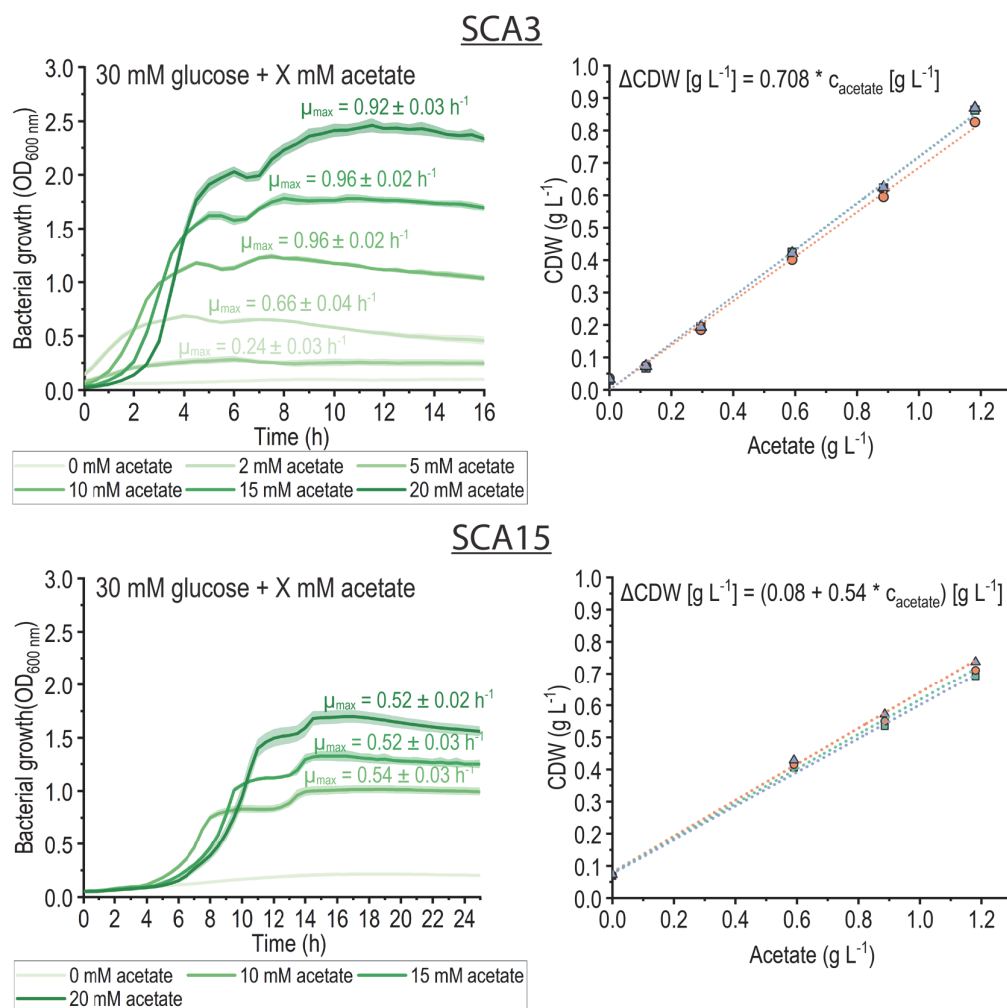


Figure 4.6. Acetate-dependent growth of the synthetic C2-auxotroph strains SCA3 and SCA15. The experiments were performed in microtiter plates (96-well). Left panels: growth in minimal medium with 30 mM glucose and varying concentrations of acetate. Error bars, representing the standard deviation from three biological replicates, are indicated by filled areas around the curves. Right panels: linear correlation of biomass yield and supplied acetate concentration. The slope and intersection values in the equation displayed in the right panels represent the average values from three independent correlations performed on biological replicates. The slope values obtained via linear regression for each strain had a standard deviation of < 3.3%.

Table 4.2. Quantitative physiology parameters of engineered strains in minimal medium with glucose and acetate. Maximum exponential growth rates (μ_{\max}) were determined via Gaussian Process regression for growth experiments in microtiter plates. Biomass yields Y_{XS} in gram cell dry weight (g_{CDW}) per gram of substrate (g_S) were calculated for each indicated substrate (S). Given are the average values \pm standard deviation from at least three biological replicates.

Strain	Carbon sources	μ_{\max} [h ⁻¹]	Biomass yield Y_{XS} [$g_{CDW} g_S^{-1}$]
KT2440	30 mM glucose	0.78 \pm 0.07	0.37 \pm 0.02 (S: glucose)
KT2440	30 mM glucose 40 mM acetate	0.98 \pm 0.05	-
KT2440	5-20 mM acetate	0.77 \pm 0.14	0.33 \pm 0.01 (S: acetate)
SCA3	30 mM glucose	-	-
SCA3	30 mM glucose 5 mM acetate	0.66 \pm 0.00	0.65 \pm 0.02 (S: acetate)
SCA3	30 mM glucose 10-20 mM acetate	0.95 \pm 0.02	0.71 \pm 0.01 (S: acetate)
SCA3	5-20 mM acetate	0.61 \pm 0.07	0.34 \pm 0.06 (S: acetate)
SCA15	30 mM glucose	-	- (S: acetate)
SCA15	30 mM glucose 5 mM acetate	0.56 \pm 0.02	0.71 \pm 0.06 (S: acetate)
SCA15	30 mM glucose 10-20 mM acetate	0.53 \pm 0.03	0.60 \pm 0.08 (S: acetate)
SCA15	5-20 mM acetate	-	- (S: acetate)

4.2.3. Quantitative proteome analysis exposes the dependency of synthetic C2 auxotrophs on acetate and highlights bottlenecks for a functional phosphoketolase pathway

To uncover the effects of removing intracellular Ac-CoA sources, the protein content of the exponentially growing strains SCA3 and KT2440 was analyzed via mass spectrometry. Cells were grown in minimal medium supplemented with 30 mM glucose and 30 mM K-Ac, whereby a total of 110 proteins were significantly differently [false discovery rate (FDR) of $\leq 5\%$] expressed with an absolute $\log_2(\text{fold change})$ of ≥ 1 (Figure 4.7). Among these, 45 were identified to have metabolic functions (Table 4.S2).

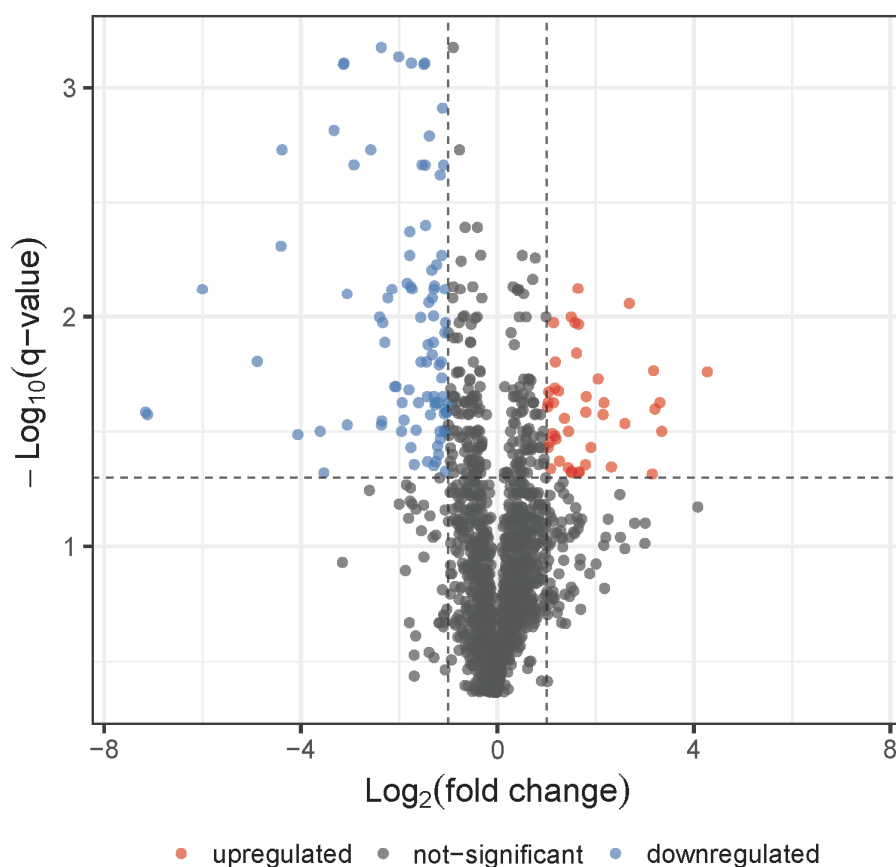


Figure 4.7. Volcano plot of mass spectrometry results showing differentially expressed proteins in strain SCA3 compared to *P. putida* KT2440. Both strains (with three biological replicates) were grown in DBM medium supplemented with 30 mM glucose and 30 mM K-Ac and harvested in the mid-exponential phase to measure the entire protein content of biomass. Each point in the plot represents an individual protein. The horizontal intersection is set at a q-value (FDR) of ≤ 0.05 ; the vertical intersections are placed for an absolute fold-change of ≥ 2 .

Within central carbon metabolism, a down-regulation of gluconokinase (GnuK), glucose 6-phosphate 1-dehydrogenase (ZwfA²⁹⁵), and 6-phosphogluconolactonase (Pgl) was observed together with an up-regulation of 2-keto-gluconate-6-P (2K6PG) reductase (KguD) (**Figure 4.8**). This pattern suggests a shift from the preferred glucose utilization route (i.e., glucose oxidation and gluconate uptake¹⁰⁵) towards further oxidation to 2KG and utilization thereof. We had observed before that engineered *P. putida* strains convert supplied glucose into 2KG at significant rates if implemented genetic modifications hampered their growth^{296,297}. The resulting accumulation of 2KG is the consequence of a missing regulatory mechanism that couples the cells' substrate uptake rate to the activities of the periplasmic dehydrogenases under glucose excess.

Strain SCA3 showed a diverging pattern in the expression of enzymes involved in the anaplerotic reactions connecting the downstream EMP route with the TCA cycle. Compared to wild-type strain KT2440, the oxaloacetate (Oaa)-producing pyruvate carboxykinase (PycA and PycB) was down-regulated by 70%. On the other hand, the Oaa-consuming oxaloacetate decarboxylase (OadC, *PP_1389*) was up-regulated by a factor of 6.4. Simultaneously, the two enzymes constituting the glyoxylate shunt, isocitrate lyase (AceA) and malate synthase (GlcB), were 3.5- and 2.0-fold more abundant in SCA3. Furthermore, two enzymes associated with fatty acid degradation (and conversely, acetyl-CoA formation), acetyl-CoA acetyltransferase (YqeF, 3.5-fold) and β -ketoacyl-CoA thiolase subunit β (FadA, 1.6-fold) were elevated. (3*R*)-3-Hydroxydecanoyl-ACP dehydratase (FabA), associated with fatty acid biosynthesis, was down-regulated 0.6-fold. These enzyme concentration changes suggest a more substantial utilization of acetate as carbon substrate for central metabolism as opposed to energy conservation. The abundance of fatty acid metabolism enzymes implies a recruitment of lipid pools to replenish Ac-CoA. The activity of the glyoxylate shunt is essential for utilizing acetate as a carbon source since it bypasses the two decarboxylation steps of the TCA cycle. The thereby conserved carbon could be further fed into the gluconeogenic route, as indicated by OadC overexpression.

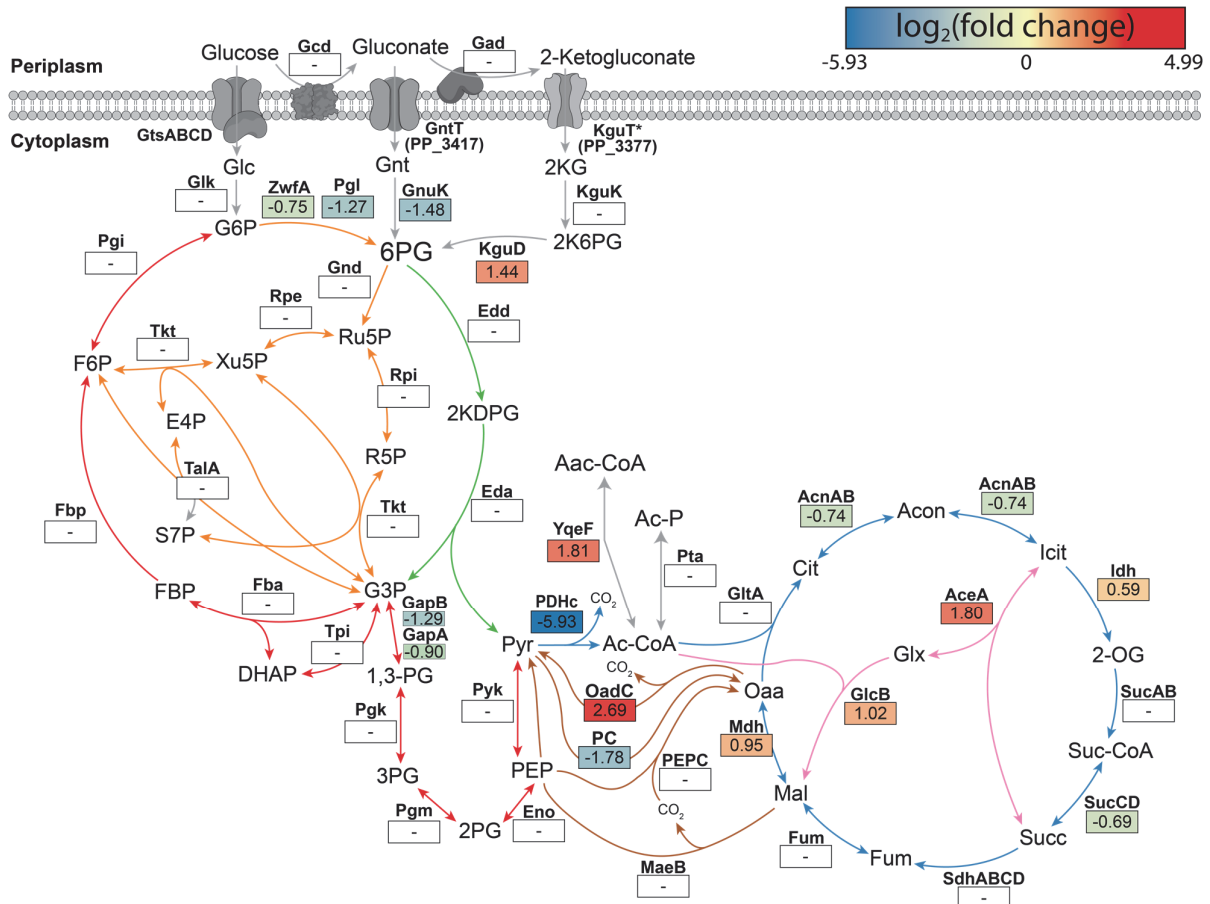


Figure 4.8. Changes in protein expression within central carbon metabolism for strain SCA3 compared to *P. putida* KT2440. The two strains were grown in DBM medium supplemented with 30 mM glucose and 30 mM acetate. Shown are the $\log_2(\text{fold change})$ values for significantly differentially expressed proteins (q -value of 0.05). The reactions are categorized into the ED pathway (green), the PP (orange), the EMP route (red), the TCA cycle (blue), the glyoxylate shunt (pink), and the anaplerotic reactions (brown). A list of abbreviations is given in Figure 4.3. Additional abbreviations: Aac-CoA, acetoacetyl-coenzyme A; YqeF, acetyl-CoA acetyltransferase; OadC, oxaloacetate decarboxylase.

Next, the *P. putida* proteome was analyzed regarding the abundance of enzymes carrying a higher in silico flux in the designed phosphoketolase shunt-utilizing strain (Section 4.2.1) compared to the wild-type model iJN1411. Edd and Eda were included in the analysis as an indication of ED pathway activity. These two reactions were predicted to be absent under ideal flux distributions. Wild-type strain KT2440 was grown in minimal medium supplemented with 30 mM glucose (\pm 30 mM acetate), and biomass was sampled in the mid-exponential phase. For an easier comparison of expression levels, the quantile-normalized protein abundances were normalized to the

housekeeping protein RNA polymerase sigma factor RpoD. **Figure 4.9** shows a comparison of the relative protein abundances for KT2440 grown on glucose as well as the cells grown on glucose and K-Ac. Most enzymes within the upstream glycolysis were produced at statistically significantly lower rates in the presence of acetate as co-substrate. However, none of the abundances was changed by more than 50%. Only Pta was expressed 7.8-fold higher in the presence of glucose and acetate compared with glucose as the sole carbon source. While its functionality in the conversion of Ac-P to Ac-CoA was experimentally demonstrated²⁶⁹, the low Pta abundance in glucose-grown *P. putida* suggests a potential bottleneck for a functional PK pathway.

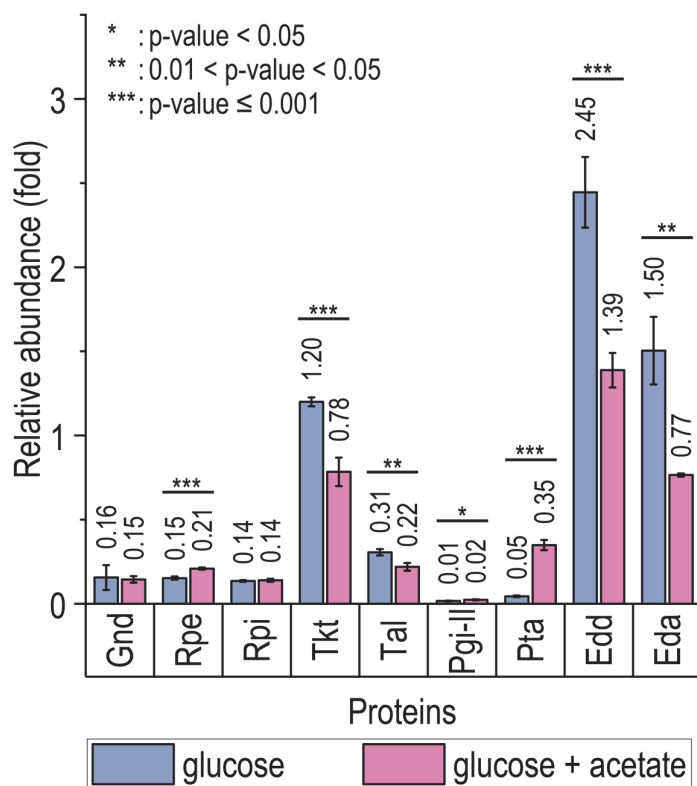


Figure 4.9. Protein abundance of selected central carbon metabolism genes in *P. putida* KT2440 grown on glucose and glucose + acetate. The strain was cultured in minimal medium supplemented with 30 mM glucose \pm 30 mM K-Ac. Quantile-normalized values were normalized to the abundance of RpoD in each sample. Error bars indicate the standard deviation of three biological replicates.

The flux through the PPP is low in *P. putida* KT2440 and optimized for the precise supply of biomass precursors, as exposed both by in silico analysis and confirmed experimentally in glucose-grown cells¹⁰⁵. Therefore, it was not surprising that the protein levels of all PPP enzymes were low in all test conditions except for transketolase (Tkt) and transaldolase (Tal). These two enzymes catalyze the interconversion of PPP

metabolites and act simultaneously on two substrates. Flux control over these reactions is likely exerted on a metabolite level. Despite high catalyst concentrations, the reactions can only occur if the remaining PPP reactions provide the substrates involved. High basal levels of Tkt and Tal allow for a quicker response to changes in the flux distribution within the EDMP network (**Section 2.1.3**).

4.2.4. Implementing the phosphoketolase pathway in a synthetic C2 auxotroph restores prototrophy on glucose

After confirming that the synthetic C2-auxotrophic designs could not utilize glucose as the sole carbon substrate, the PK pathway was implemented. To this end, the original gene sequence encoding the bifunctional phosphoketolase Xfpk^{BA} from *Bifidobacterium adolescentis* E194 was amplified via PCR and introduced into a landing pad in the intergenic region between *PP_0013* (*gyrB*) and *PP_5421* in the chromosome of SCA3 (**Section 3.4.3**), yielding strain SCA3_{PK} (**Table 4.4**). Additionally, the strain was transformed with plasmid pS438-*pta*^{EC}. This plasmid served two functions in SCA3_{PK}: the abundance of the native Pta in *P. putida* was found to be low in glucose-grown wild-type KT2440 and SCA3 (see **Section 4.2.3**). Consequently, overexpression of *pta* from *E. coli* (*pta*^{EC}) should complement the essential phosphate acetyltransferase activity for the Ac-P produced by Xfpk^{BA}. The XylS/*Pm* expression system was used to this end. In this setup, the plasmid-borne XylS should also initiate transcription from the *Pm* promoter controlling the expression of *xfpk*^{BA} in the chromosome.

The production and functionality of Xfpk^{BA} were tested in vitro with cell lysates via indirect chemical detection through the hydroxamate method (**Figure 4.10**). To this end, the soluble fraction of cell-free extracts obtained from strains SCA3/pS438-*pta*^{EC} and SCA3_{PK}/pS438-*pta*^{EC} were adjusted to a final total protein concentration of 5.9 mg mL⁻¹, and Ac-P formation from F6P was monitored over time.

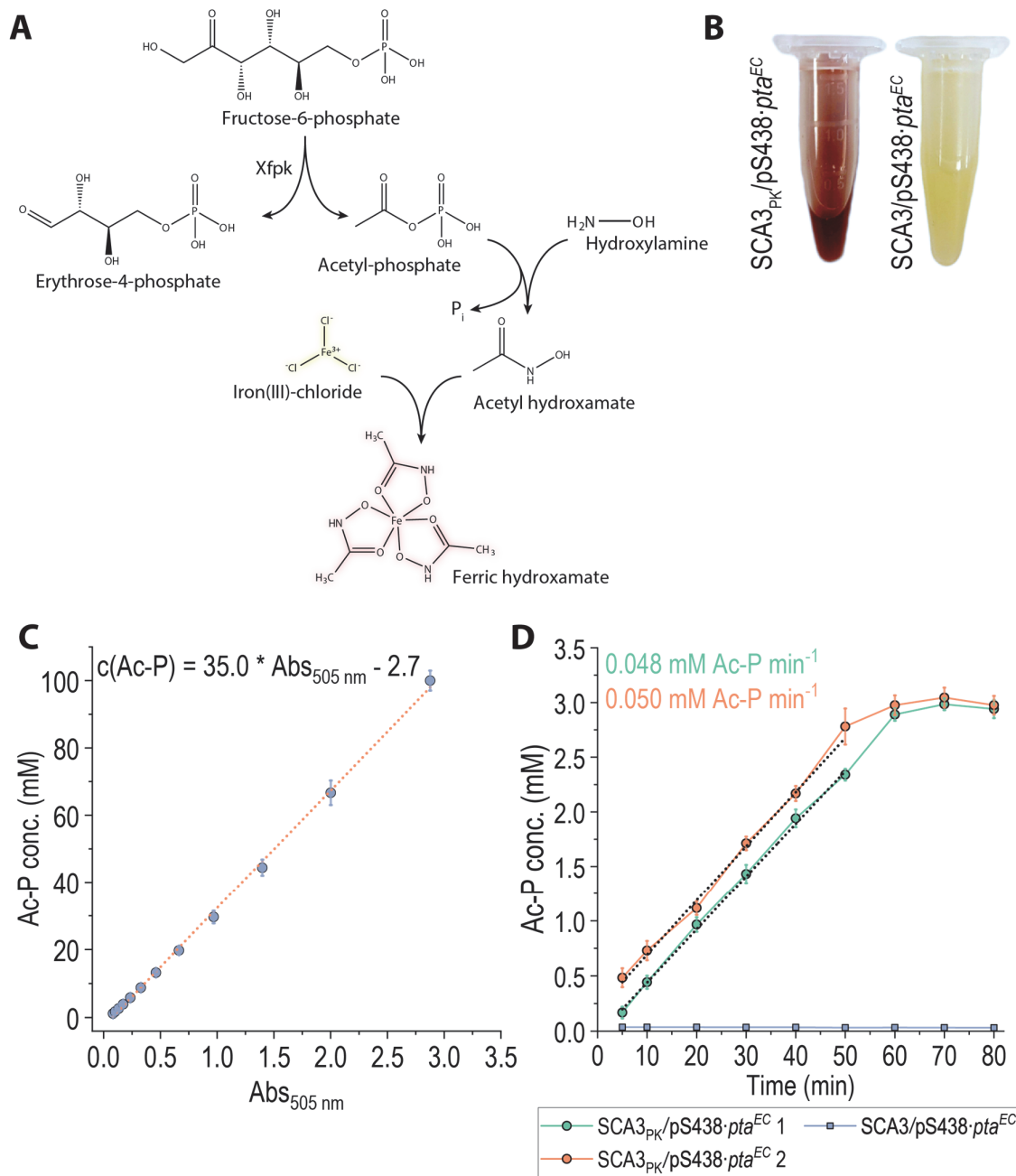


Figure 4.10. In vitro assay for the determination of phosphoketolase activity. Cell lysates were prepared from cultures grown in LB medium supplemented with 0.5 mM 3-*m*Bz. Total protein concentrations of 5.9 mg mL⁻¹ were used for the conversion of F6P to Ac-P. The concentration of the latter was determined using the hydroxamate method. **(A)** Reaction scheme of the PK assay via the hydroxamate method. **(B)** Photo of reaction samples with enzymatic conversion for 1 h followed by the chemical conversion of Ac-P to ferric hydroxamate. The red color for strain SCA3_{PK}/pS438-*pta*^{EC} indicates the formation of Ac-P by the cell extract. **(C)** Calibration curve made to quantify produced Ac-P from absorbance measurements at 505 nm ($Abs_{505\text{ nm}}$). The calibration was performed with three serial dilutions of Ac-P. **(D)** Results of the hydroxamate assay for the strains SCA3/pS438-*pta*^{EC} and SCA3_{PK}/pS438-*pta*^{EC}. Each strain was tested with two biological replicates, and each clone was screened with three technical replicates. Only one of two biological replicates is shown for strain SCA3/pS438-*pta*^{EC}. Error bars represent the standard deviation obtained from technical replicates.

No formation of Ac-P was observed for the strain without *xfpk*^{BA} (SCA3/pS438-*pta*^{EC}). Cell lysates of strain SCA3_{PK}/pS438-*pta*^{EC} converted 51.3 mM F6P into 2.95 mM Ac-P in 1 h with a specific activity of 0.083 mM Ac-P mg protein⁻¹ min⁻¹. The hexose isomerase (Pgi-I) that was shown to be produced at low concentrations (**Figure 4.9**) could have caused additional depletion of F6P in the reaction mixtures. Regardless, the results of the hydroxamate assay indicated that Xfpk^{BA} was produced and was active in *P. putida* at 30°C. Two other Xfpk variants, chromosomally introduced in SCA3 as codon-optimized sequences of the *xfpk* genes from *Pseudomonas fluorescens* F113 and *Bifidobacterium mongoliense* YIT 10443, were tested under the same conditions but showed no significant formation of Ac-P (data not shown).

To test whether Xfpk^{BA} could restore growth of a synthetic C2 auxotroph, strains SCA3_{PK}/pS438-*pta*^{EC} and SCA3/pS438-*pta*^{EC} were cultured in minimal medium supplemented with 10 mM glucose as well as 0.5 mM 3-*mBz*, with and without an additional 5 mM K-Ac. The expression of both *xfba*^{BA} and *pta*^{EC} enabled growth of SCA3_{PK}/pS438-*pta*^{EC}, with an Y_{XS} of 0.02 g_{CDW} g_{glc}⁻¹ and a μ_{max} of 0.06 h⁻¹ (**Figure 4.11A**). The expression of only *pta*^{EC} had no effect on growth.

The two reactions performed by 6-phosphogluconate dehydrogenase (Gnd) and ribulose 5-phosphate 3-epimerase (Rpe) were highly elevated in the optimal flux prediction obtained with iJN1411 for a C2-auxotrophic design compared to the *wild-type* model (**Section 4.2.1**). However, analysis of the whole proteome of *P. putida* KT2440 and SCA3 showed no significant alteration in the low protein abundances of Gnd and Rpe (**Section 4.2.3**). Therefore, the expression of *gntZ* and *rpe* was artificially enhanced via the chromosomal integration of a Tn7-encoded, synthetic *gntZ-rpe* operon on plasmid pTn7-*P*_{14g}(*BCD10*)→*gntZ-rpe* (**Table 4.5**). The expression of *gntZ* was controlled by the strong, constitutive *P*_{14g} promoter²⁹⁸ and the bi-cistronic translational coupling sequence *BCD10*²⁹⁹. The two genes within the operon were translationally coupled by overlapping the Stop codon (in bold) of *gntZ* and the Start codon of *rpe* (underlined): ATGA. The chromosomal integration was achieved by cloning the synthetic operon into a mini-Tn7 transposon on the plasmid pTn7. Overexpression of *gntZ* and *rpe* led to an increased μ_{max} by a factor of two and improved the biomass yield by two-thirds for the resulting strain SCA3_{PK-Tn}/pS438-*pta*^{EC} compared to SCA3_{PK}/pS438-*pta*^{EC} (**Figure 4.11B**).

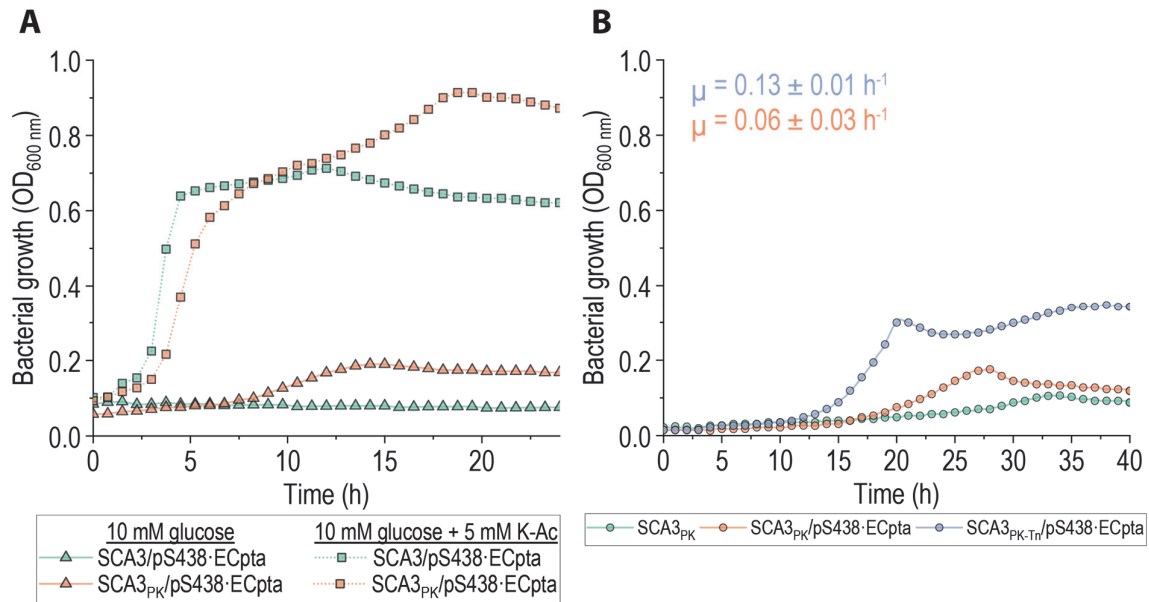


Figure 4.11 The expression of *xfpk*^{BA} restores growth of a synthetic C2 auxotroph on glucose. The strains were cultured in microtiter plates (96-well) in DBM medium supplemented with 10 mM glucose and 0.5 mM 3-*mBz* ± 5 mM K-Ac. **(A)** Comparison of SCA3 harboring plasmid pS438-*pta*^{EC} with and without chromosomally integrated *xfpk*^{BA}. **(B)** Effect of *gntZ* and *rpe* overexpression on the growth of SCA3_{PK}. The lag times varied considerably between three replicates performed for each strain and condition. Thus, only one of three replicates is shown. The OD_{600 nm} increase for strain SCA3_{PK} could be attributed to the formation of colored compounds produced from 3-*mBz* via oxidation. Maximum observed growth rates and biomass yields are summarized in **Table 4.2**.

As predicted by FBA simulations, the implementation of a phosphoketolase combined with increasing Gnd, Rpe, and Pta production proved to be a successful strategy to restore growth in a C2-auxotroph strain. The growth rate and biomass yield observed for strain SCA3_{PK}/pS438-*pta*^{EC} was deemed sufficient to support adaptive evolution on the new metabolic network architecture.

4.2.5. Adaptive laboratory evolution enabled the integration of the phosphoketolase pathway into the metabolic network of *P. putida*

To optimize the flux through the implemented pathway, strain SCA3_{PK-Tn}/pS438·pta^{EC}, as well as SCA3, SCA3/pS438·pta^{EC}, and SCA3_{Tn}/pS438·pta^{EC} were subject to ALE. Evolution was performed in 24-well deep-well plates filled with 2 mL DBM medium supplemented with 30 mM glucose and 0.5 mM 3-*m*Bz. A volume of 50 μ l (after glucose cultures) or 20 μ l (after culture steps with glucose and acetate) of each culture was passed into fresh medium every other day. For every second passage, the medium contained an additional 20 mM of K-Ac to recover biomass at higher concentrations. After 1 month of continued cultivation, ALE was continued using DBM medium supplemented with only glucose.

After an estimated number of 140 generations (ca. 2 months), no significant difference in growth was observed for the strains SCA3, SCA3/pS438·pta^{EC}, and SCA3_{Tn}/pS438·pta^{EC} (results not shown). However, the Y_{XS} of SCA3_{PK-Tn}/pS438·pta^{EC} increased to 0.09 g_{CDW} g_{glc}⁻¹ and μ_{max} to 0.28 h⁻¹, representing an increase from the pre-evolved strain by factors of 3 and 2, respectively (Figure 4.12 and Table 4.3). The evolved strain grew at one-third the maximum rate of the wild-type *P. putida* KT2440. The enhanced growth observed for the evolved strain on glucose was stable even after five sub-culturing steps in a rich medium (LB). Hence, evolution rather than adaptation appeared to be responsible for the improved phenotype.

When grown on gluconate instead of glucose, the growth rate was not significantly altered. However, evolved SCA3_{PK-Tn}/pS438·pta^{EC} reached only 36% cell density compared to growth on glucose. This suggested a stoichiometric bottleneck in the production of energy or reducing equivalents on gluconate. During growth on glucose, 26% of membrane-bound ubiquinol in the electron transport chain is predicted to be produced by direct glucose oxidation (FBA with iJN1411), acting as an implicit ATP source. Alternatively, *P. putida* can produce NAD(P)H via the oxidation of glucose 6-phosphate, contributing to the *intracellular* pool of reducing equivalents.

Table 4.3. Quantitative physiology parameters of glucose-grown PK-shunt strains. Maximum exponential growth rates (μ_{\max}) were determined via Gaussian Process regression for growth experiments in microtiter plates. Biomass yields Y_{XS} in gram cell dry weight (g_{CDW}) per gram of substrate (g_S) were calculated for each indicated substrate (S). Given are the average values \pm standard deviation from at least three biological replicates.

Strain	Carbon sources	μ_{\max} [h^{-1}]	Biomass yield Y_{XS} [$g_{CDW} g_S^{-1}$]
SCA3 _{PK} /pS438· <i>pta</i> ^{EC} (pre-evolved / evolved)	10 or 30 mM glucose	0.06 \pm 0.03	0.02 \pm 0.01 (S: glucose)
SCA3 _{PK-Tn} /pS438· <i>pta</i> ^{EC} (pre-evolved)	10 or 30 mM glucose	0.13 \pm 0.01	0.03 \pm 0.01 (S: glucose)
SCA3 _{PK-Tn} /pS438· <i>pta</i> ^{EC} (evolved)	5-30 mM glucose	0.28 \pm 0.03	0.09 \pm 0.01 (S: glucose)
SCA3 _{PK-Tn} /pS438· <i>pta</i> ^{EC} (evolved)	5-30 mM gluconate	0.23 \pm 0.03	0.03 \pm 0.01 (S: glucose)

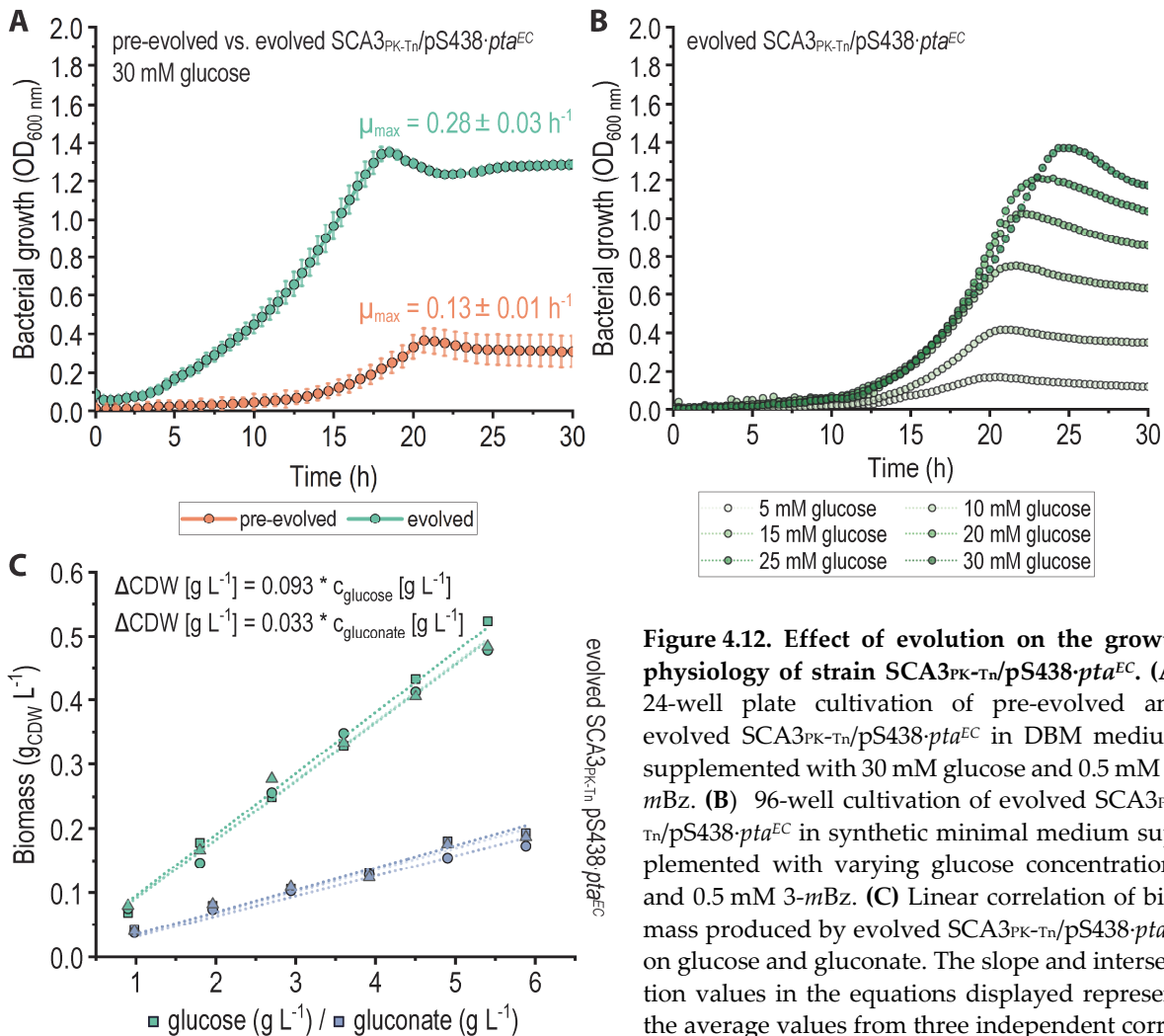


Figure 4.12. Effect of evolution on the growth physiology of strain SCA3_{PK-Tn}/pS438·*pta*^{EC}. (A) 24-well plate cultivation of pre-evolved and evolved SCA3_{PK-Tn}/pS438·*pta*^{EC} in DBM medium supplemented with 30 mM glucose and 0.5 mM 3-*mBz*. (B) 96-well cultivation of evolved SCA3_{PK-Tn}/pS438·*pta*^{EC} in synthetic minimal medium supplemented with varying glucose concentrations and 0.5 mM 3-*mBz*. (C) Linear correlation of biomass produced by evolved SCA3_{PK-Tn}/pS438·*pta*^{EC} on glucose and gluconate. The slope and intersection values in the equations displayed represent the average values from three independent correlations performed on biological replicates. Maximum observed growth rates and biomass yields are summarized in **Table 4.3**.

Comparative proteome analysis of glucose-grown *SCA3_{PK-Tn}/pS438-pta^{EC}* performed on cultures before and after evolution did not reveal any significant changes in the production of proteins that could explain the improved growth. However, the pre-evolved clones displayed a greatly increased variation in protein content, reflected in large Euclidean distances between each strains' dataset (**Figure 4.13A**). This high fluctuation in protein abundance prevented the identification of significant differences between the two groups and could have masked relevant changes.

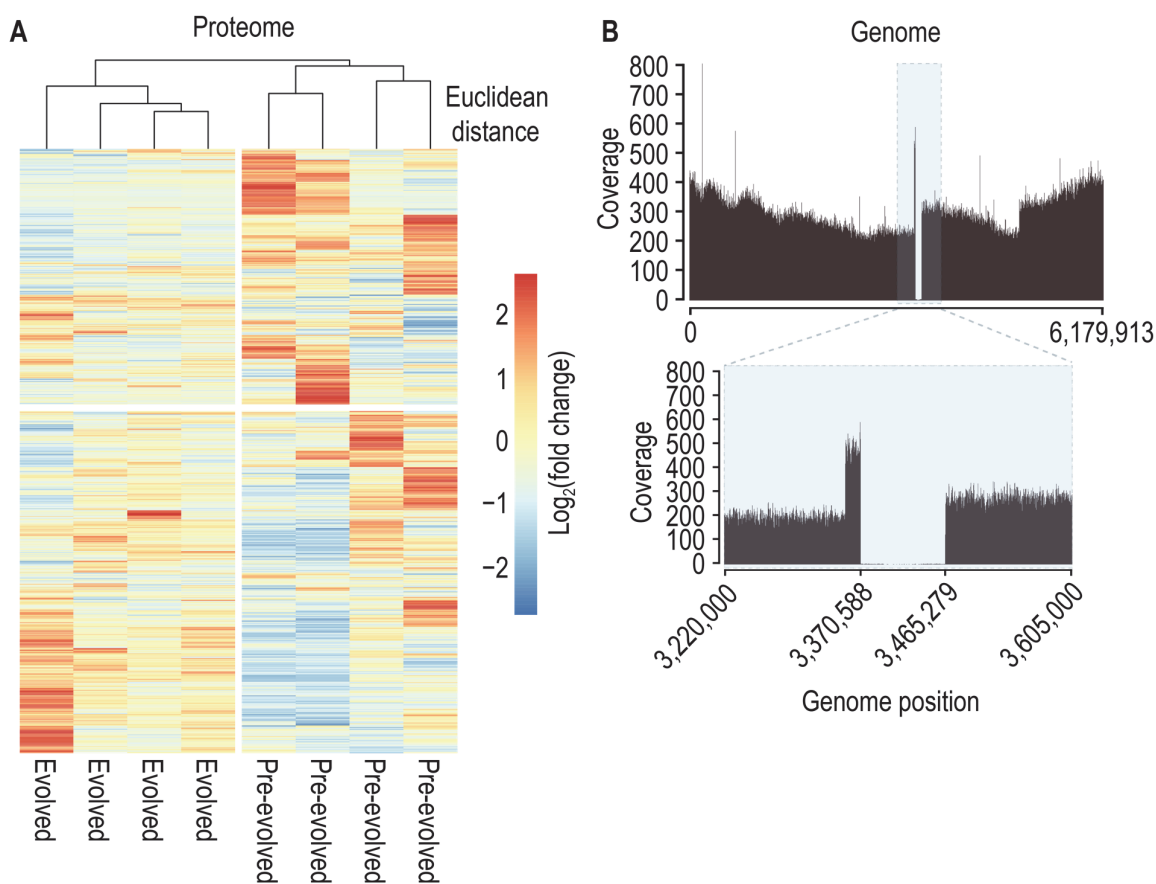


Figure 4.13. Omics approaches to identify the effects of evolution on *SCA3_{PK-Tn}/pS438-pta^{EC}*. **(A)** Whole-proteome heat map of the evolved and pre-evolved strain with four biological replicates. The protein abundance values were quantile normalized, log₂-transformed and plotted based on their Euclidean distance. **(B)** Absence of a DNA segment in the chromosome of evolved *SCA3_{PK-Tn}/pS438-pta^{EC}* during whole-genome sequencing. The sequenced reads (raw reads) were cleared from adapter sequences, low-quality reads, and reads with N > 10% (N represents the base cannot be determined). Then, the filtered reads were aligned to the constructed chromosomal sequence of *SCA3_{PK-Tn}/pS438-pta^{EC}*. In two out of four sequences clones, a chromosomal segment comprising 94,691 bp was almost fully absent, with a maximum local coverage of 7.

Four evolved SCA3_{PK-Tn}/pS438·*pta*^{EC} clones with enhanced growth on glucose, and four pre-evolved clones were subjected to whole-genome sequencing. Polymorphisms that were identified in both pre-evolved and evolved clones were discarded. No mutations were found in plasmid pS438·*pta*^{EC}. In the chromosomal sequence, a segment of 94,691 bp was almost entirely absent in the read coverage of two out of four evolved SCA3_{PK-Tn}/pS438·*pta*^{EC} clones (**Figure 4.12B**). This chromosomal region stretches from *PP_2985* to *PP_3089*, and harbors the previously identified prophage 2 with a length of 35.6-kb (*PP_3026-PP_3066*)^{241,300}. The loss of this prophage has not been reported so far in *P. putida* KT2440. The excised segment is furthermore located 1,111 bp downstream of the transposon Tn4652, which was shown to be activated under carbon starvation^{247,301}.

A full list of genes located within the absent region is given in **Table 4.S3**. Apart from many unknown proteins, an array of functions contributing to the production of pyocins are encoded within this region, as well as proteins with predicted regulatory and enzymatic roles. Among the potential regulatory proteins are FlaR (DNA topology modulation kinase), *PP_3006* (ECF family RNA polymerase sigma-70 factor), *PP_3002* (AraC family transcriptional regulator), ClpP (ATP-dependent protease), *PP_5558* (Xre family transcriptional regulator), *PP_3086* (RNA polymerase sigma-70 factor), *PP_3075* (putative transcriptional regulator), and *PP_3087* (excinuclease ABC subunit A). While the exact functions of these proteins have not been characterized, particularly the loss of *flaR*, *PP_3006*, *clpP*, *PP_3086*, and *PP_3086* could have caused systemic effects on DNA topology, DNA transcription, or protein degradation. Within the set of enzymes encoded in the missing chromosomal region, *PP_3071*, encoding an acetoacetyl-CoA synthetase, could have a direct effect on the intracellular Ac-CoA concentrations. The absence of the 94.7-kb chromosomal sequence was confirmed in the respective two clones via PCR-amplification of the region (**Figure 4.S4**).

Only one location within the chromosome was found to be mutated consistently in every evolved clone. In all four sequenced genomes, guanine in position 437 of the *PP_1608* coding sequence (CDS) was mutated to adenine, causing a Gly¹⁴⁶→Asp sub-

stitution in the tRNA^{Ile}-lysidine(34) synthetase TilS. This enzyme was found to be essential for the majority of all known eubacteria, with one of the few exceptions being *B. adolescentis*³⁰². TilS is involved in the maturation of the isoleucine tRNA recognizing AUA codons in the mRNA (tRNA^{Ile2}, **Figure 4.14A**). Thereby, lysine is attached to cytidine in the wobble position of the anticodon within the tRNA precursor, creating 2-lysyl-cytidine (lysidine, L). This changes the base-pairing specificity at this position (tRNA nucleotide number 34) from guanine to adenine. Consequently, tRNA^{Ile2} recognizes AUA instead of AUG. At the same time, the methionine attached to the precursor (CAU is a positive determinant for methionyl-tRNA synthetase³⁰³) is replaced by isoleucine. Without the action of TilS, the LAU-tRNA^{Ile2} precursor acts as CAU-tRNA^{Met}, and AUA codons in mRNA molecules cannot be translated correctly³⁰².

We next wanted to shed light on the potential effects caused by the Gly146→Asp substitution in TilS. To this end, we employed the SWISS-MODEL software in Alignment mode to create homology models of *P. putida* TilS based on the solved crystal structures of *Geobacillus kaustophilus* TilS (TilS^{GK}) in complex with tRNA (PDB id: 3A2K; 27.34% identity)³⁰⁴ as well as *E. coli* MesJ (MesJ^{EC}) without bound ligands (PDB id: 1NI5; 42.11% identity)³⁰⁵. The two models shared a high degree of structural similarity, particularly in their N-termini, harboring the catalytic center. Using PyMOL (version 1.1), the homology model created with 1NI5 was aligned to the 3A2K-based model as a proxy for the binding position of the tRNA in the active center. The resulting homology model of *P. putida* TilS with 1NI5, aligned to the tRNA in 3A2K, is shown in **Figure 4.14B**. A close-up view of the enzyme's substrate-binding pocket harboring the CAU anticodon of the tRNA^{Ile2} precursor is provided in **Figure 4.14C**. Residues that were found to be essential for recognizing the anticodon loop, Asp¹¹⁶, Glu¹¹⁹, Arg¹²⁷, Arg¹⁴¹, Arg¹⁸⁴, Gln²⁶³, and Leu²⁶⁶ are highly conserved and were found in the same positions as described in the crystal structure of TilS^{GK}³⁰⁴. The mutated Gly¹⁴⁶ residue is positioned close to the three anticodon nucleotides (**Figure 4.14D**). Granted that the exact 3D structure of *P. putida* TilS is not known, the proximity of Gly¹⁴⁶ to the catalytic center and its substitution's high prevalence in the evolved strain population suggests an altering effect on the enzyme's catalytic performance by the mutation.

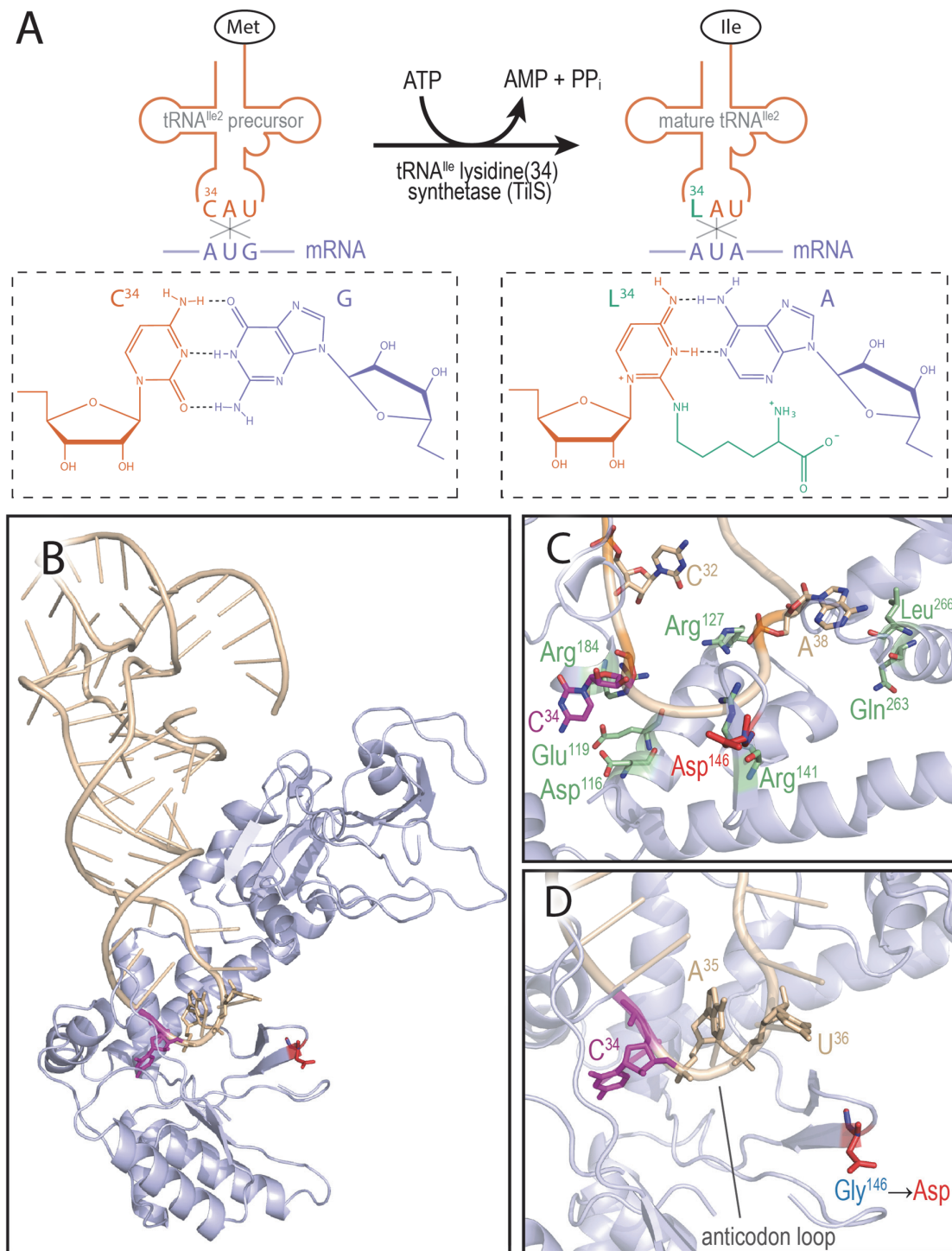


Figure 4.14. The effect of mutated TilS in strain SCA3_{PK-Tn}/pS438-pta^{EC}. (A) Reaction performed by TilS. Energized by ATP hydrolysis, L-lysine is attached to cytosine in position 34 of the tRNA^{Met} precursor molecule³⁰². The base-pairing specificity changes from G to A. Consequently, L-methionine (Met) loaded onto the precursor tRNA is replaced by L-isoleucine (Ile). (B) 3D structure of a homology model (violet) obtained for *P. putida* TilS using *E. coli* MesJ (PDB id: 1NI5) as the structural framework and the similarity to *G. kaustophilus* TilS (PDB id: 3A2K) to position the tRNA^{Met} precursor (beige) within the structure. C³⁴ is highlighted in magenta. (C) Conservation of amino acids involved in recognizing the precursor tRNA. Residues that were shown to interact with nucleotides³⁰⁴ are highlighted in green. The Gly¹⁴⁶→Asp mutation is drawn in red. (D) Position of the mutated residue relative to the anticodon of the tRNA substrate.

The codon ATA is present at an overall frequency of 0.21% in *P. putida* KT2440³⁰⁶. Compared to the other two triplets, ATT (21%) and ATC (74%), ATA encodes 4.5% of isoleucines within all CDSs. A modified catalytic efficiency of TilS could affect the intracellular tRNA^{Ile2} pools, causing system-wide alterations in the translation efficiency of proteins harboring an ATA codon in their encoding gene sequence.

4.2.6. The PK pathway enables the conservation of carbon during growth on glucose

To characterize the physiology of the evolved PK-utilizing SCA3_{PK-Tn}/pS438-*pta*^{EC} compared to wild-type strain KT2440 under controlled conditions, aerobic batch fermentations were performed in bioreactors. Glucose was used as the only carbon substrate at a concentration of 30 mM. **Figure 4.15A** shows the time-resolved measurements for the dissolved oxygen concentration (DO), biomass as OD_{600 nm}, differential CO₂ production rates, and corresponding metabolite concentrations. The list of compounds measured via HPLC comprised glucose, Gnt, 2KG, pyruvate, succinate, and acetate.

Wild-type strain KT2440 reached its maximum cell density at an OD_{600 nm} of 5.4 within 11 h. The growth rate throughout the exponential phase (μ) was 0.54 h⁻¹, with a maximum value of 0.65 h⁻¹ (**Figure 4.15B**). Concomitant with a temporary secretion of Gnt (≤ 2.4 mM) and 2KG (≤ 3.2 mM), all six-carbon variants were consumed entirely with a combined consumption rate (q_s) of 1.70 g_{C6} g_{CDW}⁻¹ h⁻¹ (9.34 mmol_{C6} g_{CDW}⁻¹ h⁻¹). The biomass yield on the substrate (Y_{XS}) was 0.33 g_{CDW} g_{C6}⁻¹ (0.06 g_{CDW} mmol_{C6}⁻¹). No metabolites other than the three six-carbon moieties were detected in the medium. *P. putida* KT2440 generated 1.74 mol of CO₂ per C-mol of produced biomass (**Figure 4.15C**), at a production rate of 1.76 ± 0.62 mmol g_{CDW}⁻¹ h⁻¹ over the growth phase. Maintenance requirements were not considered for the calculation of any physiological parameter.

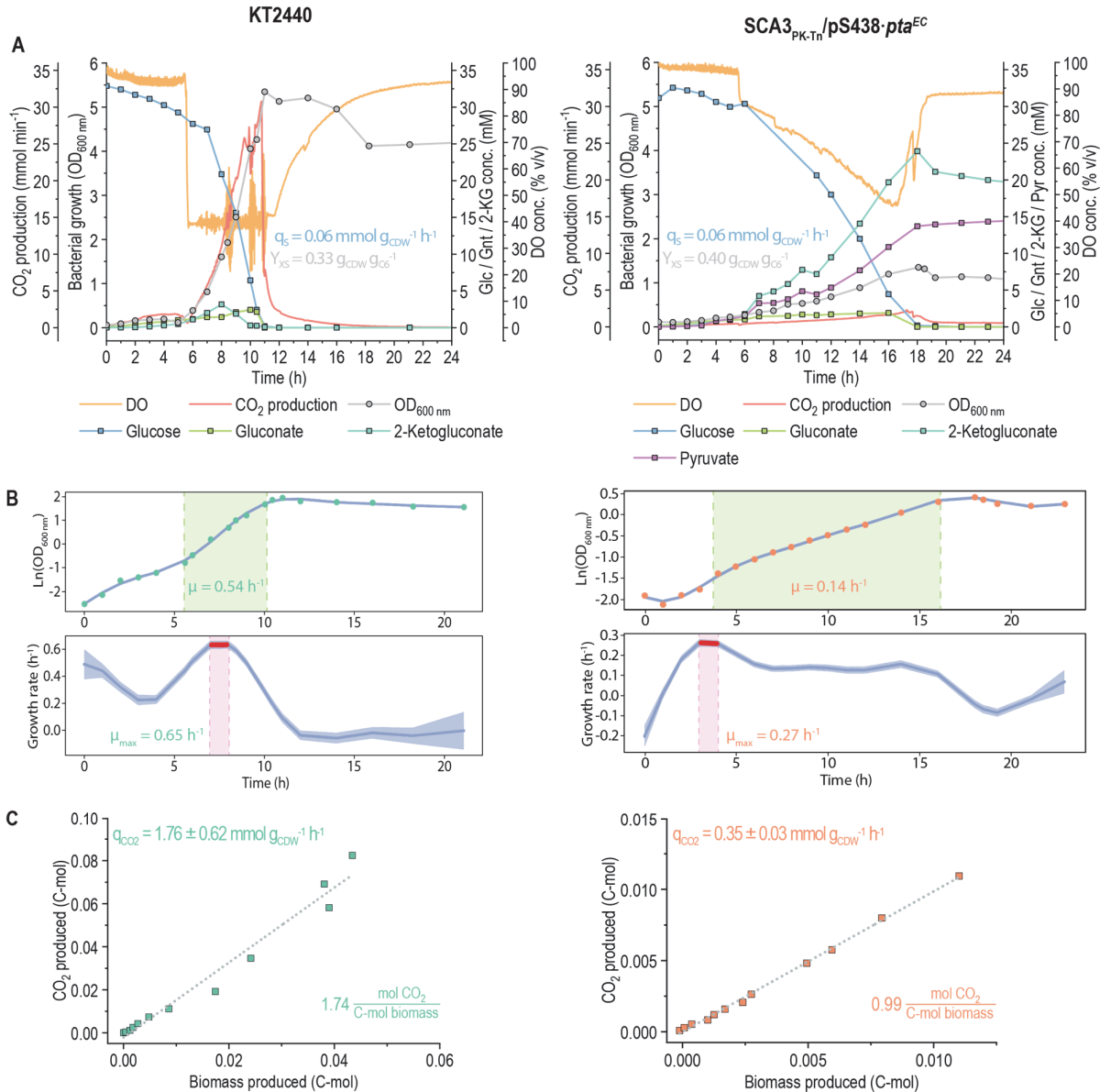


Figure 4.15 Bioreactor fermentations of *P. putida* KT2440 and SCA3_{PK-Tn}/pS438-pta^{EC}. The cells were grown in lab-scale bioreactors in batch mode. The culture medium was DBM medium supplemented with 30 mM glucose and, for SCA3_{PK-Tn}/pS438-pta^{EC}, 0.5 mM 3-*m*Bz. **(A)** Selected process parameters and concentrations of measured metabolite and biomass over time. The CO₂ production rate was calculated as the difference in CO₂ flux (mmol min⁻¹) in the gas phase flowing into vs. outside of the bioreactors. No pyruvate could be detected in the medium of wild-type strain KT2440. **(B)** Determination of growth rates (μ) via linear regression of Ln-transformed OD_{600 nm} (upper panels) or maximum growth rates (μ_{max}) via Gaussian process correlation. Blue lines represent growth curves simulated by Gaussian process regression. The sections highlighted in red illustrate the maximum observed growth rates. Green-highlighted sections indicate the time window for the determination of μ via linear regression. **(C)** Correlation of the cumulative CO₂ produced (C-mol) with the produced biomass (C-mol) at sampling time points.

Strain SCA3_{PK-Tn}/pS438-*pta*^{EC} grew with a μ of 0.14 h⁻¹ (μ_{\max} : 0.27 h⁻¹) to a maximum OD_{600 nm} of 1.5 within 18 h. The growth profile thereby closely resembled that previously observed during physiological characterizations in 24-well plates (**Figure 4.12**). Glucose and its two oxidized products were consumed with a combined q_s of 0.35 g_{C6} g_{CDW}⁻¹ h⁻¹ (2.50 mmol_{C6} g_{CDW}⁻¹ h⁻¹). The PK strain formed biomass with a Y_{XS} of 0.40 g_{CDW} g_{C6}⁻¹ (0.06 g_{CDW} mmol_{C6}⁻¹). While the per-mole biomass yield was equal to that of the wild-type strain, SCA3_{PK-Tn}/pS438-*pta*^{EC} additionally secreted significant amounts of pyruvate (14.6 mM) into the medium with a specific rate of 3.76 mmol g_{CDW}⁻¹ h⁻¹. The pyruvate yield on the six-carbon substrates was 1.50 mol mol⁻¹. Pyruvate production occurred in parallel to the consumption of the three substrate moieties, and no re-consumption occurred after the cells had reached the stationary phase. The accumulation of pyruvate indicates a strong activity of the ED pathway, involving the splitting of 2KDPG into pyruvate and G3P. When exposed to glycolytic substrates or pyruvate, the cells' regulatory status could prevent the utilization of the produced pyruvate through gluconeogenic routes or anaplerotic reactions. With 50% of six-carbon substrates ending up in pyruvate (C3) after cleavage by Eda, and 1.5 mol pyruvate being produced per mol of consumed glucose, it can be estimated that at least three-fourth of the substrate entering the cells was processed through the ED pathway. This fraction was found to be 90 to 100% in wild-type strain KT2440^{105,307,308}.

The PK-supplemented glycolysis reduced the amount of CO₂ per C-mol of biomass by 43% (0.99 mol C-mol⁻¹) compared to the *pure* ED pathway in the wild type. The biomass-specific CO₂ production rate was 0.35 ± 0.03 mmol g_{CDW}⁻¹ h⁻¹. However, the lack of NADH production that would accompany pyruvate decarboxylation caused a bottleneck in energy production. This resulted in the oxidation of two-thirds of the supplied glucose to 2KG, which was secreted into the medium. Transport of 2KG across the cytoplasmic membrane has not been thoroughly studied in *P. putida*. It is assumed that the uptake is mediated by the major facilitator superfamily (MFS) transporter KguT³⁰⁹ and was shown to occur against a concentration gradient³¹⁰, likely enabled via the symport of H⁺. Once inside the cytoplasm, 2KG is activated via phosphorylation by KguK to yield 2K6PG. The utilization of 2KG further requires the NADPH-dependent reduction of 2K6PG to 6PG¹⁰⁵. However, the electrons initially removed in the periplasmic oxidation of Gnt are directly transferred onto elements of the electron transport chain in the membrane and are not available to replenish the pool of soluble reducing equivalents. After inactivation of PDHc and with the predominant use of the ED pathway, the intracellular electron carriers can only be recharged in central metabolism via the oxidation of G3P, after funneling pyruvate into the TCA cycle through anaplerotic reactions, or by recycling G3P in the EDEMP cycle. With pyruvate as a dead-end metabolite, insufficient amounts of NAD(P)H are being produced to utilize

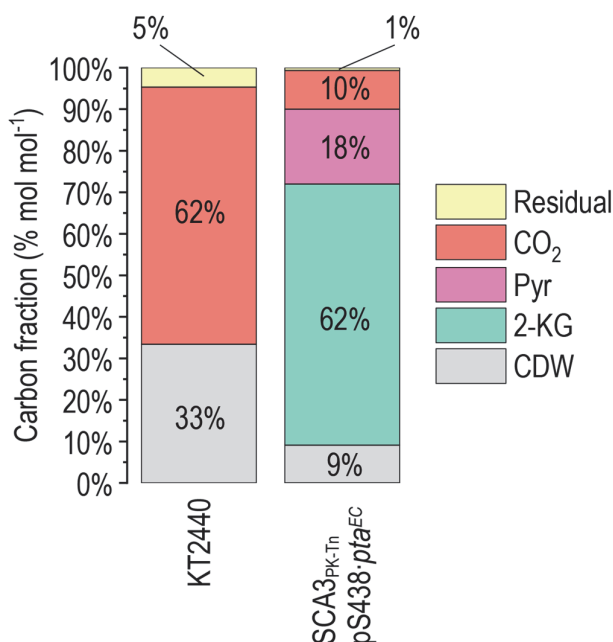


Figure 4.16 Carbon balance for bioreactor batch fermentations. Shown are all carbon-containing entities measured at the end of the growth phases for each strain. The carbon fractions represent the relative value of each entity compared to the overall amount of C-mol at the beginning of the fermentations. The amount of CO₂ was determined via the integration of measured CO₂ production rates over the whole time period.

2KG as source of carbon and energy. With a significant fraction of glucose being exclusively used as energy source, the per-gram biomass yield on the combined pool of all three six-carbon moieties was higher compared to wild-type strain KT2440.

Figure 4.16 shows the carbon balance, including all measured carbon-containing entities, at the end of the growth phase for strain KT2440 (11 h) and SCA3_{PK-Tn}/pS438·*pta*^{EC} (18 h). A residual amount of carbon could not be attributed to any of the measured components, likely due to inaccuracies in the measurement of metabolite and biomass concentrations or the volume left in the bioreactor. Both strains had fully consumed all supplied glucose by the end of the growth phase. The only carbon species identified for KT2440 were biomass (one-third) and CO₂ (two-thirds). On the other hand, strain SCA3_{PK-Tn}/pS438·*pta*^{EC} converted 80% of the supplied carbon into 2KG and pyruvate.

4.2.7. FBA-guided reconstruction of metabolic fluxes in strain

SCA3_{PK-Tn}/pS438·*pta*^{EC}

The co-utilization of the ED pathway and the PK shunt resulted in the pronounced overflow of 2KG and pyruvate. The metabolic quandary faced by *P. putida* due to the resulting imbalances is illustrated by an optimized flux distribution based on the observed phenotype (**Figure 4.17**). We again performed FBA using the created C2-auxotroph variant of model iJN1411 with the implemented PK reactions. This time, we fixed specific flux rates determined for the strain SCA3_{PK-Tn}/pS438·*pta*^{EC} during bioreactor fermentation. The glucose uptake rate was set to the experimentally determined consumption rate of 9.72 mmol g_{CDW}⁻¹ h⁻¹. Since 62% of glucose-derived carbon was found in secreted 2KG, its export reaction was set to a value of 6.0 mmol g_{CDW}⁻¹ h⁻¹. Based on the pyruvate yield, three-fourth of the carbon entering the cells was estimated to be processed through the ED pathway. Thus, the activity of Edd was fixed at 7.30 mmol g_{CDW}⁻¹ h⁻¹. Lastly, the flux through the PK pathway was estimated from the measured in vitro Fpk activity. Assuming that the quantified soluble protein fraction constitutes 45% (w/w) of biomass, the measured activity was calculated as 1.20 mmol g_{CDW}⁻¹ h⁻¹.

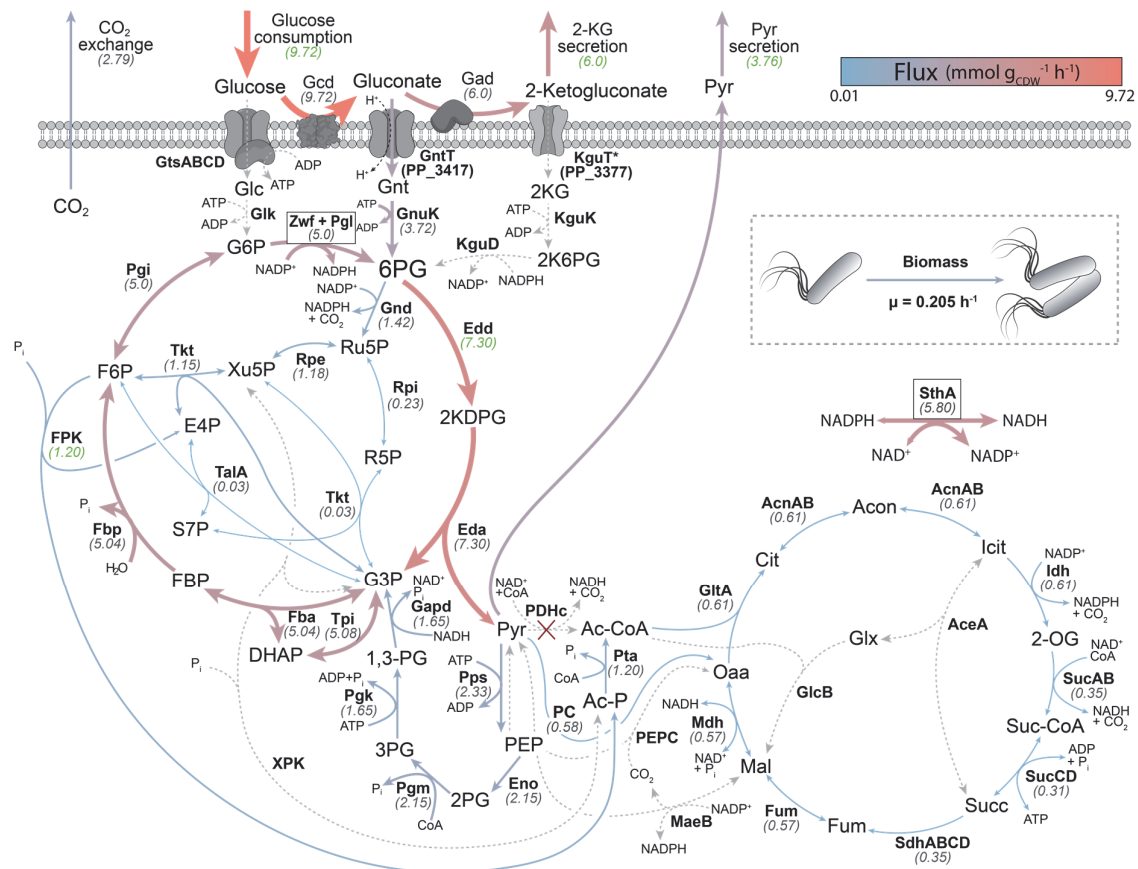


Figure 4.17. Flux distribution predicted by iJN1411 for strain *SCA3_{PK-Tn}/ps438-pta^{EC}*. Experimentally determined rates were set as fixed parameters (flux values in green), and the flux distribution was optimized for biomass production via FBA. A list of abbreviations is given in **Figure 4.3**. Additional abbreviations: Pps, phosphoenolpyruvate synthase; SthA, soluble pyridine nucleotide transhydrogenase

With the imposed constraints, the model predicted a growth rate of 0.21 h^{-1} and provided a potential flux distribution for *SCA3_{PK-Tn}/ps438-pta^{EC}*. The carbon skeleton of glucose is assimilated exclusively through the 6PG node via the import of Gnt. All of the 2KG produced from glucose is secreted. Pyruvate produced from the ED pathway is secreted at a fraction of 52% and replenishes the TCA cycle with 8%. Another 32% is directed back into biomass precursors and the ED pathway through gluconeogenesis. Within the cycle, 69% of the carbon initially processed through the ED pathway is recycled to generate NADPH. This carbon recycling is responsible for producing the majority of this electron carrier (66%), in addition to a 19% contribution by Gnd and 8% by Idh. A highly active pyridine nucleotide transhydrogenase (SthA) reaction converts a large portion of NADPH to NADH for energy generation, accounting for 70% of the NADH production in the flux distribution.

Concomitant with the low flux of pyruvate to oxaloacetate, the PK pathway provides 40% of the carbon to replenish the TCA cycle. Consequently, only half of the Ac-CoA produced is available for biomass production. However, the estimated flux through the PK pathway based on in-vitro experiments could vary significantly from the actual reaction rate in vivo. The specific activity of Xfpk on Xu5P has not been determined, and the fluxes depend strongly on the reactant concentrations in the cytoplasm, which are not known. Under the given flux distribution, the model suggests a CO₂ production rate of 2.79 mmol g_{CDW}⁻¹ h⁻¹, which is significantly higher than the experimentally determined rate for SCA3_{PK-Tn}/pS438-*pta*^{EC}.

4.3. Discussion

4.3.1. A synthetic C2 auxotroph of *P. putida* provides a tight selection regime for Ac-CoA producing pathways and reveals unknown metabolic connectivities

In this study, we employed a genome-scale model-guided approach to design synthetic C2-auxotroph selection platforms based on *P. putida*. The auxotrophy of the created strains was experimentally confirmed and shown to be reversible by the external addition of acetate. Thus, the SCA strains can be easily propagated by supplying acetate or by cultivation in complex media. The strong dependency of biomass formation on acetate provides access to a large evolutionary space in which gradual improvements in the Ac-CoA supply should stimulate fitness gains up to a great extent.

The deletion of *aceEF* proved to be sufficient to disrupt growth on glycolytic substrates. For strain SCA3, which *aceEF* deletion was combined with $\Delta bkdAA$ and $\Delta ltaE$, no effect of evolution on restoring prototrophy on glucose was observed. However, the additional deletions identified might be a prerequisite for the selection strategy to work with carbon substrates other than (acidic) sugars. This was illustrated by the ability of all SCA strains to use citrate as the sole carbon source. In SCA15, all genes identified to provide a source of Ac-CoA, Ac-P, acetate, or acetaldehyde were deleted, and the strain was unable to form biomass in FBA simulations. However, the strain still demonstrated growth on citrate. Consequently, the additional deletion of *glcB*, *gltA*, and *prpC* was performed to rule out reversibility of the three putative irreversible reactions malate synthase³¹¹, citrate synthase^{312,313}, and 2-methyl citrate synthase^{314,315} under restrictive conditions.

The elimination of GlcB, GltA and PrpC did not affect growth on citrate in SCA18. Hence, there appear to be unknown enzymatic functions in *P. putida* that establish a biochemical route from citrate to Ac-CoA. However, removing the three Ac-CoA-consuming reactions associated with the TCA cycle and most Ac-CoA forming reactions could be beneficial for the strain's use in certain applications: A complete decoupling of C2 metabolism from the physiological metabolic network could enable the targeted

incorporation of functionalized acetate derivatives into products. For example, fluoroacetate (F-Ac) has been shown to be toxic to cells through inhibition of the aconitase after entering the TCA cycle³¹⁶. However, the wide product range accessible through Ac-CoA makes F-Ac an attractive substrate for the *in vivo* production of fluorinated compounds. One can devise strategies to utilize a $\Delta aceEF \Delta gltA \Delta glcB$ strain for bioproduction with resting cells. The whole-cell biocatalyst could first be propagated by supplying a tailored combination of an (acidic) sugar, acetate, and an organic acid to feed the TCA cycle. Once the substrates are depleted, F-Ac and other required (co-)reactants can be fed to quiescent cells or cell lysates to carry out the formation of fluorinated products without the interference of Ac-CoA.

4.3.2. The integration of the phosphoketolase pathway into the metabolic network occurred via stabilization of the total protein content

The predictions obtained by FBA informed our proof-of-concept strategy to implement an alternative phosphoketolase-based glycolysis in a synthetic C2-auxotroph strain background. Chromosomal integration of *B. adolescentis* Xfpk and plasmid-based expression of *E. coli* pta provided sufficient flux through the PK-pathway to establish bradytrophic growth on glucose. In response to the low abundances of GntZ and Rpe observed in whole-proteome analyses, the production of both enzymes was artificially increased, further enhancing growth on glucose.

Adaptive evolution enabled strain SCA3_{PK-Tn}/pS438-pta^{EC} to make another leap towards restoring its growth ability on glucose. To identify the mechanisms responsible for the improved growth rate and biomass yield, we analyzed changes in the proteome that had occurred during evolution. However, the only observation was a significantly reduced variability in the protein abundance profiles of the evolved strain. Rather than causing gain-of-function by up- or down-regulating specific proteins, the effects of evolution may have had a stabilizing effect for an advantageous proteome profile. This notion is supported by the potential effects proposed for the only mutation found consistently in the mutated strain, the substitution of Gly¹⁴⁶ in TtlS by aspartate. Acting on the fundamental level of protein translation, the altered supply rate

for a specific tRNA could have genome-wide implications for the production of proteins.

Rare codons can arrest translation of a polypeptide due to the rarity of their cognate tRNAs^{317,318}. The precise position of rare codons within a coding sequence can be essential for the correct folding of proteins and contribute to their catalytic function^{319,320}. However, in addition to modulating the translation rate and folding of proteins, rare codons may also play a strategic role in the global regulation of gene expression. In *E. coli*, the gene *lacZ* encoding β -galactosidase has 5 rare AGG codons encoding L-arginine (L-arg) within the first 25 codons. Replacing these codons with more abundant variants uncoupled LacZ production from regulatory mechanisms that naturally prevent its translation in stationary phase³²¹. In addition, artificially increasing the supply of rare L-arg tRNAs (translating AGG and AGA codons) increased the abundance of a variety of proteins during stationary phase significantly. One of these proteins was the product of *hns*, which encodes a nucleoid-associated protein involved in global transcriptional repression (silencing)³²²⁻³²⁵. A single AGA codon at position 19 was found to be responsible for stationary phase repression³²¹. These results highlighted the presence of global regulatory mechanisms based on the availability of rare tRNAs.

Early rare ATA codons are found in the *P. putida* genome within many genes. The most notable among these are the global regulators *crp*, encoding the cAMP receptor protein^{326,327}, *PP_0994*, encoding a putative RNA polymerase σ -factor, and *spoT*, encoding a bifunctional (p)ppGpp synthase/hydrolase involved in *stringent response*^{328,329}. Due to their role in central metabolism, other genes worth mentioning are *PP_0652* (gluconate transporter), *cyoA* and *cyoB* (cytochrome bo terminal oxidase subunits), and *pgl* (6-phosphogluconolactonase). With ATA codons being involved in the translation rate of these proteins, changes in the abundance of tRNA^{Ile2} could serve as a global regulatory mechanism similar to ones observed for AGG/AGA codons in *E. coli*.

4.3.3. Sequence analysis of potential TiS substrates proposes new functions for previously identified tRNA sequences

Curiously, we could not identify any tRNA^{Ile} with CAU or AAU anticodons annotated in the chromosomal sequence of KT2440 (Accession: PRJNA267). One can find three genes assigned with a tRNA^{Ile} function: *PP_t05*, *PP_t35*, and *PP_t50*. The nucleotide sequence of these genes is identical, and all three encode for a tRNA^{Ile} recognizing the most frequent AUC codon (**Figure 4.18A**). However, the alternative Ile-encoding codons are found at relative frequencies of 21% (AUU) and 4.5% (AUA), respectively³⁰⁶. Using the tRNA screening tool ARAGORN³³⁰, we analyzed the whole genome sequence of *P. putida* KT2440 for unidentified tRNA genes. Five so far undiscovered sequences were predicted to encode for tRNA^{Trp}, tRNA^{Thr}, tRNA^{Cys}, and 2x tRNA^{Ala} (**Table 4.S4**). However, secondary structure predictions for those supposed tRNA sequences using the algorithm developed by M. Andronescu et al.³³¹ in Geneious (version 2021.1.1) showed no similarity to the *canonical* tRNA fold structure (not shown). No new sequence could be identified to provide for the missing tRNA^{Ile} functions.

We then analyzed the sequences of annotated tRNA^{Met} variants for patterns that might indicate cryptic tRNA^{Ile} functions since they share the same anticodon with AUA-tRNA^{Ile2} precursors. *P. putida* harbors six annotated Met-tRNAs (**Figure 4.18B**). Three of them, *PP_t65*, *PP_t66*, and *PP_t67* are identical, and *PP_t49* deviates from that sequence by only 5 nucleotides (out of 77). The two remaining Met-tRNAs, *PP_t70* and *PP_t71*, share a 78% sequence identity and are both 56% identical with the first four genes. The online tool tRNAscan-SE³³² was used to identify the function of all six variants. Based on their sequence homology to computationally characterized tRNAs in the GtRNAdb database, *PP_t65*, *PP_t66*, *PP_t67*, and *PP_t49* were assigned the role of an N-formylmethionine tRNA (tRNA^{fMet}), while *PP_t70* is a supposed elongator methionine tRNA (tRNA^{Met}), and *PP_t49* functions as tRNA^{Ile2}. However, a closer look at the sequence features of the tRNAs at stake paints a different picture.

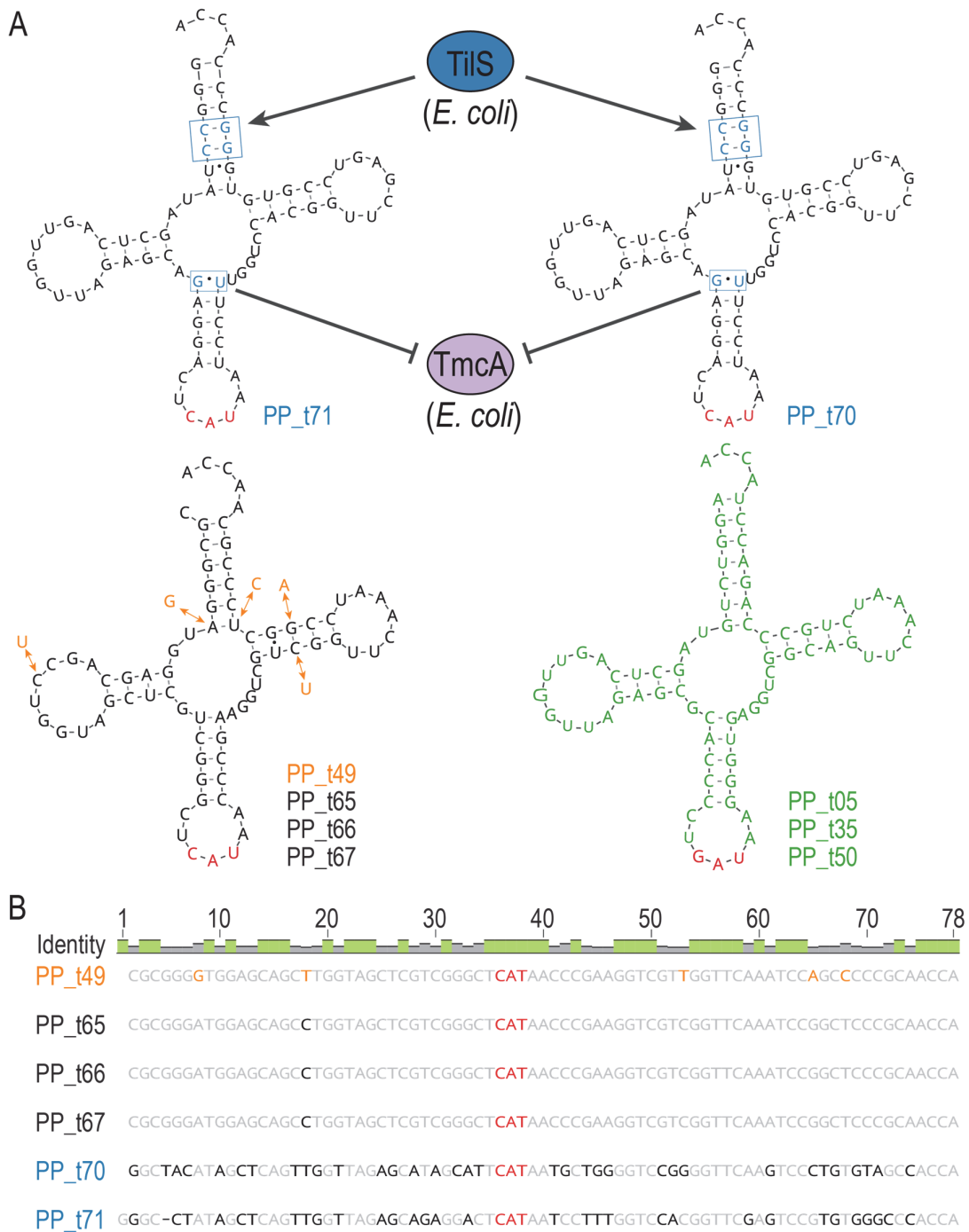


Figure 4.18. Analysis of potential tRNA substrates for TiIS. (A) Sequence and secondary structure prediction for the three identical Ile-tRNAs (green), four nearly identical Met-tRNAs (black and orange), and two putative UAU-tRNA^{Ile2} precursors (blue) annotated in the genome of *P. putida* KT2440. **(B)** Alignment of genes annotated as Met-tRNA. Identical nucleotides in all six sequences are drawn in grey, positions deviant in at least one variant are drawn in black. Green bars in the Identity row indicate conserved nucleotides. Anticodons are highlighted in red. Sequence features within the tRNA^{Ile2} precursors that were shown to guide the interactions with TiIS and TmcA in *E. coli* are highlighted with blue boxes.

The enzymes responsible for the post-transcriptional modification of tRNA^{Met} and tRNA^{Ile2} have been studied in detail by Y. Ikeuchi et al.³³³. Similar to the modification of the wobble base in the CAU anticodon by TilS, tRNA^{Met} cytidine acetyltransferase (TmcA) attaches an acetyl group to cytosine in position 34 to ensure the precise recognition of the mRNA-AUG codon. TmcA was shown to recognize specific sequence features in mainly the anticodon stem of tRNA^{Met}. Conversely, TilS was suggested to interact strongly with two consecutive C-G base pairs in the amino acid acceptor stem of tRNA^{Ile2}. Furthermore, a G28-U46 wobble base pair at the top of the anticodon loop was shown to inhibit the incorrect interaction of tRNA^{Ile2} with TmcA. *PP_t71* and *PP_t70* exhibit the same sequence features that were found to be essential for the differential recognition of tRNA^{Ile2} by TilS and TmcA (**Figure 4.18A**). Based on this sequence analysis, we propose a tRNA^{Ile2} function for these two genes.

None of the annotated tRNA^{Met} genes in *P. putida* carry the features considered relevant for TmcA recognition. Moreover, the genome of strain KT2440 does not harbor any gene with an assigned tRNA^{Met} cytidine acetyltransferase function, and no amino acid sequence with significant homology to *E. coli* TmcA could be found for any member of the *P. putida* group (using the BLASTP search engine). Thus, the mechanisms for how initiator tRNA^{Met} is distinguished from elongator tRNA^{Met} in these species is unclear. Lastly, our analysis could not reveal any gene encoding for AAU-tRNA^{Ile}, despite a considerable amount of Ile-encoding ATT codons in *P. putida*'s genome.

4.3.4. A flux split between the ED and PK pathways creates a metabolic imbalance in synthetic C2 auxotrophs

During batch fermentation on glucose, the evolved PK-utilizing strain SCA3_{PK-Tn}/pS438-*pta*^{EC} secreted significant amounts of pyruvate and 2KG. Disproportionate production of 2KG can occur in *P. putida* in two scenarios. (i) Genetic manipulations (e.g., by introducing bottlenecks in the supply of biomass constituents) or toxic effects from medium components may impede the typically rapid growth. As a result, the periplasmic dehydrogenases convert glucose into its acid forms faster than they can be utilized for biomass formation. However, if central metabolism is intact, 2KG

is fully assimilated by the cells after glucose and Gnt are depleted. This behavior bears a striking resemblance to the phenomenon of acetate overflow production in glucose-grown *E. coli*³³⁴.

(ii) Disrupting the *supply* of NAD(P)H or high levels of oxidative stress (increasing NADPH *demands*) can cause shortages within the pool of soluble electron carriers used to feed anabolic reactions and fuel the electron transport chain for energy production. To maintain a high and homeostatic energy charge $([ATP] + 0.5 [ADP])/([ATP] + [ADP] + [AMP])$, required to drive biosynthetic reactions³³⁵⁻³³⁷, glucose can be utilized as energy source without degrading its carbon skeleton. The electrons removed from glucose or gluconate during periplasmic oxidation are transferred to ubiquinones in the cytoplasmic membrane, fueling the electron transfer chain^{338,339}. Consequently, they cannot contribute to replenishing the intracellular pool of reducing equivalents.

In wild-type *P. putida* KT2440 growing on glucose, NADH is produced predominantly by PDHc, 2-oxoglutarate dehydrogenase (SucAB), and malate dehydrogenase (MDH). The primary reactions producing NADPH are, in order of their contribution, isocitrate dehydrogenase (Icd), malic enzyme (MaeB), G3P dehydrogenase (Gap), Glucose-6-P 1-dehydrogenase (Zwf), and 6-phosphogluconate dehydrogenase Gnd¹⁰⁵. In strain SCA3_{PK-Tn}/pS438-*pta*^{EC}, a significant substrate fraction is processed via the ED pathway, indicated by the accumulation of pyruvate. This route yields 2 moles of NAD(P)H per mol of glucose. However, if glucose is oxidized to 2KG in the periplasm, 1 mol of NADPH is required to reduce 2K6PG to 6PG before entering the ED pathway. Thus, the net yield of intracellular reducing equivalents sums up to zero. The lack of re-consumption of pyruvate suggests a low carbon flux from glycolysis into the TCA cycle. Consequently, only little NAD(P)H is provided by the reactions catalyzed by SucAB, MDH, Icd, and MaeB.

We used the quantitative phenotypical parameters observed during the bioreactor fermentation with strain SCA3_{PK-Tn}/pS438-*pta*^{EC} to approximate the flux distribution via in silico modeling. Even if the FBA results obtained do not reflect the exact metabolite fluxes in the engineered strain, they enabled drawing relevant conclusions to inform further engineering strategies. One such case is that glycolytic metabolites appear to

be poorly connected to the TCA cycle. This imbalance could be resolved by overexpressing anaplerotic enzymes. It is noteworthy that *pckA* (encoding phosphoenolpyruvate carboxykinase) contains a frameshift and therefore the open reading frame is classified as a pseudogene³⁴⁰. With an increased flux to the TCA cycle, a smaller fraction of carbon would need to be recycled in the ED/EMP cycle. In addition, increased NADPH production would allow the use of 2KG as a carbon source, which further increases the biomass yield on glucose.

In the ideal flux distribution obtained with iJN1411 (**Section 4.2.1**) for a PK-based glycolysis, the ED pathway and the oxidative glucose utilization route through 2KG were completely inactive. Pyr was produced via the lower glycolysis from G3P provided by activities within the PPP. While the production of PPP enzymes may need to be further increased to support a high metabolite turnover, the *gad* operon and *edd/eda* present themselves as targets for additional genome reductions.

4.4. Outlook

The functionality of a heterologously implemented phosphoketolase pathway was demonstrated here in an obligate aerobic species. *P. putida* KT2440 was engineered to be fully dependent on the new glycolytic route to supply essential Ac-CoA. During adaptive laboratory evolution on the new metabolic network architecture, a single point mutation was identified with potential system-wide effects on the proteome composition. To investigate the consequences of the Gly¹⁴⁶→Asp substitution, the G⁴³⁷→A mutation in *tilS* will be retro-engineered into both the pre-evolved strain SCA3_{PK-Tn}/pS438-*pta*^{EC} and the wild-type strain KT2440. The mutants harboring TilS^{Gly146Asp} will be analyzed for changes in their protein content as well as physiology. Mutations in *E. coli* that have been shown to enhance growth on glucose often had positive pleiotropic effects on other carbon sources³⁴¹. Hence, it will be interesting to investigate how the *tilS* mutation affects the growth of *P. putida* under alternative culture conditions. Likewise, the effects which resulted from excision of the 95-kb chromosomal segment in some clones during evolution will be subjected to closer scrutiny.

A single point mutation seems to have mediated increased growth performance on glucose in strains engineered with the PK-dependent route. However, detailed physiological characterization revealed far-from-ideal utilization of the substrate under the new metabolic regime. Thus, the strain will be subjected to continued evolution to reveal additional mechanisms to improve PK pathway performance that might not be obvious from the predicted flux distributions. If the PK pathway can be efficiently implemented, it can be utilized to produce Ac-CoA-derived products. To fully exploit the carbon-conserving nature of this metabolic route, it can be combined with a complete decoupling of C2 metabolism from the TCA cycle, as implemented in strain SCA18. The resulting strains could be used for growth-decoupled fermentation strategies to maximize the conversion of glycolytic substrates into value-added products.

The mode of glucose assimilation in the currently evolved SCA3_{PK-Tn}/pS438-*pta*^{EC} points to obvious targets for further strain engineering. The ED pathway and periplasmic gluconate oxidation should be removed to reduce the production of the overflow

metabolites 2KG and pyruvate. Additional deletion of glucose dehydrogenase, combined with alternative, more efficient glucose import systems, could provide a more energy-efficient way of transport into the cells. Relocating all glucose oxidation steps to the cytoplasmic compartment would allow cells to better distribute the reducing power by taking advantage of the multiple equilibration systems that distinguish *Pseudomonas* species. Removal of the ED pathway could force all flux through the pentose phosphate pathway, with a concomitant high NADPH formation rate that could be exploited in various bioproduction pathways.

The flux analysis performed via in silico modeling can only serve as a proxy for the real in vivo flux distribution. An experimental approach to determine the contribution of each biochemical reaction will help identify metabolic bottlenecks and confirm the obtained results. Glucose labeled with ^{13}C in carbon positions 3 and 4 was identified as a suitable substrate to decipher all fluxes in central carbon metabolism, including the two reactions performed by Xfpk.

Notwithstanding the hitherto moderate performance of the PK pathway, the implemented genetic modifications created a strain that accumulates substantial amounts of pyruvate. If 2KG secretion can be prevented, a PK-ED pathway hybrid could provide ample substrate amounts for production pathways that use pyruvate as an entry metabolite.

Recently, a rather exotic application that could make use of the presented C2-selection platform has gained traction in our laboratory: the biological production of fluorinated chemicals enabled by in vivo fluorination³⁴². Using the universal methyl-donor S-adenosyl-L-methionine (SAM) as substrate, the fluorinase enzyme (5'-fluoro-5'-deoxyadenosine synthase) attaches inorganic fluoride (F^-) by releasing an L-methionine residue, yielding 5'-fluoro-5'-deoxyadenosine. This fluorinated compound can further be processed in a cascade of enzymatic reactions, eventually yielding fluoroacetate (F-Ac, **Figure 4.19**). The fluorinase is the only enzyme found in nature that can catalyze F-C bond formation, and F-Ac is one of the two end-products produced by *Streptomyces cattleya*³⁴³, the native host of the route. Using a suitable dehalogenase, fluorine can again be released, yielding acetate, which can be assimilated to Ac-CoA by, e.g., Ac-

CoA synthetase. If the outlined fluorination pathway can be established with an efficiency that provides Ac-CoA at growth-supporting rates, a synthetic C2-auxotroph selection platform could help to improve the pathway through evolutionary mechanisms.

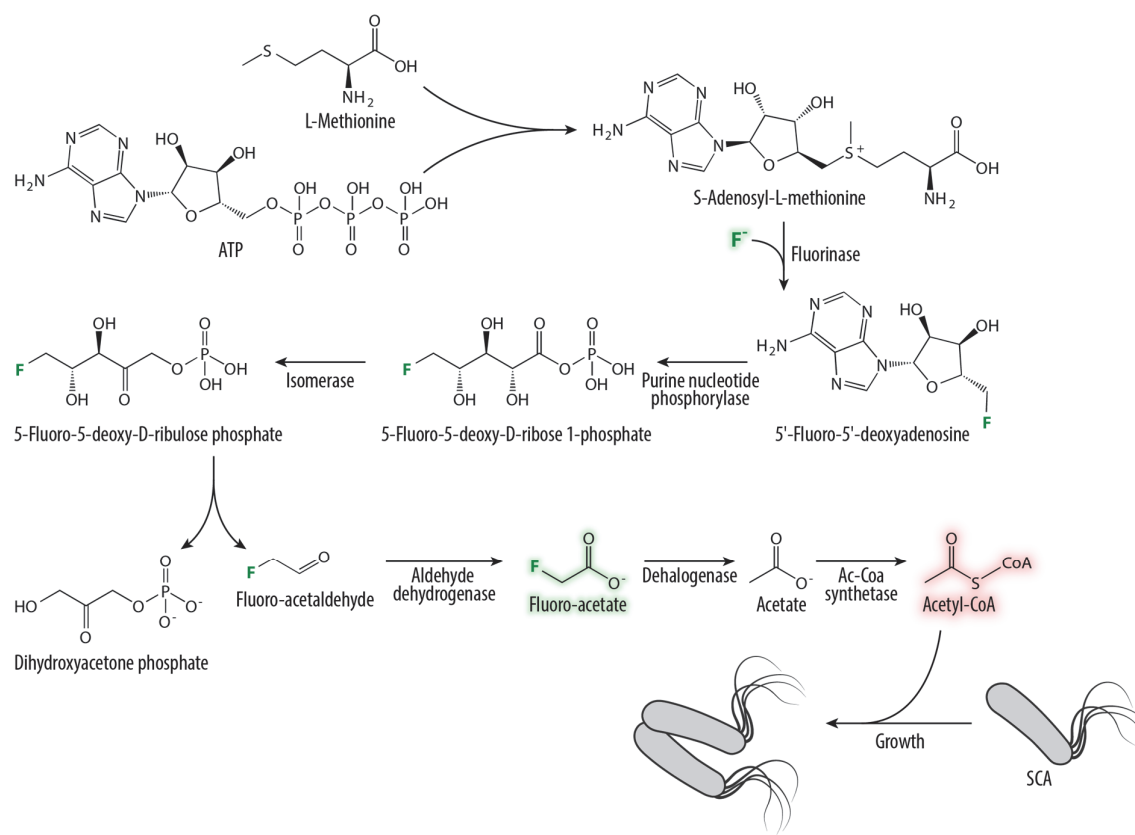


Figure 4.19 Reaction scheme for a biofluorination pathway amenable to evolutionary engineering via a synthetic C2-auxotrophy. The reactions from S-Adenosyl-L-methionine to fluoro-acetate are natively present in *S. cattleya*. Two subsequent reactions tie the biofluorination pathway to central carbon metabolism to restore prototrophy in SCA strains.

4.5. Materials and Methods

Table 4.4. Bacterial strains used in this chapter.

Strain	Relevant characteristics	Reference or source
<i>Escherichia coli</i>		
DH5 α λ pir	Cloning host; F- λ - <i>endA1 glnX44(AS) thiE1 recA1 relA1 spoT1 gyrA96(Nal^R) rfbC1 deoR nupG Φ80(lacZΔM15) Δ(argF-lac)U169 <i>hsdR17(r_K m_K⁺)</i>, λpir lysogen</i>	Platt et al. ²⁵⁸
<i>Pseudomonas putida</i>		
KT2440	Wild-type strain, derived from <i>P. putida</i> mt-2 ²⁶⁰ cured of the TOL plasmid pWW0	Bagdasarian et al. ²⁶¹
SCA1	KT2440 Δ aceEF	This work
SCA3	KT2440 Δ bkdAA Δ ltaE Δ aceEF	This work
SCA8 _{PD}	KT2440 Δ bkdAA Δ pcaBDC Δ paaEDCBA Δ davBA Δ gabT Δ glcB Δ hmgABC ^a Δ mmsA2	This work
SCA9	KT2440 Δ bkdAA Δ pcaBDC Δ paaEDCBA Δ davBA Δ gabT Δ glcB Δ hmgABC ^a Δ mmsA2 Δ aceEF	This work
SCA14 _{PD}	KT2440 Δ bkdAA Δ ltaE Δ pcaBDC Δ paaEDCBA Δ davBA Δ gabT Δ glcB Δ hmgABC ^a Δ eutBC Δ mmsA2 Δ mmsA1 Δ acoABC Δ prpC Δ benABCD ^b	This work
SCA15	KT2440 Δ bkdAA Δ ltaE Δ pcaBDC Δ paaEDCBA Δ davBA Δ gabT Δ glcB Δ hmgABC ^a Δ eutBC Δ mmsA2 Δ mmsA1 Δ acoABC Δ prpC Δ benABCD ^b Δ aceEF	This work
SCA18	KT2440 Δ bkdAA Δ ltaE Δ pcaBDC Δ paaEDCBA Δ davBA Δ gabT Δ glcB Δ hmgABC ^a Δ eutBC Δ mmsA2 Δ mmsA1 Δ acoABC Δ prpC Δ benABCD ^b Δ aceEF Δ glpR Δ gltA Δ crc	This work
SCA3 _{PK}	KT2440 Δ bkdAA Δ ltaE Δ aceEF LP:: <i>xfpk</i> ^{BA} SCA3 with <i>B. adolescentis</i> <i>xfpk</i> chromosomally integrated into a "landing pad" between <i>PP_0013</i> and <i>PP_5421</i> .	This work
SCA3 _{PK-Tn}	KT2440 Δ bkdAA Δ ltaE Δ aceEF LP:: <i>xfpk</i> ^{BA} <i>attTn7::gntZ-rpe</i> SCA3 _{PK} with the translationally coupled genes <i>gntZ</i> and <i>rpe</i> chromosomally integrated at site <i>attTn7</i> .	This work

- a** The deletion of *hmgABC* causes the formation of a brown pigment when cells are grown in LB medium, indicating the accumulation of 2,5-OH-PhAc that, after oxidation to a quinoid derivative, polymerizes spontaneously and generates melanic compounds³⁴⁴.
- b** The *benABCD* operon was removed to avoid the degradation of the inducer 3-methylbenzoate and the associated browning of culture media (see **Chapter 3**).

Table 4.5. Plasmids used in this chapter.

Plasmid name	Relevant characteristics ^a	Source or reference
pGNW2	Suicide vector used for genetic manipulations in Gram-negative bacteria; <i>oriT</i> , <i>traJ</i> , <i>lacZα</i> , <i>ori</i> (R6K), $P_{14g}(BCD2) \rightarrow msfGFP$; Km ^R	See Chapter 3
pSNW2	Derivative of vector pGNW2 with the translation initiation sequence of <i>msfGFP</i> replaced by the very strong translational coupling sequence <i>BCD2</i>	See Chapter 3
pQURE6-H	Conditionally-replicating vector; derivative of vector pJBSD1 carrying $XylS/Pm \rightarrow I-SceI$ and $P_{14g}(BCD2) \rightarrow mRFP$; Gm ^R	See Chapter 3
pSNW2- $\Delta aceEF$	Derivative of pGNW2 carrying HAs to delete <i>aceEF</i> in <i>P. putida</i> KT2440	This study
pSNW2- $\Delta gltA$	Derivative of pGNW2 carrying HAs to delete <i>gltA</i> in <i>P. putida</i> KT2440	This study
pSNW2- $\Delta acoABC$	Derivative of pGNW2 carrying HAs to delete <i>acoABC</i> in <i>P. putida</i> KT2440	This study
pSNW2- $\Delta amaC-dpkA$	Derivative of pGNW2 carrying HAs to delete <i>amaC-dpkA</i> in <i>P. putida</i> KT2440	This study
pSNW2- $\Delta bkdAA$	Derivative of pGNW2 carrying HAs to delete <i>bkdAA</i> in <i>P. putida</i> KT2440	This study
pSNW2- Δcrc	Derivative of pGNW2 carrying HAs to delete <i>crc</i> in <i>P. putida</i> KT2440	This study
pSNW2- $\Delta davBA$	Derivative of pGNW2 carrying HAs to delete <i>davBA</i> in <i>P. putida</i> KT2440	This study
pSNW2- $\Delta eutBC$	Derivative of pGNW2 carrying HAs to delete <i>eutBC</i> in <i>P. putida</i> KT2440	This study
pSNW2- $\Delta gabT$	Derivative of pGNW2 carrying HAs to delete <i>gabT</i> in <i>P. putida</i> KT2440	This study
pSNW2- $\Delta glcB$	Derivative of pGNW2 carrying HAs to delete <i>glcB</i> in <i>P. putida</i> KT2440	This study
pSNW2- $\Delta hmgABC$	Derivative of pGNW2 carrying HAs to delete <i>hmgABC</i> in <i>P. putida</i> KT2440	This study
pSNW2- $\Delta ltaE$	Derivative of pGNW2 carrying HAs to delete <i>ltaE</i> in <i>P. putida</i> KT2440	This study
pSNW2- $\Delta mmsA1$	Derivative of pGNW2 carrying HAs to delete <i>mmsA1</i> in <i>P. putida</i> KT2440	This study
pSNW2- $\Delta mmsA2$	Derivative of pGNW2 carrying HAs to delete <i>mmsA2</i> in <i>P. putida</i> KT2440	This study

pSNW2- Δ <i>paaEDCBA</i>	Derivative of pGNW2 carrying HAs to delete <i>paaEDCBA</i> in <i>P. putida</i> KT2440	This study
pSNW2- Δ <i>pcaBDC</i>	Derivative of pGNW2 carrying HAs to delete <i>pcaBDC</i> in <i>P. putida</i> KT2440	This study
pSNW2- Δ <i>prpC</i>	Derivative of pGNW2 carrying HAs to delete <i>prpC</i> in <i>P. putida</i> KT2440	This study
pTn7-M	Tn7 integration vector; <i>oriV</i> (R6K); Km ^R , Gm ^R	Choi et al. ³⁴⁵
pTn7- <i>P</i> _{14g} (<i>BCD10</i>) \rightarrow <i>gntZ-rpe</i>	Derivative of pTn7-M used for chromosomal integration of a synthetic <i>gntZ-rpe</i> operon under the control of <i>P</i> _{14g} (<i>BCD10</i>)	This study
pTNS2	Helper plasmid constitutively expressing the <i>tnsABCD</i> genes encoding the Tn7 transposase; <i>oriV</i> (R6K); Amp ^R	Choi et al. ³⁴⁵
pS438- <i>pta</i> ^{EC}	Expression vector; <i>oriV</i> (<i>pBBR1</i>), Strep ^R ; <i>XylS/Pm</i> \rightarrow <i>pta</i> ^{EC}	This work

a Antibiotic markers: *Km*, kanamycin; *Nal*, nalidixic acid; and *Rif*, rifampicin.

Bacterial strains and culture conditions

The bacterial strains employed in this study are listed in **Table 4.4**. *E. coli* and *P. putida* were incubated at 37°C and 30°C, respectively. For cell propagation and storage, routine cloning procedures, and during genome engineering manipulations, cells were grown in lysogeny broth (LB) medium (10 g L⁻¹ tryptone, 5 g L⁻¹ yeast extract, and 10 g L⁻¹ NaCl). Liquid cultures were performed using either 50-ml centrifuge tubes with a medium volume of 5-10 mL, or in 500-mL Erlenmeyer flasks covered with cellulose plugs (Carl Roth, Karlsruhe, Germany) and with a medium volume of 50 mL. All liquid cultures were agitated at 250 rpm (MaxQ™8000 incubator; ThermoFisher Scientific, Waltham, MA, USA). Solid culture media contained an additional 15 g L⁻¹ agar. Selection of plasmid-harboring cells was achieved by adding kanamycin (Km), gentamicin (Gm), or streptomycin (Sm) when required at 50 µg mL⁻¹, 10 µg mL⁻¹, and 50 µg mL⁻¹, respectively.

For phenotypic characterizations in microtiter plates as well as fermentations in shaken flasks, the experiments were performed in synthetic Hartman's de Bont minimal (DBM) medium³⁴⁶ additionally buffered with 5 g L⁻¹ 3-(*N*-morpholino)propane sulfonic acid (MOPS) at pH 7.0 and supplemented with different carbon compounds

as explained in the text. Before the plate reader experiments with SCA strains in **Section 4.2.2**, the cells were pre-grown in LB medium. For all other experiments, the pre-culture media were identical to those used for the experiment. The precultures were harvested by centrifugation at 8,000 g for 2 min, washed with DBM medium without the addition of any carbon substrate, and resuspended in the final media of the experiment at the desired start-optical density at 600 nm ($OD_{600\text{ nm}}$). Cell growth was monitored by measuring the absorbance at 630 nm ($Abs_{630\text{ nm}}$; for 96-well plate reader experiments with ELx808, BioTek Instruments; Winooski, VT, USA) or 600 nm (for shaken flask experiments, bioreactor fermentations, and 24-well plate reader experiments with Synergy H1, BioTek Instruments; Winooski, VT, USA). The $OD_{600\text{ nm}}$ was estimated from plate reader $Abs_{630\text{ nm}}$ values via multiplying the values by correlation factors previously determined for the employed microtiter plate-readers and spectrophotometers. Adaptive laboratory evolution (ALE) of strains was performed in 24-well deep-well plates covered with a Sandwich Cover (PreSens Precision Sensing, Regensburg, Germany) and filled with 2 mL DBM medium per well. The ALE procedure is described in the Results text.

Cloning procedures and plasmid construction

All plasmids used in this work are listed in **Table 5.5**. Oligonucleotides used for the PCR-amplification of fragments and genotyping via colony PCR are listed in **Table 4.S1**. Uracil-excision (*USER*) cloning²⁰³ was used for the construction of all plasmids. The AMUSER tool was employed for the design of oligonucleotides³⁴⁷. All genetic manipulations followed the protocol described in **Chapter 3**. DNA fragments employed in assembly reactions were amplified using the PhusionTM U high-fidelity DNA polymerase (Thermo Fisher Scientific, Waltham, Massachusetts, USA) according to the manufacturer's specifications. The identity and correctness of all plasmids and DNA constructs were confirmed by sequencing. For genotyping experiments after cloning procedures and genome manipulations, colony PCRs were performed using the commercial OneTaqTM master mix (New England BioLabs; Ipswich, MA, USA) according to the manufacturer's instructions. *E. coli* DH5 α λ pir was employed for all cloning purposes. Chemically competent *E.coli* cells were prepared and transformed

with plasmids according to well-established protocols³⁴⁸. *P. putida* was rendered electro-competent following the protocol of Choi, Kumar et al.³⁴⁹ (**Chapter 3**).

GSMM simulations

The most recent genome-scale metabolic network reconstruction (genome-scale metabolic model, GSMM) for *P. putida*, iJN1411³⁵⁰, was subjected to Flux Balance Analysis (FBA³⁵¹) within the COBRAPy toolbox³⁵² to predict optimal flux distributions and to identify reactions contributing to a supply of Ac-CoA. The growth-limiting determinants, the glucose-uptake rate, and ATP maintenance requirement were fixed at rates of 6.3 mmol g_{CDW} h⁻¹ and 0.92 mmol g_{CDW} h⁻¹, respectively [experimentally determined by del Castillo et al.³⁵³ and Ebert et al.³³⁷, respectively]. After an initial deletion of reactions performed by the PDHc, the following analytic steps were iterated several times to identify potential alternative sources of Ac-CoA (reaction loops were not permitted):

1. Optimization of flux distribution for biomass formation
2. Identification of the Ac-CoA-forming reaction with the highest flux under the current distribution
3. Tracing of the fluxes leading to Ac-CoA formation to identify the metabolic pathway involved
4. Removal of the initial entry reaction of the pathway, simultaneously avoiding the creation of auxotrophies

The identified pathways were then analyzed regarding the flux towards the first biomass constituent in the Ac-CoA-producing pathway and ranked according to their value within the flux distribution of the 'wildtype' model. This ranking was used to inform a hierarchy of gene deletions to be established in *P. putida* to create a robust acetate auxotroph.

Targeted proteomics by mass spectrometry (MS)

The *P. putida* strains were pre-cultured overnight in DBM medium supplemented with 30 mM glucose or 30 mM glucose and 30 mM acetate. Then, experimental cultures with the identical medium were inoculated at an initial OD_{600 nm} of 0.05. Samples were taken in the mid-exponential phase, and the cells were harvested by centrifugation at 17,000 g for 2 minutes at 4°C. After removal of the supernatant, the cell pellets were frozen. Frozen cells were kept at -80°C until the processing of samples. Thawing of the cells was done on ice, and any remaining supernatant was removed after centrifugation at 15,000 g for 10 min. While kept on ice, two 3-mm zirconium oxide beads (Glen Mills, NJ, USA) were added to the samples. Immediately after removing the samples from ice, 100 µl of 95°C 6 M Guanidinium hydrochloride (GuHCl), 5 mM tris(2-carboxyethyl)phosphine (TCEP), 10 mM chloroacetamide (CAA), and 100 mM Tris-HCl pH 8.5) was added to the samples. The cells were disrupted in a Mixer Mill (MM 400 Retsch, Haan, Germany) set at 25 Hz for 5 min at room temperature, followed by 10 min in a thermal mixer at 95°C and 2000 rpm. Any cell debris was removed by centrifugation at 15,000 g for 10 min, after which 50 µl of supernatant was collected and diluted with 50 µl of 50 mM ammonium bicarbonate. Based on protein concentration quantification (via the Bradford method with BSA concentration standards³⁵⁴), 100 µg of protein was used for tryptic digestion. Tryptic digestion was carried out at constant shaking (400 rpm) for 8 h, after which 10 µl of 10% trifluoroacetic acid (TFA) was added, and samples were ready for StageTipping, using C18 as resin (Empore, 3M, USA).

For sample analysis, a CapLC system (Thermo Scientific) coupled to an Orbitrap Q exactive HF-X mass spectrometer (Thermo Scientific) was used. First, samples were captured at a flow rate of 10 µl/min on a pre-column (µ-precolumn C18 PepMap 100, 5 µm, 100Å). Subsequently, the peptides were separated on an 15 cm C18 easy spray column (PepMap RSLC C18 2µm, 100Å, 150 µm×15cm) at a flow rate of 1.2 µl/min, with an applied gradient from 4% (v/v) acetonitrile in water to 76% (v/v) over a total of 60 minutes. While spraying the samples into the mass spectrometer, the instrument operated in *data-dependent* mode using the following settings: MS-level scans were

performed with Orbitrap resolution set to 60,000; AGC Target 3.0e6; maximum injection time 50 ms; intensity threshold 5.0e3; dynamic exclusion 25 s. Data-dependent MS2 selection was performed in Top 20 Speed mode with HCD collision energy set to 28% (AGC target 1.0e4, maximum injection time 22 ms, Isolation window 1.2 m/z).

For analysis of the thermo raw files, Proteome discoverer 2.4 was used with the following settings:

Fixed modifications: Carbamidomethyl (C); Variable modifications: oxidation of methionine residues; First search mass tolerance: 20 ppm; MS/MS tolerance: 20 ppm; Trypsin as enzyme, allowing one missing cleavage; the false-discovery rate (FDR) was set at 0.1%; the match-between-runs window was set to 0.7 min. Only unique peptides were considered for quantification. Protein abundances were normalization based on the total peptide amount. To assign the detected peptides to their functions, a protein database consisting of the *Pseudomonas putida* reference proteome (UP000000556) was used, supplemented with heterologously expressed proteins.

Statistical analysis of proteomics data

Proteomics data, acquired as described above, were analyzed using a customized R script in RStudio (version 1.3.1093), developed as part of this thesis. Only proteins that were detected in all samples within an analysis were considered. The abundance values were normalized via quantile normalization using the R-package *qsmooth*. Next, the Student's t-test was performed with the build-in *dt()* function. Based on the individual p-values and their total distribution, the false-discovery rate (FDR) for each protein was calculated via the *qvalue* package. The q-value threshold for significant observations was set at a value of 0.05. Fold-change comparison between groups was performed on log₂-transformed data. Volcano plots were generated with the *ggplot* package. The *heatmap* package was used to create heatmaps of protein abundances within all samples. Proteins showing an abundance change of ≥ 1.4 fold (log₂-fold change of 0.49) and a q-value of ≤ 0.05 were considered differentially expressed.

Bioreactor fermentations

The batch fermentations were performed in BIOSTAT® Qplus 1-L bioreactors (Sartorius, Göttingen, Germany) with a working culture volume of 800 mL. Precultures were grown overnight in 500-mL Erlenmeyer flasks filled with 10% (v/v) DBM medium supplemented with 5 g L⁻¹ MOPS and 30 mM glucose. The same medium was used in the bioreactors. The precultures were harvested by centrifugation at 4,000 g for 10 min and resuspended in culture medium to inoculate the bioreactors. Aeration of the vessels was achieved via horseshoe-shaped spargers with ambient air at a flow rate of 0.824 L min⁻¹. The dissolved oxygen concentration (DO) was measured online using an oxygen electrode and kept above 40% of saturation by increasing the stirring speed from 500 to 1000 min⁻¹. The lower stirring speed threshold was reduced to 250 min⁻¹ after 5.5 h to reduce the shear stress on the cells and biofilm formation. Sigma-Aldrich Antifoam 204 reagent (MilliporeSigma, St. Louis, Missouri, USA) was added to reduce foaming by adding single droplets when required (only for strain KT2440). The cultures were maintained at 30°C and pH 7.0 by online measurements with standard thermometers and pH electrodes and the addition of 7 M NaOH. The composition of the off-gas was analyzed online with a Prima BT Bench Top Process mass spectrometer (Thermo Fisher Scientific, Waltham, Massachusetts, USA).

Physiological parameters for the strains KT2440 and SCA3_{PK-Tr}/pS438-EC_{pta} were quantified as follows: The growth was followed via OD_{600 nm} measurements and, for strain KT2440, cell-dry-weight (CDW) determination with a Moisture analyzer WBA-110M (witeg Labortechnik Wertheim, Germany). CDW values were derived from OD_{600 nm} measurements by applying a correlation factor obtained from standard curves with the absorbance and CDW determinations for KT2440. Growth rates μ were determined from linear correlations of Ln-transformed OD_{600 nm} values or Gaussian Process regression as described in the Results. Biomass yields on glucose Y_{xs} (or the sum of all six-carbon moieties) were obtained as the slope of linear correlations of biomass (g_{CDW} L⁻¹)-over-substrate (g_s L⁻¹) plots. Pyruvate yields on the six-carbon substrates (Y_{ps}) were obtained via the same procedure. Substrate consumption rates q_s were calculated via the following equation:

$$q_S = \frac{\mu}{Y_{XS}} .$$

Pyruvate and 2-ketogluconate production rates q_P were calculated by employing the equation

$$q_P = Y_{PS} \cdot q_S .$$

The CO₂ production was calculated from the different CO₂ contents of the in-gas and the off-gas. Dissolved inorganic carbon species (carbonate and dissolved CO₂) were neglected. The amount of C-mol in biomass was derived from the cell dry weight and a previously published elemental biomass composition of *P. putida* KT2440³⁵⁵.

Metabolite analyses via HPLC

Sugars and organic acids were analyzed using a Dionex Ultimate 3000 HPLC with an Aminex® HPX-87X Ion Exclusion (300 × 7.8 mm) column (BioRad, Hercules, CA) as well as RI-150 refractive index and UV (260, 277, 304 and 210 nm) detectors. For analysis, the column was maintained at 65°C and a 5 mM H₂SO₄ solution was used as mobile phase at a flowrate of 0.5 mL min⁻¹. HPLC data were processed using the Chromeleon 7.1.3 software (Thermo Fisher Scientific), and compound concentrations were calculated from peak areas using calibration curves with five different standard concentrations.

Determination of in vitro phosphoketolase activity

PK activity was determined in cell lysates according to the hydroxamate method adapted from Lipmann and Tuttle^{356,357}. This assay utilizes the reaction of enzymatically produced Ac-P with hydroxylamine to form hydroxamate and inorganic phosphate. The hydroxamate is converted into a ferric hydroxamate complex via the addition of FeCl₃ (**Figure 4.10A**). The complex exhibits an orange-brown to purplish-brown color, depending on the concentration, and can be measured spectrophotometrically between 480 at 540 nm. The yellow FeCl₃ shows no absorption at these wavelengths.

P. putida strains were cultured overnight in 50 ml LB medium supplemented with 0.5 mM 3-*mBz* to induce *xfpk* expression. All following steps were performed on ice

and with pre-chilled solutions. The cells were collected by centrifugation at 5,000 g for 10 minutes at 4°C, washed twice with phosphate buffer (0.05 M phosphate buffer, 0.5 g L⁻¹ L-cysteine, and 1 mM MgCl₂; pH 6.5) and suspended in 3 ml. The suspensions were split into 1-mL aliquots in 2-mL cryotubes, and 0.3 g of acid-washed glass beads were added. The cells were lysed using a bead-beater homogenizer (BioSpec Products, Bartlesville, USA) at 6000 rpm for two times 20 s. Clear lysates were obtained by centrifugation at 17,000 g for 2 min at 4°C. The protein concentration was determined via the Bradford assay³⁵⁴ and all lysates were adjusted to the lowest concentration measured by adding phosphate buffer.

The enzyme assay was performed in 1.5-mL micro reaction tubes. Therefore, 600 µL of lysate was added to 150 µL of halogen solution (6 mg mL⁻¹ NaF and 10 mg mL⁻¹ iodoacetic acid) and 150 µL of 80 mg mL⁻¹ D-fructose-6-phosphate. The reaction mixtures were incubated at 30°C, and 75-µL samples were taken 10-min intervals. The samples were added into wells of a 96-well plate pre-filled with 75 µL 2 M hydroxylamine (freshly adjusted to pH 7 with 1 M HCl) and incubated for 10 min at room temperature. Subsequently, 50 µL 150 mg mL⁻¹ trichloroacetic acid, 50 µL 4 M HCl, and 50 µL 50 g L⁻¹ FeCl₃ in 0.1 M HCl were added. After the last sample was processed, the absorption at 505 nm was measured for all samples in a Synergy H1 plate reader (BioTek Instruments; Winooski, VT, USA). A calibration curve with Ac-P lithium salt was created by subjecting solutions of different concentrations to the same assay procedure.

Whole-genome sequencing

The sequencing of chromosomal (and plasmid) DNA to analyze effects of evolution was performed by Novogene (Cambridge, UK). The DNA content of strains was purified using the PureLink™ Genomic DNA Mini Kit (Invitrogen, California, USA). The raw data was processed in Geneious Prime 2021.1.1 (Biomatters Ltd.) by read pairing, trimming (*BBDuk* plugin) and mapping to the reference genome sequence. Sequence polymorphisms were identified by using the build-in *Annotate and Predict* functions. Single-nucleotide polymorphisms (SNPs) found in both pre-evolved and evolved clones were discarded.

Data and statistical analyses

All experiments, except for bioreactor fermentations, were performed with at least three biological replicates, and the mean values \pm standard deviation are presented. Statistical significances were determined by calculating p-values with the T.Test function in Microsoft Excel 2016. Maximum exponential growth rates (μ_{\max}) were determined by Gaussian process regression using the Python-based tool deODorizer³⁵⁸. Average specific growth rates over the exponential phase (μ) were determined by fitting Ln-transformed OD_{600 nm} data versus time to linear regressions. All linear regressions as well as the visualization of data was performed in OriginPro 2021 (OriginLab Corporation). Figures and Illustrations were created in OriginPro 2021 and Adobe Illustrator 2020. Geneious Prime 2021.1.1 (Biomatters Ltd.) served as a database for any kind of DNA sequences, design plasmids and constructs, and analyze Sanger sequencing results.

4.6. Supplementary Material

Table 4.S1. Oligonucleotides used in this chapter. Sequences used for the construction of the same plasmid via *USER* cloning are shaded in the same tone.

Name	Sequence (5'→3')	Application
pSNW- <i>USER</i> _F	AGTCGACCUUGCAGGCATGCAAGCTTCT	Linearization of suicide vector pSNW for HA insertion
pSNW- <i>USER</i> _R	AGGATCUAGAGGATCCCCGGGTACCG	Linearization of suicide vector pSNW for HA insertion
Seq-pSNW_F	TGTA AACGACGGCCAGT	Amplification and sequencing of the insert region on pSNW
Seq-pSNW_R	ATGACCATGATTACGCCGG	Amplification and sequencing of the insert region on pSNW
<i>aceEF</i> _HA1_F	AGATCCUCGAAGACTCGCTTGAAGAGG	Amplification of HA1 for the deletion of <i>aceEF</i>
<i>aceEF</i> _HA1_R	AGCCATGUAAGCCAGCACACTGC	Amplification of HA1 for the deletion of <i>aceEF</i>
<i>aceEF</i> _HA2_F	ACATGGCUTGCTCCAGGG	Amplification of HA2 for the deletion of <i>aceEF</i>
<i>aceEF</i> _HA2_R	AGGTCGACUCGATGAACTGCTGGTTGCG	Amplification of HA2 for the deletion of <i>aceEF</i>
<i>aceEF</i> _g-check_F	GTTTGGCTGGAGATTTTGGG	Genotyping for the chromosomal <i>aceEF</i> region via colony PCR
<i>aceEF</i> _g-check_R	CCTTGATCGGCGTGAATAG	Genotyping for the chromosomal <i>aceEF</i> region via colony PCR
<i>aceEF</i> _F	GCGCGCTCATTCGCGTACCTGACAT	sgRNA for <i>aceEF</i> deletion
<i>aceEF</i> _R	AAACATGTCAGGTACGCGAATGAGC	sgRNA for <i>aceEF</i> deletion
Seq-LP_F	ACCAACTTTTCCGCTTTGCAC	Amplification and sequencing of the chromosomal landing pad
Seq-LP_R	CGAAAGACTGGGCCTTTCGT	Amplification and sequencing of the chromosomal landing pad
<i>gltA</i> _HA1_F	AGATCCUCTAGCATAAAGCATGATGGC	Amplification of HA1 for the deletion of <i>gltA</i>
<i>gltA</i> _HA1_R	ACATAGCUTACATGTGGCCTCCTATT	Amplification of HA1 for the deletion of <i>gltA</i>
<i>gltA</i> _HA2_F	AGCTATGUAAGCTGCAGTAGCCGAAC	Amplification of HA2 for the deletion of <i>gltA</i>
<i>gltA</i> _HA2_R	AGGTCGACUGTTGGCGGAGGTTCTCAAG	Amplification of HA2 for the deletion of <i>gltA</i>
<i>gltA</i> _g-check_F	TCCCTCTATAGTGGTGCCGG	Genotyping for the chromosomal <i>gltA</i> region via colony PCR
<i>gltA</i> _g-check_R	TACCTGCCGGAAGAGAAGGG	Genotyping for the chromosomal <i>gltA</i> region via colony PCR
<i>acoABC</i> _HA1_F	AGATCCUGTGCCTGAACAACAGCTGG	Amplification of HA1 for the deletion of <i>acoABC</i>
<i>acoABC</i> _HA1_R	ACATCTUGTTGTTCTCCGGGG	Amplification of HA1 for the deletion of <i>acoABC</i>
<i>acoABC</i> _HA2_F	AAGATGUAAGCCCTTTTCGTGAGCCT	Amplification of HA2 for the deletion of <i>acoABC</i>
<i>acoABC</i> _HA2_R	AGGTCGACUCCACTACAACGGTTTGCCC	Amplification of HA2 for the deletion of <i>acoABC</i>
<i>acoABC</i> _g-check_F	CGAATTTGCCGAGCATGACA	Genotyping for the chromosomal <i>acoABC</i> region via colony PCR
<i>acoABC</i> _g-check_R	CACCAGTCCACCTTGATCTG	Genotyping for the chromosomal <i>acoABC</i> region via colony PCR
<i>amaC-dpkA</i> _HA1_F	AGATCCUATCGGCAGGAACAGTGTCC	Amplification of HA1 for the deletion of <i>amaC-dpkA</i>

<i>amaC-dpkA_HA1_R</i>	ACCGTTGTGUAACCTCGCCAACGGGCCAAC	Amplification of HA1 for the deletion of <i>amaC-dpkA</i>
<i>amaC-dpkA_HA2_F</i>	ACACAACGGUGCTGGTGGAAAG	Amplification of HA2 for the deletion of <i>amaC-dpkA</i>
<i>amaC-dpkA_HA2_R</i>	AGGTCGACUTCTGGCGGTATTCGTGTACG	Amplification of HA2 for the deletion of <i>amaC-dpkA</i>
<i>amaC-dpkA_g-check_F</i>	CACGGAAAGGTTGCACTTGC	Genotyping for the chromosomal <i>amaC-dpkA</i> region via colony PCR
<i>amaC-dpkA_g-check_R</i>	GATCAGTTGGCTCATGCTGC	Genotyping for the chromosomal <i>amaC-dpkA</i> region via colony PCR
<i>bkdAA_HA1_F</i>	AGATCCUGGTCATCAGGTAGCACTCC	Amplification of HA1 for the deletion of <i>bkdAA</i>
<i>bkdAA_HA1_R</i>	ATCTCACAUCAATGCTTTTTACGCTCGCTCGG	Amplification of HA1 for the deletion of <i>bkdAA</i>
<i>bkdAA_HA2_F</i>	ATGTGAGAUGAACGACCACAACAACAG	Amplification of HA2 for the deletion of <i>bkdAA</i>
<i>bkdAA_HA2_R</i>	AGGTCGACTCCAGGAAGATTACGGGTCCG	Amplification of HA2 for the deletion of <i>bkdAA</i>
<i>bkdAA_g-check_F</i>	CCTGCTCAGCAAAGGCAATC	Genotyping for the chromosomal <i>bkdAA</i> region via colony PCR
<i>bkdAA_g-check_R</i>	ATGGTCATGGTAGTGGTGGC	Genotyping for the chromosomal <i>bkdAA</i> region via colony PCR
<i>crc_HA1_F</i>	ACCTCCAGUGATGATCTGCATGACCTCACGAATGG	Amplification of HA1 for the deletion of <i>crc</i>
<i>crc_HA1_R</i>	ACATAAAUGGCCCATAAATCTCGTG	Amplification of HA1 for the deletion of <i>crc</i>
<i>crc_HA2_F</i>	ATTTATGUAAGGCCATTGGGGCTGCAT	Amplification of HA2 for the deletion of <i>crc</i>
<i>crc_HA2_R</i>	AGCTCTTGAUACGCCATGCTCGCTTTGGC	Amplification of HA2 for the deletion of <i>crc</i>
<i>crc_g-check_F</i>	ACAGCACATCGAACGGGATC	Genotyping for the chromosomal <i>crc</i> region via colony PCR
<i>crc_g-check_R</i>	TGCTATGGCACCTCAAGCG	Genotyping for the chromosomal <i>crc</i> region via colony PCR
<i>davBA_HA1_F</i>	AGATCCUCTGGGCCAGAGTGTGATAGG	Amplification of HA1 for the deletion of <i>davBA</i>
<i>davBA_HA1_R</i>	ACATGAAUAGACCTTGCCAGAGAG	Amplification of HA1 for the deletion of <i>davBA</i>
<i>davBA_HA2_F</i>	ATTCATGUGACAGGGCCGCTATGC	Amplification of HA2 for the deletion of <i>davBA</i>
<i>davBA_HA2_R</i>	AGGTCGACUTGGATCACTTCGCGTTCACG	Amplification of HA2 for the deletion of <i>davBA</i>
<i>davBA_g-check_F</i>	AGCGTATGTCGGGATCAAGG	Genotyping for the chromosomal <i>davBA</i> region via colony PCR
<i>davBA_g-check_R</i>	GGGTACCGAGGAAGAACAGG	Genotyping for the chromosomal <i>davBA</i> region via colony PCR
<i>eutBC_HA1_F</i>	AGATCCUAGATCTTCGCCCTGTCCC	Amplification of HA1 for the deletion of <i>eutBC</i>
<i>eutBC_HA1_R</i>	ATTTTTACAUACAGAATCTCCAGAGCC	Amplification of HA1 for the deletion of <i>eutBC</i>
<i>eutBC_HA2_F</i>	ATGTAAAAAUUCTGTCACGGAAGGC	Amplification of HA2 for the deletion of <i>eutBC</i>
<i>eutBC_HA2_R</i>	AGGTCGACUACCCGATGGATTCGTAAGTC	Amplification of HA2 for the deletion of <i>eutBC</i>
<i>eutBC_g-check_F</i>	CTACCCTGTCTTACGTGCTG	Genotyping for the chromosomal <i>eutBC</i> region via colony PCR
<i>eutBC_g-check_R</i>	TAAATCACCGATTCGTCCCG	Genotyping for the chromosomal <i>eutBC</i> region via colony PCR
<i>gabT_HA1_F</i>	AGATCCUCAAGGTAGGCTGACAGG	Amplification of HA1 for the deletion of <i>gabT</i>
<i>gabT_HA1_R</i>	ATGTGAUGTGACGCGCTTCAGAA	Amplification of HA1 for the deletion of <i>gabT</i>

<i>gabT</i> _HA2_F	ATCACAUAAATGCCCTCATTGCGCC	Amplification of HA2 for the deletion of <i>gabT</i>
<i>gabT</i> _HA2_R	AGGTCGACUGTCCAGGAACACATCGAGG	Amplification of HA2 for the deletion of <i>gabT</i>
<i>gabT</i> _g-check_F	CTCATCGCCAACTACTCCTG	Genotyping for the chromosomal <i>gabT</i> region via colony PCR
<i>gabT</i> _g-check_R	CCTGATCTCCAACGAAGTGG	Genotyping for the chromosomal <i>gabT</i> region via colony PCR
<i>glcB</i> _HA1_F	AGATCCUACTGGGCAATACGTTGACC	Amplification of HA1 for the deletion of <i>glcB</i>
<i>glcB</i> _HA1_R	ACATTGCUTGCCTCACTCTGC	Amplification of HA1 for the deletion of <i>glcB</i>
<i>glcB</i> _HA2_F	AGCAATGUAAGCAGCATCTGCTGCCAG	Amplification of HA2 for the deletion of <i>glcB</i>
<i>glcB</i> _HA2_R	AGGTCGACUGCGGTCTAATGCTGAAGC	Amplification of HA2 for the deletion of <i>glcB</i>
<i>glcB</i> _g-check_F	GTTTGGATGTCTGCCAAGGC	Genotyping for the chromosomal <i>glcB</i> region via colony PCR
<i>glcB</i> _g-check_R	TCCTGTACCTGAAAAGCCGG	Genotyping for the chromosomal <i>glcB</i> region via colony PCR
<i>hmgABC</i> _HA1_F	AGATCCUAACCGATCTGGGTCACCAC	Amplification of HA1 for the deletion of <i>hmgABC</i>
<i>hmgABC</i> _HA1_R	AGCCATCGAUGCCTCCGGATTTTG	Amplification of HA1 for the deletion of <i>hmgABC</i>
<i>hmgABC</i> _HA2_F	ATCGATGGCUCAGTGAAGTGAACGGTTC	Amplification of HA2 for the deletion of <i>hmgABC</i>
<i>hmgABC</i> _HA2_R	AGGTCGACUGGCCATCCTCGCTTTG	Amplification of HA2 for the deletion of <i>hmgABC</i>
<i>hmgABC</i> _g-check_F	ATCCTGTTCGGCAAACCAC	Genotyping for the chromosomal <i>hmgABC</i> region via colony PCR
<i>hmgABC</i> _g-check_R	GGTGAGCGACTACATGACTC	Genotyping for the chromosomal <i>hmgABC</i> region via colony PCR
<i>ltaE</i> _HA1_F	AGATCCUACCTTGTCTACGTGCTCG	Amplification of HA1 for the deletion of <i>ltaE</i>
<i>ltaE</i> _HA1_R	ATGGCACGGUCCTGTGAAC	Amplification of HA1 for the deletion of <i>ltaE</i>
<i>ltaE</i> _HA2_F	ACCGTGCCAUGTGAGCGAGACCGGGGCC	Amplification of HA2 for the deletion of <i>ltaE</i>
<i>ltaE</i> _HA2_R	AGGTCGACUCGGTCGATGAAGTGCTC	Amplification of HA2 for the deletion of <i>ltaE</i>
<i>ltaE</i> _g-check_F	TGGCGATGTTATGACTGGTG	Genotyping for the chromosomal <i>ltaE</i> region via colony PCR
<i>ltaE</i> _g-check_R	TAGAGCACATCAGCGACATG	Genotyping for the chromosomal <i>ltaE</i> region via colony PCR
<i>mmsA1</i> _HA1_F	AGATCCUAGACCTTCATGAACCAGCCG	Amplification of HA1 for the deletion of <i>mmsA1</i>
<i>mmsA1</i> _HA1_R	ACTTCCCTUACATGCAAACTCCAGATAAACAAAGG	Amplification of HA1 for the deletion of <i>mmsA1</i>
<i>mmsA1</i> _HA2_F	AAGGGAAGUAGATGAAGCGGG	Amplification of HA2 for the deletion of <i>mmsA1</i>
<i>mmsA1</i> _HA2_R	AGGTCGACUTCCTCAGAGCCTGTCAAGC	Amplification of HA2 for the deletion of <i>mmsA1</i>
<i>mmsA1</i> _g-check_F	CTGTTGGCGAAACCCTGAAC	Genotyping for the chromosomal <i>mmsA1</i> region via colony PCR
<i>mmsA1</i> _g-check_R	GCTTCAAACACTTGGCTCGC	Genotyping for the chromosomal <i>mmsA1</i> region via colony PCR
<i>mmsA2</i> _HA1_F	AGATCCUCAGGATGTCCACCGAAATTGC	Amplification of HA1 for the deletion of <i>mmsA2</i>
<i>mmsA2</i> _HA1_R	ACTCCTTACAUCTGCGTTCTCCTTGGAAATTG	Amplification of HA1 for the deletion of <i>mmsA2</i>
<i>mmsA2</i> _HA2_F	ATGTAAGGAGUACGTCATGCGTATCG	Amplification of HA2 for the deletion of <i>mmsA2</i>
<i>mmsA2</i> _HA2_R	AGGTCGACUGCAGGTTGTTGCAGATCTTGG	Amplification of HA2 for the deletion of <i>mmsA2</i>
<i>mmsA2</i> _g-check_F	GACAGGCTGATGAAATGCGG	Genotyping for the chromosomal <i>mmsA2</i> region via colony PCR

<i>mmsA2_g-check_R</i>	TCAGGTCGAACAGGTTTCAGC	Genotyping for the chromosomal <i>mmsA2</i> region via colony PCR
<i>paaEDCBA_HA1_F</i>	AGATCCUGTGAATGACGGCGCTTGC	Amplification of HA1 for the deletion of <i>paaEDCBA</i>
<i>paaEDCBA_HA1_R</i>	ACATGGCUTCACCTCGAATTGTTC	Amplification of HA1 for the deletion of <i>paaEDCBA</i>
<i>paaEDCBA_HA2_F</i>	AGCCATGUAGACCGAGTCGGCTGCTTC	Amplification of HA2 for the deletion of <i>paaEDCBA</i>
<i>paaEDCBA_HA2_R</i>	AGGTCGACUCCAGCAGGGTGAAGCAGAC	Amplification of HA2 for the deletion of <i>paaEDCBA</i>
<i>paaEDCBA_g-check_F</i>	GTTACCGAACTGAACGCAGC	Genotyping for the chromosomal <i>paaEDCBA</i> region via colony PCR
<i>paaEDCBA_g-check_R</i>	GCTTGACCTTGCTGTTGAGC	Genotyping for the chromosomal <i>paaEDCBA</i> region via colony PCR
<i>pcaBDC_HA1_F</i>	AGATCCUATGCAGAAGTACCTGGTCAAC	Amplification of HA1 for the deletion of <i>pcaBDC</i>
<i>pcaBDC_HA1_R</i>	ACGGTTTACAUGCAGCGTCCTTAATCATC	Amplification of HA1 for the deletion of <i>pcaBDC</i>
<i>pcaBDC_HA2_F</i>	ATGTAAACCGUGATCACGGGCAG	Amplification of HA2 for the deletion of <i>pcaBDC</i>
<i>pcaBDC_HA2_R</i>	AGGTCGACUGAGCCAATACGCCAACTACC	Amplification of HA2 for the deletion of <i>pcaBDC</i>
<i>pcaBDC_g-check_F</i>	AAACCCTGGGGATGGAAAAC	Genotyping for the chromosomal <i>pcaBDC</i> region via colony PCR
<i>pcaBDC_g-check_R</i>	TCTGTGTGGTCTACTTGCG	Genotyping for the chromosomal <i>pcaBDC</i> region via colony PCR
<i>prpC_HA1_F</i>	AGATCCUCCGTATCAAAGCTGCCGTC	Amplification of HA1 for the deletion of <i>prpC</i>
<i>prpC_HA1_R</i>	ATTCACAUUGTGTTCCTTTCTTGAA	Amplification of HA1 for the deletion of <i>prpC</i>
<i>prpC_HA2_F</i>	ATGTGAUAGCTATAGAGAGGCAACC	Amplification of HA2 for the deletion of <i>prpC</i>
<i>prpC_HA2_R</i>	AGGTCGACUGTGGTCGACGATCAGTTGC	Amplification of HA2 for the deletion of <i>prpC</i>
<i>prpC_g-check_F</i>	ACGTGTCGTTGGTGCTGTAC	Genotyping for the chromosomal <i>prpC</i> region via colony PCR
<i>prpC_g-check_R</i>	GTATGGCAAGCCGTCGTAGG	Genotyping for the chromosomal <i>prpC</i> region via colony PCR
<i>xfpk_F</i>	ATGACGAGUCCTGTTATTGGCA	Amplification of <i>xfpk</i> for integration into pGNW2-LPR
<i>xfpk_R</i>	ATCTCACUCGTTATCGCCAGCG	Amplification of <i>xfpk</i> for integration into pGNW2-LPR
pGNW2-LP_F	AGTGAGAUAGTGCTAGTGTAGATCGC	Linearization of pGNW2-LPR to replace <i>rfp</i> with <i>xfpk</i>
pGNW2-LP_R	ACTCGTCAUTAGAAAACCTCCTTAGCATGATTA	Linearization of pGNW2-LPR to replace <i>rfp</i> with <i>xfpk</i>
<i>pta^{EC}_F</i>	ATCGTTTUAATGATTATTGAACGTTGTCGTGAA	Amplification of <i>pta</i> from the chromosome of <i>E. coli</i> DH5 α
<i>pta^{EC}_R</i>	AGTCATUGGGACCGTTCATTCAACC	Amplification of <i>pta</i> from the chromosome of <i>E. coli</i> DH5 α
pS438-BCD10_F	AATGACUGGGAAAACCTGGC	Linearization of pS438-BCD10 for the integration of <i>pta^{EC}</i>
pS438-BCD10_R	AGAAACGAUCCTCCGCATGATTAA GATGTTTCAGTACG	Linearization of pS438-BCD10 for the integration of <i>pta^{EC}</i>
<i>gntZ_F</i>	AATGCAACUGGGAATCATCGG	Amplification of <i>gntZ</i> from the chromosome of <i>P. putida</i> KT2440
<i>gntZ_R</i>	AGGGGTTCAUTCGCCTTTCTTCTCGAC	Amplification of <i>gntZ</i> from the chromosome of <i>P. putida</i> KT2440
<i>rpe_F</i>	ATGAACCCCUACGCTATTGCCCC	Amplification of <i>rpe</i> from the chromosome of <i>P. putida</i> KT2440

<i>rpe</i> _R	ACGTTGUAATCATGGCGGGCCAGGGC	Amplification of <i>rpe</i> from the chromosome of <i>P. putida</i> KT2440
P _{14g(BCD10)} _F	ACAAGGCUCTCGCGGCCA	Amplification of P _{14g(BCD10)} from pS628(BCD10)→msfGFP (Chapter 5)
P _{14g(BCD10)} _R	AGTTGCATUAGAAACGATCCTCCGCATG	Amplification of P _{14g(BCD10)} from pS628(BCD10)→msfGFP (Chapter 5)
pTn7·xylS_F	ACGAACGUAGTGCCTAGGCCGCGCCGC	Linearization of pTn7·xylS ²³⁸ for the integration of P _{14g(BCD10)} , <i>gntZ</i> , and <i>rpe</i>
pTn7·xylS_R	AGCCTTGUAGGACACTGCACTTTATGCTGGTTATGC	Linearization of pTn7·xylS ²³⁸ for the integration of P _{14g(BCD10)} , <i>gntZ</i> , and <i>rpe</i>
seq_attTn7_F	CGAGCTGGTCGTGTTCCG	Genotyping of the <i>attTn7</i> region
seq_attTn7_R	GCACCAACTTGTTAAAGCCG	Genotyping of the <i>attTn7</i> region

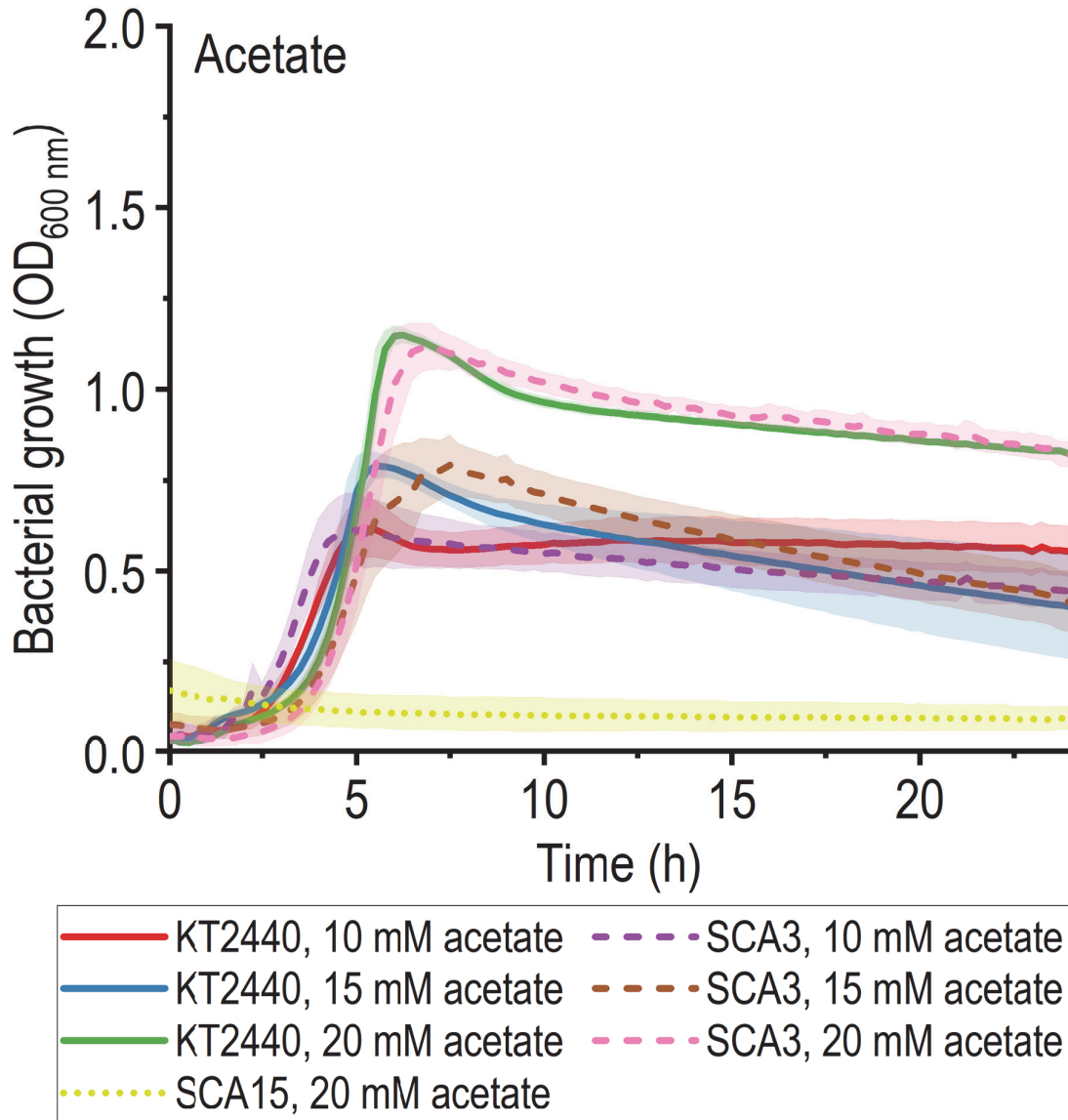


Figure 4.S1. Growth of *P. putida* KT2440, SCA3, and SCA15 in minimal medium supplemented with acetate. The strains were cultured in 96-well plates filled with 200 μ l LB medium per well. Error bars, representing the standard deviation from three biological replicates, are indicated by filled areas around the curves.

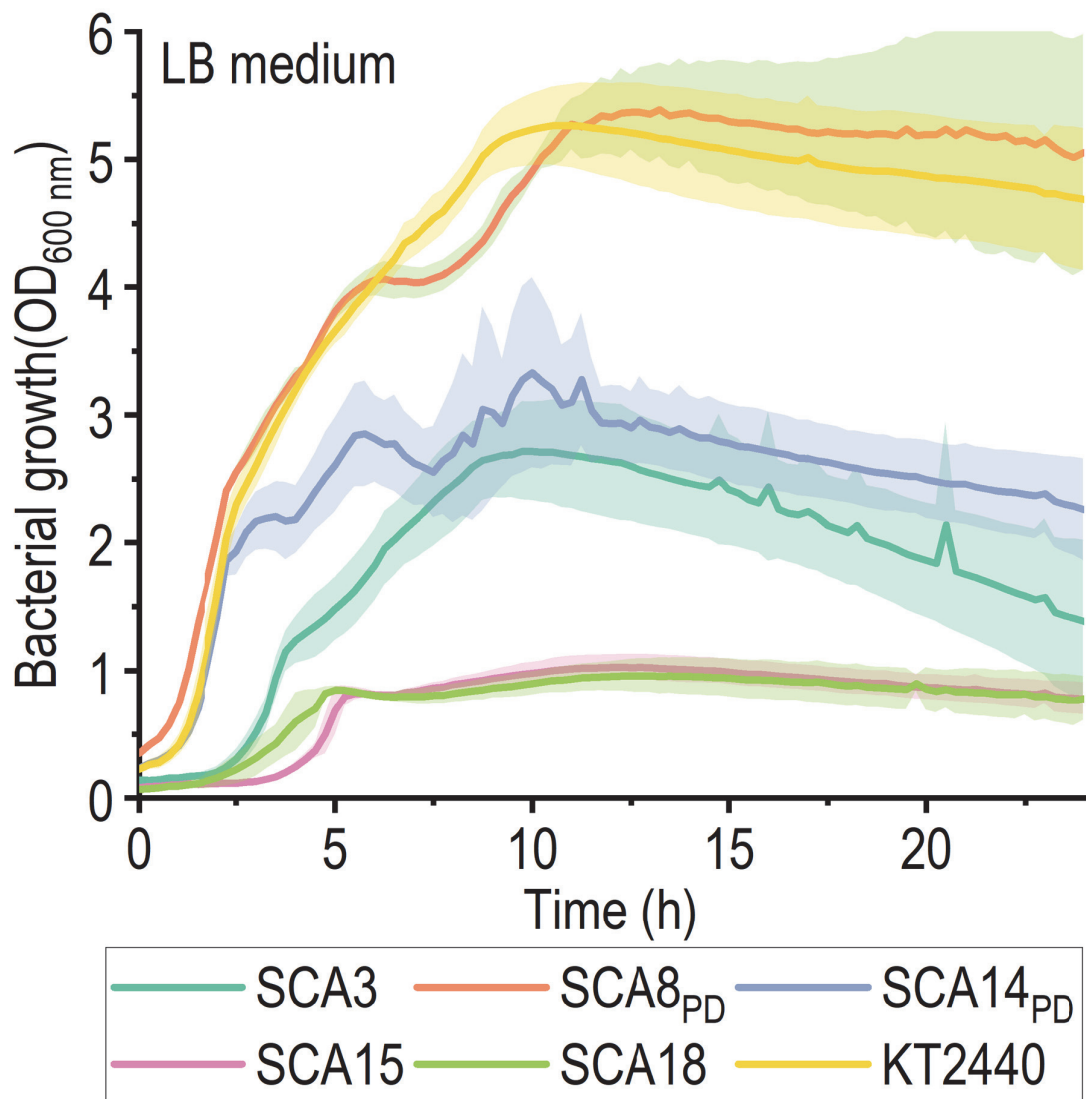


Figure 4.S2. Growth of *P. putida* KT2440 and engineered SCA strains in LB medium. The strains were cultured in 96-well plates filled with 200 μ l LB medium per well. Error bars, representing the standard deviation from three biological replicates, are indicated by filled areas around the curves.

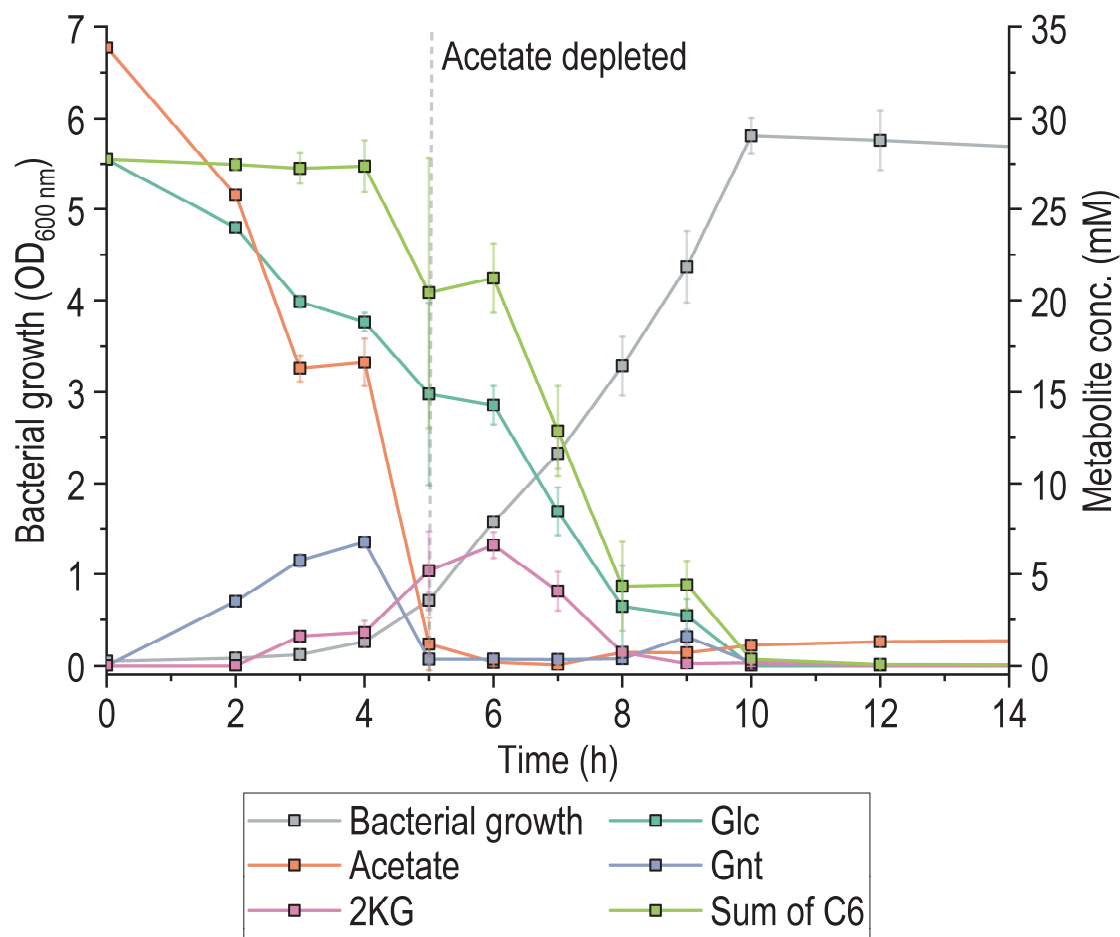


Figure 4.S3. Co-consumption of glucose and acetate in *P. putida* KT2440. The strain was grown in DBM medium supplemented with 5 g L⁻¹ (28 mM) glucose and 2 g L⁻¹ (34 mM) acetate. To distinguish the utilization of glucose as energy source as opposed to the assimilation of its carbon skeleton, the three six-carbon (C6) moieties glucose (Glc), gluconate (Gnt), and 2-ketogluconate (2KG) were combined into the *Sum of C6*. During acetate consumption, glucose is only used as an energy source (via the oxidation to Gnt and 2KG). The assimilation of glucose-derived carbon is initiated after acetate has been depleted (indicated by a dashed line). Error bars represent the standard deviation from three biological replicates.

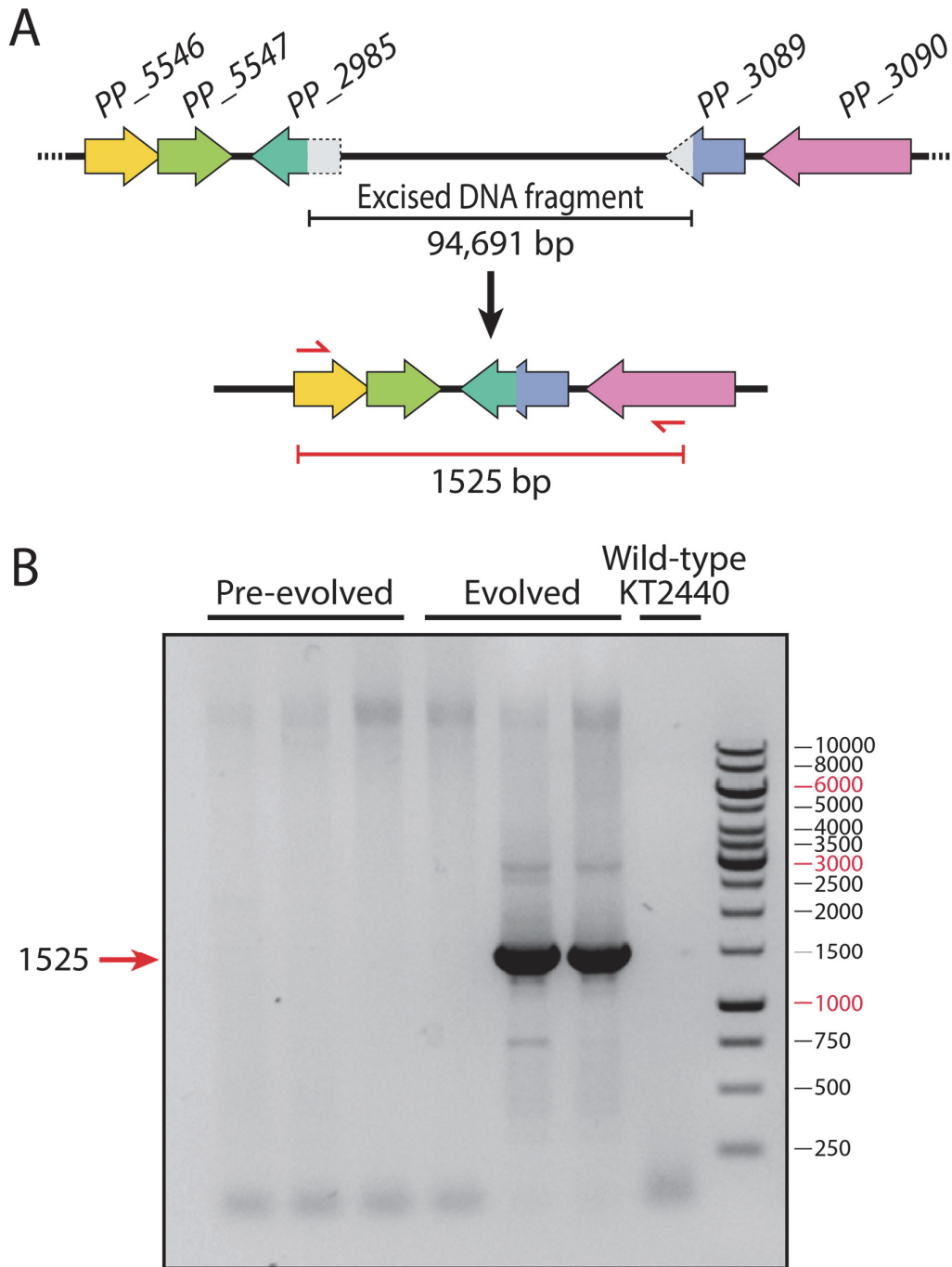


Figure 4.S4. Verification of DNA excision during the evolution of strain SCA3_{PK-Tn}/pS438-*pta*^{EC}. To verify the absence of a 94,691-bp stretch of DNA in the chromosome of 2 out of 4 evolved SCA3_{PK-Tn}/pS438-*pta*^{EC} clones, the respective region was amplified via PCR. **(A)** Re-arrangement of the chromosomal sequences during the excision. The binding regions of the primers used for PCR amplification are indicated in red. **(B)** Results of agarose gel electrophoresis with the amplified PCR fragments. The purified chromosomal DNA samples that had been analyzed by next-generation sequencing were used as the templates. A 1525-bp amplicon provides additional evidence for the absence of the DNA sequence identified as missing in the genome analyses.

Table 4.S2. Changes in protein expression for strain SCA3 compared to *P. putida* KT2440. Both strains were cultured in minimal medium supplemented with 30 mM glucose and 30 mM K-Ac. Genes with symbol names in bold were deleted in SCA3. The listed table entries represent significant changes with a q-value threshold of 0.05, filtered for proteins with an identified enzymatic function according to the KEGG database (https://www.genome.jp/kegg-bin/show_pathway?ppu01100). Abundance changes with a log₂(fold change) of ≥ 2 are highlighted with bold numbers.

Ensembl Gene ID	Enzyme	Gene Symbol	fold-change
PP_5270	D-amino acid:quinone oxidoreductase	<i>dadA-2; dadA-II</i>	8.90
PP_1389	oxaloacetate decarboxylase		6.44
PP_0542	ethanolamine ammonia-lyase subunit β	<i>eutC</i>	6.04
PP_2679	quinoprotein ethanol dehydrogenase	<i>qedH-II</i>	4.50
PP_4636	acetyl-CoA acetyltransferase	<i>yqeF</i>	3.50
PP_4116	isocitrate lyase	<i>aceA</i>	3.49
PP_3148	glutamine synthetase		3.47
PP_5132	dihydrofolate reductase	<i>folA</i>	2.84
PP_0596	ω-amino acid-pyruvate aminotransferase		2.73
PP_3376	phosphonate dehydrogenase	<i>kguD; ptxD</i>	2.72
PP_2341	6-carboxytetrahydropterin synthase QueD	<i>queD</i>	2.25
PP_1347	glutathione S-transferase family protein		2.12
PP_0372	acetylornithine aminotransferase	<i>aruC</i>	2.05
PP_0356	malate synthase G	<i>glcB</i>	2.03
PP_0751	malate:quinone oxidoreductase	<i>mgo-1; mgo-I</i>	1.94
PP_5332	hypothetical protein		1.93
PP_2151	pyridine nucleotide transhydrogenase	<i>sthA</i>	1.91
PP_2913	5-aminolevulinatase dehydratase	<i>hemB-1; hemB</i>	1.81
PP_1261	2-ketoaldonate reductase/hydroxypyruvate/glyoxylate reductase	<i>ghrB</i>	1.71
PP_1832	oxidase		1.67
PP_0762	glycerate dehydrogenase	<i>hprA</i>	1.60
PP_2137	β-ketoadipyl-CoA thiolase subunit β	<i>fadA; pcaF-II</i>	1.55
PP_4577	hypothetical protein		1.53
PP_0840	serine acetyltransferase	<i>cysE</i>	1.51
PP_4012	isocitrate dehydrogenase	<i>idh</i>	1.50
PP_1332	UDP-N-acetylmuramoyl-L-alanyl-D-glutamate-2,6-diaminopimelate ligase	<i>murE</i>	1.45
PP_5183	glutamylpolyamine synthetase	<i>spuB</i>	1.45
PP_0392	dihydroneopterin aldolase	<i>folB</i>	1.44
PP_1989	aspartate-semialdehyde dehydrogenase	<i>asd</i>	1.44
PP_1346	glutamate N-acetyltransferase/amino acid acetyltransferase	<i>argJ</i>	1.39
PP_1031	IMP dehydrogenase and single strand DNA binding factor	<i>guaB</i>	1.36
PP_1823	GTP cyclohydrolase I	<i>folE; folEA-I</i>	1.34
PP_0722	ribose-phosphate pyrophosphokinase	<i>prsA; prs</i>	1.32
PP_2536	glutathione S-transferase family protein		1.29
PP_1657	modified nucleoside triphosphate pyrophosphohydrolyase	<i>mazG</i>	1.25
PP_0517	6,7-dimethyl-8-ribityllumazine synthase	<i>ribH; PSEEN_RS02765</i>	1.17
PP_1338	UDP-N-acetylmuramate-L-alanine ligase	<i>murC</i>	1.15
PP_1530	2,3,4,5-tetrahydropyridine-2,6-dicarboxylate N-succinyltransferase	<i>dapD</i>	1.10

PP_0967	histidinol-phosphate aminotransferase	<i>hisC</i>	0.81
PP_0516	bifunctional 3,4-dihydroxy-2-butanone 4-phosphate synthase/GTP cyclohydrolase II	<i>ribBA-1; ribAB-I</i>	0.80
PP_1403	β -D-glucoside glucohydrolase	<i>bglX</i>	0.78
PP_1616	glutathione-dependent formaldehyde dehydrogenase	<i>frmA</i>	0.78
PP_1611	2-dehydro-3-deoxyphosphooctonate aldolase	<i>kdsA-1; kdsA-I</i>	0.77
PP_0292	phosphoribosylformimino-5-aminoimidazole carboxamide ribonucleotide isomerase	<i>hisA</i>	0.76
PP_0560	type II 3-dehydroquinone dehydratase	<i>aroQ-1; aroQ-I</i>	0.76
PP_0842	cysteine desulfurase	<i>iscS; iscS-I</i>	0.75
PP_1470	homoserine dehydrogenase	<i>hom</i>	0.75
PP_5285	bifunctional 4'-phosphopantothienylcysteine decarboxylase/phosphopantothienylcysteine synthetase	<i>coaBC; dfp</i>	0.75
PP_1807	2-dehydro-3-deoxyphosphooctonate aldolase	<i>kdsA-2; kdsA-II</i>	0.73
PP_3219	alkansulfonate monooxygenase		0.72
PP_0366	dethiobiotin synthetase	<i>bioD</i>	0.72
PP_1593	uridylate kinase	<i>pyrH</i>	0.71
PP_4122	NADH-quinone oxidoreductase subunit E	<i>nuoE</i>	0.71
PP_1617	S-formylglutathione hydrolase/S-lactoylglutathione hydrolase	<i>frmC</i>	0.71
PP_1231	quinolinate synthase iron-sulfur cluster subunit	<i>nadA</i>	0.70
PP_0328	formaldehyde dehydrogenase	<i>fdhA</i>	0.69
PP_0421	anthranilate phosphoribosyltransferase	<i>trpD</i>	0.68
PP_2371	sulfite reductase hemoprotein subunit β	<i>cysI</i>	0.67
PP_4123	NADH-quinone oxidoreductase subunit F	<i>nuoF</i>	0.67
PP_5149	threonine deaminase	<i>ilvA-2; ilvA-II</i>	0.66
PP_1677	adenosyl-cobyrinic acid synthase	<i>cobQ</i>	0.65
PP_0581	3-oxoacyl-ACP reductase	<i>fabG;</i>	0.65
PP_3540	hydroxymethylglutaryl-CoA lyase	<i>mvaB</i>	0.64
PP_4126	NADH-quinone oxidoreductase subunit I	<i>nuoI</i>	0.63
PP_4186	bifunctional succinyl-CoA synthetase subunit β /glutaryl-CoA synthetase subunit β	<i>sucC</i>	0.63
PP_1610	CTP synthase	<i>pyrG</i>	0.63
PP_4174	3R-3-hydroxydecanoyl-ACP dehydratase	<i>fabA</i>	0.61
PP_4185	succinyl-CoA synthetase subunit α	<i>sucD</i>	0.61
PP_0083	tryptophan synthase subunit β	<i>trpB</i>	0.61
PP_2339	aconitate hydratase B	<i>acnB</i>	0.60
PP_4042	Glucose 6-phosphate 1-dehydrogenase	<i>zwfA</i>	0.59
PP_4679	acetolactate synthase small subunit	<i>ilvH</i>	0.57
PP_5075	glutamate synthase subunit β	<i>gltD</i>	0.57
PP_2017	aminopeptidase N	<i>pepN</i>	0.56
PP_0582	thiolase family protein		0.55
PP_0794	1-phosphofructokinase monomer	<i>fruK</i>	0.55
PP_1481	medium chain aldehyde dehydrogenase	<i>patD</i>	0.54
PP_0989	glycine cleavage system protein H	<i>gcvH; gcvH-I</i>	0.54
PP_4065	methylcrotonyl-CoA carboxylase biotin-containing subunit β	<i>mccB</i>	0.52
PP_0988	glycine dehydrogenase	<i>gcvP-1; gcvP-I</i>	0.50
PP_0417	anthranilate synthase component 1	<i>trpE</i>	0.49
PP_4479	arginine N-succinyltransferase subunit β	<i>aruG; astA-I</i>	0.49
PP_3410	precorrin-4 C(11)-methyltransferase	<i>cobM</i>	0.48
PP_0323	sarcosine oxidase subunit β	<i>soxB</i>	0.48
PP_4922	phosphomethylpyrimidine synthase	<i>thiC</i>	0.47
PP_5186	acetylornithine deacetylase	<i>argE</i>	0.46

PP_4124	NADH-quinone oxidoreductase subunit G	<i>nuoG</i>	0.46
PP_0073	coproporphyrinogen-III oxidase	<i>hemF</i>	0.44
PP_2338	2-methylcitrate dehydratase	<i>prpD</i>	0.43
PP_3189	cytosine deaminase/isoguanine deaminase	<i>codA</i>	0.42
PP_5346	pyruvate carboxylase subunit B	<i>oadA; pycB</i>	0.42
PP_1023	6-phosphogluconolactonase	<i>pgl</i>	0.41
PP_2149	glyceraldehyde-3-phosphate dehydrogenase	<i>gap-2; gapB</i>	0.41
PP_0986	aminomethyltransferase	<i>gcvT-1; gcvT-1</i>	0.41
PP_1874	hydroperoxy fatty acid reductase Gpx1	<i>gpx</i>	0.39
PP_5128	dihydroxy-acid dehydratase	<i>ilvD</i>	0.38
PP_0365	malonyl-ACP O-methyltransferase	<i>bioC</i>	0.38
PP_0363	8-amino-7-oxononanoate synthase	<i>bioF</i>	0.37
PP_0293	imidazole glycerol phosphate synthase subunit HisF	<i>hisF</i>	0.37
PP_3416	D-gluconate kinase	<i>gnuK</i>	0.36
PP_0339	pyruvate dehydrogenase E1 component	<i>aceE</i>	0.30
PP_5033	urocanate hydratase	<i>hutU</i>	0.30
PP_0362	biotin synthase	<i>bioB</i>	0.29
PP_5347	pyruvate carboxylase subunit A	<i>accC-2; pycA</i>	0.29
PP_5184	glutamylpolyamine synthetase	<i>spul</i>	0.25
PP_4977	5,10-methylenetetrahydrofolate reductase	<i>metF</i>	0.21
PP_3790	diaminopimelate epimerase	<i>dapF;</i>	0.20
PP_4967	methionine adenosyltransferase	<i>metK</i>	0.17
PP_0321	Low specificity L-threonine aldolase	<i>ltaE</i>	0.03
PP_0338	AceF-S-acetyldihydroliipoate	<i>aceF</i>	0.01
PP_4401	2-oxoisovalerate dehydrogenase subunit α	<i>bkdAA</i>	n.d.

Table 4.S3. Genes located within the chromosomal region deleted in two out of four evolved SCA3_{PK-Tn}/pS438-*pta*^{EC}.

Ensembl Gene ID	Enzyme	Gene Symbol
PP_2985	hypothetical protein	
PP_5548	hypothetical protein	
PP_2986	oxidoreductase	
PP_2987	hypothetical protein	
PP_2988	alcohol dehydrogenase	
PP_2989	short-chain dehydrogenase/reductase family oxidoreductase	
PP_2990	MerR family transcriptional regulator	
PP_2991	hypothetical protein	
PP_2992	hypothetical protein	
PP_2994	FMN-binding oxidoreductase	
PP_2995	DNA topology modulation kinase FlaR	
PP_2996	hypothetical protein	
PP_2997	protein CnmA	
PP_2998	2-dehydropantoate 2-reductase	
PP_2999	glyoxalase family protein	
PP_3000	MaoC domain-containing protein	
PP_3001	CAIB/BAIF family protein	
PP_3002	shikimate dehydrogenase-like protein	
PP_3003	3-dehydroquinone dehydratase	<i>aroQ-III</i>
PP_3004	hypothetical protein	
PP_3005	hypothetical protein	
PP_3006	ECF family RNA polymerase sigma-70 factor	
PP_3007	hypothetical protein	
PP_3008	hypothetical protein	
PP_3009	hypothetical protein	
PP_3010	hypothetical protein	
PP_3011	hypothetical protein	
PP_3012	hypothetical protein	
PP_3013	hypothetical protein	
PP_3014	hypothetical protein	
PP_5549	hypothetical protein	
PP_3015	medium-chain acyl-CoA ligase domain-containing protein	
PP_3016	lipopolysaccharide core biosynthesis protein	
PP_3017	O6-methylguanine-DNA methyltransferase	<i>ogt</i>
PP_3018	hypothetical protein	
PP_3019	carbon-nitrogen hydrolase family protein	
PP_3020	serine/threonine protein phosphatase	
PP_3021	LysE family transporter	
PP_3022	AraC family transcriptional regulator	
PP_3024	hypothetical protein	
PP_5550	hypothetical protein	
PP_5551	hypothetical protein	
PP_3025	LysE family transporter	
PP_3026	recombinase	
PP_3027	hypothetical protein	
PP_3028	hypothetical protein	
PP_3029	DNA cytosine methyltransferase family protein	
PP_3030	hypothetical protein	
PP_3031	Pyocin activator protein PrtN	<i>prtN</i>

PP_3032	DNA-binding protein Roi-like protein	
PP_5552	hypothetical protein	
PP_5553	hypothetical protein	
PP_3033	CI/C2 family transcriptional regulator	
PP_3034	hypothetical protein	
PP_3035	hypothetical protein	
PP_5554	hypothetical protein	
PP_3036	hypothetical protein	
PP_5555	hypothetical protein	
PP_3037	DksA/TraR family C4-type zinc finger protein	
PP_3038	TraC domain-containing protein	
PP_3039	hypothetical protein	
PP_3040	holin	
PP_3041	hypothetical protein	
PP_3042	terminase large subunit	
PP_3043	hypothetical protein	
PP_3044	lambda family portal protein	
PP_3045	ATP-dependent protease ClpP	
PP_3046	hypothetical protein	
PP_3047	hypothetical protein	
PP_3048	hypothetical protein	
PP_3049	hypothetical protein	
PP_3050	hypothetical protein	
PP_3051	pyocin R2_PP	gpV
PP_3052	hypothetical protein	
PP_3053	pyocin R2_PP baseplate protein	gpW
PP_3054	pyocin R2_PP baseplate/tail fiber protein	gpJ
PP_3055	pyocin R2_PP tail formation protein	gpI
PP_3056	tail fiber protein	
PP_3057	pectinesterase	
PP_3058	hypothetical protein	
PP_3059	tail sheath protein	
PP_3060	tail sheath protein	
PP_3061	hypothetical protein	
PP_3062	tail length determination protein	
PP_3063	pyocin R2_PP tail formation protein	gpU
PP_3064	pyocin R2_PP tail component	gpX
PP_3065	pyocin R2_PP tail formation protein	gpD
PP_3066	lytic enzyme	
PP_5556	bacteriophage lysis protein	
PP_5557	hypothetical protein	
PP_3067	hypothetical protein	
PP_5558	Xre family transcriptional regulator	
PP_3069	outer membrane autotransporter	
PP_3070	PpiC-type peptidyl-prolyl <i>cis-trans</i> isomerase	ppiC-I
PP_3071	acetoacetyl-CoA synthetase	aacs
PP_3072	ecotin	eco
PP_3073	3-hydroxybutyrate dehydrogenase	hbdH
PP_3074	citrate transporter	bhbP
PP_3075	transcriptional regulator	
PP_3076	ABC transporter permease	
PP_3077	ABC transporter permease	
PP_3078	ABC transporter substrate-binding protein	
PP_3079	peptidyl-prolyl <i>cis-trans</i> isomerase	ppiC-II
PP_3080	phospho-2-dehydro-3-deoxyheptonate aldolase	aroF-II

PP_5559	hypothetical protein
PP_3081	hypothetical protein
PP_5560	hypothetical protein
PP_3082	membrane protein
PP_3083	membrane protein
PP_3084	ferric siderophore receptor
PP_3085	transmembrane sensor
PP_3086	RNA polymerase sigma-70 factor
PP_3087	excinuclease ABC subunit A
PP_3088	hypothetical protein
PP_3089	hypothetical protein

Table 4.S4. Not annotated tRNA sequences in the chromosomal sequence of *P. putida* KT2440 identified with ARAGORN.

tRNA type	Genomic location	sequence
tRNA ^{Ala}	Inside the CDS of malate dehydrogenase <i>PP_0654</i> (same strand)	5'-GGTGAGCTGGCGCAGGGCAAGGCGCTGGACGTTTGG-CAGGCGGCTGTGGATTCAGGTTCCGA-TACCCATGTTACGGC-3'
tRNA ^{Ala}	Inside the CDS of <i>quiP</i> (<i>PP_1108</i> , oppo-site strand)	5'-GCCAGCTTCTGGCTGGCAGCCGCCAGGGCTGG-CAGCCCCGGCAACTGGCTGGCCAGGTTCAGGCCCTT-GAGCTTGTCC-3'
tRNA ^{Cys}	Inside the CDS of acetyltransferase <i>PP_2957</i> (same strand)	5'-CCACCATCTTCATGACGGCAGGGCACGGCGGTT-GCAGCCCGCAGGGGCTTGAC-TGGCGCCTGGCGCCGCGGGTT-CGAGGTGTGCATGGTGGTC-3'
tRNA ^{Trp}	Inside the CDS of <i>sad-II</i> (<i>PP_3151</i> , opposite strand)	5'-ACTGGCGGTAGCCAACCTTGCGCGTT-GCAGCGCCGCTCCAGTGCGGCGTCGGTGTGCGAACGGGT-AGGTGCCGATCTGCTCGCCGCTG -3'
tRNA ^{Thr}	Between <i>PP_3550</i> and <i>PP_3551</i> (overlap on same strand)	5'-ACCGCCCTTACGCAGGCCCTGGCAGGGGCGGCCTT-GTGTGTCGCATGGGCCGAGGGCGCGCCTGCGGG-GGCGGTG-3'

4.7. References for Chapter 4

- 59 Nørholm, M. H. H. **Meta Synthetic Biology: Controlling the Evolution of Engineered Living Systems.** *Microbial Biotechnology* **12**, 35-37, doi: <https://doi.org/10.1111/1751-7915.13350> (2019).
- 105 Nickel, P. I., Chavarría, M., Fuhrer, T., Sauer, U. & de Lorenzo, V. ***Pseudomonas putida* KT2440 Strain Metabolizes Glucose through a Cycle Formed by Enzymes of the Entner-Doudoroff, Embden-Meyerhof-Parnas, and Pentose Phosphate Pathways.** *Journal of Biological Chemistry* **290**, 25920-25932, doi: [10.1074/jbc.M115.687749](https://doi.org/10.1074/jbc.M115.687749) (2015).
- 114 Sudarsan, S., Dethlefsen, S., Blank, L. M., Siemann-Herzberg, M. & Schmid, A. **The Functional Structure of Central Carbon Metabolism in *Pseudomonas putida* KT2440.** *Applied Environmental Microbiology* **80**, 5292-5303, doi: [10.1128/AEM.01643-14](https://doi.org/10.1128/AEM.01643-14) (2014).
- 203 Cavaleiro, A. M., Kim, S. H., Seppala, S., Nielsen, M. T. & Norholm, M. H. **Accurate DNA Assembly and Genome Engineering with Optimized Uracil Excision Cloning.** *ACS Synthetic Biology* **4**, 1042-1046, doi: [10.1021/acssynbio.5b00113](https://doi.org/10.1021/acssynbio.5b00113) (2015).
- 238 Volke, D. C., Turlin, J., Mol, V. & Nickel, P. I. **Physical Decoupling of XylS/*Pm* Regulatory Elements and Conditional Proteolysis Enable Precise Control of Gene Expression in *Pseudomonas putida*.** *Microbial Biotechnology* **13**, 222-232, doi: [10.1111/1751-7915.13383](https://doi.org/10.1111/1751-7915.13383) (2020).
- 241 Martínez-García, E., Jatsenko, T., Kivisaar, M. & de Lorenzo, V. **Freeing *Pseudomonas putida* KT2440 of Its Proviral Load Strengthens Endurance to Environmental Stresses.** *Environmental Microbiology* **17**, 76-90, doi: [10.1111/1462-2920.12492](https://doi.org/10.1111/1462-2920.12492) (2015).
- 247 Ilves, H., Horak, R. & Kivisaar, M. **Involvement of Sigma(S) in Starvation-Induced Transposition of *Pseudomonas putida* Transposon Tn4652.** *Journal of Bacteriology* **183**, 5445-5448, doi: [10.1128/jb.183.18.5445-5448.2001](https://doi.org/10.1128/jb.183.18.5445-5448.2001) (2001).
- 258 Platt, R., Drescher, C., Park, S. K. & Phillips, G. J. **Genetic System for Reversible Integration of DNA Constructs and *lacZ* Gene Fusions into the *Escherichia coli* Chromosome.** *Plasmid* **43**, 12-23, doi: [10.1006/plas.1999.1433](https://doi.org/10.1006/plas.1999.1433) (2000).
- 260 Worsey, M. J. & Williams, P. A. **Metabolism of Toluene and Xylenes by *Pseudomonas putida* (Arvilla) mt-2: Evidence for a New Function of the TOL Plasmid.** *Journal of Bacteriology* **124**, 7-13, doi: [10.1128/JB.124.1.7-13.1975](https://doi.org/10.1128/JB.124.1.7-13.1975) (1975).

- 261 Bagdasarian, M., Lurz, R., Rückert, B., Franklin, F. C. H., Bagdasarian, M. M., Frey, J. & Timmis, K. N. **Specific Purpose Plasmid Cloning Vectors. Ii. Broad Host Range, High Copy Number, Rsf1010-Derived Vectors, and a Host-Vector System for Gene Cloning in *Pseudomonas*.** *Gene* **16**, 237-247, doi: 10.1016/0378-1119(81)90080-9 (1981).
- 262 Novak, M., Pfeiffer, T., Lenski, R. E., Sauer, U. & Bonhoeffer, S. **Experimental Tests for an Evolutionary Trade-Off between Growth Rate and Yield in *E. coli*.** *The American Naturalist* **168**, 242-251, doi: 10.1086/506527 (2006).
- 263 Shi, L. & Tu, B. P. **Acetyl-Coa and the Regulation of Metabolism: Mechanisms and Consequences.** *Current Opinion in Cell Biology* **33**, 125-131, doi: 10.1016/j.ceb.2015.02.003 (2015).
- 264 Lu, X., Liu, Y., Yang, Y., Wang, S., Wang, Q., Wang, X., Yan, Z., Cheng, J., Liu, C., Yang, X., Luo, H., Yang, S., Gou, J., Ye, L., Lu, L. et al. **Constructing a Synthetic Pathway for Acetyl-Coenzyme a from One-Carbon through Enzyme Design.** *Nature Communications* **10**, 1378, doi: 10.1038/s41467-019-09095-z (2019).
- 265 Ebert, B. E., Kurth, F., Grund, M., Blank, L. M. & Schmid, A. **Response of *Pseudomonas putida* KT2440 to Increased NADH and ATP Demand.** *Applied and Environmental Microbiology* **77**, 6597-6605, doi: 10.1128/aem.05588-11 (2011).
- 266 Poblete-Castro, I., Becker, J., Dohnt, K., dos Santos, V. M. & Wittmann, C. **Industrial Biotechnology of *Pseudomonas putida* and Related Species.** *Applied Microbiology and Biotechnology* **93**, 2279-2290, doi: 10.1007/s00253-012-3928-0 (2012).
- 267 Isken, S., Derks, A., Wolffs, P. F. G. & de Bont, J. A. M. **Effect of Organic Solvents on the Yield of Solvent-Tolerant *Pseudomonas putida* S12.** *Applied and Environmental Microbiology* **65**, 2631-2635, doi: 10.1128/aem.65.6.2631-2635.1999 (1999).
- 268 Chohnan, S., Furukawa, H., Fujio, T., Nishihara, H. & Takamura, Y. **Changes in the Size and Composition of Intracellular Pools of Nonesterified Coenzyme a and Coenzyme a Thioesters in Aerobic and Facultatively Anaerobic Bacteria.** *Applied Environmental Microbiology* **63**, 553-560, doi: 10.1128/AEM.63.2.553-560.1997 (1997).
- 269 Nickel, P. I. & de Lorenzo, V. **Engineering an Anaerobic Metabolic Regime in *Pseudomonas putida* KT2440 for the Anoxic Biodegradation of 1,3-Dichloroprop-1-ene.** *Metabolic Engineering* **15**, 98-112, doi: 10.1016/j.ymben.2012.09.006 (2013).

- 270 Hervás, A. B., Canosa, I. & Santero, E. **Regulation of Glutamate Dehydrogenase Expression in *Pseudomonas putida* Results from Its Direct Repression by NtrC under Nitrogen-Limiting Conditions.** *Molecular Microbiology* **78**, 305-319, doi: 10.1111/j.1365-2958.2010.07329.x (2010).
- 271 Kuhn, M. L., Zemaitaitis, B., Hu, L. I., Sahu, A., Sorensen, D., Minasov, G., Lima, B. P., Scholle, M., Mrksich, M., Anderson, W. F., Gibson, B. W., Schilling, B. & Wolfe, A. J. **Structural, Kinetic and Proteomic Characterization of Acetyl Phosphate-Dependent Bacterial Protein Acetylation.** *PloS One* **9**, e94816, doi: 10.1371/journal.pone.0094816 (2014).
- 272 Scardovi, V. & Trovatelli, L. D. **The Fructose-6-Phosphate Shunt as Peculiar Pattern of Hexose Degradation in the Genus *Bifidobacterium*.** *Annali Di Microbiologia Ed Enzimologia*, 19-29, doi: 10.1371/journal.pone.0172176 (1965).
- 273 Tittmann, K. **Sweet Siblings with Different Faces: The Mechanisms of Fbp and F6P Aldolase, Transaldolase, Transketolase and Phosphoketolase Revisited in Light of Recent Structural Data.** *Bioorg Chem* **57**, 263-280, doi: 10.1016/j.bioorg.2014.09.001 (2014).
- 274 Sánchez, B., Zúñiga, M., González-Candelas, F., de los Reyes-Gavilán, C. G. & Margolles, A. **Bacterial and Eukaryotic Phosphoketolases: Phylogeny, Distribution and Evolution.** *Microbial Physiology* **18**, 37-51, doi: 10.1159/000274310 (2010).
- 275 Scheidig, A. J., Horvath, D. & Szedlacsek, S. E. **Crystal Structure of a Xylulose 5-Phosphate Phosphoketolase. Insights into the Substrate Specificity for Xylulose 5-Phosphate.** *Journal of Structural Biology* **207**, 85-102, doi: <https://doi.org/10.1016/j.jsb.2019.04.017> (2019).
- 276 Bergman, A., Siewers, V., Nielsen, J. & Chen, Y. **Functional Expression and Evaluation of Heterologous Phosphoketolases in *Saccharomyces cerevisiae*.** *Amb Express* **6**, doi: 10.1186/s13568-016-0290-0 (2016).
- 277 Henard, C. A., Freed, E. F. & Guarnieri, M. T. **Phosphoketolase Pathway Engineering for Carbon-Efficient Biocatalysis.** *Current Opinion in Biotechnology* **36**, 183-188, doi: <https://doi.org/10.1016/j.copbio.2015.08.018> (2015).
- 278 Bogorad, I. W., Lin, T.-S. & Liao, J. C. **Synthetic Non-Oxidative Glycolysis Enables Complete Carbon Conservation.** *Nature* **502**, 693-697, doi: 10.1038/nature12575 (2013).

- 279 Lin, P. P., Jaeger, A. J., Wu, T.-Y., Xu, S. C., Lee, A. S., Gao, F., Chen, P.-W. & Liao, J. C. **Construction and Evolution of an *Escherichia coli* Strain Relying on Nonoxidative Glycolysis for Sugar Catabolism.** *Proceedings of the National Academy of Sciences* **115**, 3538-3546, doi: 10.1073/pnas.1802191115 (2018).
- 280 Kocharin, K., Siewers, V. & Nielsen, J. **Improved Polyhydroxybutyrate Production by *Saccharomyces cerevisiae* through the Use of the Phosphoketolase Pathway.** *Biotechnology and Bioengineering* **110**, 2216-2224, doi: <https://doi.org/10.1002/bit.24888> (2013).
- 281 de Jong, B. W., Shi, S., Siewers, V. & Nielsen, J. **Improved Production of Fatty Acid Ethyl Esters in *Saccharomyces cerevisiae* through up-Regulation of the Ethanol Degradation Pathway and Expression of the Heterologous Phosphoketolase Pathway.** *Microbial Cell Factories* **13**, 39, doi: 10.1186/1475-2859-13-39 (2014).
- 282 Hellgren, J., Godina, A., Nielsen, J. & Siewers, V. **Promiscuous Phosphoketolase and Metabolic Rewiring Enables Novel Non-Oxidative Glycolysis in Yeast for High-Yield Production of Acetyl-Coa Derived Products.** *Metabolic Engineering* **62**, 150-160, doi: <https://doi.org/10.1016/j.ymben.2020.09.003> (2020).
- 283 Dele-Osibanjo, T., Li, Q., Zhang, X., Guo, X., Feng, J., Liu, J., Sun, X., Wang, X., Zhou, W., Zheng, P., Sun, J. & Ma, Y. **Growth-Coupled Evolution of Phosphoketolase to Improve L-Glutamate Production by *Corynebacterium glutamicum*.** *Applied Microbiology and Biotechnology* **103**, 8413-8425, doi: 10.1007/s00253-019-10043-6 (2019).
- 284 Clomburg, J. M. & Gonzalez, R. **Biofuel Production in *Escherichia coli*: The Role of Metabolic Engineering and Synthetic Biology.** *Applied Microbiology and Biotechnology* **86**, 419-434, doi: 10.1007/s00253-010-2446-1 (2010).
- 285 Campos, J. M., Stamford, T. L., Sarubbo, L. A., de Luna, J. M., Rufino, R. D. & Banat, I. M. **Microbial Biosurfactants as Additives for Food Industries.** *Biotechnol Prog* **29**, 1097-1108, doi: 10.1002/btpr.1796 (2013).
- 286 Vijayendra, S. V. N. & Shamala, T. R. **Film Forming Microbial Biopolymers for Commercial Applications—a Review.** *Critical Reviews in Biotechnology* **34**, 338-357, doi: 10.3109/07388551.2013.798254 (2014).
- 287 Dabbagh, F., Moradpour, Z. & Ghasemian, A. **Microbial Products and Biotechnological Applications Thereof: Proteins, Enzymes, Secondary Metabolites, and Valuable Chemicals.** in *Microbial Interventions in Agriculture and Environment: Volume 3: Soil and Crop Health Management* (eds Dhananjaya Pratap Singh & Ratna Prabha) 385-432 (Springer Singapore, 2019).

- 288 Shepelin, D., Hansen, A. S. L., Lennen, R., Luo, H. & Herrgård, M. J. **Selecting the Best: Evolutionary Engineering of Chemical Production in Microbes.** *Genes (Basel)* **9**, doi: 10.3390/genes9050249 (2018).
- 289 Dragosits, M. & Mattanovich, D. **Adaptive Laboratory Evolution -- Principles and Applications for Biotechnology.** *Microb Cell Fact* **12**, 64, doi: 10.1186/1475-2859-12-64 (2013).
- 290 Fernández-Cabezón, L., Cros, A. & Nikel, P. I. **Evolutionary Approaches for Engineering Industrially Relevant Phenotypes in Bacterial Cell Factories.** *Biotechnology Journal* **14**, 1800439, doi: <https://doi.org/10.1002/biot.201800439> (2019).
- 291 Mundhada, H., Seoane, J. M., Schneider, K., Koza, A., Christensen, H. B., Klein, T., Phaneuf, P. V., Herrgard, M., Feist, A. M. & Nielsen, A. T. **Increased Production of L-Serine in Escherichia coli through Adaptive Laboratory Evolution.** *Metabolic Engineering* **39**, 141-150, doi: 10.1016/j.ymben.2016.11.008 (2017).
- 292 Rühl, J., Hein, E.-M., Hayen, H., Schmid, A. & Blank, L. M. **The Glycerophospholipid Inventory of *Pseudomonas putida* Is Conserved between Strains and Enables Growth Condition-Related Alterations.** *Microb Biotechnol* **5**, 45-58, doi: 10.1111/j.1751-7915.2011.00286.x (2012).
- 293 Huang, M., Oppermann, F. B. & Steinbüchel, A. **Molecular Characterization of the *Pseudomonas putida* 2,3-Butanediol Catabolic Pathway.** *FEMS Microbiol Lett* **124**, 141-150, doi: 10.1111/j.1574-6968.1994.tb07276.x (1994).
- 294 Nikel, P. I., Chavarría, M., Fuhrer, T., Sauer, U. & de Lorenzo, V. ***Pseudomonas putida* KT2440 Strain Metabolizes Glucose through a Cycle Formed by Enzymes of the Entner-Doudoroff, Embden-Meyerhof-Parnas, and Pentose Phosphate Pathways*.** *Journal of Biological Chemistry* **290**, 25920-25932, doi: <https://doi.org/10.1074/jbc.M115.687749> (2015).
- 295 Volke, D. C., Olavarria, K. & Nikel, P. I. **Cofactor Specificity of Glucose-6-Phosphate Dehydrogenase Isozymes in *Pseudomonas putida* Reveals a General Principle Underlying Glycolytic Strategies in Bacteria.** *BioRxiv* **6**, 2021.2001.2008.426012, doi: 10.1101/2021.01.08.426012 (2021).
- 296 Wirth, N. T., Nitschel, R., Ankenbauer, A., Blombach, B. & Takors, R. **Metabolic Engineering of *Pseudomonas putida* KT2440 for the Production of Isobutanol** Master of Science thesis, University of Stuttgart, (2017).

- 297 Nitschel, R., Ankenbauer, A., Welsch, I., Wirth, N. T., Massner, C., Ahmad, N., McColm, S., Borges, F., Fotheringham, I., Takors, R. & Blombach, B. **Engineering *Pseudomonas putida* KT2440 for the Production of Isobutanol.** *Eng Life Sci* **20**, 148-159, doi: 10.1002/elsc.201900151 (2020).
- 298 Zobel, S., Benedetti, I., Eisenbach, L., de Lorenzo, V., Wierckx, N. & Blank, L. M. **Tn7-Based Device for Calibrated Heterologous Gene Expression in *Pseudomonas putida*.** *ACS Synthetic Biology* **4**, 1341-1351, doi: 10.1021/acssynbio.5b00058 (2015).
- 299 Mutalik, V. K., Guimaraes, J. C., Cambray, G., Lam, C., Christoffersen, M. J., Mai, Q. A., Tran, A. B., Paull, M., Keasling, J. D., Arkin, A. P. & Endy, D. **Precise and Reliable Gene Expression Via Standard Transcription and Translation Initiation Elements.** *Nature Methods* **10**, 354-360, doi: 10.1038/nmeth.2404 (2013).
- 300 Wu, X., Monchy, S., Taghavi, S., Zhu, W., Ramos, J. & van der Lelie, D. **Comparative Genomics and Functional Analysis of Niche-Specific Adaptation in *Pseudomonas putida*.** *FEMS Microbiology Reviews* **35**, 299-323, doi: 10.1111/j.1574-6976.2010.00249.x (2011).
- 301 Martínez-García, E., Nikel, P. I., Aparicio, T. & de Lorenzo, V. ***Pseudomonas* 2.0: Genetic Upgrading of *P. putida* KT2440 as an Enhanced Host for Heterologous Gene Expression.** *Microbial Cell Factories* **13**, 159, doi: 10.1186/s12934-014-0159-3 (2014).
- 302 Suzuki, T. & Miyauchi, K. **Discovery and Characterization of tRNA^{ile} Lysidine Synthetase (Tils).** *FEBS Letters* **584**, 272-277, doi: 10.1016/j.febslet.2009.11.085 (2010).
- 303 Muramatsu, T., Nishikawa, K., Nemoto, F., Kuchino, Y., Nishimura, S., Miyazawa, T. & Yokoyama, S. **Codon and Amino-Acid Specificities of a Transfer RNA Are Both Converted by a Single Post-Transcriptional Modification.** *Nature* **336**, 179-181, doi: 10.1038/336179a0 (1988).
- 304 Nakanishi, K., Bonnefond, L., Kimura, S., Suzuki, T., Ishitani, R. & Nureki, O. **Structural Basis for Translational Fidelity Ensured by Transfer RNA Lysidine Synthetase.** *Nature* **461**, 1144-1148, doi: 10.1038/nature08474 (2009).
- 305 Gu, M., Burling, T., Lima, C. D. & Burley, S. K. (RCSB Protein Data Bank, 2003).
- 306 Magill, D. J., Krylov, V. N., Shaburova, O. V., McGrath, J. W., Allen, C. C. R., Quinn, J. P. & Kulakov, L. A. **Pf16 and Phipmw: Expanding the Realm of *Pseudomonas putida* Bacteriophages.** *PloS One* **12**, e0184307, doi: 10.1371/journal.pone.0184307 (2017).

- 307 Kohlstedt, M. & Wittmann, C. **Gc-Ms-Based ¹³C Metabolic Flux Analysis Resolves the Parallel and Cyclic Glucose Metabolism of *Pseudomonas putida* KT2440 and *Pseudomonas aeruginosa* Pao1.** *Metabolic Engineering* **54**, 35-53, doi: 10.1016/j.ymben.2019.01.008 (2019).
- 308 Blank, L. M., Ionidis, G., Ebert, B. E., Bühler, B. & Schmid, A. **Metabolic Response of *Pseudomonas putida* During Redox Biocatalysis in the Presence of a Second Octanol Phase.** *The FEBS Journal* **275**, 5173-5190, doi: 10.1111/j.1742-4658.2008.06648.x (2008).
- 309 Daddaoua, A., Krell, T., Alfonso, C., Morel, B. & Ramos, J.-L. **Compartmentalized Glucose Metabolism in *Pseudomonas putida* Is Controlled by the Ptxs Repressor.** *Journal of Bacteriology* **192**, 4357-4366, doi: 10.1128/JB.00520-10 (2010).
- 310 Torrontegui, D., Díaz, R. & Cánovas, J. L. **The Uptake of 2-Ketogluconate by *Pseudomonas putida*.** *Archives of Microbiology* **110**, 43-48, doi: 10.1007/bf00416967 (1976).
- 311 McVey, A. C., Medarametla, P., Chee, X., Bartlett, S., Poso, A., Spring, D. R., Rahman, T. & Welch, M. **Structural and Functional Characterization of Malate Synthase G from Opportunistic Pathogen *Pseudomonas aeruginosa*.** *Biochemistry* **56**, 5539-5549, doi: 10.1021/acs.biochem.7b00852 (2017).
- 312 Sievers, M., Stöckli, M. & Teuber, M. **Purification and Properties of Citrate Synthase from *Acetobacter Europaes*.** *FEMS Microbiology Letters* **146**, 53-58, doi: 10.1111/j.1574-6968.1997.tb10170.x (1997).
- 313 Klinke, S., Dauner, M., Scott, G., Kessler, B. & Witholt, B. **Inactivation of Isocitrate Lyase Leads to Increased Production of Medium-Chain-Length Poly(3-Hydroxyalkanoates) in *Pseudomonas putida*.** *Applied Environmental Microbiology* **66**, 909-913, doi: 10.1128/aem.66.3.909-913.2000 (2000).
- 314 Brock, M., Fischer, R., Linder, D. & Buckel, W. **Methylcitrate Synthase from *Aspergillus Nidulans*: Implications for Propionate as an Antifungal Agent.** *Molecular Microbiology* **35**, 961-973, doi: 10.1046/j.1365-2958.2000.01737.x (2000).
- 315 Maerker, C., Rohde, M., Brakhage, A. A. & Brock, M. **Methylcitrate Synthase from *Aspergillus Fumigatus*.** *The FEBS Journal* **272**, 3615-3630, doi: 10.1111/j.1742-4658.2005.04784.x (2005).
- 316 Goncharov, N. V., Jenkins, R. O. & Radilov, A. S. **Toxicology of Fluoroacetate: A Review, with Possible Directions for Therapy Research.** *Journal of Applied Toxicology* **26**, 148-161, doi: 10.1002/jat.1118 (2006).

- 317 Bonekamp, F. & Jensen, K. F. **The Agg Codon Is Translated Slowly in *E. coli* Even at Very Low Expression Levels.** *Nucleic Acids Research* **16**, 3013-3024, doi: 10.1093/nar/16.7.3013 (1988).
- 318 Wang, Y., Li, C., Khan, M. R. I., Wang, Y., Ruan, Y., Zhao, B., Zhang, B., Ma, X., Zhang, K., Zhao, X., Ye, G., Guo, X., Feng, G., He, L. & Ma, G. **An Engineered Rare Codon Device for Optimization of Metabolic Pathways.** *Scientific Reports* **6**, 20608, doi: 10.1038/srep20608 (2016).
- 319 Fang, J., Zou, L., Zhou, X., Cheng, B. & Fan, J. **Synonymous Rare Arginine Codons and tRNA Abundance Affect Protein Production and Quality of Tsv Protease Variant.** *PloS One* **9**, e112254-e112254, doi: 10.1371/journal.pone.0112254 (2014).
- 320 Thangadurai, C., Suthakaran, P., Barfal, P., Anandaraj, B., Pradhan, S. N., Ramalingam, S. & Murugan, V. **Rare Codon Priority and Its Position Specificity at the 5' of the Gene Modulates Heterologous Protein Expression in *Escherichia coli*.** *Biochemical and Biophysical Research Communications* **376**, 647-652, doi: 10.1016/j.bbrc.2008.09.024 (2008).
- 321 Chen, G. T. & Inouye, M. **Role of the Aga/Agg Codons, the Rarest Codons in Global Gene Expression in *Escherichia coli*.** *Genes and Development* **8**, 2641-2652, doi: 10.1101/gad.8.21.2641 (1994).
- 322 Bertin, P., Lejeune, P., Laurent-Winter, C. & Danchin, A. **Mutations in Bgly, the Structural Gene for the DNA-Binding Protein H1, Affect Expression of Several *Escherichia coli* Genes.** *Biochimie* **72**, 889-891, doi: 10.1016/0300-9084(90)90008-5 (1990).
- 323 Sonden, B. & Uhlin, B. E. **Coordinated and Differential Expression of Histone-Like Proteins in *Escherichia coli*: Regulation and Function of the H-Ns Analog Stpa.** *The EMBO Journal* **15**, 4970-4980, doi: (1996).
- 324 Ueguchi, C., Suzuki, T., Yoshida, T., Tanaka, K. & Mizuno, T. **Systematic Mutational Analysis Revealing the Functional Domain Organization of *Escherichia coli* Nucleoid Protein H-Ns.** *Journal of Molecular Biology* **263**, 149-162, doi: 10.1006/jmbi.1996.0566 (1996).
- 325 Grainger, D. C., Hurd, D., Goldberg, M. D. & Busby, S. J. **Association of Nucleoid Proteins with Coding and Non-Coding Segments of the *Escherichia coli* Genome.** *Nucleic Acids Research* **34**, 4642-4652, doi: 10.1093/nar/gkl542 (2006).

- 326 Arce-Rodríguez, A., Durante-Rodríguez, G., Platero, R., Krell, T., Calles, B. & de Lorenzo, V. **The Crp Regulator of *Pseudomonas putida*: Evidence of an Unusually High Affinity for Its Physiological Effector, Camp.** *Environmental Microbiology* **14**, 702-713, doi: 10.1111/j.1462-2920.2011.02622.x (2012).
- 327 Herrera, M. C., Daddaoua, A., Fernández-Escamilla, A. & Ramos, J.-L. **Involvement of the Global Crp Regulator in Cyclic Amp-Dependent Utilization of Aromatic Amino Acids by *Pseudomonas putida*.** *Journal of Bacteriology* **194**, 406-412, doi: 10.1128/jb.06353-11 (2012).
- 328 Díaz-Salazar, C., Calero, P., Espinosa-Portero, R., Jiménez-Fernández, A., Wirebrand, L., Velasco-Domínguez, M. G., López-Sánchez, A., Shingler, V. & Govantes, F. **The Stringent Response Promotes Biofilm Dispersal in *Pseudomonas putida*.** *Scientific Reports* **7**, 18055, doi: 10.1038/s41598-017-18518-0 (2017).
- 329 Potrykus, K. & Cashel, M. **(P)Pppp: Still Magical?** *Annual Reviews in Microbiology* **62**, 35-51, doi: 10.1146/annurev.micro.62.081307.162903 (2008).
- 330 Laslett, D. & Canback, B. **Aragorn, a Program to Detect tRNA Genes and Tmrna Genes in Nucleotide Sequences.** *Nucleic Acids Research* **32**, 11-16, doi: 10.1093/nar/gkh152 (2004).
- 331 Andronescu, M., Condon, A., Hoos, H. H., Mathews, D. H. & Murphy, K. P. **Computational Approaches for RNA Energy Parameter Estimation.** *RNA Society* **16**, 2304-2318, doi: 10.1261/rna.1950510 (2010).
- 332 Lowe, T. M. & Chan, P. P. **tRNAscan-Se on-Line: Integrating Search and Context for Analysis of Transfer RNA Genes.** *Nucleic Acids Research* **44**, W54-57, doi: 10.1093/nar/gkw413 (2016).
- 333 Ikeuchi, Y., Kitahara, K. & Suzuki, T. **The RNA Acetyltransferase Driven by ATP Hydrolysis Synthesizes N4-Acetylcytidine of tRNA Anticodon.** *The EMBO Journal* **27**, 2194-2203, doi: 10.1038/emboj.2008.154 (2008).
- 334 Valgepea, K., Adamberg, K., Nahku, R., Lahtvee, P.-J., Arike, L. & Vilu, R. **Systems Biology Approach Reveals That Overflow Metabolism of Acetate in *Escherichia coli* Is Triggered by Carbon Catabolite Repression of Acetyl-Coa Synthetase.** *BMC systems biology* **4**, 166, doi: 10.1186/1752-0509-4-166 (2010).
- 335 Atkinson, D. E. **The Energy Charge of the Adenylate Pool as a Regulatory Parameter. Interaction with Feedback Modifiers.** *Biochemistry* **7**, 4030-4034, doi: 10.1021/bi00851a033 (1968).

- 336 Andersen, K. B. & von Meyenburg, K. **Charges of Nicotinamide Adenine Nucleotides and Adenylate Energy Charge as Regulatory Parameters of the Metabolism in *Escherichia coli*.** *Journal of Biological Chemistry* **252**, 4151-4156, doi: 10.1016/S0021-9258(17)40245-6 (1977).
- 337 Ebert, B. E., Kurth, F., Grund, M., Blank, L. M. & Schmid, A. **Response of *Pseudomonas putida* KT2440 to Increased NADH and ATP Demand.** *Applied Environmental Microbiology* **77**, 6597-6605, doi: 10.1128/AEM.05588-11 (2011).
- 338 An, R. & Moe, L. A. **Regulation of Pyrroloquinoline Quinone-Dependent Glucose Dehydrogenase Activity in the Model Rhizosphere-Dwelling Bacterium *Pseudomonas putida* KT2440.** *Applied Environmental Microbiology* **82**, 4955-4964, doi: 10.1128/AEM.00813-16 (2016).
- 339 Matsushita, K., Shinagawa, E., Adachi, O. & Ameyama, M. **Membrane-Bound D-Gluconate Dehydrogenase from *Pseudomonas aeruginosa*. Its Kinetic Properties and a Reconstitution of Gluconate Oxidase.** *Journal of Biochemistry* **86**, 249-256, doi: 10.1093/oxfordjournals.jbchem.a132508 (1979).
- 340 Nickel, P. I., Chavarria, M., Fuhrer, T., Sauer, U. & de Lorenzo, V. ***Pseudomonas putida* KT2440 Strain Metabolizes Glucose through a Cycle Formed by Enzymes of the Entner-Doudoroff, Embden-Meyerhof-Parnas, and Pentose Phosphate Pathways.** *Journal of Biological Chemistry* **290**, 25920-25932, doi: 10.1074/jbc.M115.687749 (2015).
- 341 Ostrowski, E. A., Rozen, D. E. & Lenski, R. E. **Pleiotropic Effects of Beneficial Mutations in *Escherichia coli*.** *Evolution* **59**, 2343-2352, doi: 10.1111/j.0014-3820.2005.tb00944.x (2005).
- 342 Calero, P., Volke, D. C., Lowe, P. T., Gotfredsen, C. H., O'Hagan, D. & Nickel, P. I. **A Fluoride-Responsive Genetic Circuit Enables in Vivo Biofluorination in Engineered *Pseudomonas putida*.** *Nature Communications* **11**, 5045, doi: 10.1038/s41467-020-18813-x (2020).
- 343 Zhu, X., Robinson, D. A., McEwan, A. R., O'Hagan, D. & Naismith, J. H. **Mechanism of Enzymatic Fluorination in *Streptomyces Cattleya*.** *Journal of the American Chemical Society* **129**, 14597-14604, doi: 10.1021/ja0731569 (2007).
- 344 Arias-Barrau, E., Olivera, E. R., Luengo, J. M., Fernández, C., Galán, B., García, J. L., Díaz, E. & Miñambres, B. **The Homogentisate Pathway: A Central Catabolic Pathway Involved in the Degradation of L-Phenylalanine, L-Tyrosine, and 3-Hydroxyphenylacetate in *Pseudomonas putida*.** *Journal of bacteriology* **186**, 5062-5077, doi: 10.1128/JB.186.15.5062-5077.2004 (2004).

- 345 Choi, K. H., Gaynor, J. B., White, K. G., Lopez, C., Bosio, C. M., Karkhoff-Schweizer, R. R. & Schweizer, H. P. **A Tn7-Based Broad-Range Bacterial Cloning and Expression System.** *Nature Methods* **2**, 443-448, doi: 10.1038/nmeth765 (2005).
- 346 Hartmans, S., Smits, J. P., van der Werf, M. J., Volkering, F. & de Bont, J. A. **Metabolism of Styrene Oxide and 2-Phenylethanol in the Styrene-Degrading Xanthobacter Strain 124x.** *Applied and environmental microbiology* **55**, 2850-2855, doi: 10.1128/AEM.55.11.2850-2855.1989 (1989).
- 347 Genee, H. J., Bonde, M. T., Bagger, F. O., Jespersen, J. B., Sommer, M. O. A., Wernersson, R. & Olsen, L. R. **Software-Supported USER Cloning Strategies for Site-Directed Mutagenesis and DNA Assembly.** *A C S Synthetic Biology* **4**, 342-349, doi: 10.1021/sb500194z (2015).
- 348 Elder, R. T. **Cloning Techniques Molecular Cloning: A Laboratory Manual T. Maniatis E. R. Pritsch J. Sambrook.** *Bioscience* **33**, 721-722, doi: 10.2307/1309366 (1983).
- 349 Choi, K. H., Kumar, A. & Schweizer, H. P. **A 10-Min Method for Preparation of Highly Electrocompetent *Pseudomonas aeruginosa* Cells: Application for DNA Fragment Transfer between Chromosomes and Plasmid Transformation.** *Journal of Microbiological Methods* **64**, 391-397, doi: 10.1016/j.mimet.2005.06.001 (2006).
- 350 Nogales, J., Gudmundsson, S., Duque, E., Ramos, J. L. & Palsson, B. O. **Expanding the Computable Reactome in *Pseudomonas putida* Reveals Metabolic Cycles Providing Robustness.** *bioRxiv*, 139121, doi: 10.1101/139121 (2017).
- 351 Orth, J. D., Thiele, I. & Palsson, B. **What Is Flux Balance Analysis?** *Nat Biotechnol* **28**, 245-248, doi: 10.1038/nbt.1614 (2010).
- 352 Ebrahim, A., Lerman, J. A., Palsson, B. O. & Hyduke, D. R. **Cobrapy: Constraints-Based Reconstruction and Analysis for Python.** *BMC Syst Biol* **7**, 74, doi: 10.1186/1752-0509-7-74 (2013).
- 353 del Castillo, T., Ramos, J. L., Rodríguez-Herva, J. J., Fuhrer, T., Sauer, U. & Duque, E. **Convergent Peripheral Pathways Catalyze Initial Glucose Catabolism in *Pseudomonas putida*: Genomic and Flux Analysis.** *Journal of Bacteriology* **189**, 5142-5152, doi: 10.1128/jb.00203-07 (2007).
- 354 He, F. **Bradford Protein Assay.** *Bio-protocol* **1**, e45, doi: 10.21769/BioProtoc.45 (2011).

- 355 van Duuren, J. B. J. H., Puchařka, J., Mars, A. E., Bůcker, R., Eggink, G., Wittmann, C. & dos Santos, V. A. P. M. **Reconciling in Vivo and in Silico Key Biological Parameters of *Pseudomonas putida* KT2440 During Growth on Glucose under Carbon-Limited Condition.** *BMC Biotechnology* **13**, 93, doi: 10.1186/1472-6750-13-93 (2013).
- 356 Lipmann, F. & Tuttle, L. C. **A Specific Micromethod for the Determination of Acyl Phosphates.** *Journal of Biological Chemistry* **159**, 21-28, doi: 10.1016/S0021-9258(19)51298-4 (1945).
- 357 Racker, E. **[29d] Fructose-6-Phosphate Phosphoketolase from *Acetobacter Xylinum*: F-6-P+Pi→Acetyl-P+E-4-P+H₂O.** in *Methods in Enzymology* Vol. 5 *Methods in Enzymology* 276-280 (Academic Press, 1962).
- 358 Swain, P. S., Stevenson, K., Leary, A., Montano-Gutierrez, L. F., Clark, I. B. N., Vogel, J. & Pilizota, T. **Inferring Time Derivatives Including Cell Growth Rates Using Gaussian Processes.** *Nature Communications* **7**, 13766, doi: 10.1038/ncomms13766 (2016).

Chapter 5: Combinatorial pathway balancing enables the production of the novel fluorinated building block 2-fluoromuconate in engineered *P. putida* KT2440

Summary

Muconic acid (MA) is a high value-added platform chemical that finds applications in the production of various products such as engineering polymers, carpets, textiles, and lubricants. The global market, valued at US\$ 90.1 in 2020, is expected to grow further owing to the increasing demand for MA-derived materials. Since its *cis,cis* isomer is a natural intermediate in microbial catabolic pathways for the degradation of aromatic hydrocarbons, great efforts are being deployed to establish biotechnological processes for MA production from sustainable resources. Despite the widespread use of products accessible through the platform chemical, the benefits of introducing halogen atoms into their molecular structure have not yet been explored. The incorporation of fluorine into polymers can significantly enhance properties like high resistance to solvents, acids, and bases. Previous reports suggested that the enzymatic machinery of some pseudomonads is capable of converting fluorinated arenes to fluoromuconic acid via the canonical β -keto adipate pathway. *P. putida* is a natural degrader of aromatic compounds and assimilates benzoic acid via this *ortho*-cleavage pathway. Therefore, we sought to investigate whether the biochemical functions encoded in the *ben* and *cat* gene clusters in *P. putida* are also capable of metabolizing fluorobenzoic acids. While the native enzymes were able to convert 3-fluorobenzoate (3-FBz) to 2-fluoro-*cis,cis*-muconic acid (2-FMA), the biochemical reactions were highly imbalanced, resulting in significant accumulation of the toxic intermediate 3-fluorocatechol and incomplete substrate conversion. A rigorous analysis of the expression systems orchestrating *ben* and *cat* expression revealed strikingly different responses to the fluorinated analogs of their natural inducers. To balance the catalytic activities for a complete bioconversion, a combinatorial approach was pursued to orthogonalize gene expression of key enzymatic steps. The final strains were able to convert 3-FBz to 2-FMA at the maximum theoretical yield. Upscaling of the established bioconversion process could establish 2-FMA as a novel platform chemical for the production of new fluorinated materials.

5.1. Introduction

5.1.1. Halogenated *cis,cis*-muconates – promising platform compounds for industrial applications

Cis,cis-muconate (*ccMA*) is a high value-added product with conjugated double bonds and two reactive dicarboxylic groups, which facilitate its use in a large variety of reactions as a building block or intermediate to produce commodity and specialty chemicals³⁵⁹⁻³⁶⁶. The unique configuration of functional groups makes *ccMA* particularly suitable for polymerization reactions that yield synthetic resins and biodegradable polymers^{359,362}. The list of compounds accessible through *ccMA* (summarized in **Figure 5.1**) includes many commercially important commodity chemicals such as adipic acid (listed among the top 50 bulk chemicals³⁶⁷), terephthalic acid, caprolactam, and trimellitic acid. These molecules have a wide variety of uses in the manufacture of nylon-6,6, polytrimethylene terephthalate, polyethylene terephthalate, dimethyl terephthalate, trimellitic anhydride, industrial plastics, resins, polyester polyols, food ingredients, pharmaceuticals, plasticizers, cosmetics, and engineering polymers³⁶³.

Over the past few decades, numerous efforts have been put into replacing the established oil-based processes for the production of *ccMA* and products thereof with biotechnological processes^{364,366-377}. The thereby employed approaches can be categorized into two strategies: (i) *de novo* production of aromatic precursor compounds from sugars or glycerol via the shikimate pathway, followed by conversion to catechol and ring-cleavage to yield *ccMA* or (ii) direct conversion of aromatic carbon feedstocks to *ccMA*. Strategy (i) was primarily employed in the so-called ‘classical’ model organisms like *Escherichia coli* (*E. coli*), *Saccharomyces cerevisiae* (*S. cerevisiae*), or *Corynebacterium glutamicum* (*C. glutamicum*). For strategy (ii), the inherent biochemical capabilities and stress resistance properties of natural degraders of aromatic hydrocarbons (e.g., *P. putida*, *Arthrobacter* sp.) were exploited³⁷⁸. Although *ccMA* production methods are widely available (both using traditional chemical synthesis and bio-based approaches), this molecule's structural scope remains somewhat restricted to post-production modifications. The potential of a biotechnological source of *ccMA* can be multiplied by introducing halogen atoms (X) into the product and its derivatives, giving

access to products that can hardly be synthesized chemically. Replacing a hydrogen atom with fluorine or chlorine in a pharmaceutical compound structure has become an essential structural manipulation in modern pharmaceuticals. Even a single halogen atom can significantly enhance the chemical properties of drugs and chemical building blocks³⁷⁹⁻³⁸².

For this reason, about half of the most successful drugs (blockbuster molecules) contain fluorine³⁸³. Amongst all drugs approved by the FDA within the last three decades, 18% contain fluorine³⁸⁴, and 15% have at least one chlorine atom in their structure^{385,386}. Furthermore, fluorine plays a vital role in the modern agrochemical industry, with 16% of all licensed products constituting fluorochemicals³⁸⁴. Since the targeted introduction of halogens (especially fluorine) into a complex organic structure is very difficult to achieve through chemical synthesis, there is a demand for emergent strategies towards the synthesis of halogenated building blocks³⁸⁷.

The effect of fluorination on *cc*MA-derived products is of particular interest for polymer applications. As a general trend, the introduction of fluorine into a polymer structure brings about different degrees of inertness to acids, bases, solvents, and oils, a low dielectric constant, low refractive indexes, high resistance to aging and oxidation, and low surface tension³⁸⁸. Bio-based solutions for the production of such halogenated building-blocks are urgently needed since the traditional approaches to fluorination involve highly-reactive, often unspecific reagents. On this background, this study aims at developing an efficient process to produce halogenated *cis,cis*-muconate via whole-cell bioconversion using engineered *P. putida* KT2440.

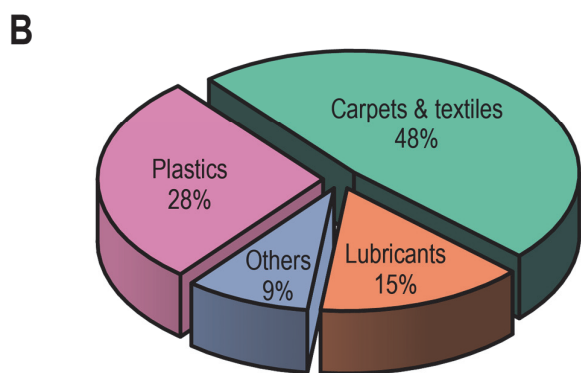
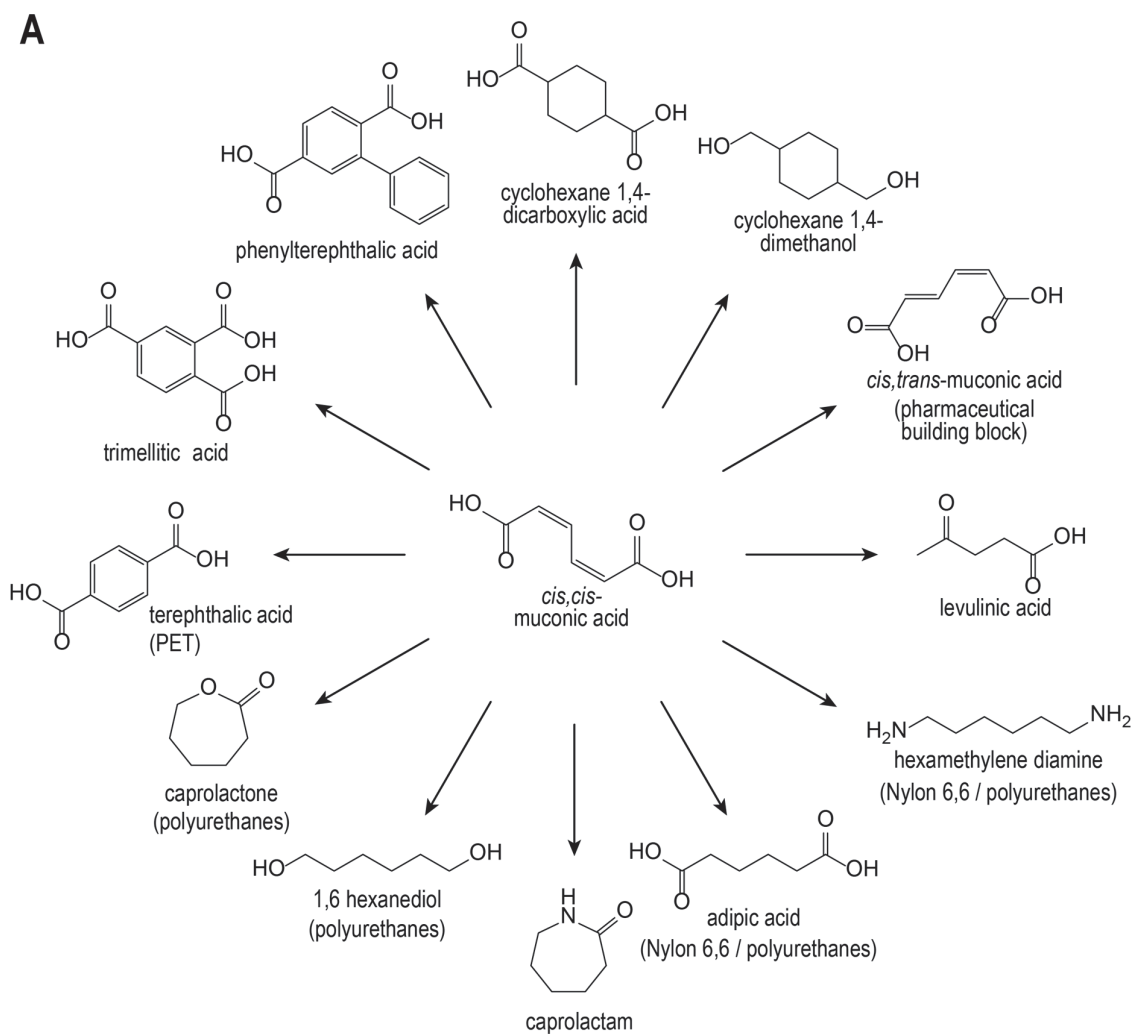


Figure 5.1: Chemical compounds derived from *cis,cis*-muconate (A), and the market share of ccMA-derived products (B).

[adapted from <https://www.greencarcongress.com/2011/11/amyris-20111101.html> and Khalil et al.³⁶¹]

5.1.2. The discovery of a chlorobenzoate-degrading bacterium paved the way for the valorization of halogenated aromatics

With a rapidly rising importance of halogen-substituted aromatic compounds as structural constituents in pesticides and pharmaceutical agents, microbiologists in the second half of the 19th century set out to study the microbial degradation of halogenated hydrocarbons and their ecological impact³⁸⁹⁻³⁹³. In the course of these endeavors, a number of bacterial species were identified that demonstrated biological activity on mono-fluorinated and -chlorinated derivatives of benzoate. Several species belonged to the bacterial *Pseudomonas* group. In particular, *Pseudomonas knackmussii* (formerly known as *Pseudomonas* strain B13) was amongst the earliest discovered and most extensively studied species^{391,394-396}. Isolated from a sewage plant by incubating the samples with 3-chlorobenzoate as the sole carbon source, the degradation of 2-, 3-, and 4-chlorobenzoate (2-, 3-, 4-CBz) as well as 2-, 3-, and 4-fluorobenzoate (2-, 3-, 4-FBz) was found to proceed in this bacterium through three initial steps of an enzymatic cascade (**Figure 5.2 B**). This route includes (i) a 1,2-dioxygenase that converts the benzoate (Bz) substrate into its 1,2-dihydro-1,2-dihydroxybenzoate (DHB) form, (ii) a 1,2-DHB dehydrogenase that releases a CO₂ moiety and restores the aromatic character of the six-carbon ring structure, yielding a catechol, and (iii) a second 1,2-dioxygenase that catalyzes the *ortho*-cleavage of the ring structure, resulting in (X-)ccMA.

The position of the halogen-substitution on the aromatic ring determines the biodegradability of the corresponding compound via this pathway [Schreiber et al.³⁹⁵ and **Figure 5.2 B**]. When acting on 4-X-benzoate, steps (i) and (ii) will yield 4-X-catechol and subsequently 3-X-*cis,cis*-muconate (3-XMA). This metabolite can be further degraded into TCA cycle metabolites with concomitant dehalogenation. The action of benzoate-1,2-dioxygenase (i) on 3-X-benzoate can result in either 3- or 4-X-catechol, further leading to 2-X-*cis,cis*-muconate (2-XMA) and 3-XMA, respectively. Dioxygenase attack on 2-X-benzoate with hydroxylation at the C1 and C2 positions of the aromatic ring can mediate the release of the halogen atom by either spontaneous elimination of fluoride or 1,2-DHB dehydrogenase activity, resulting in dechlorination³⁹⁷. If the hydroxylation is performed at the C1 and C6 positions (1,6-hydroxylation), it will

ultimately lead to the production of 3-X-catechol, and consequently, 2-XMA. 2-fluoro-*cis,cis*-muconate (2-FMA) was proposed to be a potent inhibitor of the enzyme catalyzing its further conversion, muconate cycloisomerase, thus acting as a dead-end metabolite. On the other hand, 2-chloro-*cis,cis*-muconate can be utilized by muconate cycloisomerase culminating in the release of chloride³⁹⁸.

Fluorobenzoate metabolization by *P. knackmussii* reportedly requires pre-incubation with 3-chlorobenzoate (3-CBz) due to the fluoro-analogs' inability to induce the expression of genes encoding the required catechol-1,2-dioxygenase³⁹⁵. Furthermore, two distinct catechol-1,2-dioxygenases were found in 3-CBz-grown *P. knackmussii* that displayed significantly different activities towards non-substituted catechol and halogenated catechols and that were differentially expressed in cells exposed to benzoate and 3-CBz³⁹⁹. The first enzymatic step (benzoate-1,2-dioxygenase), whose regioselectivity determines the eventual biochemical route and the consequently formed muconate derivative, has a strong bias for one of the two possible substrate orientations in its catalytic center, dependent on which halogenated substrate is used^{400,401}. The dearth of DNA technologies at the time of these studies precluded an in-depth characterization of mutants, and methods employed for the biochemical studies of *P. knackmussii* did not identify the genes encoding the characterized enzymes. The full genome of *P. knackmussii* was sequenced and published by Miyazaki et al.⁴⁰² only in 2015, which allows for a detailed functional genomic analysis of the enzymatic complement of this bacterium (further discussed in **Section 5.2.1**).

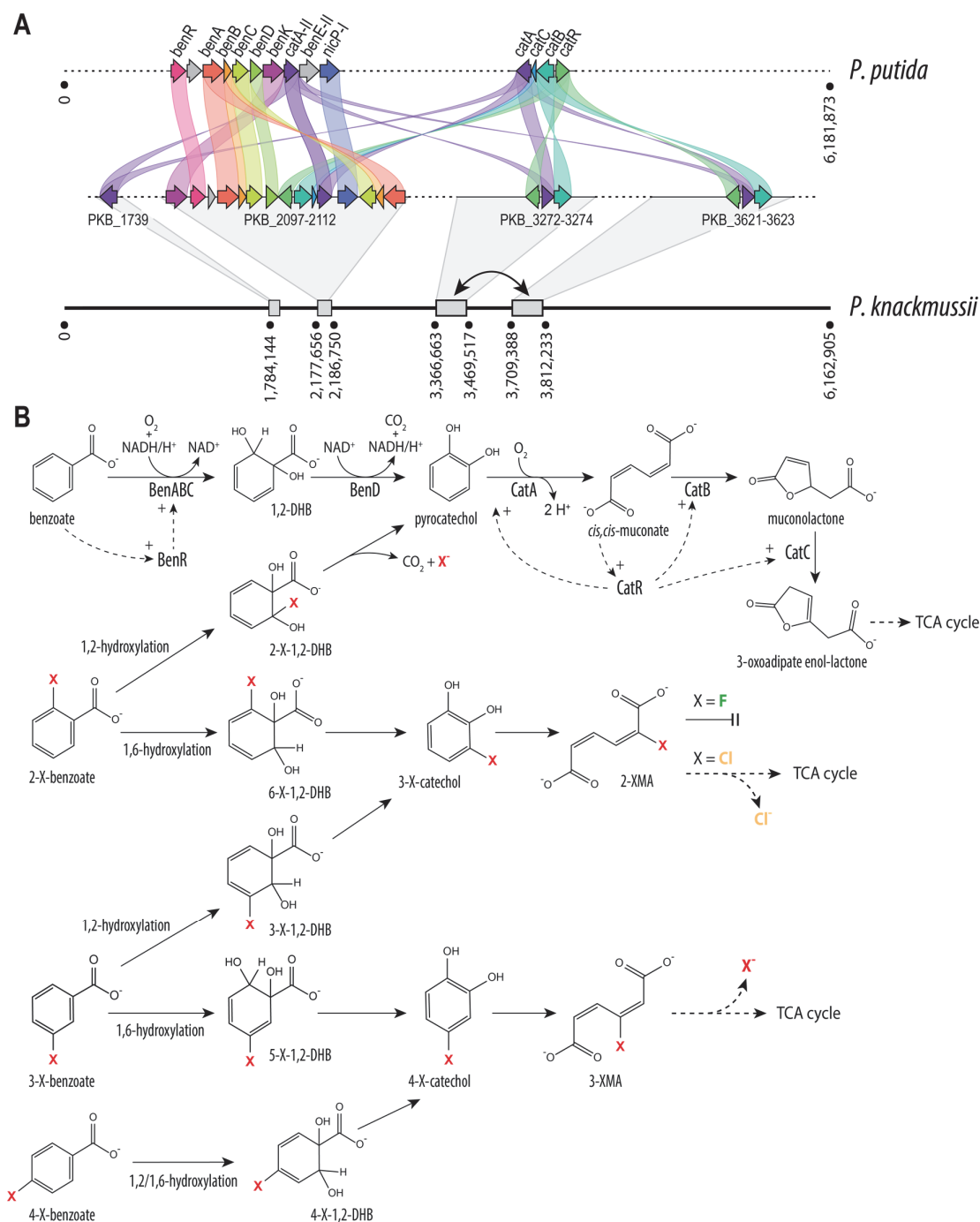


Figure 5.2. (Halo)benzoate degradation in *Pseudomonas*. (A) Chromosomal organization of genes involved in the *ortho*-cleavage pathway. (B) Scheme of the biochemical activities acting on benzoate, as well as its halogen (X)-substituted derivatives 2-XBz, 3XBz, and 4-XBz. Positive transcriptional regulation by BenR and CatR in *P. putida* is indicated by a '+' symbol. Abbreviations: *benABC*, benzoate 1,2-dioxygenase; *benD*, 1,2-DHB dehydrogenase; *catA*, catechol 1,2-dioxygenase; *catB*, muconate cycloisomerase; *catC*, muconolactone delta-isomerase; BenR, transcriptional regulator (XylS homolog); CatR, LysR family transcriptional regulator; 1,2-DHB, 1,2-dihydroxybenzoate; 2-X-1,2-DHB, 2-X-1,2-dihydroxybenzoate; 3-X-1,2-DHB, 3-X-1,2-dihydroxybenzoate; 4-X-1,2-DHB, 4-X-1,2-dihydroxybenzoate; 5-X-1,2-DHB, 5-X-1,2-dihydroxybenzoate; 6-X-1,2-DHB, 6-X-1,2-dihydroxybenzoate; 2-XMA, 2-X-*cis,cis*-muconate; 3-XMA, 3-X-*cis,cis*-muconate.

5.2. Results

5.2.1. Similarities and differences in the enzymatic repertoire of *P. putida* and *P. knackmussii* revealed by comparative genome analysis

The metabolic pathway leading from XBz to XMA in *P. knackmussii* conspicuously resembles the *ortho*-cleavage route characterized in *P. putida* for Bz assimilation. *P. putida* strain mt-2 and its TOL plasmid-free variant KT2440 have been extensively studied due to their native ability to degrade and consume recalcitrant xenobiotic compounds such as toluene and xylenes⁸⁷. Both strains (and engineered variants) are now used in several applications for the valorization of lignocellulosytic feedstocks, particularly for the production of *cc*MA^{97,98,377,403}. We thus wondered if *P. putida* KT2440 was able to perform the necessary reactions to convert XBz into XMA and performed analyses on the genomic sequence of both *P. putida* and *P. knackmussii* to identify the genes relevant for the bioconversion (**Figure 5.2 A**).

Enzymes involved in the *ortho*-cleavage pathway (also called β -keto adipate pathway) in *P. putida* are encoded in genes located in two distinct clusters at distant locations on the chromosome. One cluster, controlled by the Bz-binding activator protein BenR and its associated promoter P_{ben} , involves genes encoding benzoate-1,2-dioxygenase (*benA*, *benB*, and *benC*), 1,2-dihydro-1,2-dihydroxybenzoate (DHB) dehydrogenase (*benD*), several putative transporters predicted to assist in the uptake of benzoate derivatives (*benK*, *benE-II*, and *nicP-I*), as well as one of two catechol-1,2-dioxygenases (*catA-II*). A second catechol-1,2-dioxygenase (*catA*), sharing 77% amino acid sequence homology with *CatA-II*, is located within a second gene cluster, further containing genes encoding the two enzymes that process *cc*MA, muconate cycloisomerase (*catB*) and muconolactone δ -isomerase (*catC*). These genes are transcriptionally controlled by the activator *CatR* that responds to the intracellular concentrations of *cc*MA.

Homology comparisons of the *P. putida* amino acid sequences with *P. knackmussii*'s genome revealed the presence of four separated loci that harbor genes potentially relevant for the conversion of FBz. All genes identified in *P. knackmussii*, *P. putida* KT2440, and the TOL plasmid pWW0 of strain mt-2 are listed in **Table 5.1**. In *P. putida* KT2440,

the catalytic activities of the benzoate *ortho*-cleavage pathway are distributed between two clusters [(1.) *benA*, *benB*, *benC*, *benD*, and *catA-II*, and (2.) *catB*, *catC*, and *catA*]. Orthologs of these genes, all displaying $\geq 75\%$ homology to their *P. putida* equivalents, are located within a single locus (*PKB_2100* - *PKB_2107*) in the chromosome of *P. knackmussii*. As in *P. putida* (*catA* and *catA-II*), two highly homologous catechol-1,2-dioxygenase genes are present, one being part of the *ortho*-cleavage pathway cluster (*PKB_2107*) and the other (*PKB_1739*) in proximity to several putative genes involved in phenol degradation (*PKB_1742* - *PKB_1746*), the respective enzymes of which convert phenol into catechol. Additional orthologs to *catA* and *catB*, displaying significantly lower homologies to their *P. putida* counterparts (about 30%), are found in identical copies (*PKB_3273/PKB_3622* and *PKB_3274/PKB_3623*) as the result of an extensive genomic duplication that comprises a stretch of around 102,850 bp (**Figure 5.2**). This DNA segment, termed *clc*, residing in two locations with 99% sequence identity in *P. knackmussii*'s chromosome, was identified as a self-transferable element and was found to be the primary genetic determinant involved in the success of several *molecular breeding* applications that resulted in recipient strains capable of degrading specific chloroaromatics, hitherto thought to be non-biodegradable⁴⁰⁴⁻⁴⁰⁷. For example, the genetic transfer of a *clc* copy enabled growth on 3-chlorobenzoate in a *Pseudomonas aeruginosa* PAO1 transconjugant⁴⁰⁸. The identified roles for genes involved in the *ortho*-cleavage pathway, with sequences located within *clc* predominantly responsible for chlorobenzoate degradation, disagree with the initially assigned functions in the publication of *P. knackmussii*'s genome⁴⁰².

Table 5.1. Genes encoding enzymes involved in the biodegradation of fluorinated benzoates in *P. knackmussii* and their homologs in *P. putida* KT2440 (or in the catabolic pWW0 TOL plasmid of strain mt-2). Table rows are shaded to indicate the respective genes' location within separate clusters in the chromosome of *P. knackmussii*. Homology values are based on the amino acid sequences of proteins encoded by the listed genes.

<i>P. knackmussii</i> gene	<i>P. putida</i> KT2440 protein with highest homology % identical	pWW0 protein with highest homology % identical	Encoded function
PKB_1739	CatA-II (PP_3166) 78.3% CatA (PP_3713) 74.1%	none	catechol 1,2-dioxygenase
PKB_2098	BenR (PP_3159) 72.6%	XylS 58.7%	Transcriptional regulator (XylS homolog)
PKB_2100	BenA (PP_3161) 86.7%	XylX 71.7%	benzoate 1,2-dioxygenase subunit alpha
PKB_2101	BenB (PP_3162) 83.9%	XylY 77.2%	benzoate 1,2-dioxygenase subunit beta
PKB_2102	BenC (PP_3163) 84.8%	XylZ 85.2%	benzoate 1,2-dioxygenase electron transfer component
PKB_2103	BenD (PP_3164) 79.7%	XylL 77.0%	1,2-dihydroxybenzoate dehydrogenase
PKB_2104	CatR (PP_3716) 81.5%	none	HTH-type transcriptional regulator
PKB_2105	CatB (PP_3715) 85%	none	muconate cycloisomerase
PKB_2106	CatC (PP_3714) 92.7%	none	muconolactone delta-isomerase
PKB_2107	CatA-II (PP_3166) 80.5% CatA (PP_3713) 75.2%	none	catechol 1,2-dioxygenase
PKB_3272	YnfL (PP_5071) 32.6% CatR (PP_3716) 33.0%	none	LysR family transcriptional regulator
PKB_3273	CatA (PP_3713) 31.3% CatA-II (PP_3166) 29.1%	none	catechol 1,2-dioxygenase
PKB_3274	CatB (PP_3715) 42.0%	none	muconate cycloisomerase
PKB_3621 (identical to PKB_3272)	YnfL (PP_5071) 32.6% CatR (PP_3716) 33.0%	none	LysR family transcriptional regulator
PKB_3622 (identical to PKB_3273)	CatA (PP_3713) 31.3% CatA-II (PP_3166) 29.1%	none	catechol 1,2-dioxygenase
PKB_3623 (identical to PKB_3274)	CatB (PP_3715) 42.0%	none	muconate and cycloisomerase

5.2.2. An incompatibility of *P. putida* catechol 1,2-dioxygenases with chlorocatechols prevents the utilization of chlorobenzoates

P. knackmussii was initially isolated from sewage samples based on its ability to utilize 3-CBz as the sole source of carbon and energy, while 4-CBz reportedly did support its growth only after transformation with the TOL plasmid pWW0^{409,410}, which harbors a toluate dioxygenase with a high substrate promiscuity⁴¹¹. 3-CBz-grown cells did furthermore show no dioxygenation activity on 2-CBz and 4-CBz in whole-cell biocatalysis studies⁴¹².

We were interested in how this strain and *P. putida* KT2440 respond to cultivation with each of the chlorinated benzoates with glucose as co-substrate. To this end, both strains were cultured in synthetic de Bont minimal (DBM) medium supplemented with 30 mM glucose and 10 mM of either 2-, 3-, or 4-CBz (**Figure 5.3**). Throughout the cultivation (32 h), neither of the strains consumed any of the supplied 2- and 4-CBz. As expected, *P. knackmussii* was able to completely consume all 3-CBz within 11 to 23 h with an overall specific consumption rate of 1.59 mmol g_{CDW}⁻¹ h⁻¹. *P. putida*, on the other hand, did not show any activity on 3-CBz. No other products of the *ortho*-cleavage pathway could be detected at significant concentrations by means of liquid chromatography.

The only chlorinated substrate previously studied with *P. putida* KT2440 benzoate 1,2-dioxygenase (BenABC) was 3-CBz, with an in vitro activity of 47% relative to the activity with Bz²²². In *Pseudomonas putida* (*arvilla*) C-1, benzoate 1,2-dioxygenase was shown to have activities of 11%, 71%, and 1% on 2-CBz, 3-CBz, and 4-CBz compared to benzoate, respectively. These results suggest that at least for 3-CBz, the biochemical capabilities of *P. putida* are not the only reason for the lack of substrate consumption. Therefore, a set of reporter plasmids was constructed to explore the transcriptional activity of the different catabolic promoters that could play a role in the processing of XBz. Vector pSEVA627M was adopted as the backbone⁴¹³. Besides the low-copy-number origin of vegetative replication *oriV*(RK2) and a gentamicin resistance determinant, each plasmid harbored the *msfGFP* reporter gene under the control of the bicistronic translational coupling sequence *BCD10*⁴¹⁴. Transcriptional control was

exerted by the promoters P_m , P_{ben} , or P_{cat} , as well as their respective cognate activator protein XylS, BenR, or CatR.

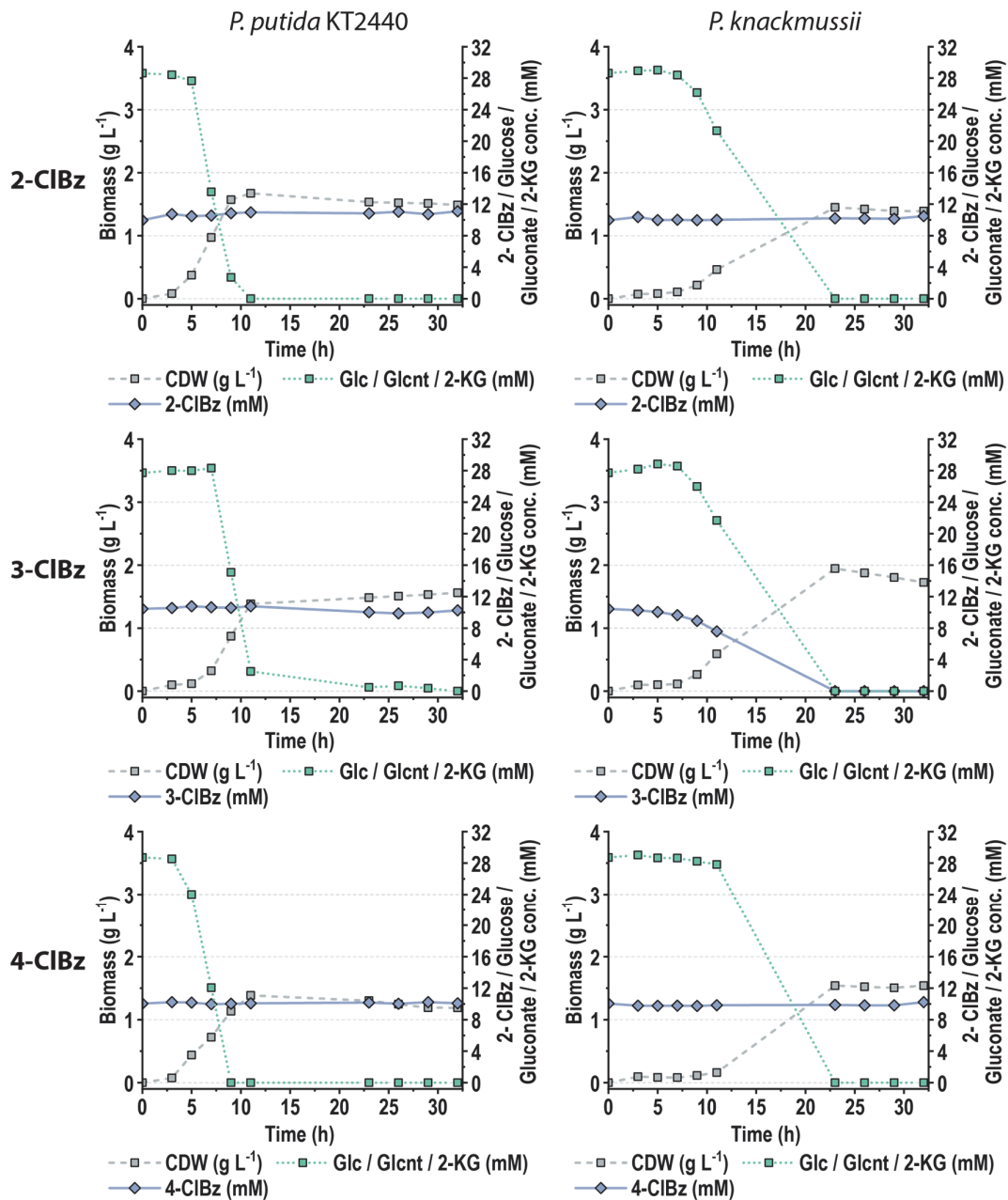


Figure 5.3. Utilization of chlorobenzoates by *P. putida* KT2440 and *P. knackmussii* with glucose as co-substrate. Cells were cultured in Erlenmeyer flasks filled with 10% (v/v) DBM medium supplemented with 30 mM glucose and 10 mM of 2-CIBz, 3-CIBz, or 4-CIBz. CDW, cell dry weight.

The reporter plasmids were delivered into *P. putida* KT2440, and the strains were cultured in microtiter plates with DBM medium containing 30 mM glucose as well as 10 mM of 2-, 3-, or 4-CBz to measure the kinetics of *msfGFP* fluorescence and growth. An additional *P. putida* strain, harboring a reporter plasmid with *msfGFP* under the transcriptional control of the constitutive P_{tac} promoter, was used as a standard for expression strength normalization. The observed expression rates, determined as the slopes of fluorescence-over-OD_{600 nm} plots, are displayed in **Figure 5.4**. In contrast to what had been previously reported for *XylS/P_m* in *E. coli*, the only chloro-substituted benzoate that induced this system was 3-CBz, with an expression strength comparable to that provided by 3-methylbenzoate (3-*mBz*, further discussed in **Section 5.2.5**). The BenR/*P_{ben}* system responded strongly to 2-CBz and 3-CBz, with a much higher expression strength than with benzoate (see **Section 5.2.5**). 4-CBz caused only a slight induction of *msfGFP* expression by BenR/*P_{ben}*. The CatR/*P_{cat}* system showed no induction by any of the CBz variants. Instead, the observed fluorescence was significantly lower than the one provided by the system without any inducer compounds.

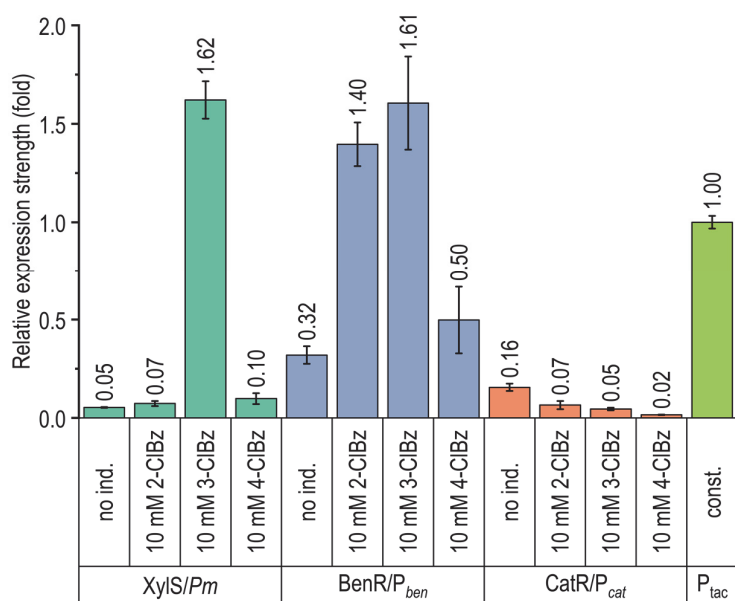


Figure 5.4. Inducibility of *ortho*-cleavage pathway expression systems by chloro-benzoates. The inducible promoter systems *XylS/P_m*, BenR/*P_{ben}*, and CatR/*P_{cat}* were cloned into pSEVA627M upstream of the *msfGFP* gene and delivered into *P. putida* KT2440. The strains were cultured in microtiter plates in minimal medium supplemented with 30 mM glucose as well as 10 mM of 2-, 3-, or 4-CIBz. The given expression strengths were normalized to the obtained rate of P_{tac} . Error bars represent the standard deviation from three biological replicates. no ind.: no addition of inducer compound; const.: constitutive promoter.

The growth of reporter plasmid-harboring *P. putida* under the screening conditions is shown in **Figure 5.5**. Only mild toxic effects could be observed for any of the chlorinated benzoates in strains harboring pS628(*BCD10*)→*msfGFP* or pS62P_{cat}(*BCD10*)→*msfGFP*. However, the strain transformed with pS62P_{ben}(*BCD10*)→*msfGFP* exhibited increased sensitivity to 2-CBz and especially 3-CBz, which suppressed growth almost entirely. The amplified expression of *ben* genes in response to increased concentrations of BenR appears to promote CBz toxicity by either an enhanced uptake or a faster conversion of CBz. Intriguingly, this strong toxic effect of 3-CBz cannot be seen in cells harboring natural concentrations of BenR. The catabolite repression control system may sufficiently suppress BenR/P_{ben} not to cause overexpression of the *ben* genes.

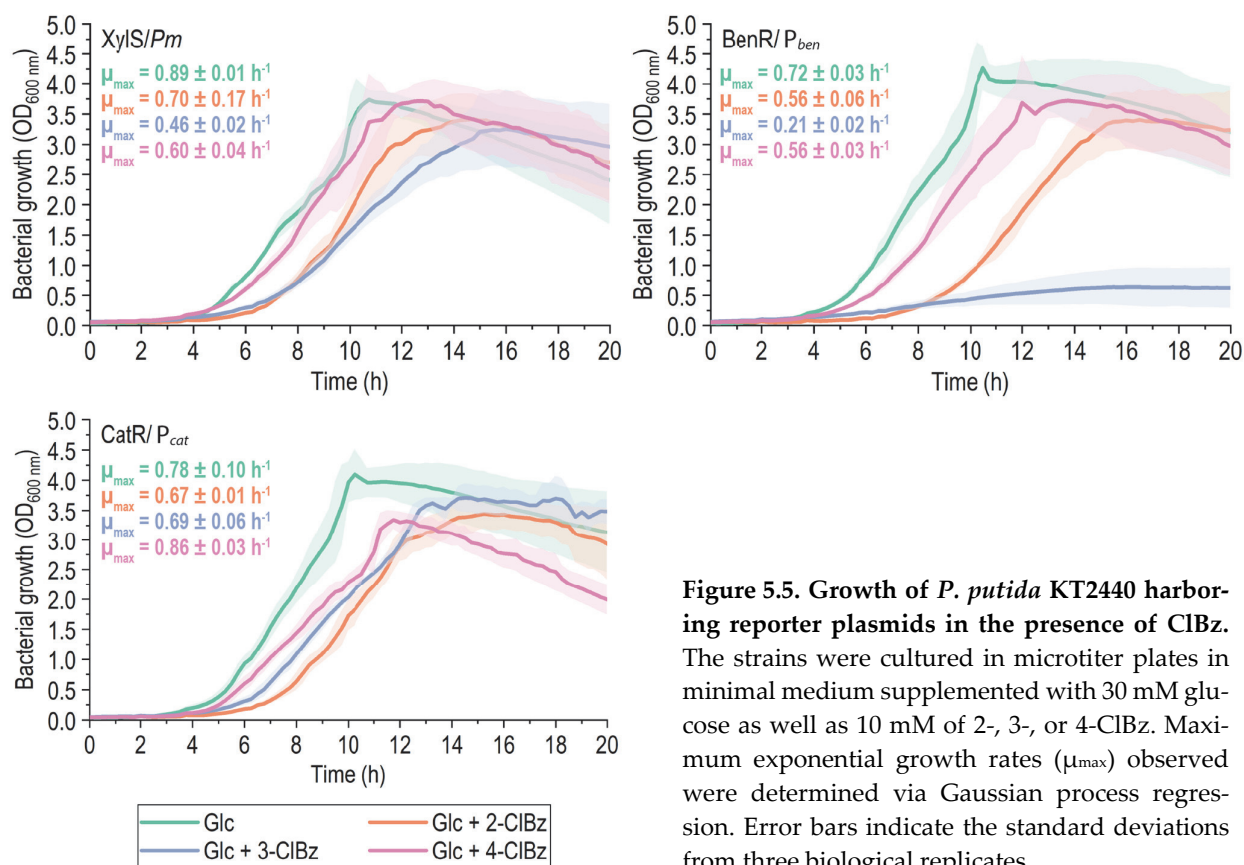


Figure 5.5. Growth of *P. putida* KT2440 harboring reporter plasmids in the presence of ClBz. The strains were cultured in microtiter plates in minimal medium supplemented with 30 mM glucose as well as 10 mM of 2-, 3-, or 4-ClBz. Maximum exponential growth rates (μ_{\max}) observed were determined via Gaussian process regression. Error bars indicate the standard deviations from three biological replicates.

The results obtained with the reporter plasmids indicate that monochlorinated benzoates can enter the *P. putida* cells and cause induction of the *ben* genes. The complete lack of expression by the CatR/ P_{cat} system in response to CBz suggests that either the substrates are not getting converted into chloromuconates efficiently or that the compounds cannot recruit CatR to bind to its cognate promoter. 2- and 3-chloro-muconate may exert an inhibiting effect on the binding of CatR to P_{cat} , as proposed by the decreased *msfGFP* expression in the presence of CBz. The fact that the CBz concentrations remained stable throughout the bioconversion experiment (**Figure 5.3**), as well as the increased toxic effects of CBz for cells with higher BenR concentrations, support the notion of a bottleneck within the *ortho*-cleavage pathway. This phenomenon, probably linked to the step of catechol 1,2-dioxygenation, would cause the accumulation of chlorinated catechols. Indeed, both CatA orthologs in *P. putida* were shown to have only very little activity on 4-chlorocatechol²²³. Due to the inability of *P. putida* to produce chlorinated *ccMA*, we focused our attention on the production of fluoro-*cis,cis*-muconate. A biotechnological source for the *fluorinated* platform chemical suggests itself as the more impactful endeavor given the eminent effects of fluorination for synthetic polymers and the difficulties associated with precise chemical fluorination.

5.2.3. *P. putida* KT2440 outcompetes *P. knackmussii* as a whole-cell biocatalyst for conversion of fluoro-substituted benzoates into fluoro-muconate

To examine the suitability of the two *Pseudomonas* species at stake for the bioconversion of 2- or 3-FBz to 2-FMA, both *P. knackmussii* and *P. putida* KT2440 were cultured in microtiter plates in DBM medium supplemented with 30 mM glucose (or 30 mM potassium benzoate) and varying concentrations of metabolites involved in the bioconversion process (**Figure 5.6**). During bioconversion studies with 4-FBz, we observed that 3-fluoro-*cis,cis*-muconate (3-FMA) is highly unstable under acidic pH (data not shown). This phenomenon is due to a cycloisomerization reaction that causes the fluorine atom to be released, as reported by Schmidt et al.⁴¹⁵. The instability of 3-FMA disqualified it as a target product and made 4-FBz an unsuitable substrate for the production of fluorinated *ccMA*.

The maximum exponential growth rates (μ_{\max}) observed in this experiment are listed in **Table 5.2**. Within the course of 50 h, no growth was detectable for *P. knackmussii* on benzoate as the sole source of carbon, while *P. putida* grew with a μ_{\max} of $0.73 \pm 0.20 \text{ h}^{-1}$. These results contradict those in previous publications on *P. knackmussii*, in which the species was shown to grow on benzoate⁴¹⁰. The bacterium might require an increased adaptation time to benzoate as the growth substrate. With glucose as the primary source of carbon and energy, *P. putida* grew 2.5 times faster than *P. knackmussii*. 2-FBz exerted only mild toxic effects on *P. putida*, which grew with 57% of the maximum rate on glucose and without any noticeable effect on the duration of the lag phase even in the presence of 20 mM 2-FBz. *P. knackmussii*, on the other hand, was unable to grow within the course of the experiment (50 h) at this highest concentration and showed significantly increased lag phases as well as reduced growth rates at 10 mM and 15 mM of 2-FBz. The detrimental impact of the second bioconversion substrate (3-FBz) on the growth of both species was more severe than 2-FBz. *P. putida* could grow with 3-FBz up to 10 mM but with a substantially reduced μ_{\max} . *P. knackmussii* was almost entirely inhibited at 5 mM 3-FBz no growth was noticeable at concentrations of $\geq 10 \text{ mM}$.

Depending on the fluoro-substitution's position on benzoate, the three 1,2-dihydroxybenzenes, catechol, 3-FC, and 4-FC, are produced as intermediary metabolites. No significant toxic effect was observed in the presence of up to 2 mM catechol on both *P. putida* and *P. knackmussii*. The physiological response to the two fluorinated catechol derivatives was more pronounced. While 3-FC had a more substantial effect on both strains' growth rate, the presence of 4-FC had a more noticeable impact on the duration of lag phases. However, in both cases, *P. putida* demonstrated higher resistance to the toxic effects of both 3-FC and 4-FC than *P. knackmussii*. Neither of the two strains could grow with 2-FBz or 3-FBz as the sole source of carbon (**Table 5.2**).

Table 5.2. Growth rates of selected strains used in this chapter. The experiment was performed in 96-well microtiter plates with each well containing 200 μ l DBM medium with 5 g L⁻¹ MOPS and varying concentrations of carbon sources and metabolites involved in the bioconversion process. Maximum growth rates were determined by Gaussian process regression. Each experiment was performed with three biological replicates. Growth rates are given as average values \pm standard deviation.

Strain / media additives	Maximum growth rate μ_{\max} (h ⁻¹)			
	<i>P. putida</i> KT2440	<i>P. knack-</i> <i>mussii</i>	PMP1021 pSEVA228	PMP1043
30 mM glucose	0.98 \pm 0.20	0.40 \pm 0.08	0.76 \pm 0.16	0.91 \pm 0.12
30 mM Bz (+ 0.5 mM 3- <i>m</i> Bz)	0.73 \pm 0.14	no growth	0.16 \pm 0.09	0.39 \pm 0.03
30 mM 2-FBz	no growth	n.d.	n.d.	no growth
30 mM 3-FBz	no growth	n.d.	n.d.	no growth
30 mM 4-FBz	no growth	n.d.	n.d.	no growth
30 mM glucose, 1 mM catechol	0.83 \pm 0.17	0.36 \pm 0.06	0.83 \pm 0.13	n.d.
30 mM glucose, 2 mM catechol	0.78 \pm 0.14	0.32 \pm 0.01	0.89 \pm 0.11	n.d.
30 mM glucose, 1 mM 3-FC	0.63 \pm 0.10	0.22 \pm 0.05	0.49 \pm 0.03	n.d.
30 mM glucose, 2 mM 3-FC	0.37 \pm 0.01	0.12 \pm 0.02	0.22 \pm 0.02	no growth
30 mM glucose, 5 mM 3-FC	no growth	no growth	no growth	no growth
30 mM glucose, 1 mM 4-FC	0.60 \pm 0.11	0.24 \pm 0.03	0.63 \pm 0.19	n.d.
30 mM glucose, 2 mM 4-FC	0.76 \pm 0.08	0.30 \pm 0.01	0.50 \pm 0.05	0.76 \pm 0.13
30 mM glucose, 5 mM 4-FC	no growth	no growth	no growth	no growth
30 mM glucose, 10 mM 2-FBz	0.65 \pm 0.13	0.26 \pm 0.02	n.d.	n.d.
30 mM glucose, 15 mM 2-FBz	0.61 \pm 0.12	0.22 \pm 0.03	n.d.	n.d.
30 mM glucose, 20 mM 2-FBz	0.56 \pm 0.14	no growth	n.d.	n.d.
30 mM glucose, 5 mM 3-FBz	0.39 \pm 0.19	0.05 \pm 0.01	0.39 \pm 0.06	n.d.
30 mM glucose, 10 mM 3-FBz	0.14 \pm 0.08	no growth	0.38 \pm 0.08	0.45 \pm 0.02
30 mM glucose, 15 mM 3-FBz	no growth	no growth	0.36 \pm 0.07	0.45 \pm 0.03
30 mM glucose, 20 mM 3-FBz	no growth	no growth	0.35 \pm 0.08	0.46 \pm 0.02
30 mM glucose, 30 mM 3-FBz	no growth	no growth	n.d.	0.24 \pm 0.04
30 mM glucose, 40 mM 3-FBz	no growth	no growth	n.d.	0.23 \pm 0.05
30 mM glucose, 50 mM 3-FBz	no growth	no growth	n.d.	0.20 \pm 0.04
30 mM glucose, 10 mM 2-FMA	1.04 \pm 0.09	n.d.	n.d.	0.98 \pm 0.15
30 mM glucose, 15 mM 2-FMA	0.66 \pm 0.04	n.d.	n.d.	0.51 \pm 0.05
30 mM glucose, 20 mM 2-FMA	0.24 \pm 0.05	n.d.	n.d.	0.22 \pm 0.02
30 mM glucose, 20 mM 2-FMA	no growth	n.d.	n.d.	no growth

n.d., not determined

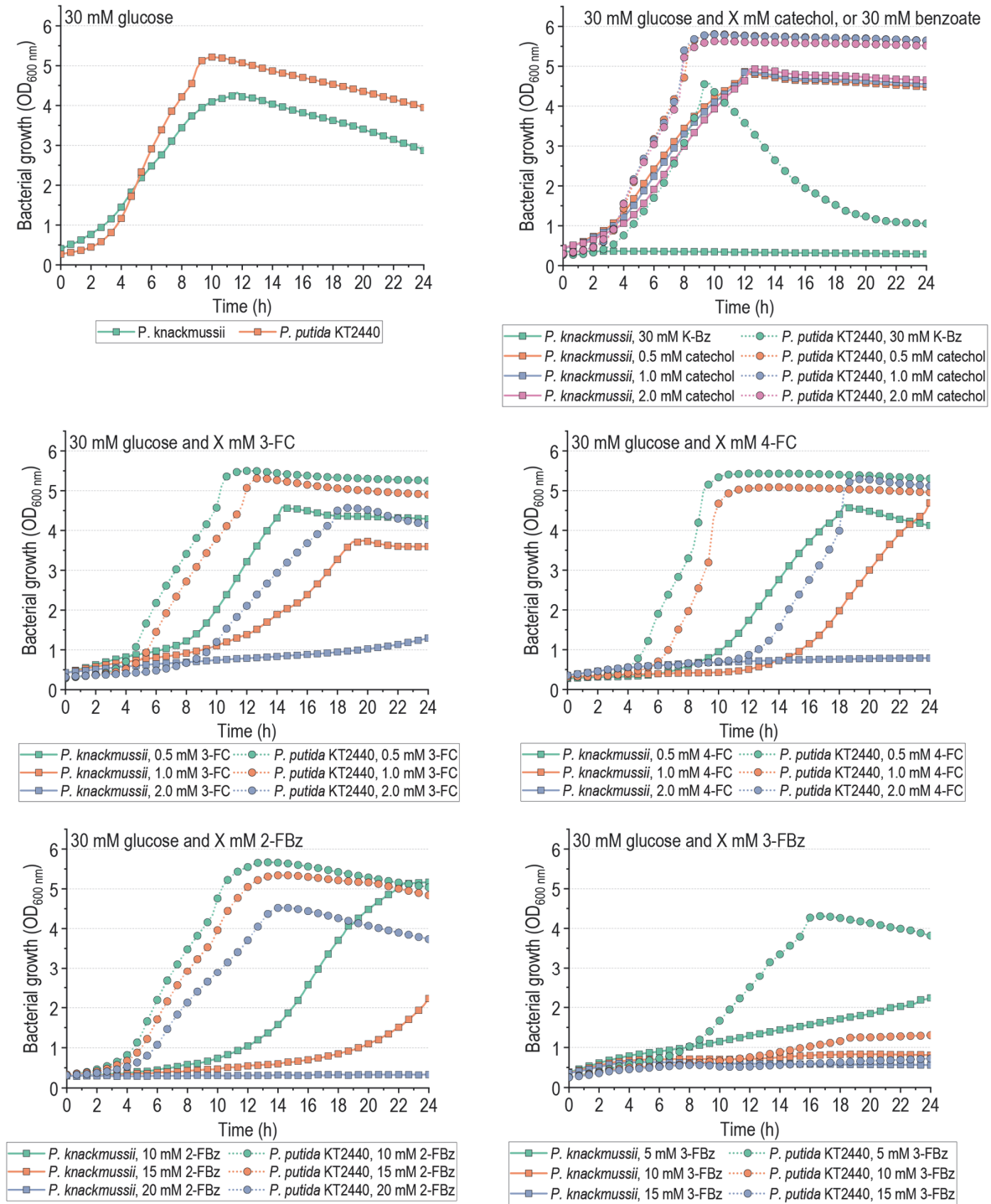


Figure 5.6. Physiological response to fluorinated and nonfluorinated *ortho*-cleavage pathway metabolites. *P. knackmussii* and *P. putida* KT2440 were cultured in microtiter plates with 200 μ l DBM medium supplemented with 30 mM glucose or potassium benzoate (K-Bz) as the source of carbon and energy, as well as varying concentrations of metabolites involved in the bioconversion process.

After establishing the physiological response of *P. knackmussii* and *P. putida* to the metabolites involved in the bioconversion of FBz to 2-FMA, the two species were subjected to a fermentation experiment in shaken flasks containing DBM medium supplemented with 30 mM glucose as well as 10 mM of 2-FBz or 3-FBz. The growth was monitored via OD_{600 nm} measurements. To calculate biomass-specific conversion rates, the absorbance values were converted to cell dry weight concentrations (g_{CDW} L⁻¹).

Culture supernatants obtained during the fermentation were analyzed via ¹⁹F Nuclear Magnetic Resonance (NMR) Spectroscopy (**Figure 5.7**). Based on the chemical shifts reported in previous work⁴¹⁶, The signals at -107.5, -113.0, -113.9, -118.9, and -136.2 ppm were identified as 2-FMA, 3-F-DHB, 3-FBz, 5-F-DHB, and 3-FC, respectively. The identities of these compounds were further confirmed by utilizing ¹H, ¹H-¹³C heteronuclear single quantum coherence spectroscopy (HSQC; 1-bond ¹H-¹³C correlations) and ¹H-¹³C heteronuclear multiple bond correlation (HMBC, 2-4 bonds ¹H-¹³C correlations) NMR experiments (spectra not shown). The observed multiplet splittings due to ¹⁹F-¹H couplings for the ¹⁹F signals were used to identify which ¹H signals originated from the same molecule as the corresponding ¹⁹F signal. The ¹H NMR signals were then further matched with ¹³C NMR signals using the HSQC and HMBC NMR experiments. From these observations, it was possible to identify the compounds reliably. Free fluoride (F⁻) is observed at around -120 ppm. However, the exact chemical shift depends on the sample properties (pH, temperature, concentration). As expected, the F⁻ signal does not show any multiplet splitting.

The concentrations of 3-FBz, catechol, 3-FC, 4-FC, and ccMA were quantified in the samples via high-performance liquid chromatography (HPLC) with commercial standards. Using HPLC-quantified 3-FBz, 3-FC, and 4-FC as internal standards, the remaining fluorinated metabolites could be quantified based on their ¹⁹F NMR signals. The results obtained for the NMR experiments furthermore allowed the identification of all fluorometabolites in the HPLC spectra (**Figure 5.8 C**).

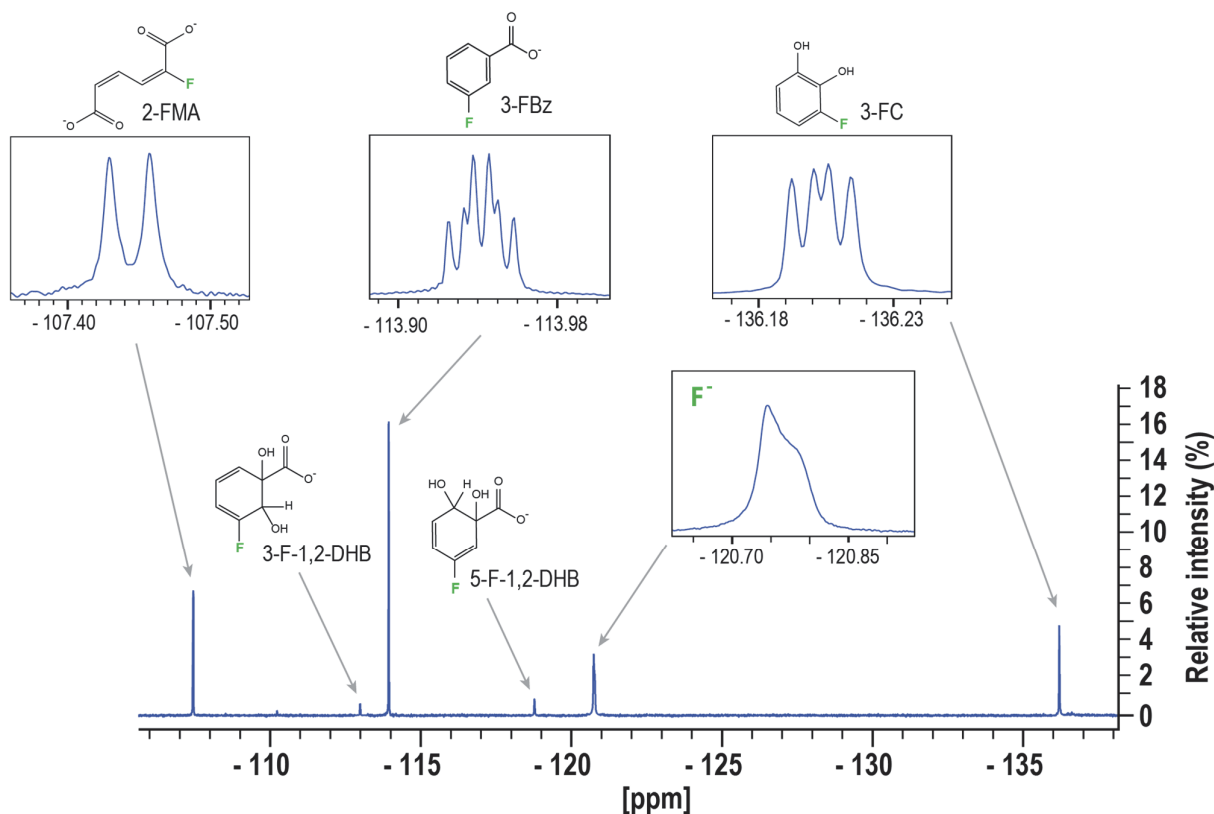


Figure 5.7. Coupled ^{19}F NMR spectrum of the culture supernatant of *P. putida* KT2440 during the conversion of 3-FBz. The shown data represents the sample taken after 20 h of cultivation. 2-FMA, 2-fluoro-*cis,cis*-muconate; 3-F-1,2-DHB, 3-fluoro-1,2-dihydroxybenzoate; 3-FBz, 3-fluorobenzoate, 5-F-1,2-DHB, 5-fluoro-1,2-dihydroxybenzoate; 3-FC, 3-fluorocatechol; F^- , free fluoride.

P. putida completely consumed 2-FBz within 20 h with a substrate uptake rate (q_s) of $1.07 \text{ mmol g}_{\text{CDW}}^{-1} \text{ h}^{-1}$ (Figure 5.8). 2-FMA was the only compound detectable after substrate depletion, at a concentration of 1.34 mM and produced at a product formation rate q_p of $0.12 \text{ mmol g}_{\text{CDW}}^{-1} \text{ h}^{-1}$. Neither 3-FC nor 4-FC were detected at any point in time. After an initial consumption of 2-FBz with a q_s of $0.81 \text{ mmol g}_{\text{CDW}}^{-1} \text{ h}^{-1}$ for about 20 h, *P. knackmussii* stopped converting any further substrate (final concentration: 3.2 mM). Out of the 6 mM substrate consumed, about 1 mM 2-FMA was produced at a product formation rate q_p of $0.06 \text{ mmol g}_{\text{CDW}}^{-1} \text{ h}^{-1}$. Furthermore, *ccMA* could be detected in the culture supernatant at a maximum concentration of 1.55 mM after 30 h, which continued to be consumed slowly (but not completely) until the end of the fermentation (50 h). For both species, the amount of 2-FMA produced represented 14% of the 3-FBz consumed (product yield coefficient $Y_{\text{SP}} = 0.14 \text{ mol mol}^{-1}$).

With 3-FBz, *P. putida* consumed the substrate until a time between 7 and 20 h with a q_s of $0.98 \text{ mmol g}_{\text{CDW}}^{-1} \text{ h}^{-1}$, after which the 3-FBz concentration remained constant. Within the first 7 h, all 3-FBz consumed was converted into 3-FC until it reached a concentration of 1 mM. In the course of the next 13 h, 40% of 3-FC in the supernatant was converted into 2-FMA, combined with a fraction of additionally consumed 3-FBz at a combined product formation rate q_p of $0.06 \text{ mmol g}_{\text{CDW}}^{-1} \text{ h}^{-1}$. At the end of the fermentation, 3.48 mM 3-FBz had been converted into 1.38 mM 2-FMA, corresponding to a product yield Y_{SP} of $0.41 \text{ mol mol}^{-1}$, as well as 0.52 mM 3-FC. The combined metabolite concentrations (2-FMA and 3-FC) summed up to 1.90 mM, representing 55% of the consumed 3-FBz. Considering the previously established toxicity of 3-FC, its accumulation was identified as a significant bottleneck for an efficient and prolonged bioconversion process in *P. putida*.

Also, with *P. knackmussii*, 3-FBz consumption occurred only within the first 7-20 h of the fermentation, with a q_s of $1.01 \text{ mmol g}_{\text{CDW}}^{-1} \text{ h}^{-1}$. After an initial increase of 3-FC up to 0.94 mM in the culture supernatant, the catechol derivative was completely re-consumed until 20 h. From a total concentration of 2.93 mM consumed 3-FBz, *P. knackmussii* produced 1.64 mM 2-FMA [corresponding to 56% of the substrate (Y_{SP} : $0.56 \text{ mol mol}^{-1}$)] with a rate q_p of $0.09 \text{ mM g}_{\text{CDW}}^{-1} \text{ h}^{-1}$. In none of the conditions tested, significant amounts of 4-FC could be detected in the culture supernatants. Thus, the enzymes performing the di-oxygenation on fluorinated catechol derivatives that both species are equipped with seem to have a higher efficiency on 4-FC than 3-FC. This explains the reduced growth-inhibiting effect of 4-FC after a prolonged lag phase, as described before.

The asymmetrical use of the non-productive 1,2-dioxygenation route with 2-FBz causes fluorine to be lost by about 85%, in contrast to 50% with 3-FBz. The 3-F-substituted benzoate consequently represents the most suitable precursor compound to produce 2-FMA. A faster growth rate, higher biomass yield on glucose, and higher resistance to toxic effects of pathway intermediates make *P. putida* stand out as the bacterial platform better suited as a whole-cell biocatalyst for the bioconversion of fluoro-benzoate into 2-FMA.

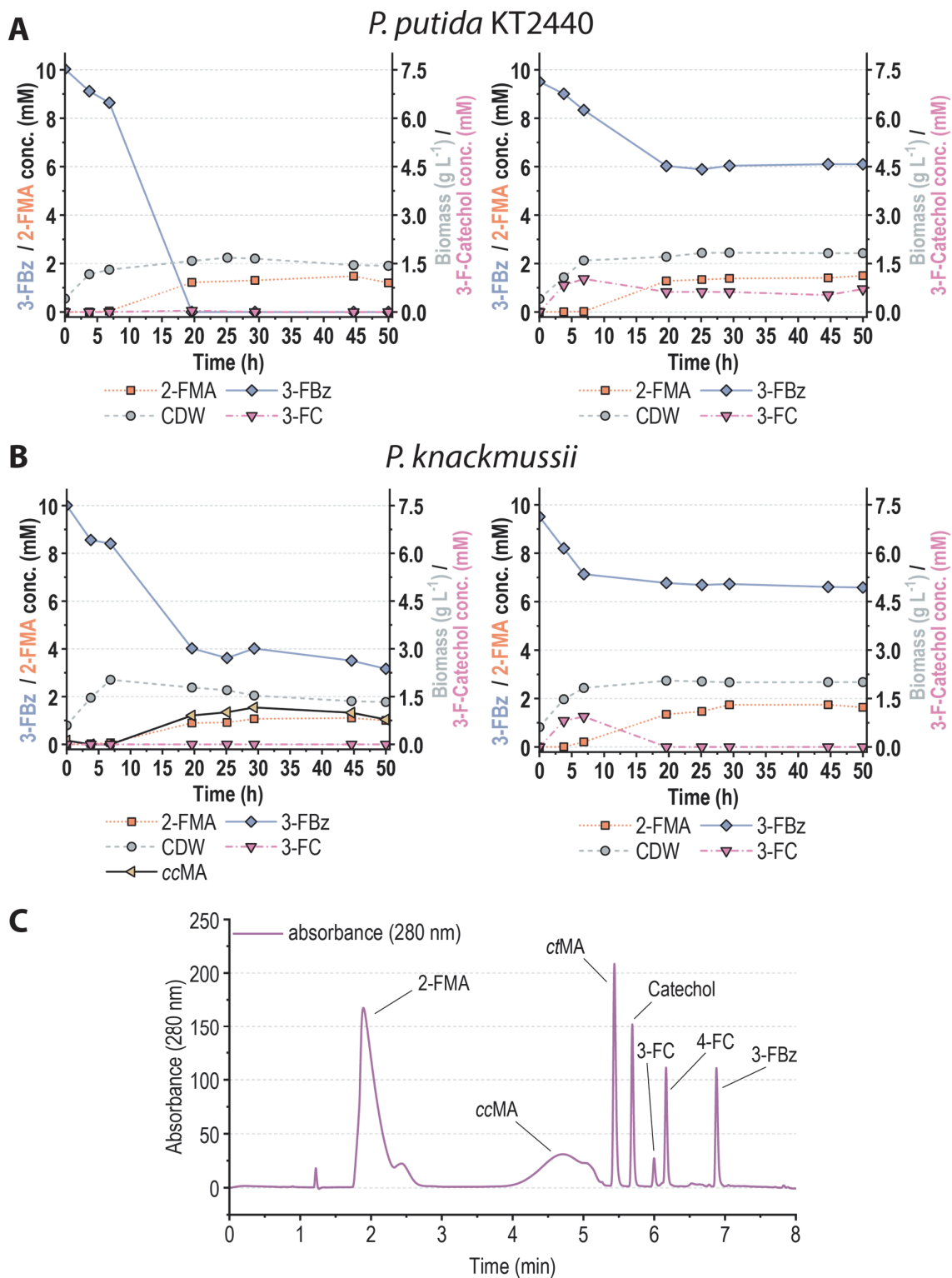


Figure 5.8. Utilization of fluorobenzoates by *P. putida* KT2440 and *P. knackmussii*. Cells were cultured in Erlenmeyer flasks filled with 10% (v/v) DBM medium supplemented with 30 mM glucose and 10 mM of the respective fluoro-benzoate. **(A-B)** Time course of extracellular metabolite concentrations (mM) and biomass ($\text{g}_{\text{CDW}} \text{L}^{-1}$). **(C)** HPLC chromatogram of a calibration standard containing 1 mM of each compound with UV absorption measured at 280 nm.

5.2.4. Engineering strategies to increase 3-fluorobenzoate bioconversion performance in *P. putida* KT2440

Analysis of the metabolites in the supernatant during fermentation experiments with *P. putida* and 3-FBz revealed a bottleneck in the last biochemical step of the upper *ortho*-cleavage pathway (i.e., the conversion of 3-FC into 2-FMA). Following an approach commonly employed in microbial strain engineering, a first set of genome manipulations was performed in *P. putida* KT2440. The aim of this procedure was to increase the enzyme availability of different steps of the bioconversion pathway by implementing constitutive promoters. Thereby, special attention was given to the two catechol 1,2-dioxygenases.

All strains constructed are listed in **Table 5.4**; the nomenclature employed for the engineered strains is illustrated in **Figure 5.9**. The modifications comprised the replacement of the native P_{ben} promoter upstream of *benA* with the constitutive P_{tac} promoter, the insertion of P_{tac} upstream of 28 bp 5' UTR of *benD*, and the insertion of the P_{EM7} promoter sequence upstream of 29 bp 5' UTR of *catA*. Approaches to insert a regulatory element comprising P_{tac} and a translational coupling sequence (bi-cistronic designs – *BCD2* or *BCD10*⁴¹⁴) upstream of *catA* or *catA-II* failed due to the consistent emergence of mutations within the -35 region of P_{tac} in the cloning host *E. coli* harboring the respective genome editing plasmid. This suggested a toxic effect of strong and constitutive catechol 1,2-dioxygenase gene overexpression.

As an alternative strategy to increase catechol 1,2-dioxygenase activity, the three *catA* homologs from *P. knackmussii* were cloned into vector pSEVA634, controlled by the IPTG-inducible Laclq/P_{trc} system, and inserted into *P. putida* KT2440. Following a similar strategy as employed by Kohlstedt et al.³⁷³ for *ccMA*, further *P. putida* KT2440 strains were constructed with in-frame deletions of the two genes *catB* and *catC* to avoid (3-F-)*cis,cis*-muconate degradation. In additional strain variants, the *catBC* gene sequences were replaced by additional copies of *catA* or *catA-II*, putting them under the control of the native CatR/P_{cat} regulatory system (with predicted translation rates of 1934 for *catA* and 503 for *catA-II*).

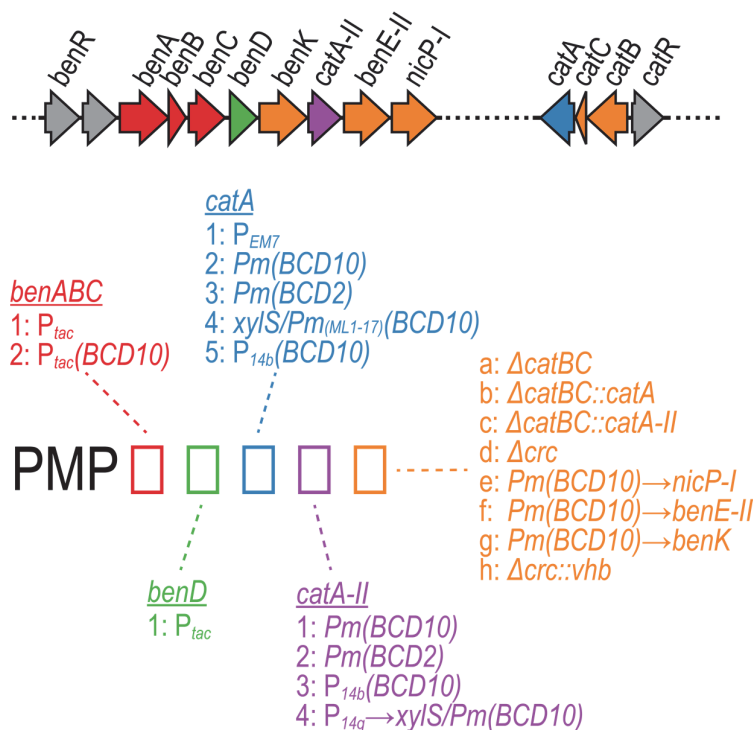


Figure 5.9. Schematic representation of the nomenclature employed in this study for engineered 2-F-muconate-producing *Pseudomonas putida* (PMP) strains.

All first-generation strains (Table 5.4) were subjected to a bioconversion experiment in Erlenmeyer flasks filled to 10% with DBM medium supplemented with 30 mM glucose and 10 mM 3-FBz, and with an initial biomass concentration of 0.175 g L⁻¹. Within 24 h, all cultures reached a terminal state in which no further 3-FBz was consumed, and all extracellular metabolites measured remained at constant concentrations in the culture supernatants (Figure 5.10). A comparison of these final states of the fermentations allowed conclusions to be drawn about the balance of biochemical activities involved in converting 3-FBz into 2-FMA. The pathway in wild-type *P. putida* is not optimized to process halogenated benzoate derivatives, which became apparent in the accumulation of fluorinated catechol intermediates. This accumulation is slightly decreased by replacing the P_{ben} promoter with the P_{tac} promoter. The insertion of P_{tac} upstream of *benD* increased 3-FBz consumption significantly and led to a 3-FC formation to an about five-fold higher concentration than with wild-type *P. putida*. The promoter integration could have also caused elevated expression levels for genes downstream of *benD*. The high flux towards 3-FC indicates a significant, rate-limiting role of either BenD or the benzoate H⁺ symporter BenK. However, such an increased flux within the

pathway's upper reactions without increased catechol *detoxification* was detrimental to cell viability and bioconversion efficiency.

This apparent bottleneck was addressed via the overexpression of *catA*, which was shown to be the ortholog predominantly involved in benzoate metabolism²²³, by the P_{EM7} promoter (strain PMP0010). However, besides increasing 3-FBz consumption, the constitutive overexpression of *catA* had detrimental effects on catechol 1,2-dioxygenase activity, resulting in a near-complete accumulation of all 3-FBz having entered the 1,2-dioxygenation pathway in 3-FC. The deletion of *catBC* also caused a higher accumulation of 3-FC in all respective strains (PMP0000a and PMP0100a). Additional expression of *benABC* or *benD* by P_{tac} brought about comparable effects in a $\Delta catBC$ background as with *catBC* intact (PMP1000a and PMP0100a vs. PMP1000 and PMP0100).

Also, the implementation of additional copies of *catA* or *catA-II* under P_{cat} control in place of *catBC* did not show any positive effect on the conversion of 3-FC into 2-FMA (strains PMP0000b, PMP0000c, PMP0100b, and PMP0100c). In addition to > 2 mM 3-FC and < 0.9 mM 2-FMA, each of the seven $\Delta catBC$ strains accumulated a new, unquantified by-product eluting at 4.0 min with an absorption maximum at 277.5 nm and with a molecular weight of 299.06 g mol⁻¹ (as determined by LC-MS). The molecular weight and fragmentation pattern were compatible with either of the two C₁₂H₁₃NO₈ compounds 3-[bis(carboxymethyl)amino]methyl-2,4-dihydroxybenzoic acid or 3-[bis(carboxymethyl)amino]methyl-4,5-dihydroxybenzoic acid (data not shown). Potential biochemical routes leading to these two compounds' production could not be identified, and a post-hoc chemical modification (e.g., reaction with medium components) cannot be ruled out. The most significant detriment to the bioconversion performance was caused by the three *P. knackmussii* *catA* orthologs' expression from a medium-copy-number plasmid. While 3-FBz uptake was greatly enhanced, with nearly all substrate being consumed within 24 h, almost 50% of the initial 3-FBz was converted to 3-FC, with final concentrations of about 5 mM.

Only $P_{tac} \rightarrow benABC$ had a balancing effect on the pathway's enzyme activities of the manipulations tested. Efforts to increase the enzyme abundance of catechol 1,2-dioxygenase appeared to reduce the rate at which its reaction was performed while at the same time enhancing 3-FBz consumption.

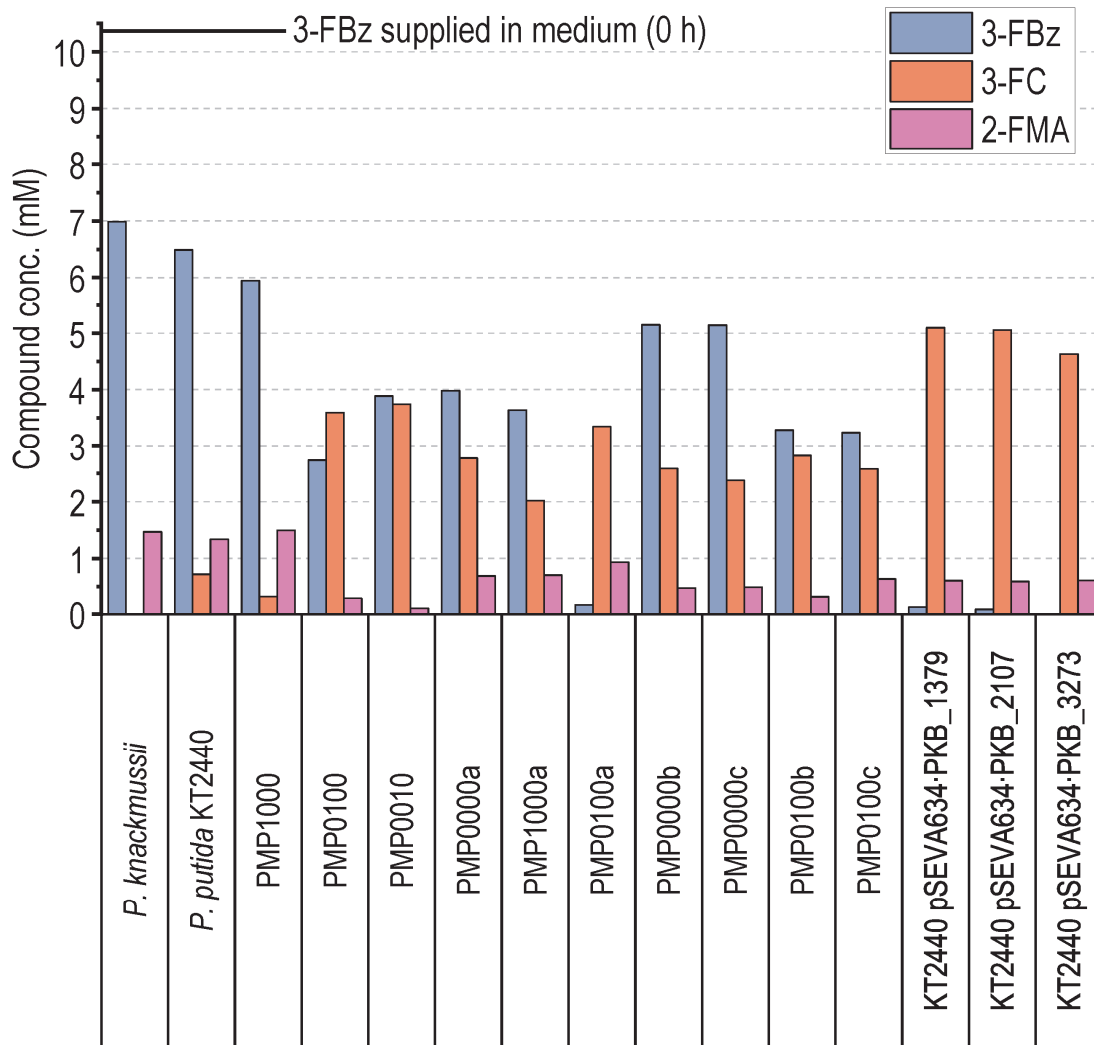


Figure 5.10. Bioconversion performance of first-generation strains in shaken flask fermentations. The strains were cultured in Erlenmeyer flasks filled with 10% (v/v) DBM medium supplemented with 30 mM glucose and 10 mM 3-FBz. Shown are the extracellular metabolite concentrations measured after 24 h of cultivation.

5.2.5. Characterization of expression devices to balance bioconversion of 3-fluorobenzoate to 2-fluoro-*cis,cis*-muconate

To get a better understanding of the effects caused by the defined genomic manipulations within *first-generation* strains, all regulatory sequences involved in the strain engineering process were subjected to a quantitative analysis. To this end, the previously deployed reporter plasmids (**Section 5.2.2**) were used to characterize the response of expression systems involved in fluoro-benzoate utilization. The plasmids harboring *XylS/P_m*, *BenR/P_{ben}*, and *CatR/P_{cat}* were complemented with a set of constitutive promoters with different strengths and variants of the *XylS/P_m* system with a reported divergent response compared to the natural sequence. A complete list of reporter constructs tested is summarized in **Table 5.5**. *P. putida* KT2440 harboring each of the reporter plasmids was cultured in DBM medium supplemented with 30 mM glucose, 10 µg mL⁻¹ gentamicin, and, if applicable, varying concentrations of inducer compounds.

A comparison of the effects brought about by different bi-cistronic translational coupling sequences (*BCD*) as translation initiation sequences (*TIS*) is shown in **Figure 5.11 A**. The five chosen *BCD* variants showed the same effect on translation initiation as published for *E. coli* by Mutalik et al.⁴¹⁴, with relative rates as follows: *BCD2* > *BCD1* > *BCD7* > *BCD10* > *BCD20*. With the set of translational coupling sequences tested, the expression of target genes can be tuned within an about 2.3-fold range. Since the *BCD* sequences qualitatively behaved comparable to the data originally published for *E. coli*⁴¹⁴, it is expected that any of the other published variants can be chosen to provide translation initiation at even lower rates.

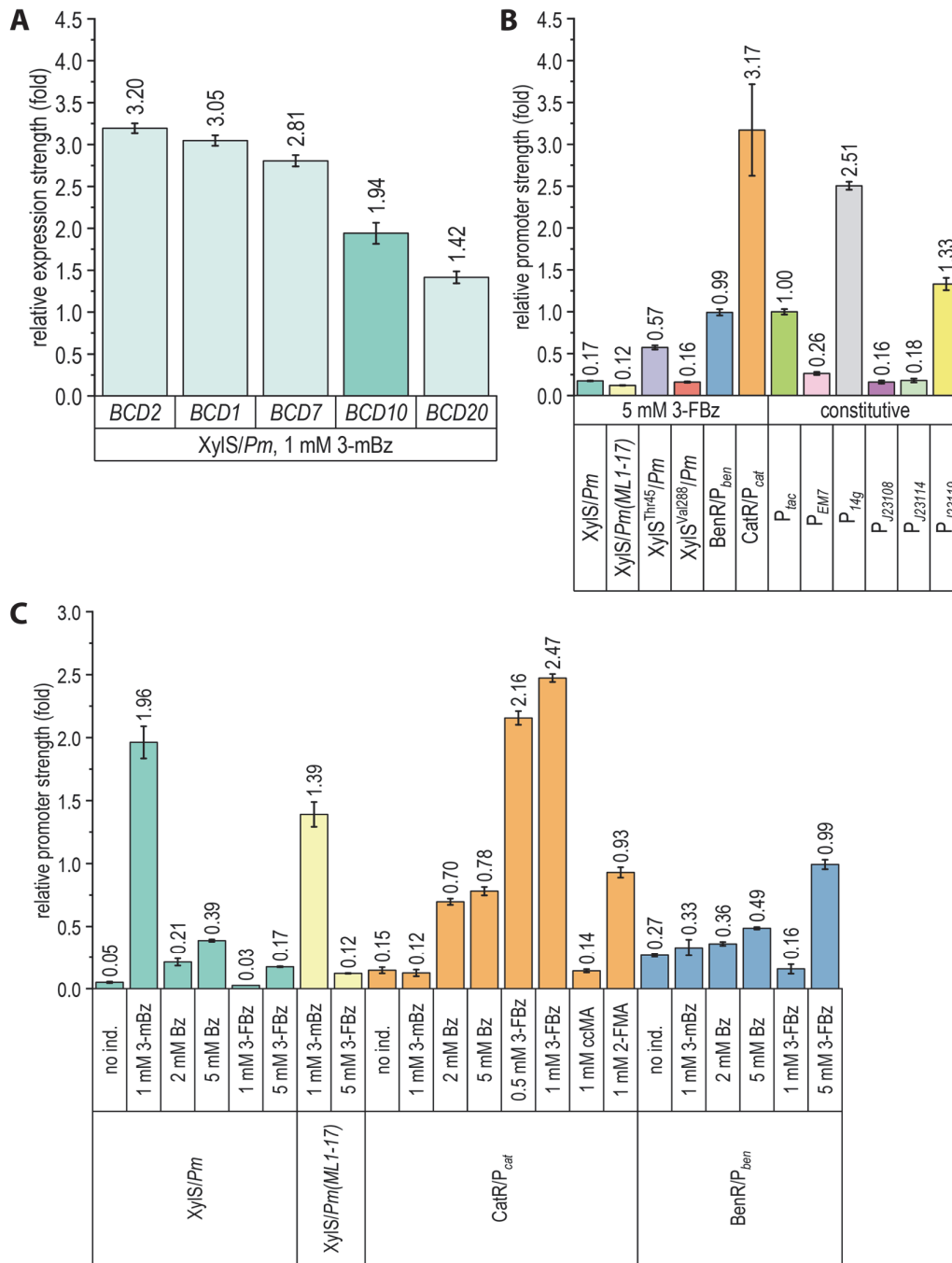


Figure 5.11. Quantitative comparison for expression systems used in this study. The different inducible (XylS/Pm, BenR/P_{ben}, CatR/P_{cat}) and constitutive (P_{tac}, P_{EM7}, P_{14g}, P_{J23108}, P_{J23114}, P_{J23119}) promoters, as well as different BCD sequences, were cloned upstream of the *msfGFP* gene in pSEVA627M and delivered into *P. putida* KT2440. The strains were cultured in microtiter plates in DBM medium supplemented with 30 mM glucose and varying concentrations of different inducer compounds. **(A)** Efficiency of BCD sequences in initiating mRNA translation. **(B)** Relative transcriptional strengths of promoter systems used during strain engineering under bioconversion conditions with BCD10 as TIS. **(C)** Inducibility of the promoter systems controlling the expression of *ortho*-cleavage pathway genes, as well as XylS/Pm, with the translation initiation sequence BCD10. The given expression strengths were normalized to the obtained expression strength of P_{tac}. Error bars represent the standard deviation from three biological replicates. no ind.: no inducer compound.

Figure 5.11 C shows a comparison of the transcription strength provided by the native CatR/ P_{cat} and BenR/ P_{ben} systems, as well as the XylS/ P_m system and its variant XylS/ $P_{m(ML1-17)}$, reported to provide a higher expression strength than wild-type P_m^{417} . The induction strengths in the presence of the native XylS/ P_m inducer 3-methyl benzoate (3-*mBz*), the native substrate of the *ortho*-cleavage pathway benzoate, the bio-conversion substrate 3-FBz, and, for CatR/ P_{cat} , its co-inducer compounds *ccMA* and 2-FMA were systematically compared in these experiments.

With both 3-*mBz* and 3-FBz as inducers, *msfGFP* expression under $P_{m(ML1-17)}$ control amounted to only 70-80% of the expression provided by wild-type P_m . The XylS/ P_m system was induced to 94% by 1 mM of 3-*mBz* compared with 5 mM of the inducer and only to about 50% with 0.1 mM 3-*mBz* during the first 6 h of cultivation, with maximum fluorescence values measured being only 9% of those of the fully induced system (not shown). In contrast, with Bz and 3-FBz there was a nearly linear dependency between inducer concentration and *msfGFP* production in the range between 1 and 5 mM. However, even at 5 mM inducer concentration, the *msfGFP* expression from P_m was only 20% and 9% of that elicited by 1 mM 3-*mBz* for Bz and 3-FBz, respectively. The system was not induced with 1 mM 3-FBz. These results are in contrast to previously reported results with $P_m \rightarrow lacZ$ fusion constructs, where XylS/ P_m was shown to respond to 1 mM 3-FBz with an induction strength of approximately 50% compared to 1 mM 3-*mBz*⁴¹⁸. However, those studies had been conducted in *E. coli*, whose different metabolic capacity and regulation might have affected the transport of the inducer compounds and the XylS/ P_m system regulation.

The CatR/ P_{cat} system had the highest expression strength and was almost entirely induced with as little as 0.5 mM 3-FBz. The addition of 1 mM 3-*mBz* elicited no response, and only 32% of fluorescence was observed with 5 mM Bz as compared to induction by 3-FBz. Furthermore, the system responded 6.7-fold more strongly to 1 mM 2-FMA than to 1 mM *ccMA*, which did not cause any significant induction. The expression with CatR/ P_{cat} was 2.7-fold higher with 3-FBz than with 2-FMA, indicating a more efficient uptake of 3-FBz, which is converted intracellularly to 2-FMA. The more vigorous response to 3-FBz and 2-FMA compared with Bz and *ccMA* could be caused either

by a stronger interaction of CatR with the fluoro-substituted muconate or a more substantial intracellular accumulation of 2-FMA, because *ccMA* can be further consumed by the CatR/*P_{cat}*-regulated muconate lactonizing enzyme.

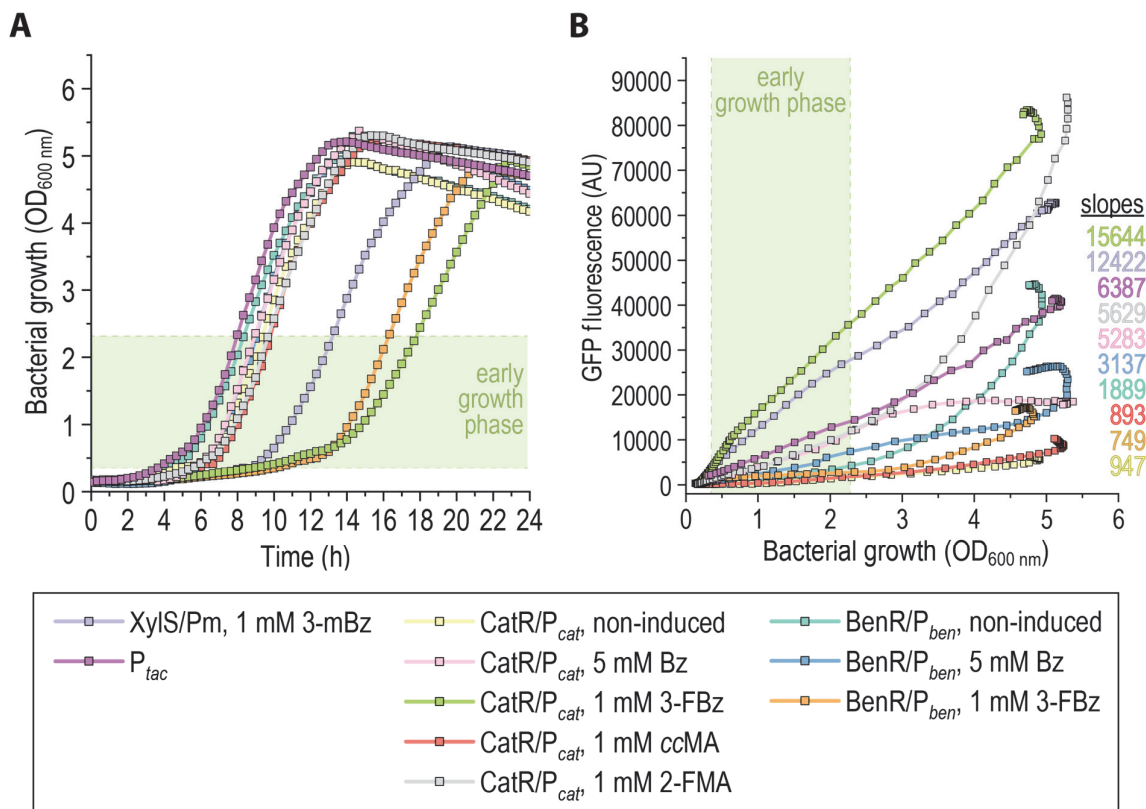


Figure 5.12. Characterization of expression systems used in this study. *P. putida* KT2440 harboring pSEVA627M plasmid derivatives with *BCD10* and different promoters controlling the expression of *msfGFP* were cultured in microtiter plates in minimal medium supplemented with 30 mM glucose as growth substrate. (A) Growth of bacteria as measured by the change in OD_{600 nm} over time. (B) *msfGFP* fluorescence over OD_{600 nm} for each strain.

The BenR/*P_{ben}* system displayed a high basal expression without the addition of any inducer, and only a slight increase in *msfGFP* formation could be observed with 1 mM 3-*mBz* and 2 mM Bz. With 5 mM of Bz, the induction was increased by 81% compared to the non-induced system. With 3-FBz supplied in the medium, BenR/*P_{ben}* showed almost no induction at an inducer concentration of 1 mM. However, supplementing 3-FBz at 5 mM caused a strong *msfGFP* signal, which was twice as high as with 5 mM Bz and comparable to *P_{tac}*. As with XylS, it has been shown that overproduction of BenR can cause activation from its associated promoter in the absence of an inducer compound^{49,213-215}, likely through the spontaneous formation of active dimeric forms.

At very high concentrations, the BenR/ P_{ben} system was shown to be fully induced and not to respond further to the presence of benzoate⁴¹⁹. By increasing the *benR* copy numbers via its expression from a plasmid, the resulting enhanced BenR concentration could be responsible for the system's high basal expression.

The translation of BenR mRNA in *P. putida* KT2440 is inhibited by the catabolite repression control protein Crc which could have caused an attenuated response of the BenR/ P_{ben} system. This notion is supported by the course of *msfGFP* expression in fluorescence-over-OD_{600 nm} plots of BenR/ P_{ben} in every condition, even without any inducer compound (**Figure 5.12**). While there is a linear increase of fluorescence in the early exponential phase of the growth curve, it rises exponentially within the mid-to-late growth phase and continues to rise in the early stationary phase. This behavior could be explained by a decreased inhibition by Crc once glucose is depleted to a concentration at which it becomes growth-limiting, causing a de-repression of genes involved in the assimilation of alternative carbon sources. The presence of glucose in the medium had been shown to cause a down-regulation of the two small RNAs *crcZ* and *crcY*, which are known to inhibit Crc⁴²⁰.

An alternative explanation for the differential behavior of BenR/ P_{ben} is the recruitment of different σ -factors by the P_{ben} promoter at different growth stages. P_m was shown to recruit σ^{32} -, and σ^{38} -dependent RNA polymerases⁴²¹, with σ^{32} being active predominantly within the exponential growth phase and σ^{38} activating transcription in the stationary phase⁴²². Considering the high homology of *XylS*/ P_m and BenR/ P_{ben} , it seems plausible that similar interactions govern the transcriptional control from P_{ben} , as well.

The inducible promoter systems BenR/ P_{ben} , CatR/ P_{cat} , and *XylS*/ P_m (plus its single substitution variants *XylS*^{Thr45} and *XylS*^{Val288}) were compared to the constitutive promoters P_{tac} , P_{EM7} , P_{14g} , P_{J23108} , P_{J23114} , and P_{J23119} under 2-FMA production conditions with 5 mM 3-FBz (**Figure 5.11B**). Both *XylS* variants *XylS*^{Thr45} and *XylS*^{Val288} had been described to respond more strongly to 3-substituted Bz derivatives⁴²³. The observed transcription initiation rates ranked as follows: CatR/ P_{cat} (3.17) > P_{14g} (2.51) > P_{J23119} (1.33) > P_{tac} (1.00) = BenR/ P_{ben} (0.99) > *XylS*^{Thr45}/ P_m (0.57) > P_{EM7} (0.26) > P_{J23114} (0.18) = P_{J23108} (0.16) = *XylS*/ P_m (0.17) = *XylS*^{Val288}/ P_m (0.16) > *XylS*/ $P_{m(ML1-17)}$ (0.12).

The expression strengths of the promoter systems employed in the first round of strain engineering in the presence of 5 mM 3-FBz provide explanations for the phenotypes observed in the respective strains. At high 3-FBz concentrations, the BenR/ P_{ben} system provided an expression level comparable to P_{tac} . The slightly increased consumption observed in strain PMP1000 compared to wild-type strain KT2440 (**Figure 5.10**) may be attributed to the full induction of the *ben* operon by P_{tac} from the start of the fermentation, whereas BenR/ P_{ben} is induced only upon exposure to the substrate. The introduction of P_{tac} upstream of *benD* had a substantial effect on the 3-FBz consumption and 3-FC formation rate. Analysis of transcriptome data published for *P. putida* KT2440 under various conditions^{420,424,425} showed varying transcript levels for genes at different locations within the *ben* cluster (**Figure 5.13**). Artificially increasing the *ben* gene cluster's downstream portion appeared to have caused a higher flux of 3-FBz into the *ortho*-cleavage pathway. Thus, 1,2-DHB dehydrogenase BenD or the benzoate transport-associated proteins BenK, BenE-II, and BenF appear to rate-limiting roles in 3-FBz assimilation.

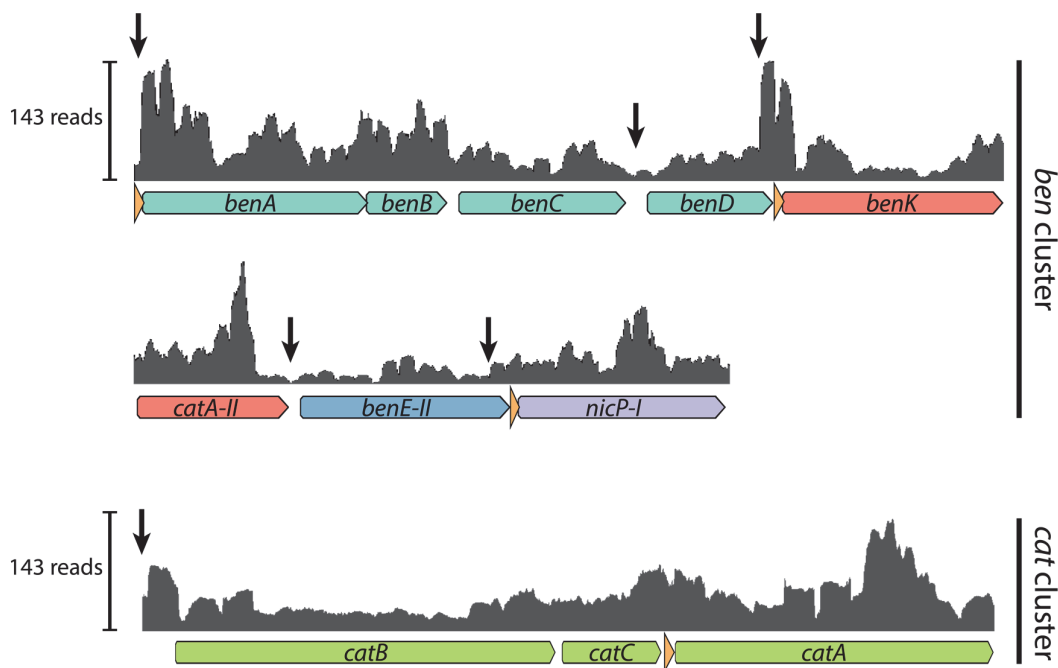


Figure 5.13. Transcriptome analysis of genes forming the *ben* and *cat* genes clusters. Accessible transcriptomics data published^{420,424,425} under various experimental conditions was pooled and mapped to the chromosome sequence of *P. putida* KT2440 (NCBI-RefSeq: NC_002947). The grey columns represent the read coverage for every nucleotide position. Orange triangles indicate identified Hfq recognition sequences. Black arrows highlight potential transcription start positions inferred from the course of coverage. The genes are drawn with colors indicating their joint expression as a transcription unit based on computational predictions on biocyc.org³¹.

A more complicated picture is drawn by the manipulations of *catA(-II)* expression by various expression modules. The native CatR/*P_{cat}* system, which controls the transcription of *catA*, was the strongest expression system observed in *P. putida* exposed to 3-FBz. On the other hand, *catA-II* is probably expressed as part of a polycistron with *benK* with incompletely characterized regulation (**Figure 5.13**). This operon is presumably subject to catabolite repression control, indicated by the presence of a recognition motif for Hfq, which was suggested to promote the binding of Crc to its targets¹¹³, upstream of *benK*.

Any effort to further increase the expression of *catA* or *catA-II* resulted in the increased accumulation of 3-FC, suggesting a decrease in the catalytic catechol 1,2-dioxygenase activity as a consequence. This effect was particularly pronounced with the plasmid-based expression of *P. knackmussii catA* orthologs controlled by *Laclq/P_{trc}*, whose expression strength with the addition of the inducer IPTG is expected to be higher than that of the constitutive *P_{tac}* promoter as a single copy in the chromosome. In the cloning host *E. coli* DH5 α λ pir, the *P. putida catA* transcript levels provided by the chosen constitutive promoters on pGNW2 plasmids (not replicated in *P. putida*) are expected to be particularly high since the plasmids are maintained at copy numbers of ~10-15⁴²⁶. Additionally, CatA concentrations are further increased by the *BCD* sequences, which are predicted to increase the translation initiation rate by a factor of 15 (*BCD2*) or 10 (*BCD10*) compared to the native *catA* translation initiation sequence (see **Table 5.4**). In *E. coli*, these high expression levels of *catA* appear to be toxic, thus providing a selection pressure to mutate the promoter sequences, while in *P. putida*, high CatA(-II) levels disrupted catechol 1,2-dioxygenase activity. Together, presented data on expression systems and the bioconversion performances of the *first-generation* strains suggest that a reduction, rather than an increase, of *catA(-II)* expression might increase the bioconversion efficiency in *P. putida*.

5.2.6. Implementation of a dynamic catechol 1,2-dioxygenase expression control enabled a balanced, complete conversion of 3-fluorobenzoate into 2-fluoro-*cis,cis*-muconate

Guided by the observations made on the effects of genetic manipulations within *first-generation* strains and the expression system characterization, the next set of strains was designed, in which *catA* or *catA-II* was set under the control of the XylS/*Pm* system that responded weakly to the bioconversion substrate 3-FBz and showed little to no induction in the absence of any inducer compound. The latter was thought to facilitate the cloning process in *E. coli*. Because 3-FBz-induced XylS/*Pm* provides transcript levels at a rate of only 7% compared to CatR/*P_{cat}* (see **Figure 5.11**), the native translation initiation sequence of *catA* and *catA-II* were replaced by *BCD10*, which, according to model predictions (RBS calculator 2.1), should increase translation initiation by about 10-fold. The changes within the regulatory sequences for *catA* and *catA-II* were furthermore combined with *P_{tac}*→*benABC*, the integration of *xylS* into the chromosome under control of its native regulatory sequences, or the chromosomal integration of the suicide plasmid pBen1 (a pGNW2-derivative), which harbors additional copies of the *benABC* and *benDK-(catA-II)* operons, each under the control of *Pm(BCD10)*, into a landing site between *PP_0013* and *PP_5421*. Strains without *xylS* integrated into the chromosome were additionally transformed with pSEVA228 or pSEVA438 (complementing pBen1) to provide the activator XylS from a plasmid. All strains created within the second round of strain engineering are listed in **Table 5.4**.

The *second-generation* strains were screened in bioconversion experiments in minimal medium supplemented with 30 mM glucose and 10 mM 3-FBz, with an initial biomass concentration of 0.175 g L⁻¹. The extracellular metabolites for each strain after 24 h of cultivation, after which they remained stable, are shown in **Figure 5.14 A**. While the individual replacement of regulatory sequences for *catA* and *catA-II* with *Pm(BCD10)* (strains PMP0020 and PMP0001) led to an increased formation of 3-FC, both manipulations combined (strain PMP0021) resulted in reduced 3-FC concentrations in the culture supernatant as well as an increase in 2-FMA concentration by about two-fold compared to wild-type *P. putida* KT2440. At the end of the experiment, about 50% of

3-FBz were still left in the medium. The implementation of $P_{tac} \rightarrow benABC$ (strain PMP1021) enhanced 3-FBz uptake, which led to the complete consumption of the substrate and a 2-FMA yield of 50% (mol/mol) without 3-FC accumulation.

This performance could only be observed if XylS was provided from a plasmid (pSEVA228) as indicated by the performance of strain PMP1041 having xylS integrated into the chromosome upstream of *catA*. This suggests that higher XylS levels are necessary to saturate both *Pm* promoters of *catA* and *catA-II*, located at distant positions within the *P. putida* chromosome. The effects of varying spatial distances between the gene encoding XylS and its associated promoter *Pm* had been comprehensively studied by Goñi-Moreno et al.⁴²⁷ and Volke et al.⁴²⁸, who demonstrated that the transcriptional output becomes more heterogeneous within a cell population at an increased regulator-promoter distance. The integration of pBen1 in a strain that had both *catA* paralogs controlled by *Pm(BCD10)* significantly reduced the substrate consumption so that only 20% of the supplied 3-FBz were depleted.

With 2-FMA as the only metabolite detected in the supernatant of PMP1021 pSEVA228, the culture broth was subjected to the purification protocol published for ccMA by Vardon et al.³⁷⁷. Following the procedure, which includes microfiltration, activated carbon treatment, pH/temperature shift crystallization, vacuum filtration, and vacuum-drying, about 34 mg 2-FMA could be recovered from 45 ml of culture broth. This mass corresponds to 84% of 2-FMA initially measured in the culture supernatant. The chromatogram of an HPLC analysis of the purified product with a UV-detection at 280 nm is shown in **Figure 5.14 B**. The elution profile of purified 2-FMA was identical to that of a commercially available, chemically synthesized standard (Ambinter, Orléans, France, product reference 33855674) and confirmed the previous identification via ¹⁹F NMR. 2-FMA showed a single absorbance maximum at 269 nm, close to the maximum of 263 nm reported in the literature³⁹⁵.

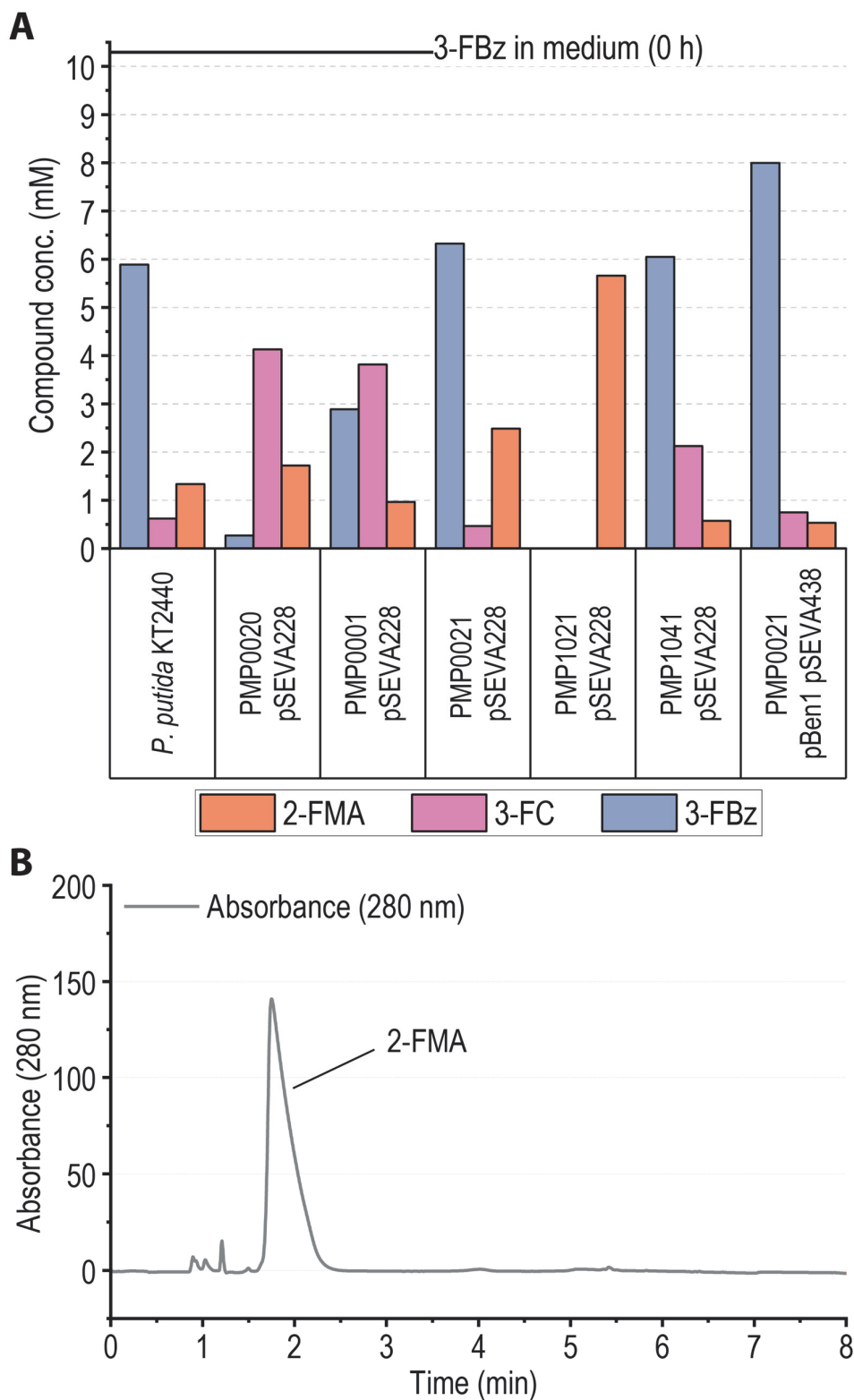


Figure 5.14. Bioconversion performance of second-generation strains. The strains were cultured in Erlenmeyer flasks filled with 10% (v/v) DBM medium supplemented with 30 mM glucose, 5 g L⁻¹ MOPS, and 10 mM 3-FBz. **(A)** Extracellular metabolite concentrations after 24 h of cultivation. **(B)** HPLC chromatogram of purified 2-FMA.

5.2.7. Further strain engineering involving genetic "off the beaten path" targets uncovers a vital role of carbon catabolite control

A suitable set of genetic manipulation had been established that enables a balanced conversion of 3-FBz into 2-FMA without the accumulation of by-products and pathway intermediates. These manipulations resulted in *P. putida* PMP1021/pSEVA228. Using PMP1021 as genetic background, an additional set of strains was created with the aim of further increasing the overall productivity of the bioconversion process:

1. The gene encoding the global catabolite repression control regulator Crc was deleted, which had been shown to bind to the mRNA of the BenR activator^{429,430} and likely other genes within the *ben* cluster (**Figure 5.13**), thereby inhibiting translation of genes involved in the *ortho*-cleavage pathway (strain PMP0021d).
2. The three genes located within the *ben* gene cluster that encode membrane proteins which are thought to be involved in benzoate uptake, *benK* (H⁺ symporter), *benE-II* (H⁺ symporter), and *nicP-I* (also named *benF*, porin OprD), were chosen as targets for expression control by *Pm(BCD10)*, yielding strains PMP1021g, PMP1021f, and PMP1021e.
3. To decipher the contribution of each of the two CatA orthologs in the bioconversion, *catA* (strain PMP1030) or *catA-II* (strain PMP1002) were put under the control of *Pm* and the stronger translation initiation sequence *BCD2* while keeping the regulation of the other catechol 1,2-dioxygenase unchanged.
4. To further increase the flux into the pathway, the native *TIS* of *benA* harboring an Hfq recognition motif (**Figure 5.13**) was replaced by *BCD10* (strain PMP2032).
5. To achieve a balanced bioconversion without introducing any plasmid into the strains, *xylS* was integrated upstream of *catA* under the control of the regulatory sequences *P_{tac}* and *BCD10* (strain PMP1051d).
6. Since two of the three biochemical reactions involved in the bioconversion require oxygen, the gene encoding the bacterial hemoglobin from *Vitreoscilla stercoraria*, *vhb*, was fused to a type II secretion system signal sequence derived from the lipoprotein-encoding gene *uxpA*⁴³¹ and integrated into the *crc* locus

under control of a *Pm(BCD10)* element (strain PMP1021h). The expression of *vhb* was expected to increase the cell's affinity to oxygen, thus increasing the bioconversion rate.

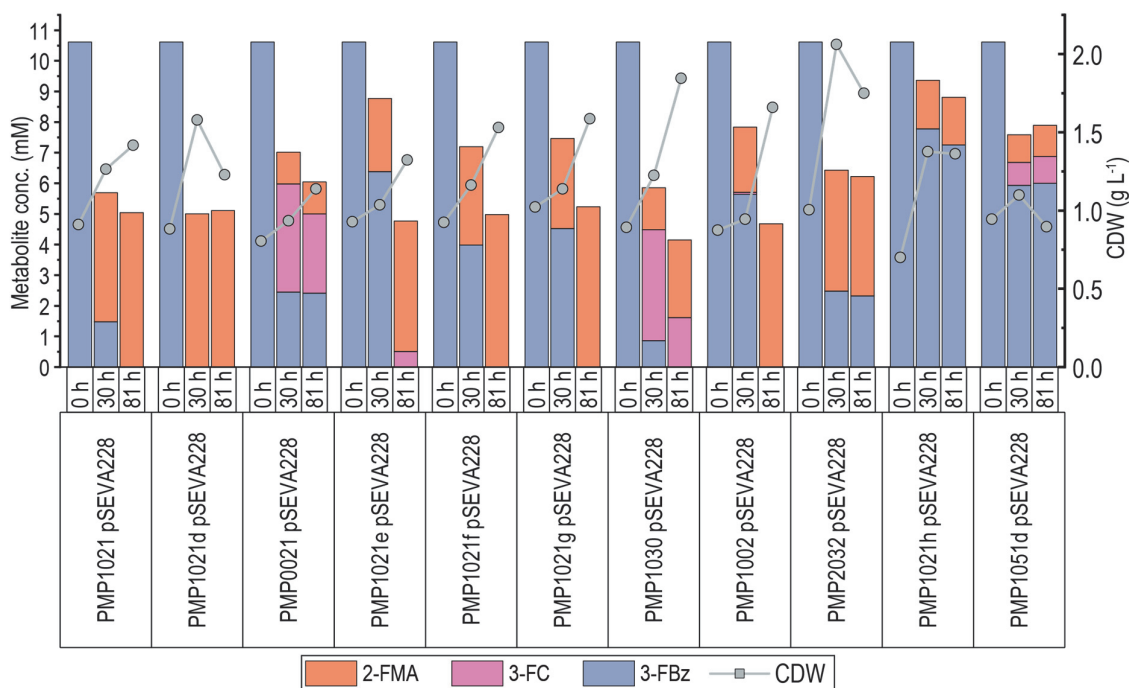


Figure 5.15. Bioconversion performance of third-generation strains. The strains were cultured in Erlenmeyer flasks filled with 10% (v/v) DBM medium supplemented with 30 mM glucose, 5 g L⁻¹ MOPS, and 10 mM 3-FBz.

Each of the strains, except for PMP1051d, was transformed with pSEVA228 to provide XylS for the genes under *Pm* control, and all were tested for their performance in the conversion of 10 mM 3-FBz with 30 mM glucose as the growth substrate. The biomass (cell dry weight – CDW), 3-FBz, 3-FC, and 2-FMA concentrations for each strain over 81 h of cultivation are summarized in **Figure 5.15**. The complete fermentation profiles for each strain are shown in **Figure 5.S1A** and **Figure 5.S1B**. It should be noted that biomass concentrations from OD_{600 nm} measurements could not be estimated reliably at (fluoro-)catechol concentrations > 0.2 mM for an extended period due to their spontaneous auto-oxidation followed by the formation of colored polymerization products⁴³².

The deletion of *crc* in PMP0021d resulted in rapid initial consumption of 7.8 mM 3-FBz within 6.5 h, accompanied by an accumulation of 3-FC to a concentration of 4.1 mM. After this time, the 3-FBz concentration remained nearly constant, and 3-FC was partially converted to 2-FMA up to a concentration of 1 mM. When P_{ben} was replaced by P_{tac} (PMP1021d), 3-FBz conversion to 2-FMA was complete and occurred at a high rate without a permanent accumulation of 3-FC (**Figure 5.S3A**). This suggests that the expression provided by P_{ben} in the absence of Crc is too high, resulting in a high substrate flux into the pathway. However, the performance of PMP1021d was not consistent between different experiments. In a subsequent fermentation, the strain displayed low biochemical activity for up to 30 h, followed by a similar substrate consumption as observed before (**Figure 5.S3B**).

The insertion of $Pm(BCD10)$ upstream of membrane protein-encoding genes resulted in a significant reduction of the 3-FBz consumption rate, with the most substantial effect apparent with strain PMP1021e (*nicP-I*, **Table 5.3**). Nonetheless, nearly all PMP1021(e/f/g) strains converted the supplied 3-FBz completely into 2-FMA at the maximum yield of 50% (mol/mol). After initial accumulation of ~1 mM 3-FC within the first 5 h, no other metabolites were found in the culture medium by the end of the fermentation, except for 0.5 mM with strain PMP1021e. The initial increase in extracellular 3-FC concentrations was likely due to a lack of *catA(-II)* induction at the start of the fermentation. Considering the weak induction strength of the *XylS/Pm* system in response to 3-FBz, the replacement of the native regulatory sequences likely resulted in a down-regulation of the transport-associated function, causing a drop in 3-FBz uptake.

While the expression of only *catA* via $Pm(BCD2)$ (strain PMP1030) did not suffice to process all flux towards 3-FC, as evident in a substantial accumulation of the intermediate, the expression control of *catA-II* (strain PMP1002) enabled a complete conversion of 3-FBz into 50% (mol/mol) 2-FMA, although with lower productivity than PMP1021. This suggests that CatA-II is the catechol 1,2-dioxygenase predominantly responsible for converting 3-FC into 2-FMA. The additional enhancement of *benA* expression via the introduction of *BCD10* (strain PMP2032) resulted in an accelerated 3-

FBz consumption. However, this effect could be attributed to an enhanced growth rate during the fermentation. The biomass-specific substrate consumption rate and the product formation rate were decreased compared to PMP1021 (**Table 5.3**).

The chromosomal integration of *xylS* under strong transcriptional and translational control upstream of *catA* did not suffice to properly induce the expression of both catechol 1,2-dioxygenase genes (strain PMP1051d). After a rapid consumption of ~2.5 mM 3-FBz that was converted into 1.2 mM 3-FC, likely due to the deletion of *crc*, the strain ceased to grow and showed only little biochemical activity in the further conversion of 3-FBz and 3-FC into 2-FMA.

A negative effect of *crc* deletion can also be seen for PMP1021h, in which the regulatory gene was replaced by the *Vitreoscilla stercoraria vhb* gene. Only one-third of the supplied 3-FBz was consumed, although with complete conversion to 2-FMA at the maximum yield. However, the bacterial hemoglobin's potential benefits for the obligate aerobic bacterium appeared in another experiment, in which the strains PMP1021d and PMP1051d were cultured in sealed glass tubes filled to 60% (v/v) with culture medium without shaking (**Figure 5.S2**). While no 3-FBz was consumed, the hemoglobin-harboring strain grew to about two-fold higher biomass concentrations than the strain without *vhb* over the course of one week, and the cells showed reduced sedimentation in the tube, indicating increased flagellar activity. These results suggest that the expression of *Vitreoscilla stercoraria vhb* might be beneficial under micro-oxic conditions like the ones that cells repeatedly experience in large bioreactors with suboptimal oxygen transfer into the medium.

Table 5.3. Performance parameters for selected strains used in this study in the bioconversion of 10 mM 3-FBz. To determine the biomass-specific 3-FBz uptake rates q_s and 2-FMA formation rates q_p , the strains were cultured in Erlenmeyer flasks filled with 10% (v/v) DBM medium supplemented with 30 mM glucose and 10 mM 3-FBz. Maximum growth rates (μ_{max}) were determined in microtiter plate experiments in the same medium.

Strain	μ_{max} [h^{-1}]	q_s [mmol $g_{CDW}^{-1} h^{-1}$]	q_p [mmol $g_{CDW}^{-1} h^{-1}$]
<i>P. knackmussii</i>	no growth	0.090 ^a	0.046 ^b
<i>P. putida</i> KT2440	0.13	0.162 ^a	0.060
PMP1021 pSEVA228	0.28	1.105	0.537 ^b
PMP1021d pSEVA228	0.13	n.d. ^c	n.d. ^c
PMP0021d pSEVA228	no growth	1.409 ^a	0.135
PMP1021e pSEVA228	0.29	0.568	0.318 ^b
PMP1021f pSEVA228	0.30	0.837	0.405 ^b
PMP1021g pSEVA228	0.27	0.742	0.358 ^b
PMP1030 pSEVA228	0.32	1.212	0.169
PMP1002 pSEVA228	0.39	0.812	0.381 ^b
PMP2032 pSEVA228	0.17	0.860	0.434 ^b
PMP1021h pSEVA228	0.24	0.410	0.208 ^b
PMP1051d pSEVA228	0.15	0.384 ^a	0.091
PMP1063	0.28	1.230	0.537 ^b
PMP1063d	0.15	1.771 ^a	0.526
PMP2063	0.41	0.248 ^a	0.128 ^b
PMP1023 pSEVA228	0.29	1.216	0.460 ^b
PMP1023 pSEVA228.2	0.25	0.930	0.385 ^b
PMP1024	0.30	1.051	0.521 ^b

^a no complete consumption of 3-FBz

^b no detectable fluorocatechol at the end of the fermentation

^c strain PMP1021d showed two distinct phases of different biochemical activity with first a period characterized by slow growth, glucose consumption, and 3-FBz consumption rates, followed by very rapid depletion of glucose and 3-FBz. The order of these phases was reverted in different experiments.

5.2.8. Constitutive expression of catechol 1,2-dioxygenase genes enables balanced 2-fluoro-*cis,cis*-muconate production in plasmid-free strains

Based on the previous observations, a fourth set of strains was designed to characterize the specific effects of $P_{tac}(BCD10) \rightarrow benABC$ and Δcrc , to enable an efficient bioconversion without the use of plasmids, and to consolidate the contributions of *catA* and *catA-II* to the conversion of 3-FC. In the resulting strains, PMP1063, PMP1063d, PMP2063, and PMP1023, either only *catA-II* or both *catA* genes were put under the control of the constitutive promoter P_{14b} , which was reported to have 25% of the strength of P_{14g} (corresponding to a value of ~ 0.63 in this study)⁴³³, as well as *BCD10*. In PMP1024, *xylS* was integrated under the control of P_{14g} and a synthetic translation initiation sequence designed with the RBS Calculator with a translation rate of 719,862, which is even higher than that predicted for *BCD2*. Fermentation profiles for each of the *fourth-generation* strains are shown in **Figure 5.16**. The results for PMP1021 and PMP1021d, which were included in the experiment as controls, are displayed in **Figure 5.S3B**.

The combination of $P_{tac} \rightarrow benABC$, $P_{14b}(BCD10) \rightarrow catA$, and $P_{14b}(BCD10) \rightarrow catA-II$ in PMP1063 enabled a complete conversion of all supplied 3-FBz at the maximum theoretical yield of 50% at the highest specific productivities observed (**Table 5.3**), without the requirement for any plasmid. Furthermore, the constitutive expression of *catA* and *catA-II* decreased the initial 3-FC accumulation compared to PMP1023, in which the catechol 1,2-dioxygenases were activated only at fermentation start with the exposure to 3-FBz.

With both *catA* and *catA-II* constitutively expressed by P_{14b} , the additional deletion of *crc* (PMP1063d) or the introduction of *BCD10* for *benABC* (PMP2063) resulted in an incomplete consumption of 3-FBz at low specific rates. Thus, both genetic modifications brought about detrimental effects to the bioconversion.

In strain PMP1023, only *catA-II* was constitutively expressed, while *catA* was under the regulation of $P_m(BCD10)$. To achieve different induction strengths for *catA*, *XylS* was provided either as its wild-type sequence (on pSEVA228) or as variant *XylS*^{Thr45} (on plasmid pSEVA228.2), which had been shown to cause a higher induction strength

in response to 3-FBz compared to the wild-type variant by a factor of 3.4 (**Figure 5.11**). PMP1023 demonstrated equal performances with pSEVA228 and pSEVA228.2, both of which were similar to that of strain PMP1021 with pSEVA228 (**Figure 5.15, Table 5.3**). The additional increase in expression for *catA* did neither result in increased bioconversion productivity nor decreased initial fluorocatechol accumulation.

Unlike strains PMP1041 and PMP1051d, in which *xylS* was integrated upstream of *catA*, its integration in proximity to *catA-II* in PMP1024 provided sufficient expression from the chromosomal *Pm* promoters to enable a complete conversion of 3-FBz. The biomass-specific substrate consumption and product formation rates were comparable to PMP1021 with pSEVA228, without the necessity for a plasmid. The results with PMP1023 and PMP1024 confirm the previous notion that the control of *catA-II* expression is the predominant mechanism that allows for an efficient conversion of 3-FC.

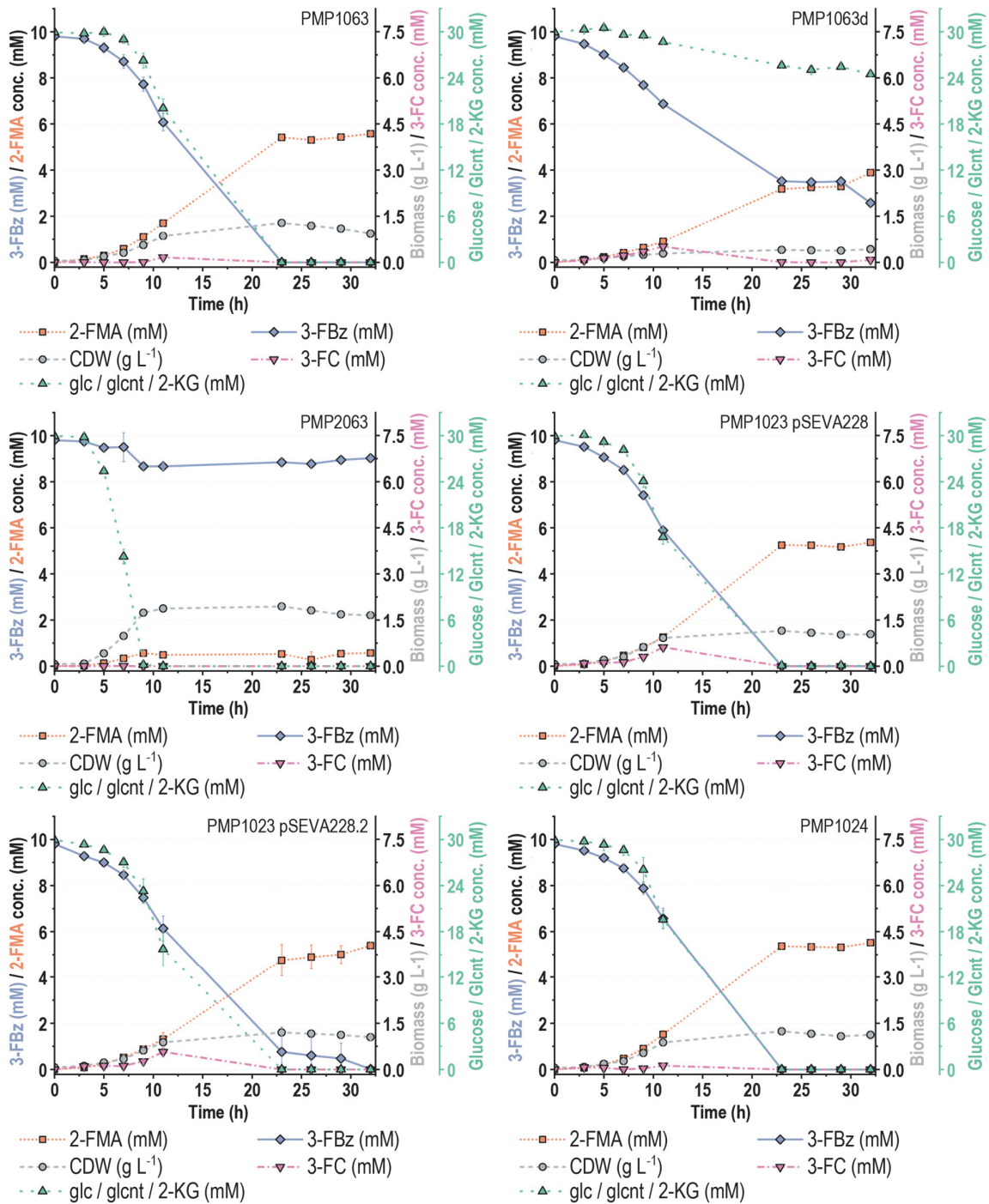


Figure 5.16. Fermentation profiles of *fourth-generation* bioconversion strains. The bioconversions were performed in Erlenmeyer flasks filled with 10% (v/v) DBM medium supplemented with 30 mM glucose and 10 mM 3-FBz. Error bars represent the standard deviations from three biological replicates.

5.2.9. Engineered *P. putida* tolerates higher 3-fluorobenzoate concentrations than the parental strain

Strain PMP1063 was tested in microtiter plate cultivations regarding its ability to use Bz as the sole source of carbon and the maximum 3-FBz concentrations tolerated in the presence of 30 mM glucose as the source of carbon and energy (**Figure 5.17A**). Up to a 3-FBz concentration of 20 mM, no toxic effects were observed, while the growth of wild-type *P. putida* KT2440 was suppressed entirely in the presence of 10 mM. PMP1063 grew up to the highest concentration of 50 mM 3-FBz, although at a significantly reduced rate and maximum biomass concentration. The apparent increase in OD_{600 nm} for KT2440 could be attributed exclusively to the formation of colored fluorocatechol polymerization products. On the other hand, no medium coloration was observed with PMP1063, indicating that the 3-FBz consumed was assimilated without the formation of fluorocatechol. The apparent lack of 3-FC accumulation and the fact that the growth deficiencies observed in the growth rate were present from the start of the cultivation suggests a toxic effect on the cells by 3-FBz itself. Interestingly, the growth rate and biomass yield of PMP1063 on benzoate were significantly reduced compared to wild-type *P. putida* KT2440.

With the 2-FMA purified from fermentation broths, the toxicity of the product on *P. putida* was investigated in microtiter plate cultivations in minimal medium with 30 mM glucose and varying concentrations of the bioconversion product (**Figure 5.17B**). With up to 10 mM 2-FMA, *P. putida* KT2440 showed a growth profile similar to cultures with glucose as the utilized only carbon compound in the medium (**Table 5.2**). At 15 mM 2-FMA, the growth rate and maximum biomass concentration were reduced by 50%, and at 25 mM 2-FMA, no growth could be detected. Exposed to 2-FMA, strain PMP1063 had a growth profile nearly identical to the wild-type strain (not shown).

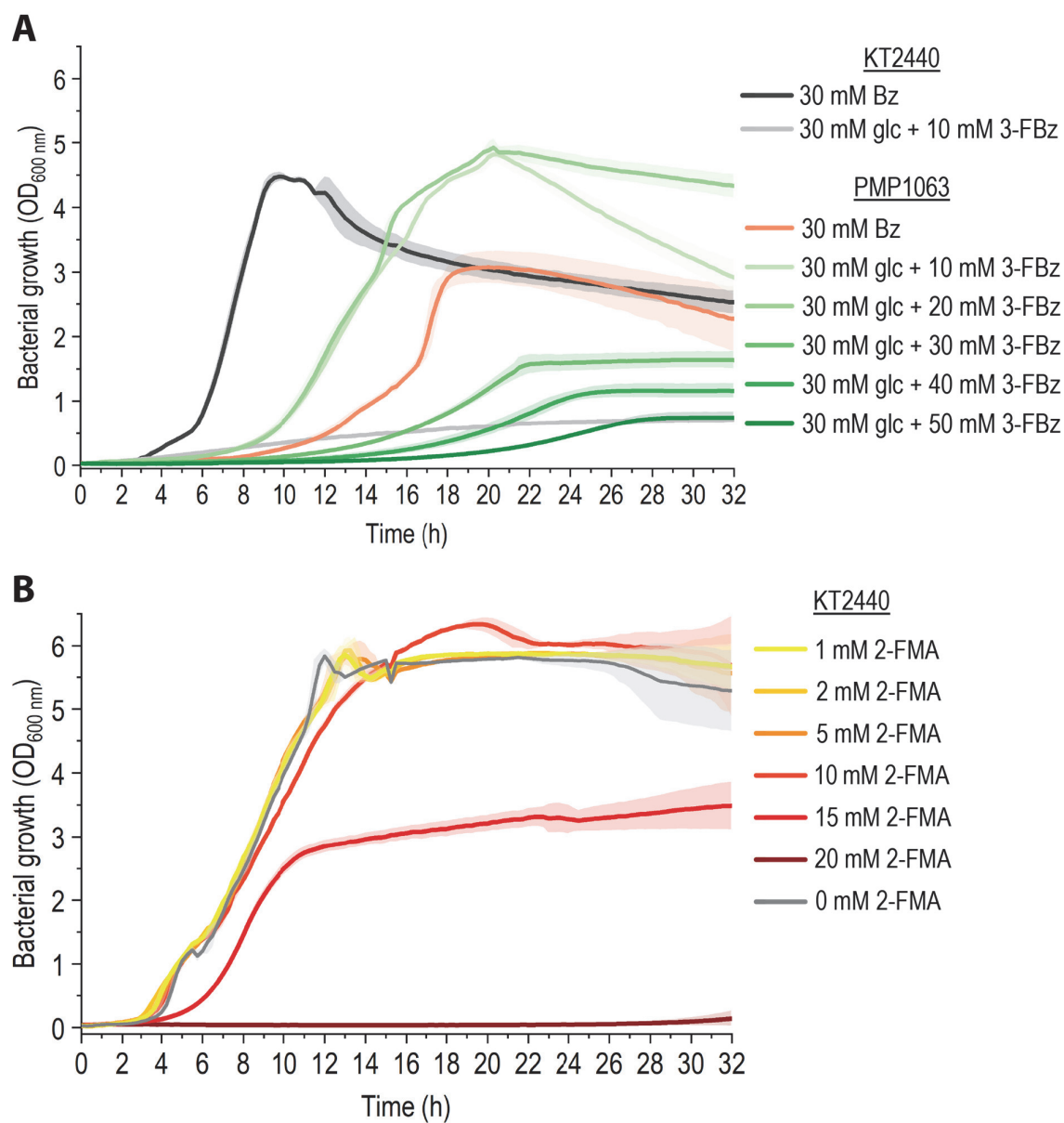


Figure 5.17. Toxicity of the bioconversion substrate product for wild-type and engineered *P. putida*. *P. putida* KT2440 and strain PMP1063 were cultured in microtiter plates with 200 μ l DBM medium with various carbon compounds. **(A)** Growth of KT2440 and PMP1063 on 30 mM benzoate or 30 mM glucose with increasing concentrations of 3-FBz. **(B)** Growth of KT2440 with 30 mM glucose and increasing 2-FMA concentrations. Error bars represent the standard deviations from three biological replicates.

Table 5.4. Bacterial strains used in this chapter.

Strain [Alias]	Genotype / Relevant characteristics	Reference or source
<i>Escherichia coli</i>		
DH5 α λ pir	Cloning host; F- λ - <i>endA1 glnX44(AS) thiE1 recA1 relA1 spoT1 gyrA96(Nal^R) rfbC1 deoR nupG Φ80(lacZΔM15) Δ(argF-lac)U169 hsdR17(rκ- mκ⁺), λ pir lysogen</i>	Platt et al. ²⁵⁸
<i>Pseudomonas</i>		
<i>P. putida</i> KT2440	Wild-type strain, derived from <i>P. putida</i> mt-2 ²⁶⁰ cured of the TOL plasmid pWW0	Bagdasarian et al. ²⁶¹
<i>P. knackmussii</i> (<i>Pseudomonas</i> sp. B13)	Wild-type strain	Stolz et al. ⁴³⁴
PMP1000 *1	$P_{tac} \rightarrow benABC$ <i>P. putida</i> KT2440 with the chromosomal <i>benABC</i> gene cluster put under the control of the constitutive P_{tac} promoter. The native, validated 5' UTR of the <i>benA</i> gene were kept unchanged, providing a predicted translation rate of 220.	This study P_{tac} : de Boer et al. ⁴³⁵ <i>benA</i> 5' UTR definition: Pérez-Pantoja et al. ²³⁷
PMP0100 *1	$P_{tac} \rightarrow benD$ <i>P. putida</i> KT2440 with the chromosomal <i>benD</i> gene under the control of the constitutive P_{tac} promoter. The native 28 bp upstream of the <i>benD</i> gene were kept unchanged, providing a putative translation initiation sequence with a predicted translation rate of 818.	This study
PMP0010 *1	$P_{EM7} \rightarrow catA$ <i>P. putida</i> KT2440 with the constitutive P_{EM7} promoter chromosomally inserted upstream of the <i>catA</i> gene. The native 29 bp upstream of the <i>catA</i> gene were kept unchanged, providing a putative translation initiation sequence with a predicted translation rate of 3211.	This study
PMP0000a *1	$\Delta catBC$ <i>P. putida</i> KT2440 with both chromosomal genes <i>catB</i> and <i>catC</i> deleted	This study
PMP0000b *1	$\Delta catBC::catA$ <i>P. putida</i> KT2440 with the genes <i>catB</i> and <i>catC</i> replaced with an additional copy of <i>catA</i> . The predicted translation rate of <i>catA</i> with the <i>catB</i> 5' UTR is 1934.	This study
PMP0000c *1	$\Delta catBC::catA-II$ <i>P. putida</i> KT2440 with the genes <i>catB</i> and <i>catC</i> replaced with an additional copy of <i>catA-II</i> . The predicted translation rate of <i>catA-II</i> with the <i>catB</i> 5' UTR is 503.	This study

PMP1000a	*1	$P_{tac} \rightarrow benABC \Delta catBC$	This study
PMP0100a	*1	$P_{tac} \rightarrow benD \Delta catBC$	This study
PMP0100b	*1	$P_{tac} \rightarrow benD \Delta catBC::catA$	This study
PMP0100c	*1	$P_{tac} \rightarrow benD \Delta catBC::catA-II$	This study
PMP0020	*2	$Pm(BCD10) \rightarrow catA$ <i>P. putida</i> KT2440 with the chromosomal gene <i>catA</i> put under the control of the inducible <i>Pm</i> promoter and the translational coupling sequence <i>BCD10</i> with predicted translation strengths of 28177 (SD1) and 331 (SD2).	This study <i>BCD10</i> : Mutalik et al. ⁴¹⁴
PMP0001	*2	$Pm(BCD10) \rightarrow catA-II$ <i>P. putida</i> KT2440 with the chromosomal gene <i>catA</i> put under the control of the inducible <i>Pm</i> promoter and the translational coupling sequence <i>BCD10</i> with predicted translation strengths of 28177 (SD1) and 134 (SD2).	This study
PMP0021	*2	$Pm(BCD10) \rightarrow catA Pm(BCD10) \rightarrow catA-II$	This study
PMP0021d	*3	$Pm(BCD10) \rightarrow catA Pm(BCD10) \rightarrow catA-II \Delta crc$ PMP1021 with the catabolite repression control gene <i>crc</i> deleted.	This study
PMP1021	*2	$P_{tac} \rightarrow benABC Pm(BCD10) \rightarrow catA Pm(BCD10) \rightarrow catA-II$	This study
PMP1041	*2	$P_{tac} \rightarrow benABC xyIS/Pm_{(ML1-17)}(BCD10) \rightarrow catA Pm(BCD10) \rightarrow catA-II$ Strain PMP1011 with the <i>xyIS</i> gene with its native regulatory sequences chromosomally integrated upstream of and encoded on the opposite DNA strand of <i>catA</i> , which is controlled by the <i>Pm</i> variant ML1-17.	This study <i>Pm</i> _(ML1-17) : Bakke et al. ⁴¹⁷
PMP0021 pBen1	*2	$Pm(BCD10) \rightarrow catA Pm(BCD10) \rightarrow catA-II$ pBen1 pSEVA438 pBen1 is a suicide plasmid harboring HAs for the chromosomal integration of additional copies of $Pm(BCD10) \rightarrow benABC$ and $Pm(BCD10) \rightarrow benDK-(catA-II)$, into a landing site between <i>PP_0013</i> and <i>PP_5421</i>	This study The use of the landing site was previously in Wirth et al. ⁴³⁶
PMP1021d	*3	$P_{tac} \rightarrow benABC Pm(BCD10) \rightarrow catA Pm(BCD10) \rightarrow catA-II \Delta crc$ PMP1021 with the catabolite repression control gene <i>crc</i> deleted.	This study
PMP1051d		$P_{tac} \rightarrow benABC P_{14g}(BCD10) \rightarrow xyIS/Pm(BCD10) \rightarrow catA Pm(BCD10) \rightarrow catA-II \Delta crc$ Strain 1021d with the <i>xyIS</i> gene chromosomally integrated under $P_{14g}(BCD10)$ control upstream of and encoded on the opposite DNA strand of <i>catA</i>	This study
PMP1021e	*3	$P_{tac} \rightarrow benABC Pm(BCD10) \rightarrow catA Pm(BCD10) \rightarrow catA-II Pm_{(ML1-17)}(BCD10) \rightarrow nicP-I$ PMP1022 with the porin-like protein-encoding gene <i>nicP-I</i> (<i>benF</i>) under the control of the inducible <i>Pm</i> promoter variant ML1-17 and the translational coupling sequence <i>BCD10</i> with predicted translation strengths of 31045 (SD1) and 72 (SD2).	This study

PMP1021f	*3	$P_{tac} \rightarrow benABC Pm(BCD10) \rightarrow catA$ $Pm(BCD10) \rightarrow catA-II Pm_{(ML1-17)} \rightarrow benE-II$	This study
		PMP1022 with the benzoate transport protein encoding gene <i>benE-II</i> put under the control of the inducible <i>Pm</i> promoter variant ML1-17 and the translational coupling sequence <i>BCD10</i> with predicted translation strengths of 31045 (SD1) and 1594 (SD2).	
PMP1021g	*3	$P_{tac} \rightarrow benABC Pm(BCD10) \rightarrow catA Pm(BCD10) \rightarrow catA-II$ $Pm_{(ML1-17)} \rightarrow benK$	This study
		PMP1022 with the benzoate MFS transporter encoding gene <i>benK</i> put under the control of the inducible <i>Pm</i> promoter variant ML1-17 and the translational coupling sequence <i>BCD10</i> with predicted translation strengths of 31045 (SD1) and 541 (SD2).	
PMP1030	*3	$P_{tac} \rightarrow benABC Pm(BCD2) \rightarrow catA$	This study <i>BCD2</i> : Mutalik et al. ⁴¹⁴
		Chromosomal <i>benABC</i> gene cluster put under the control of the constitutive P_{tac} promoter. Chromosomal gene <i>catA</i> put under the control of the inducible <i>Pm</i> promoter and the translational coupling sequence <i>BCD2</i> with predicted translation strengths of 28177 (SD1) and 18908 (SD2).	
PMP1002	*3	$P_{tac} \rightarrow benABC Pm(BCD2) \rightarrow catA-II$	This study
		Chromosomal <i>benABC</i> gene cluster put under the control of the constitutive P_{tac} promoter. Chromosomal gene <i>catA-II</i> put under the control of the inducible <i>Pm</i> promoter and the medium-strong translational coupling sequence <i>BCD2</i> with predicted translation strengths of 28177 (SD1) and 7687 (SD2).	
PMP2021	*3	$P_{tac}(BCD10) \rightarrow benABC Pm(BCD10) \rightarrow catA$ $Pm(BCD10) \rightarrow catA-II$	This study
		PMP1022 with the native 5'-UTR of <i>benABC</i> replaced with <i>BCD10</i> .	
PMP1021h	*3	$P_{tac} \rightarrow benABC Pm(BCD10) \rightarrow catA$ $Pm(BCD10) \rightarrow catA-II \Delta crc::vhb$	This study <i>uxpA</i> signal peptide: Putker et al. ⁴³¹
		PMP1011 _C with the <i>Vitreoscilla stercoraria vhb</i> gene inserted into the <i>crc</i> locus under control of <i>Pm</i> and <i>BCD10</i> and fused at the 5' end to a type II secretion system signal sequence derived from the <i>P. putida</i> KT2440 gene <i>uxpA</i>	
PMP1023		$P_{tac} \rightarrow benABC Pm(BCD10) \rightarrow catA P_{14b}(BCD10) \rightarrow catA-II$	This study
		<i>catA-II</i> under the transcriptional control of the constitutive promoter P_{14b}	P_{14b} : Zobel et al. ²⁹⁸
PMP1063		$P_{tac} \rightarrow benABC P_{14b}(BCD10) \rightarrow catA P_{14b}(BCD10) \rightarrow catA-II$	This study
		<i>catA</i> and <i>catA-II</i> under the transcriptional control of the constitutive promoter P_{14b}	
PMP1063d		$P_{tac} \rightarrow benABC P_{14b}(BCD10) \rightarrow catA P_{14b}(BCD10) \rightarrow catA-II$ Δcrc	This study
PMP2063		$P_{tac}(BCD10) \rightarrow benABC P_{14b}(BCD10) \rightarrow catA$ $P_{14b}(BCD10) \rightarrow catA-II$	

PMP2063d	$P_{tac}(BCD10) \rightarrow benABC$ $P_{14b}(BCD10) \rightarrow catA$ $P_{14b}(BCD10) \rightarrow catA-II \Delta crc$	This study
PMP2021d	$P_{tac}(BCD10) \rightarrow benABC$ $Pm(BCD10) \rightarrow catA$ $Pm(BCD10) \rightarrow catA-II \Delta crc$	This study
PMP1024	$P_{tac} \rightarrow benABC$ $Pm(BCD10) \rightarrow catA$ $P_{14g} \rightarrow xylS/Pm(BCD10) \rightarrow catA-II$ <i>catA-II</i> under the transcriptional control of <i>XylS/Pm</i> , with <i>xylS</i> chromosomally integrated upstream of <i>catA-II</i> under the control of P_{14g} and a synthetic translation initiation sequence designed with the RBS Calculator with a translation rate of 719862.	This study

5.3. Discussion

5.3.1. Divergent metabolic specializations in *P. putida* and *P. knackmussii* result in distinct processing of benzoate and its halogenated derivatives

During cultivations with chloro-substituted benzoates, 3-CBz was the only substrate consumed by *P. knackmussii*, while *P. putida* could not utilize any of the Bz derivatives. Our study on the expression systems governing the *ortho*-cleavage pathway was restricted to *P. putida* functions and could not resolve regulatory responses in *P. knackmussii*. Hence, the lack of growth on the substrates tested could stem from insufficient induction of the necessary enzymes or transport proteins with 2-CBz and 4-CBz. However, it is more plausible that the 2- and 4-substituted chlorobenzoates are incompatible with the benzoate dioxygenase of *P. knackmussii*. The strain was reportedly able to grow on 4-CBz after transformation with the TOL plasmid pWW0⁴⁰⁹, which provides a highly promiscuous toluate dioxygenase (XylX)⁴¹¹. XylX likely complemented the missing activity of the *P. knackmussii* BenABC homolog. On the other hand, the reason behind *P. putida*'s inability to assimilate chlorobenzoates seems to be a missing catechol 1,2-dioxygenase activity on chlorocatechols. This was reflected in enhanced toxic effects caused by the overproduction of *ben* gene-activating BenR with a simultaneous lack of induction for the *cat* genes. The unresponsiveness of CatR/P_{cat} to ClBz could be caused by insufficient interactions of chloromuconates with CatR or the fact that the compounds are not being produced.

Both wild-type *P. putida* and *P. knackmussii* accumulated 3-FC while assimilating 3-FBz, but no significant 4-FC concentrations could be measured in the supernatants of these cultures. The catechol 1,2-dioxygenases, present in both species, appear to have higher activities on 4-substituted catechol than on the 3-substituted derivative. The 3-FC produced in the early phase of fermentation was fully converted into 2-FMA by *P. knackmussii*, whereas *P. putida* failed to *detoxify* the compound by the end of the experiment. Besides, we observed no growth of *P. knackmussii* on benzoate as the sole carbon source in contrast to *P. putida*, which could grow well on this substrate. However, when *P. putida* was engineered to convert fluorinated compounds efficiently, its

growth on benzoate was impaired. During the assimilation of 2-FBz, *P. knackmussii* accumulated significant amounts of non-fluorinated *cc*MA. These results demonstrate the different specialization of the two pseudomonads in the utilization of non-halogenated and halogenated *ortho*-cleavage substrates and indicate contrasting regulatory and biochemical requirements for the two substrate types.

In *P. putida*, the presence of the second catechol 1,2-dioxygenase, CatA-II, was proposed to serve as a safety valve to combat high concentrations of toxic catechol. It was found to have a significantly lower affinity and specific activity on the substrate than CatA²²³, while the two orthologs had similar enzymatic properties on the substituted compounds 4-methylcatechol, 3-methylcatechol, 4-chlorocatechol, and protocatechuate. Conversely, the accumulation of catechol was higher in strains deficient in *catA* than *catA-II*. In our experiments, the expression control of only *catA-II* had a sufficiently balancing effect on the pathway flux to enable a complete conversion of 3-FBz to 2-FMA. These results suggest an essential role of *catA-II* in the assimilation of fluorinated substrates. Further characterization of the kinetic properties of both catechol 1,2-dioxygenases would help decipher both isozymes' exact role in fluorocatechol conversion.

5.3.2. The overexpression of catechol 1,2-dioxygenase genes simultaneously enhances 3-fluorobenzoate consumption and decreases 3-fluorocatechol conversion

The bottleneck in the catechol 1,2-dioxygenation step on 3-FBz apparent in the accumulation of 3-FC was initially addressed via the constitutive overexpression of *catA* genes. Consequently, 3-FBz consumption rates were greatly enhanced. However, a mere *pulling* effect via the removal of pathway intermediates seems unlikely since *catA* overexpression was also accompanied by decreased conversion of 3-FC to 2-FMA. Likewise, transcriptional effects on genes located downstream of the overexpressed *catA* do not appear to be exclusively responsible for the phenotype, as it was also observed with the plasmid-based expression of *P. knackmussii* *catA* orthologs. Van Duuren et al.⁴³⁷ demonstrated a suppressive effect of catechol on transcription from

the P_{ben} promoter in a CatR-deficient *P. putida* strain. Such an effect could not be confirmed for 3-FC in this study. Wild-type *P. putida* KT2440 and engineered PMP1063 accumulated significantly different amounts of the intermediate when exposed to 3-FBz. However, *msfGFP* expression was comparable in both strains harboring a BenR/ $P_{ben} \rightarrow msfGFP$ construct.

Fluorine engages in fundamentally different chemical interactions with its environment than hydrogen. Therefore, fluorinated ligands often display a significantly altered affinity to their receptors compared to their non-halogenated counterparts⁴³⁸⁻⁴⁴¹. The various catalytic and regulatory proteins that contribute to the functionality of the *ortho*-cleavage pathway have typically been studied in conjunction with their native substrates. The regulatory network in *P. putida* is adjusted to the assimilation of natural compounds that rarely contain halogens. The results herein were limited to phenotypes of *Pseudomonas* exposed to halogenated *ortho*-cleavage pathway metabolites. However, the observed growth behavior and fluorescence are likely the consequence of cumulative effects on several regulatory layers. Further investigation of the specific protein-ligand interactions with fluorinated substrate analogs is required to fully uncover the mechanisms behind the observed phenotypes in response to fluorocarbon compounds.

5.3.3. The targeted replacement of regulatory sequences governing the expression of *ortho*-cleavage pathway genes reveals hidden control patterns

The regulatory network controlling the expression of genes in the *ben* and *cat* gene clusters is optimized to assimilate non-halogenated metabolites, as evident in the disparate response of the BenR/ P_{ben} and CatR/ P_{cat} expression systems to Bz/FBz/CBz or *ccMA*/2-FMA. CatR/ P_{cat} was found to deliver an extremely high transcriptional output with a dynamic range of up to 14 in response to 3-FBz and 2-FMA, while no toxic effects were observed at concentrations necessary to induce the system (0.5 mM 3-FBz or up to 10 mM 2-FMA). While it will require further validation in different bacterial

hosts, the results obtained here put CatR/ P_{cat} forward as a potential new expression system for the targeted overproduction of proteins.

The expression of *ben* genes changes drastically based on the cells' metabolic state, as seen in batch cultures with glucose in *P. putida* cells expressing *msfGFP* under the control of BenR/ P_{ben} . A similar effect of physiological control mechanisms was reported on CatR/ P_{cat} ⁴⁴². Apart from a thorough characterization of the P_{ben} and P_{cat} promoters^{237,419,430,442-444}, a less complete picture is drawn about the regulatory mechanisms that control the expression of all eight genes in the *ben* cluster or the three genes within the *cat* cluster. The activity of reporter functions fused to the P_{ben} and P_{cat} promoters or the abundance of *benA* and *catB* transcripts were commonly used as a proxy for the expression of the whole gene clusters. However, our analysis of transcriptomics data^{420,424,425} published for *P. putida* grown on glucose, fructose, glycerol, and succinate or exposed to toluene or ferulic acid revealed potential transcription start sites within the *ben* cluster that were so far not reported. Furthermore, Hfq binding motifs were found upstream of *benA*, *benK*, *nicP-I*, and *catA*, in addition to the previously reported recognition sequence controlling *catR* expression⁴³⁰. However, the *ben* genes' transcript levels were relatively low under all tested conditions, making the data sensitive to technical variations. Transcriptome analysis of *P. putida* grown on benzoate could help confirm the locations of promoter sequences within the gene cluster.

The complex nature of *ortho*-cleavage pathway gene expression in *P. putida* underlines the importance of orthogonal expression systems to control the respective biochemical functions for a stable bioconversion performance. Integration of a constitutive promoter upstream of *benD* or *catA-II* caused a significantly enhanced 3-FBz consumption. The elevated transcription rates could have also affected the expression of benzoate transport-associated genes located downstream of the modified chromosomal locations. On the other hand, the control of *benK*, *benE-II*, or *nicP-I* by *Pm(BCD10)* with low transcriptional strength resulted in decreased 3-FBz consumption rates. These results suggest a rate-limiting role of substrate transport in the tested strains.

P. putida was shown to co-consume glucose and benzoate at similar rates⁴⁴⁵ while the expression of genes involved in both substrates' utilization is controlled by

Crc/Hfq^{429,446,447}. Inactivation of *crc* without replacing the native P_{ben} promoter caused a q_s increase by about 3.5-fold compared to a strain harboring *benABC* under the control of P_{tac} . However, this substantial increase in 3-FBz uptake was not counteracted by a sufficient catechol 1,2-dioxygenase activity, consequently leading to a high accumulation of 3-FC. In previous studies, deletion of *crc* was found to be beneficial for improving the production of *ccMA* from lignocellulosic feedstocks⁴⁴⁸. However, the assimilation of halogenated compounds requires alternative regulatory regimes to balance the biochemical activities involved. As demonstrated in this study, *crc* deletion hinders the cell's ability to adapt to changing culture conditions. Consequently, Δcrc strains demonstrated two distinct phases during bioconversion experiments. In the first phase, the cells replicated rapidly with a concomitant fast conversion of 3-FBz to 2-FMA. The second phase was characterized by low metabolic activity reflected in slow growth, low 3-FBz uptake rates, and low 2-FMA production rates. These two distinct periods appeared in varying orders during the cultivations (strain PMP0021d or the first experiment with strain PMP1021d vs. strain PMP1063 and the second experiment with strain PMP1021d).

Rather than merely establishing a strict hierarchy for different assimilated substrates, one of Crc's roles is to coordinate conflicting metabolic fluxes (e.g., glycolytic vs. gluconeogenic)¹⁰⁷. In a previous study, inactivation of Crc was shown to cause a disorder in the assimilation of available compounds in a complex medium, resulting in the overflow of the node metabolites pyruvate and acetate and consequently inefficient growth¹⁰⁶. Furthermore, glucose consumption was enhanced in the early and mid-exponential phases while it significantly decreased in the late exponential phase compared to the wild-type strain. In this study, the engineered strains were pre-cultured in LB medium before the bioconversion experiments in DBM medium. This was found to increase the biomass-specific productivities with the *first generation* strains compared to a preculture in minimal medium. Before the start of bioconversion experiments, the LB cultures were harvested in the late exponential to early stationary phase. With a Δcrc strain background, the metabolic state of LB-grown cells at the time of their harvest for the bioconversion experiments could impact the adaptation to the conditions in DBM medium with glucose as the growth substrate. It deserves further

investigation of how the preculture conditions affect bioconversion performances of Crc-deficient strains to exploit the remarkable maximum productivities observed for these strains reliably.

5.4. Outlook

In this study, we were able to create *P. putida* strains that efficiently perform the conversion of 3-FBz into 2-FMA at the maximum theoretical yield of 50% (mol mol⁻¹). The best-performing strain, PMP1063, was shown to grow in the presence of high 3-FBz concentrations, which will facilitate an upscaling of the bioconversion process. 2-FBz was discarded as a suitable substrate due to benzoate dioxygenase's (BDO) bias for 1,2-dihydroxylation, resulting in the loss of fluorine. However, even with 3-FBz as substrate, 50% of fluorine is lost due to the inherent biochemical mechanism of the pathway. Thus, BDO's characteristics represent the current bottleneck for a maximum product yield on FBz. The 3D structure of a BDO variant has not been resolved thus far. However, homology models of *P. putida* BenA, created with the published structures of two homologous enzymes, *Comamonas* sp. JS765 nitrobenzene dioxygenase (PDB entry: 2BMO⁴⁴⁹) and *Pseudomonas fluorescens* IP01 cumene dioxygenase (PDB entry: 1WQL⁴⁵⁰), revealed a high conservation of residues constituting the substrate-binding pocket (data not shown). The preference of BenA for the orientation of substituted benzoates can potentially be altered through rational enzyme engineering. This could be achieved by, e.g., introducing amino acids that repel the halogen atom within the substrates' unproductive orientation or cause an attraction in its favorable orientation. By shifting BenA specificity on 3-FBz towards utilizing the fluorine-conserving 1,2-dioxygenation routes, the maximum theoretical yield could be improved.

Substrate transport mechanisms for 3-FBz were not exploited in a way that would facilitate increased bioconversion productivities. However, the effects observed after manipulating the production of benzoate transport proteins suggest a limiting role of 3-FBz uptake on the strains' performance. The specific productivities can likely be further enhanced via the controlled expression of the benzoate transport-associated genes at increased rates that still allow for detoxification of 3-FC by CatA(-II).

The whole-cell biocatalyst *P. putida* KT2440 tolerated up to 15 mM of 2-FMA without severe growth defects. Its resistance can likely be further enhanced via tolerance adaptive laboratory evolution (TALE) by exposing the cells to increasing concentrations of the end product. The expected direct [decreased (re-)import or increased export of 2-FMA] or indirect (buffering of the intracellular toxic effects of 2-FMA) properties that can reduce sensitivity to 2-FMA are also likely to be beneficial for its production^{16,451}. Increased resistance to the product, combined with the existing tolerance to high concentrations of 3-FBz, will facilitate large-scale production of 2-FMA. With high amounts of 2-FMA purified from fermentation broths, the product can be characterized for its potential as a building block for polymerization reactions to yield new fluorinated polymers. 3-FBz can be synthesized through conventional organic-chemical methods⁴⁵² and is available at a low price. With the potential applications that can be predicted for 2-FMA as a new platform molecule, the described biocatalytic process represents a substantial product valorization.

5.5. Materials and Methods

Table 5.5. Plasmids used in Chapter 5.

Plasmid	Relevant characteristics ^a	Reference or source
pGNW2	Suicide vector used for genetic manipulations in Gram-negative bacteria; <i>oriT</i> , <i>traJ</i> , <i>lacZα</i> , <i>ori</i> (R6K), $P_{14g}(BCD2) \rightarrow msfGFP$; Km ^R	See Chapter 3
pSNW2	Derivative of vector pGNW2 with the translation initiation sequence of <i>msfGFP</i> replaced by the very strong translational coupling sequence <i>BCD2</i>	See Chapter 3
pSEVA628S	Helper plasmid; <i>oriV</i> (RK2), <i>xylS</i> , $Pm \rightarrow I-SceI$; Gm ^R	Martínez-García et al. ⁴⁵³
pSEVA228	Plasmid used to supply XylS for chromosomal <i>Pm</i> promoters; <i>oriV</i> (RK2), <i>xylS</i> , <i>Pm</i> ; Km ^R	Martínez-García et al. ⁴⁵³
pSEVA228.2	Plasmid used to supply XylS ^{Thr45} (XylS.2) for chromosomal <i>Pm</i> promoters; <i>oriV</i> (RK2), <i>xylS.2</i> , <i>Pm</i> ; Km ^R	Ramos et al. ⁴²³
pQURE6·H	Conditionally-replicating vector; derivative of vector pJBSD1 carrying $XylS/Pm \rightarrow I-SceI$ and $P_{14g}(BCD2) \rightarrow mRFP$; Gm ^R	See Chapter 3
pGNW2· $P_{tac} \rightarrow benABC$	Derivative of pGNW2 carrying homology arms (HAs) to replace the native P_{ben} promoter upstream of <i>benA</i> with the P_{tac} promoter sequence in <i>P. putida</i> KT2440	This study P_{tac} : de Boer et al. ⁴³⁵
pGNW2· $P_{tac} \rightarrow benD$	Derivative of pGNW2 carrying HAs to insert the P_{tac} promoter sequence upstream of <i>benD</i> in <i>P. putida</i> KT2440	This study
pGNW2· $P_{EM7} \rightarrow catA$	Derivative of pGNW2 carrying HAs to insert the P_{EM7} promoter sequence upstream of <i>catA</i> in <i>P. putida</i> KT2440	This study
pGNW2· $Pm(BCD10) \rightarrow catA$	Derivative of pGNW2 carrying HAs to insert the <i>Pm</i> promoter and the translational coupling sequence <i>BCD10</i> upstream of <i>catA</i> in <i>P. putida</i> KT2440	This study <i>BCD10</i> : Mutalik et al. ⁴¹⁴
pGNW2· $Pm(BCD2) \rightarrow catA$	Derivative of pGNW2 carrying HAs to insert the <i>Pm</i> promoter and the translational coupling sequence <i>BCD2</i> upstream of <i>catA</i> in <i>P. putida</i> KT2440	This study <i>BCD2</i> : Mutalik et al. ⁴¹⁴
pGNW2· <i>xylS</i> / $Pm_{(ML1-17)}(BCD10) \rightarrow catA$	Derivative of pGNW2 carrying HAs to insert the <i>xylS</i> gene with its native regulatory sequences, the <i>Pm</i> promoter variant <i>ML1-17</i> , and the translational coupling sequence <i>BCD10</i> upstream of <i>catA</i> in <i>P. putida</i> KT2440	This study $Pm_{(ML1-17)}$: Bakke et al. ⁴¹⁷
pGNW2· $P_{14g}(BCD10) \rightarrow xylS$ / $Pm(BCD10) \rightarrow catA$	Derivative of pGNW2 carrying HAs to insert the <i>xylS</i> gene under the control of P_{14g} and <i>BCD10</i> , the <i>Pm</i> promoter, and the translational coupling sequence <i>BCD10</i> upstream of <i>catA</i> in <i>P. putida</i> KT2440	This study

pGNW2·P _{14c} (BCD10)→ <i>xyIS/Pm</i> (BCD10)→ <i>catA</i>	Derivative of pGNW2 carrying HAs to insert the <i>xyIS</i> gene under the control of P _{14c} and BCD10, the <i>Pm</i> promoter, and the translational coupling sequence BCD10 upstream of <i>catA</i> in <i>P. putida</i> KT2440	This study
pGNW2· <i>Pm</i> (BCD10)→ <i>catA-II</i>	Derivative of pGNW2 carrying HAs to insert the <i>Pm</i> promoter and the translational coupling sequence BCD10 upstream of <i>catA-II</i> in <i>P. putida</i> KT2440	This study
pGNW2· <i>Pm</i> (BCD2)→ <i>catA-II</i>	Derivative of pGNW2 carrying HAs to insert the <i>Pm</i> promoter and the translational coupling sequence BCD2 upstream of <i>catA-II</i> in <i>P. putida</i> KT2440	This study
pSNW2· <i>Pm</i> (BCD10)→ <i>nicP-I</i>	Derivative of pGNW2 carrying HAs to insert the <i>Pm</i> promoter and the translational coupling sequence BCD10 upstream of <i>nicP-I</i> in <i>P. putida</i> KT2440	This study
pSNW2· <i>Pm</i> (BCD10)→ <i>benE-II</i>	Derivative of pGNW2 carrying HAs to insert the <i>Pm</i> promoter and the translational coupling sequence BCD10 upstream of <i>benE-II</i> in <i>P. putida</i> KT2440	This study
pSNW2· <i>Pm</i> (BCD10)→ <i>benK</i>	Derivative of pGNW2 carrying HAs to insert the <i>Pm</i> promoter and the translational coupling sequence BCD10 upstream of <i>benK</i> in <i>P. putida</i> KT2440	This study
pGNW2·Δ <i>crc</i>	Derivative of pGNW2 carrying HAs to delete <i>crc</i> in <i>P. putida</i> KT2440	This study
pGNW2·Δ <i>crc</i> :: <i>vhb</i>	Derivative of pGNW2 carrying HAs to delete <i>crc</i> in <i>P. putida</i> KT2440 and replace it with the sequence of the <i>V. stercoraria vhb</i> gene under control of <i>Pm</i> and BCD10, and fused at the 5' end to a type II secretion system signal sequence derived from the <i>P. putida</i> KT2440 gene <i>uxpA</i> .	This study <i>uxpA</i> signal peptide: Putker et al. ⁴³¹
pGNW·Δ <i>catBC</i>	Derivative of pGNW2 carrying HAs to delete <i>catBC</i> in <i>P. putida</i> KT2440	This study
pGNW·Δ <i>catBC</i> :: <i>catA</i>	Derivative of pGNW2 carrying HAs to delete <i>catBC</i> in <i>P. putida</i> KT2440 replace it with an additional copy of <i>catA</i>	This study
pGNW·Δ <i>catBC</i> :: <i>catA-II</i>	Derivative of pGNW2 carrying HAs to delete <i>catBC</i> in <i>P. putida</i> KT2440 replace it with an additional copy of <i>catA-II</i>	This study
pGNW2·P _{tac} (BCD10)→ <i>benABC</i>	Derivative of pGNW2 carrying homology arms (HAs) to replace the native P _{ben} promoter upstream of <i>benA</i> with the P _{tac} promoter sequence, and the native 5'-UTR with the translational coupling sequence BCD10 in <i>P. putida</i> KT2440.	This study
pGNW2·P _{14b} (BCD10)→ <i>catA</i>	Derivative of pGNW2 carrying homology arms (HAs) to insert the constitutive P _{14b} promoter and the translational coupling sequence BCD10 upstream of <i>catA</i> in <i>P. putida</i> KT2440.	This study P _{14b} : Zobel et al. ⁴³³
pGNW2·P _{14b} (BCD10)→ <i>catA-II</i>	Derivative of pGNW2 carrying homology arms (HAs) to insert the constitutive P _{14b} promoter and the translational coupling sequence BCD10 upstream of <i>catA-II</i> in <i>P. putida</i> KT2440.	

pGNW2·P _{14g} → <i>xylS</i> /Pm(BCD2)→ <i>catA-II</i>	Derivative of pGNW2 carrying homology arms (HAs) to insert the <i>Pm</i> promoter and the translational coupling sequence <i>BCD10</i> , as well as the gene sequence of <i>xylS</i> under the control of the strong, constitutive promoter P _{14g} , upstream of <i>catA-II</i> in <i>P. putida</i> KT2440.	This study
pS628(BCD1)→ <i>msfGFP</i>	<i>oriV</i> (RK2), <i>xylS</i> , Pm(BCD1)→ <i>msfGFP</i> ; Gm ^R	This study <i>BCD1</i> : Mutalik et al. ⁴¹⁴
pS628(BCD2)→ <i>msfGFP</i>	<i>oriV</i> (RK2), <i>xylS</i> , Pm(BCD2)→ <i>msfGFP</i> ; Gm ^R	This study
pS628(BCD7)→ <i>msfGFP</i>	<i>oriV</i> (RK2), <i>xylS</i> , Pm(BCD7)→ <i>msfGFP</i> ; Gm ^R	This study <i>BCD7</i> : Mutalik et al. ⁴¹⁴
pS628(BCD10)→ <i>msfGFP</i>	<i>oriV</i> (RK2), <i>xylS</i> , Pm(BCD10)→ <i>msfGFP</i> ; Gm ^R	This study
pS628 _(ML1-17) (BCD10)→ <i>msfGFP</i>	<i>oriV</i> (RK2), <i>xylS</i> , Pm _(ML1-17) (BCD10)→ <i>msfGFP</i> ; Gm ^R	This study
pS62P _{lac} (BCD10)→ <i>msfGFP</i>	<i>oriV</i> (RK2), P _{lac} (BCD10)→ <i>msfGFP</i> ; Gm ^R	This study
pS62P _{EM7} (BCD10)→ <i>msfGFP</i>	<i>oriV</i> (RK2), P _{EM7} (BCD10)→ <i>msfGFP</i> ; Gm ^R	This study
pS62P _{14g} (BCD10)→ <i>msfGFP</i>	<i>oriV</i> (RK2), P _{14g} (BCD10)→ <i>msfGFP</i> ; Gm ^R	This study P _{14g} : Zobel et al. ⁴³³
pS62P _{14d} (BCD10)→ <i>msfGFP</i>	<i>oriV</i> (RK2), P _{14d} (BCD10)→ <i>msfGFP</i> ; Gm ^R	This study P _{14d} : Zobel et al. ⁴³³
pS62P _{J23108} (BCD10)→ <i>msfGFP</i>	<i>oriV</i> (RK2), P _{J23108} (BCD10)→ <i>msfGFP</i> ; Gm ^R	This study
pS62P _{J23114} (BCD10)→ <i>msfGFP</i>	<i>oriV</i> (RK2), P _{J23114} (BCD10)→ <i>msfGFP</i> ; Gm ^R	This study
pS62P _{J23119} (BCD10)→ <i>msfGFP</i>	<i>oriV</i> (RK2), P _{J23119} (BCD10)→ <i>msfGFP</i> ; Gm ^R	This study
pS62P _{cat} (BCD10)→ <i>msfGFP</i>	<i>oriV</i> (RK2), <i>catR</i> , P _{cat} (BCD10)→ <i>msfGFP</i> ; Gm ^R	This study
pS62P _{ben} (BCD10)→ <i>msfGFP</i>	<i>oriV</i> (RK2), <i>benR</i> , P _{ben} (BCD10)→ <i>msfGFP</i> ; Gm ^R	This study
pSEVA634·PKB_1379	<i>oriV</i> (pBBR1), <i>lacIq</i> , P _{trc} →PKB_1379, Gm ^R	This study
pSEVA634·PKB_2107	<i>oriV</i> (pBBR1), <i>lacIq</i> , P _{trc} →PKB_2107, Gm ^R	This study
pSEVA634·PKB_3273	<i>oriV</i> (pBBR1), <i>lacIq</i> , P _{trc} →PKB_3273, Gm ^R	This study
pSEVA438	<i>oriV</i> (pBBR1), <i>xylS</i> , Pm, Sm ^R	Martínez-García et al. ⁴⁵³

Bacterial strains and culture conditions

The bacterial strains employed in this study are listed in **Table 5.4**. *E. coli* and *P. putida* were incubated at 37°C and 30°C, respectively. For cell propagation and storage, routine cloning procedures, and during genome engineering manipulations, cells were grown in lysogeny broth (LB) medium (10 g L⁻¹ tryptone, 5 g L⁻¹ yeast extract, and 10 g L⁻¹ NaCl). Liquid cultures were performed using either 50-ml centrifuge tubes with a medium volume of 5-10 mL, or in 500-mL Erlenmeyer flasks covered with cellulose plugs (Carl Roth, Karlsruhe, Germany) and with a medium volume of 50 mL. All liquid cultures were agitated at 250 rpm (MaxQ™8000 incubator; ThermoFisher

Scientific, Waltham, MA, USA). Solid culture media contained an additional 15 g L⁻¹ agar. Selection of plasmid-harboring cells was achieved by adding kanamycin (Km), gentamicin (Gm), or streptomycin (Sm) when required at 50 µg mL⁻¹, 10 µg mL⁻¹, and 50 µg mL⁻¹, respectively.

For phenotypic characterizations in microtiter plates as well as fermentations in shaken flasks, *P. putida* was pre-grown in LB medium, and the experiments were performed in synthetic Hartman's de Bont minimal (DBM) medium³⁴⁶ additionally buffered with 5 g L⁻¹ 3-(*N*-morpholino)propanesulfonic acid (MOPS) at pH 7.0 and supplemented with different carbon compounds as explained in the text. For shaken flask experiments, LB precultures were harvested by centrifugation at 4000 g for 10 min, washed with DBM medium without the addition of any carbon substrate, and resuspended in the final media of the experiment at the desired start-optical density at 600 nm (OD_{600 nm}). Cell growth was monitored by measuring the absorbance at 630 nm (Abs_{630 nm}; for plate reader experiments with ELx808, BioTek Instruments; Winooski, VT, USA) or 600 nm (for shaken flask experiments).

The OD_{600 nm} was estimated from plate reader Abs_{630 nm} values via multiplying the values by correlation factors previously determined for the employed microtiter plate-readers and spectrophotometers. To calculate quantitative cell performance parameters for shaken flask experiments, biomass concentrations (cell dry weight, g_{CDW} L⁻¹) were derived from OD_{600 nm} measurements with a correlation factor of 0.35, previously determined for the spectrophotometer employed with exponentially growing *P. putida* KT2440. Comparative phenotypical characterizations and quantifications of green fluorescence for bioreporters were performed in 96-well plates in a Synergy H1 plate reader (BioTek Instruments; Winooski, VT, USA). Therefore, the LB precultures were diluted 1:100 in the respective screening medium (DBM medium supplemented with various organic compounds). Fluorescence was measured at an excitation wavelength of 488 nm and an emission wavelength of 588 nm. The gain was set to 60.

Cloning procedures and plasmid construction

All plasmids used in this work are listed in **Table 5.5**. Uracil-excision (*USER*) cloning²⁰³ was used for the construction of all plasmids. The AMUSER tool was employed for the design of oligonucleotides³⁴⁷. All genetic manipulations followed the protocol described in **Chapter 3**. DNA fragments employed in assembly reactions were amplified using the Phusion™ U high-fidelity DNA polymerase (Thermo Fisher Scientific, Waltham, Massachusetts, USA) according to the manufacturer's specifications. The identity and correctness of all plasmids and DNA constructs were confirmed by sequencing. For genotyping experiments after cloning procedures and genome manipulations, colony PCRs were performed using the commercial OneTaq™ master mix (New England BioLabs; Ipswich, MA, USA) according to the manufacturer's instructions. *E. coli* DH5 α *λpir* was employed for all cloning purposes. Chemically competent *E. coli* cells were prepared and transformed with plasmids according to well-established protocols³⁴⁸. *P. putida* was rendered electro-competent following the protocol of Choi, Kumar et al.³⁴⁹ (**Chapter 3**).

Metabolite analyses via HPLC

For the detection of extracellular metabolites, supernatants were obtained via centrifugation of bacterial culture broths for 2 min at 13,000 *g*. 2-fluoro-*cis,cis*-muconate (2-FMA), *cis,cis*-muconate (*ccMA*), catechol, 3-fluorocatechol (3-FC), 4-fluorocatechol (4-FC), 2-chlorobenzoate (2-CBz), 3-chlorobenzoate (3-CBz), 4-chlorobenzoate (4-CBz), 2-fluorobenzoate (2-FBz), and 3-fluorobenzoate (3-FBz) were quantified using a Dionex 3000 HPLC system equipped with a Zorbax Eclipse Plus C18 column (Agilent Technologies, Santa Clara, CA, USA) that was heated to 30°C, and a guard column from Phenomenex. Separation was achieved with a mobile phase consisting of 0.05% (w/v) acetic acid and varying amounts of acetonitrile. The total runtime per sample was 8.3 min (with a separation time of 8.0 min), during which the fraction of acetonitrile was increased from 1% to 3% within the first 3 min, followed by a steady increase to 20% within 12 s, and a further steady increase to 75% within 4 min. From 7.2 to 7.5 min, the acetonitrile concentration was held at 75% and subsequently reduced to 1% within 18 s. The column was then equilibrated again at 1% acetonitrile

for further 30 s before injecting the next sample. The flow rate was set to 1 ml min⁻¹, and the injection volume was 0.75 µl. Elution of the compounds was detected by UV light at wavelengths of 210 nm, 240 nm, 280 nm, and 300 nm. HPLC data were processed using the Chromeleon 7.1.3 software (Thermo Fisher Scientific), and compound concentrations were calculated from peak areas using calibration curves with five different standard concentrations.

¹⁹F-NMR analysis

The ¹⁹F NMR spectra were acquired on a Bruker Avance III-HD spectrometer operating at a ¹⁹F frequency of 752.75 MHz ($B_0 = 18.8$ T). The spectrometer was equipped with a TCI CryoProbe, and all measurements were made at 25°C. 512 transient scans were acquired with an interscan delay of 5.6 s (0.6 s acquisition time + 5 s of recovery delay), which was tested to provide quantitative signal intensities for the relevant fluorinated species. 500 µl of sample volume was mixed with 50 ml of D₂O (Sigma-Aldrich, 99.99%) for locking and shimming. ¹⁹F chemical shifts are reported relative to CFCl₃ ($\delta_{19F} = 0.0$ ppm) using the lock signal of D₂O as a secondary reference⁴⁵⁴. Chemical shifts are reported in ppm.

Software and data analysis

Data manipulations and calculations were performed in Microsoft Excel 2016 and OriginPro 2021 (OriginLab Corporation). Figures and Illustrations were created in OriginPro 2021 and Adobe Illustrator 2020. Geneious Prime 2021.1.1 (Biomatters Ltd.) served as a database for any kind of DNA sequences, design plasmids and constructs, and analyze Sanger sequencing results. The visualization of the gene cluster comparison for *P. putida* and *P. knackmussii* shown in **Figure 5.2 A** was performed using Clinker⁴⁵⁵ with additional editing in Adobe Illustrator 2020. Maximum exponential growth rates (μ_{max}) were determined by Gaussian process regression using the Python-based tool deODorizer³⁵⁸. The prediction of translation initiation strengths for 5' untranslated region (5' UTR) mRNA sequences was performed using the online RBS

Calculator v2.1¹³³⁻¹³⁸, which can be found at https://www.denovodna.com/software/predict_rbs_calculator. The results are given in arbitrary units (au) on the RBS Calculator scale, representing the relative strength of translation. Biomass-specific 3-FBz consumption rates q_s and 2-FMA production rates q_p were determined over the timeframes of fermentations in which there was 3-FBz detectable in the culture media with the following equations:

$$q_s = \frac{1}{\bar{X}} \frac{\Delta S}{\Delta t} \quad (1)$$

$$q_p = \frac{1}{\bar{X}} \frac{\Delta P}{\Delta t} \quad (2)$$

q_s : biomass-specific substrate consumption rate ($\text{mmol}_{3\text{-FBz}} \text{g}_{\text{CDW}}^{-1} \text{h}^{-1}$)

\bar{X} : the average biomass concentration between two sampling timepoints ($\text{g}_{\text{CDW}} \text{L}^{-1}$)

ΔS : Difference in substrate concentration between two sampling timepoints ($\text{mM}_{3\text{-FBz}}$)

Δt : time between two sampling points (h)

q_p : biomass-specific product formation rate ($\text{mmol}_{2\text{FMA}} \text{g}_{\text{CDW}}^{-1} \text{h}^{-1}$)

ΔP : Difference in product concentration between two sampling timepoints ($\text{mM}_{2\text{FMA}}$)

The q_s and q_p rates displayed in **Table 5.3** are averages of the values determined individually for three biological replicates. The transcription and translation initiation strengths of various expression systems tested in bioreporter experiments were determined via linear regression of fluorescence-over- $\text{OD}_{600 \text{ nm}}$ plots in OriginPro 2021. The identified slope values were normalized by dividing them by the expression strength of the P_{tac} promoter.

5.6. Supplementary Figures

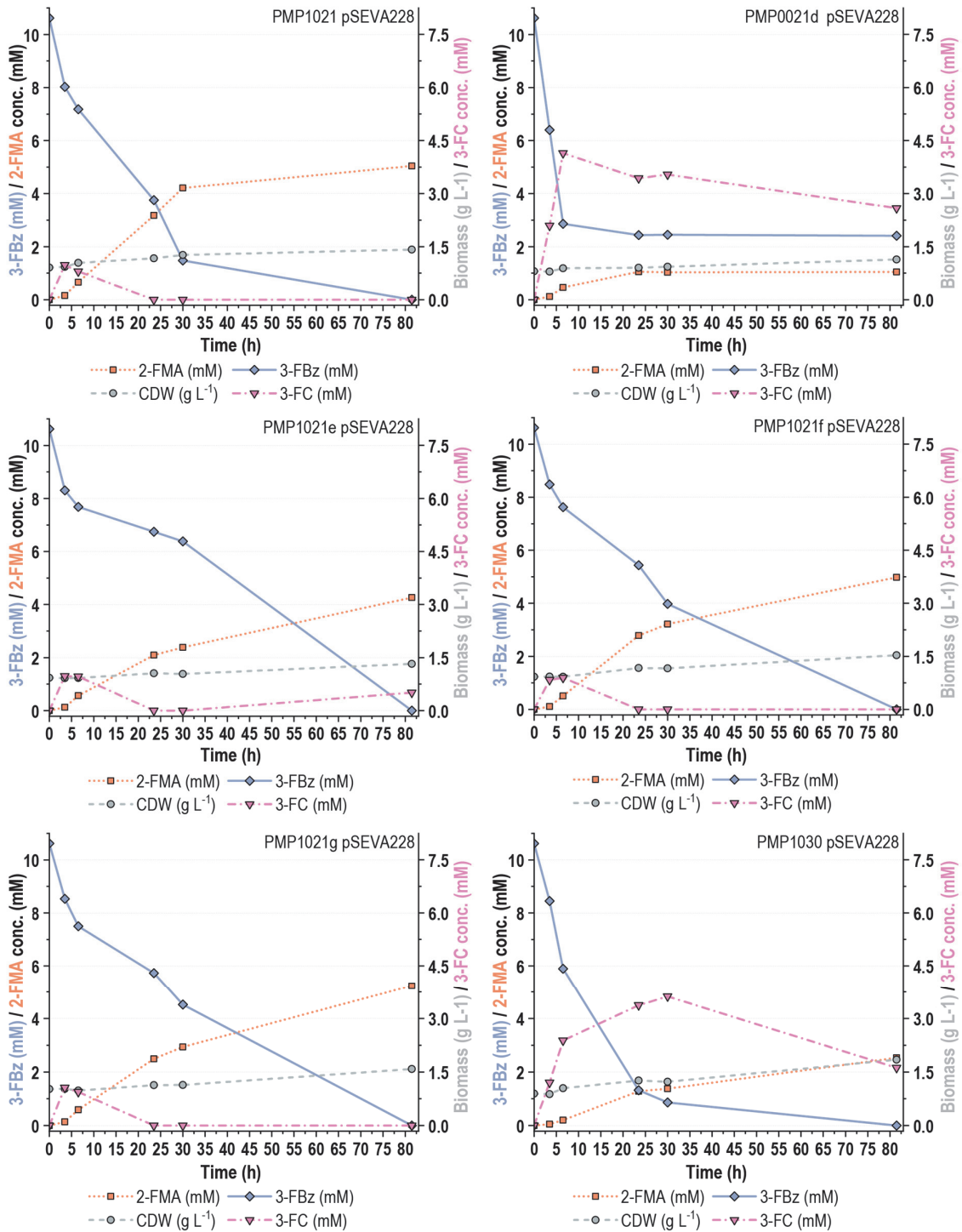


Figure 5.S1 A. Fermentation profiles of *third-generation* bioconversion strains (part A). The bioconversions were performed in Erlenmeyer flasks filled with 10% (v/v) DBM medium supplemented with 30 mM glucose and 10 mM 3-FBz.

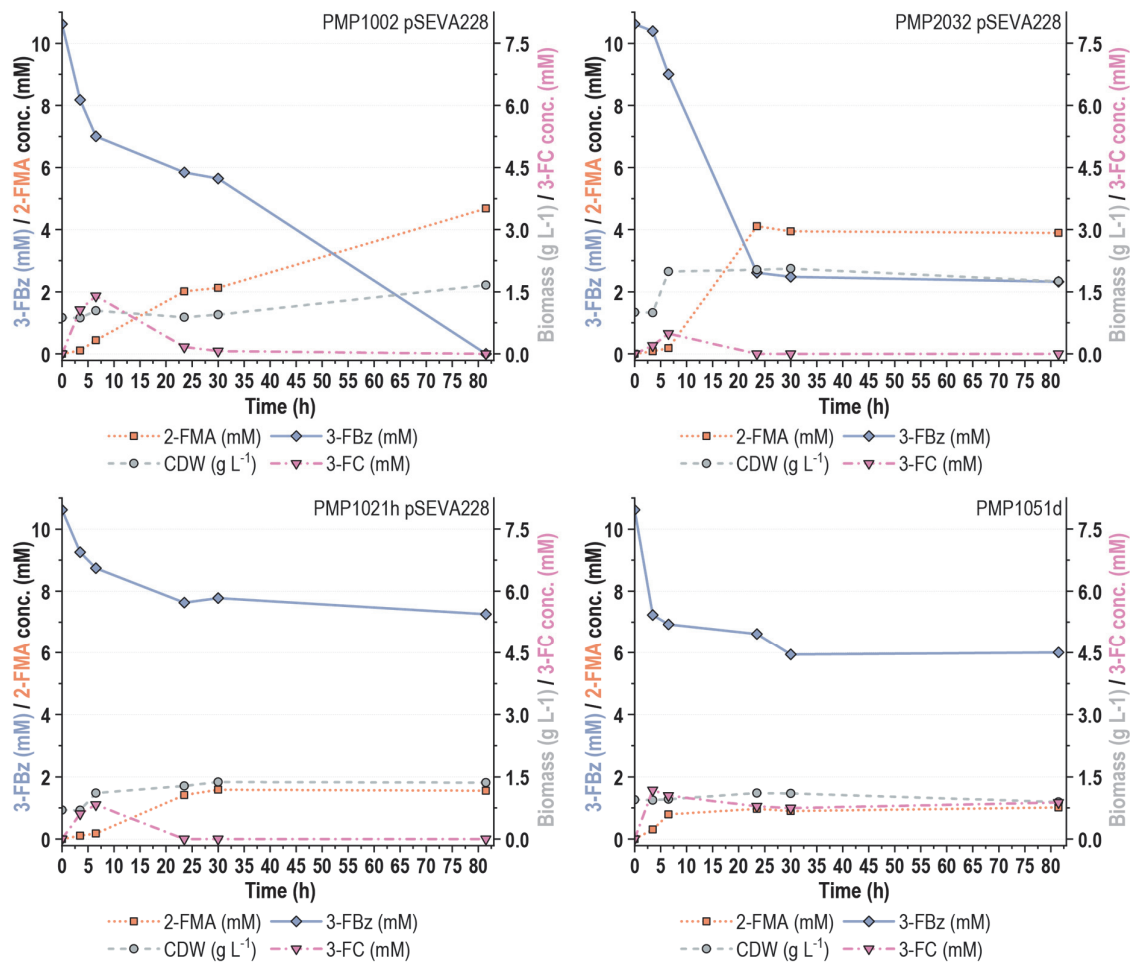


Figure 5.S1 B. Fermentation profiles of *third-generation* bioconversion strains (part B). The bioconversions were performed in Erlenmeyer flasks filled with 10% (v/v) DBM medium supplemented with 30 mM glucose and 10 mM 3-FBz.



Figure 5.S2. Effect of bacterial hemoglobin expression on *P. putida* under micro-aerobic conditions. The strains were cultured in sealed test tubes filled to 60% with DBM medium supplemented with 5 g L⁻¹ MOPS, 30 mM glucose, and 10 mM 3-FBz. The picture was taken after one week of incubation at 30°C.

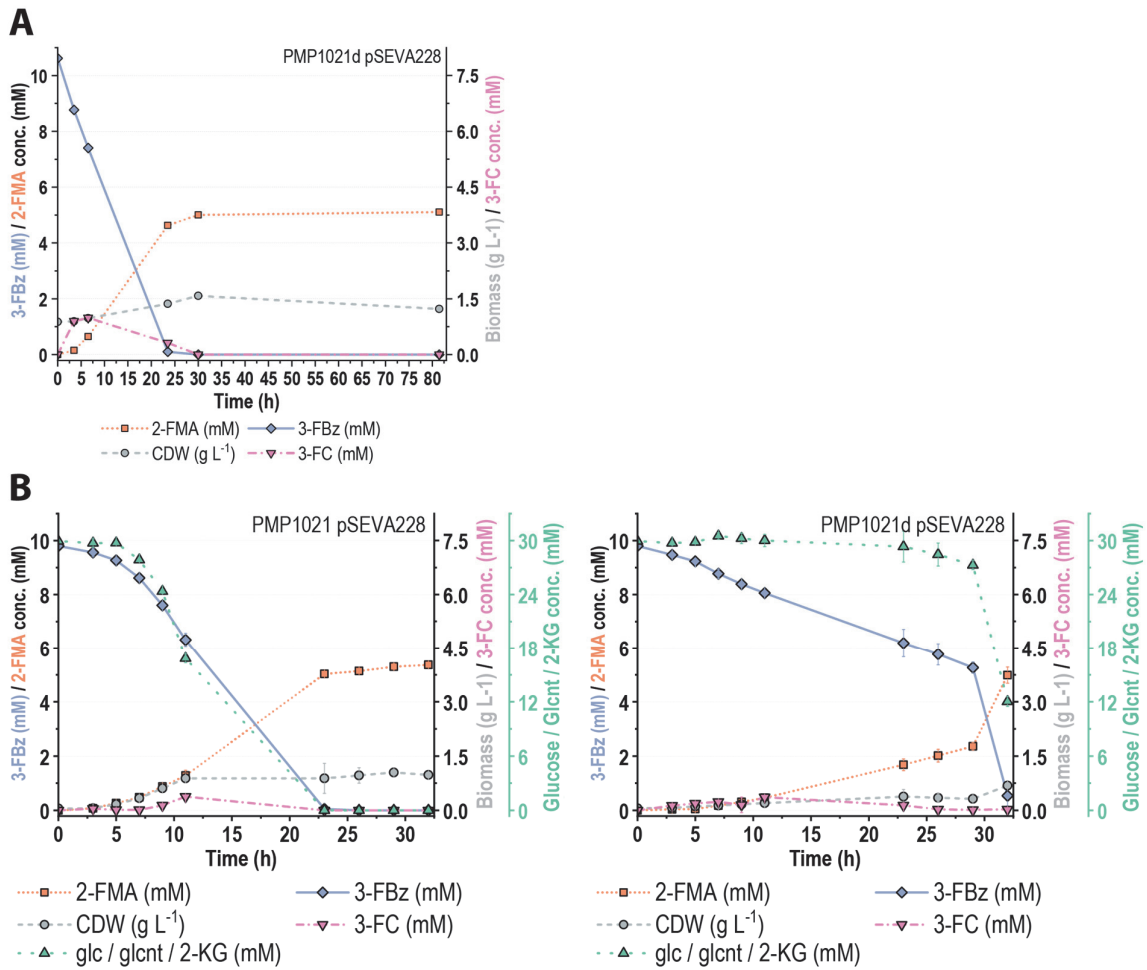


Figure 5.S3. Fermentation profiles of the control strains included in the experiment to test the performance of *fourth-generation* strains. (A) fermentation performed with PMP1021d pSEVA228 during the screening of *third-generation* strains. (B) fermentations performed with PMP1021 pSEVA228 and PMP1021d pSEVA228 during the screening of *fourth-generation* strains.

5.7. References for Chapter 5

- 16 Mukhopadhyay, A. **Tolerance Engineering in Bacteria for the Production of Advanced Biofuels and Chemicals.** *Trends in Microbiology* **23**, 498-508, doi: 10.1016/j.tim.2015.04.008 (2015).
- 31 Karp, P. D., Billington, R., Caspi, R., Fulcher, C. A., Latendresse, M., Kothari, A., Keseler, I. M., Krummenacker, M., Midford, P. E., Ong, Q., Ong, W. K., Paley, S. M. & Subhraveti, P. **The Biocyc Collection of Microbial Genomes and Metabolic Pathways.** *Briefings in Bioinformatics* **20**, 1085-1093, doi: 10.1093/bib/bbx085 (2017).
- 87 Nakazawa, T. **Travels of a *Pseudomonas*, from Japan around the World.** *Environmental Microbiology* **4**, 782-786, doi: 10.1046/j.1462-2920.2002.00310.x (2002).
- 97 Vardon, D. R., Franden, M. A., Johnson, C. W., Karp, E. M., Guarnieri, M. T., Linger, J. G., Salm, M. J., Strathmann, T. J. & Beckham, G. T. **Adipic Acid Production from Lignin.** *Energy & Environmental Science* **8**, 617-628, doi: 10.1039/C4EE03230F (2015).
- 98 Johnson, C. W., Salvachúa, D., Khanna, P., Smith, H., Peterson, D. J. & Beckham, G. T. **Enhancing Muconic Acid Production from Glucose and Lignin-Derived Aromatic Compounds Via Increased Protocatechuate Decarboxylase Activity.** *Metabolic Engineering Communications* **3**, 111-119, doi: 10.1016/j.meteno.2016.04.002 (2016).
- 106 Molina, L., La Rosa, R., Nogales, J. & Rojo, F. **Influence of the Crc Global Regulator on Substrate Uptake Rates and the Distribution of Metabolic Fluxes in *Pseudomonas putida* KT2440 Growing in a Complete Medium.** *Environmental Microbiology* **21**, 4446-4459, doi: 10.1111/1462-2920.14812 (2019).
- 107 Rojo, F. **Carbon Catabolite Repression in *Pseudomonas*: Optimizing Metabolic Versatility and Interactions with the Environment.** *FEMS Microbiology Reviews* **34**, 658-684, doi: 10.1111/j.1574-6976.2010.00218.x (2010).
- 113 Moreno, R., Hernández-Arranz, S., La Rosa, R., Yuste, L., Madhushani, A., Shingler, V. & Rojo, F. **The Crc and Hfq Proteins of *Pseudomonas putida* Cooperate in Catabolite Repression and Formation of Ribonucleic Acid Complexes with Specific Target Motifs.** *Environmental Microbiology* **17**, 105-118, doi: 10.1111/1462-2920.12499 (2015).
- 133 Salis, H. M., Mirsky, E. A. & Voigt, C. A. **Automated Design of Synthetic Ribosome Binding Sites to Control Protein Expression.** *Nature Biotechnology* **27**, 946-950, doi: 10.1038/nbt.1568 (2009).

- 134 Espah Borujeni, A., Channarasappa, A. S. & Salis, H. M. **Translation Rate Is Controlled by Coupled Trade-Offs between Site Accessibility, Selective RNA Unfolding and Sliding at Upstream Standby Sites.** *Nucleic Acids Research* **42**, 2646-2659, doi: 10.1093/nar/gkt1139 (2013).
- 135 Espah Borujeni, A. & Salis, H. M. **Translation Initiation Is Controlled by RNA Folding Kinetics Via a Ribosome Drafting Mechanism.** *Journal of the American Chemical Society* **138**, 7016-7023, doi: 10.1021/jacs.6b01453 (2016).
- 136 Espah Borujeni, A., Cetnar, D., Farasat, I., Smith, A., Lundgren, N. & Salis, H. M. **Precise Quantification of Translation Inhibition by mRNA Structures That Overlap with the Ribosomal Footprint in N-Terminal Coding Sequences.** *Nucleic Acids Research* **45**, 5437-5448, doi: 10.1093/nar/gkx061 (2017).
- 137 Cetnar, D. P. & Salis, H. M. **Systematic Quantification of Sequence and Structural Determinants Controlling mRNA Stability in Bacterial Operons.** *BioRxiv*, 2020.2007.2022.216051, doi: 10.1101/2020.07.22.216051 (2020).
- 138 Reis, A. C. & Salis, H. M. **An Automated Model Test System for Systematic Development and Improvement of Gene Expression Models.** *ACS Synthetic Biology* **9**, 3145-3156, doi: 10.1021/acssynbio.0c00394 (2020).
- 203 Cavaleiro, A. M., Kim, S. H., Seppala, S., Nielsen, M. T. & Norholm, M. H. **Accurate DNA Assembly and Genome Engineering with Optimized Uracil Excision Cloning.** *ACS Synthetic Biology* **4**, 1042-1046, doi: 10.1021/acssynbio.5b00113 (2015).
- 222 Wolfe, M. D., Altier, D. J., Stubna, A., Popescu, C. V., Münck, E. & Lipscomb, J. D. **Benzoate 1,2-Dioxygenase from *Pseudomonas putida*: Single Turnover Kinetics and Regulation of a Two-Component Rieske Dioxygenase.** *Biochemistry* **41**, 9611-9626, doi: 10.1021/bi025912n (2002).
- 223 Jiménez, J. I., Pérez-Pantoja, D., Chavarría, M., Díaz, E. & de Lorenzo, V. **A Second Chromosomal Copy of the *Cata* Gene Endows *Pseudomonas putida* mt-2 with an Enzymatic Safety Valve for Excess of Catechol.** *Environmental Microbiology* **16**, 1767-1778, doi: 10.1111/1462-2920.12361 (2014).
- 237 Pérez-Pantoja, D., Kim, J., Silva-Rocha, R. & de Lorenzo, V. **The Differential Response of the P_{ben} Promoter of *Pseudomonas putida* mt-2 to BenR and XylS Prevents Metabolic Conflicts in m-Xylene Biodegradation.** *Environmental Microbiology* **17**, 64-75, doi: 10.1111/1462-2920.12443 (2015).
- 258 Platt, R., Drescher, C., Park, S. K. & Phillips, G. J. **Genetic System for Reversible Integration of DNA Constructs and *lacZ* Gene Fusions into the *Escherichia coli* Chromosome.** *Plasmid* **43**, 12-23, doi: 10.1006/plas.1999.1433 (2000).

- 260 Worsey, M. J. & Williams, P. A. **Metabolism of Toluene and Xylenes by *Pseudomonas putida* (Arvilla) mt-2: Evidence for a New Function of the TOL Plasmid.** *Journal of Bacteriology* **124**, 7-13, doi: 10.1128/JB.124.1.7-13.1975 (1975).
- 261 Bagdasarian, M., Lurz, R., Rückert, B., Franklin, F. C. H., Bagdasarian, M. M., Frey, J. & Timmis, K. N. **Specific Purpose Plasmid Cloning Vectors. Ii. Broad Host Range, High Copy Number, RSF1010-Derived Vectors, and a Host-Vector System for Gene Cloning in *Pseudomonas*.** *Gene* **16**, 237-247, doi: 10.1016/0378-1119(81)90080-9 (1981).
- 298 Zobel, S., Benedetti, I., Eisenbach, L., de Lorenzo, V., Wierckx, N. & Blank, L. M. **Tn7-Based Device for Calibrated Heterologous Gene Expression in *Pseudomonas putida*.** *ACS Synthetic Biology* **4**, 1341-1351, doi: 10.1021/acssynbio.5b00058 (2015).
- 346 Hartmans, S., Smits, J. P., van der Werf, M. J., Volkering, F. & de Bont, J. A. **Metabolism of Styrene Oxide and 2-Phenylethanol in the Styrene-Degrading *Xanthobacter* Strain 124x.** *Applied and environmental microbiology* **55**, 2850-2855, doi: 10.1128/AEM.55.11.2850-2855.1989 (1989).
- 347 Genee, H. J., Bonde, M. T., Bagger, F. O., Jespersen, J. B., Sommer, M. O. A., Wernersson, R. & Olsen, L. R. **Software-Supported USER Cloning Strategies for Site-Directed Mutagenesis and DNA Assembly.** *A C S Synthetic Biology* **4**, 342-349, doi: 10.1021/sb500194z (2015).
- 348 Elder, R. T. **Cloning Techniques Molecular Cloning: A Laboratory Manual T. Maniatis E. R. Pritsch J. Sambrook.** *Bioscience* **33**, 721-722, doi: 10.2307/1309366 (1983).
- 349 Choi, K. H., Kumar, A. & Schweizer, H. P. **A 10-Min Method for Preparation of Highly Electrocompetent *Pseudomonas aeruginosa* Cells: Application for DNA Fragment Transfer between Chromosomes and Plasmid Transformation.** *Journal of Microbiological Methods* **64**, 391-397, doi: 10.1016/j.mimet.2005.06.001 (2006).
- 358 Swain, P. S., Stevenson, K., Leary, A., Montano-Gutierrez, L. F., Clark, I. B. N., Vogel, J. & Pilizota, T. **Inferring Time Derivatives Including Cell Growth Rates Using Gaussian Processes.** *Nature Communications* **7**, 13766, doi: 10.1038/ncomms13766 (2016).
- 359 Bui, V. & Frost, J. W. **Process for Preparing Hexamethylenediamine and Polyamides Therefrom.** WO Patent 2012141993 A1. USA patent (2012).
- 360 Coudray, L., Bui, V., Frost, J. W. & Schweitzer, D. **Process for Preparing Caprolactam and Polyamides Therefrom.** Us Patent US20130085255A1. (2012).

- 361 Khalil, I., Quintens, G., Junkers, T. & Dusselier, M. **Muconic Acid Isomers as Platform Chemicals and Monomers in the Biobased Economy.** *Green Chemistry* **22**, 1517-1541, doi: 10.1039/c9gc04161c (2020).
- 362 Carraher, J. M., Pfennig, T., Rao, R. G., Shanks, B. H. & Tessonier, J.-P. **Cis,cis-Muconic Acid Isomerization and Catalytic Conversion to Biobased Cyclic-C6-1,4-Diacid Monomers.** *Green Chemistry* **19**, 3042-3050, doi: 10.1039/C7GC00658F (2017).
- 363 Xie, N. Z., Liang, H., Huang, R. B. & Xu, P. **Biotechnological Production of Muconic Acid: Current Status and Future Prospects.** *Biotechnology Advances* **32**, 615-622, doi: 10.1016/j.biotechadv.2014.04.001 (2014).
- 364 Lu, R., Lu, F., Chen, J., Yu, W., Huang, Q., Zhang, J. & Xu, J. **Production of Diethyl Terephthalate from Biomass-Derived Muconic Acid.** *Angewandte Chemie - International Edition* **55**, 249-253, doi: 10.1002/anie.201509149 (2016).
- 365 Thompson, B., Pugh, S., Machas, M. & Nielsen, D. R. **Muconic Acid Production Via Alternative Pathways and a Synthetic "Metabolic Funnel".** *ACS Synthetic Biology* **7**, 565-575, doi: 10.1021/acssynbio.7b00331 (2018).
- 366 Becker, J., Kuhl, M., Kohlstedt, M., Starck, S. & Wittmann, C. **Metabolic Engineering of *Corynebacterium glutamicum* for the Production of cis,cis-Muconic Acid from Lignin.** *Microbial Cell Factories* **17**, 115, doi: 10.1186/s12934-018-0963-2 (2018).
- 367 Weber, C., Bruckner, C., Weinreb, S., Lehr, C., Essl, C. & Boles, E. **Biosynthesis of cis,cis-Muconic Acid and Its Aromatic Precursors, Catechol and Protocatechuic Acid, from Renewable Feedstocks by *Saccharomyces cerevisiae*.** *Applied Environmental Microbiology* **78**, 8421-8430, doi: 10.1128/AEM.01983-12 (2012).
- 368 Mizuno, S., Yoshikawa, N., Seki, M., Mikawa, T. & Imada, Y. **Microbial Production of cis,cis-Muconic Acid from Benzoic Acid.** *Applied Microbiology and Biotechnology* **28**, 20-25, doi: 10.1007/BF00250491 (1988).
- 369 Polen, T., Spelberg, M. & Bott, M. **Toward Biotechnological Production of Adipic Acid and Precursors from Biorenewables.** *Journal of Biotechnology* **167**, 75-84, doi: 10.1016/j.jbiotec.2012.07.008 (2012).
- 370 Beerthuis, R., Rothenberg, G. & Shiju, N. R. **Catalytic Routes Towards Acrylic Acid, Adipic Acid and E-Caprolactam Starting from Biorenewables.** *Green Chemistry* **17**, 1341-1361, doi: 10.1039/c4gc02076f (2015).

- 371 Kruyer, N. S. & Peralta-Yahya, P. **Metabolic Engineering Strategies to Bio-Adipic Acid Production.** *Current Opinion in Biotechnology* **45**, 136-143, doi: 10.1016/j.copbio.2017.03.006 (2017).
- 372 Mizuno, S., Yoshikawa, N., Seki, M., Mikawa, T. & Imada, Y. **Microbial Production of *cis,cis*-Muconic Acid from Benzoic Acid.** *Applied microbiology and biotechnology* **28**, doi: 10.1007/BF00250491 (1988).
- 373 Kohlstedt, M., Starck, S., Barton, N., Stolzenberger, J., Selzer, M., Mehlmann, K., Schneider, R., Pleissner, D., Rinkel, J., Dickschat, J. S., Venus, J., B.J.H. van Duuren, J. & Wittmann, C. **From Lignin to Nylon: Cascaded Chemical and Biochemical Conversion Using Metabolically Engineered *Pseudomonas putida*.** *Metabolic Engineering* **47**, 279-293, doi: 10.1016/j.ymben.2018.03.003 (2018).
- 374 Wu, C.-M., Wu, C.-C., Su, C.-C., Lee, S.-N., Lee, Y.-A. & Wu, J.-Y. **Microbial Synthesis of *cis,cis*-Muconic Acid from Benzoate by *Sphingobacterium* sp. Mutants.** *Biochemical Engineering Journal* **29**, 35-40, doi: 10.1016/j.bej.2005.02.034 (2006).
- 375 Schmidt, E. & Knackmuss, H. J. **Production of *cis,cis*-Muconate from Benzoate and 2-Fluoro-*cis,cis*-Muconate from 3-Fluorobenzoate by 3-Chlorobenzoate Degrading Bacteria.** *Applied Microbiology and Biotechnology* **20**, 351-355, doi: 10.1007/bf00270599 (1984).
- 376 Niu, W., Draths, K. M. & Frost, J. W. **Benzene-Free Synthesis of Adipic Acid.** *Biotechnology Progress* **18**, 201-211, doi: 10.1021/bp010179x (2002).
- 377 Vardon, D. R., Rorrer, N. A., Salvachúa, D., Settle, A. E., Johnson, C. W., Menart, M. J., Cleveland, N. S., Ciesielski, P. N., Steirer, K. X., Dorgan, J. R. & Beckham, G. T. ***cis,cis* -Muconic Acid: Separation and Catalysis to Bio-Adipic Acid for Nylon-6,6 Polymerization.** *Green Chemistry* **18**, 3397-3413, doi: 10.1039/c5gc02844b (2016).
- 378 Choi, S., Lee, H.-N., Park, E., Lee, S.-J. & Kim, E.-S. **Recent Advances in Microbial Production of *cis,cis*-Muconic Acid.** *Biomolecules* **10**, 1238, doi: 10.3390/biom10091238 (2020).
- 379 Inoue, M., Sumii, Y. & Shibata, N. **Contribution of Organofluorine Compounds to Pharmaceuticals.** *ACS Omega* **5**, 10633-10640, doi: 10.1021/acsomega.0c00830 (2020).
- 380 Ogawa, Y., Tokunaga, E., Kobayashi, O., Hirai, K. & Shibata, N. **Current Contributions of Organofluorine Compounds to the Agrochemical Industry.** *iScience* **23**, 101467, doi: 10.1016/j.isci.2020.101467 (2020).

- 381 Swinson, J. **Fluorine - A vital element in the medicine chest.** 26-30 (PharmaChem, 2005).
- 382 Fang, W.-Y., Ravindar, L., Rakesh, K. P., Manukumar, H. M., Shantharam, C. S., Alharbi, N. S. & Qin, H.-L. **Synthetic Approaches and Pharmaceutical Applications of Chloro-Containing Molecules for Drug Discovery: A Critical Review.** *European Journal of Medicinal Chemistry* **173**, 117-153, doi: 10.1016/j.ejmech.2019.03.063 (2019).
- 383 Mei, H., Han, J., Fustero, S., Medio-Simon, M., Sedgwick, D. M., Santi, C., Ruzziconi, R. & Soloshonok, V. A. **Fluorine-Containing Drugs Approved by the Fda in 2018.** *Chemistry – A European Journal* **25**, 11797-11819, doi: 10.1002/chem.201901840 (2019).
- 384 Ogawa, Y., Tokunaga, E., Kobayashi, O., Hirai, K. & Shibata, N. **Current Contributions of Organofluorine Compounds to the Agrochemical Industry.** *iScience* **23**, 101467-101467, doi: 10.1016/j.isci.2020.101467 (2020).
- 385 Smith, B. R., Eastman, C. M. & Njardarson, J. T. **Beyond C, H, O, and N! Analysis of the Elemental Composition of U.S. FDA Approved Drug Architectures.** *Journal of Medicinal Chemistry* **57**, 9764-9773, doi: 10.1021/jm501105n (2014).
- 386 **Centerwatch: Site Search**, <<https://www.centerwatch.com/directories/1067-fda-approved-drugs>>, accessed on (03.04.2021)
- 387 Wakefield, B. **Fluorinated Pharmaceuticals.** *Innovations in Pharmaceutical Technology*, doi: (2000).
- 388 Patterson, R., Kandelbauer, A., Müller, U. & Lammer, H. **17 - Crosslinked Thermoplastics.** in *Handbook of Thermoset Plastics* 697-737 (2014).
- 389 Behrman, E. J. & Stanier, R. Y. **Observations on the Oxidation of Halogenated Nicotinic Acids.** *Journal of Biological Chemistry* **228**, 947-953, doi: 10.1016/S0021-9258(18)70672-8 (1957).
- 390 Cain, R. B., Tranter, E. K. & Darrah, J. A. **The Utilization of Some Halogenated Aromatic Acids by Nocardia. Oxidation and Metabolism.** *Biochem J* **106**, 211-227, doi: 10.1042/bj1060211 (1968).
- 391 Kiel, M. & Engesser, K. H. **The Biodegradation Vs. Biotransformation of Fluorosubstituted Aromatics.** *Applied Microbiology and Biotechnology* **99**, 7433-7464, doi: 10.1007/s00253-015-6817-5 (2015).

- 392 Neilson, A. H. & Allard, A.-s. **Degradation and Transformation of Organic Fluorine Compounds.** *The Handbook of Environmental Chemistry Vol. 3, Part N Organofluorines 3N*, 137-202, doi: 10.1007/10721878 (2002).
- 393 Oltmanns, R. H., Muller, R., Otto, M. K. & Lingens, F. **Evidence for a New Pathway in the Bacterial Degradation of 4-Fluorobenzoate.** *Applied Environmental Microbiology* **55**, 2499-2504, doi: 10.1128/AEM.55.10.2499-2504.1989 (1989).
- 394 Goldman, P., Milne, G. W. A. & Pignataro, M. T. **Fluorine Containing Metabolites Formed from 2-Fluorobenzoic Acid by a *Pseudomonas* Species.** *Archives of Biochemistry and Biophysics* **118**, 178-184, doi: 10.1016/0003-9861(67)90295-0 (1967).
- 395 Schreiber, A., Hellwig, M., Dorn, E., Reineke, W. & Knackmuss, H. J. **Critical Reactions in Fluorobenzoic Acid Degradation by *Pseudomonas* sp. B13.** *Applied Environmental Microbiology* **39**, 58-67, doi: 10.1128/AEM.39.1.58-67.1980 (1980).
- 396 Oltmanns, R. H., Muller, R., Otto, M. K. & Lingens, F. **Evidence for a New Pathway in the Bacterial Degradation of 4-Fluorobenzoate.** *Applied and Environmental Microbiology* **55**, 2499-2504, doi: 10.1128/aem.55.10.2499-2504.1989 (1989).
- 397 Engesser, K. H., Schmidt, E. & Knackmuss, H. J. **Adaptation of *Alcaligenes Eutrophus* B9 and *Pseudomonas* sp. B13 to 2-Fluorobenzoate as Growth Substrate.** *Applied Environmental Microbiology* **39**, 68-73, doi: 10.1128/AEM.39.1.68-73.1980 (1980).
- 398 Weisshaar, M. P., Franklin, F. C. & Reineke, W. **Molecular Cloning and Expression of the 3-Chlorobenzoate-Degrading Genes from *Pseudomonas* sp. Strain B13.** *Journal of Bacteriology* **169**, 394-402, doi: 10.1128/jb.169.1.394-402.1987 (1987).
- 399 Reineke, W. & Knackmuss, H. J. **Microbial Degradation of Haloaromatics.** *Annual Review of Microbiology* **42**, 263-287, doi: 10.1146/annurev.mi.42.100188.001403 (1988).
- 400 Dorn, E. & Knackmuss, H. J. **Chemical Structure and Biodegradability of Halogenated Aromatic Compounds. Two Catechol 1,2-Dioxygenases from a 3-Chlorobenzoate-Grown *Pseudomonad*.** *Biochemical Journal* **174**, 73-84, doi: 10.1042/bj1740073 (1978).
- 401 Milne, G. W., Goldman, P. & Holtzman, J. L. **The Metabolism of 2-Fluorobenzoic Acid. II. Studies with 18-O₂.** *Journal of Biological Chemistry* **243**, 5374-5376, doi: 10.1016/S0021-9258(18)91959-9 (1968).

- 402 Miyazaki, R., Bertelli, C., Benaglio, P., Canton, J., De Coi, N., Gharib, W. H., Gjoksi, B., Goesmann, A., Greub, G., Harshman, K., Linke, B., Mikulic, J., Mueller, L., Nicolas, D., Robinson-Rechavi, M. et al. **Comparative Genome Analysis of *Pseudomonas knackmussii* B13, the First Bacterium Known to Degrade Chloroaromatic Compounds.** *Environmental Microbiology* **17**, 91-104, doi: 10.1111/1462-2920.12498 (2015).
- 403 Linger, J. G., Vardon, D. R., Guarnieri, M. T., Karp, E. M., Hunsinger, G. B., Franden, M. A., Johnson, C. W., Chupka, G., Strathmann, T. J., Pienkos, P. T. & Beckham, G. T. **Lignin Valorization through Integrated Biological Funneling and Chemical Catalysis.** *Proceedings of the National Academy of Sciences* **111**, 12013, doi: 10.1073/pnas.1410657111 (2014).
- 404 Oltmanns, R. H., Rast, H. G. & Reineke, W. **Degradation of 1,4-Dichlorobenzene by Enriched and Constructed Bacteria.** *Applied Microbiology and Biotechnology* **28**, 609-616, doi: 10.1007/BF00250421 (1988).
- 405 Mokross, H., Schmidt, E. & Reineke, W. **Degradation of 3-Chlorobiphenyl by in Vivo Constructed Hybrid Pseudomonads.** *FEMS Microbiology Letters* **59**, 179-185, doi: 10.1016/0378-1097(90)90053-s (1990).
- 406 Ravatn, R., Studer, S., Springael, D., Zehnder, A. J. & van der Meer, J. R. **Chromosomal Integration, Tandem Amplification, and Deamplification in *Pseudomonas putida* F1 of a 105-Kilobase Genetic Element Containing the Chlorocatechol Degradative Genes from *Pseudomonas* sp. Strain B13.** *Journal of Bacteriology* **180**, 4360-4369, doi: 10.1128/jb.180.17.4360-4369.1998 (1998).
- 407 Ravatn, R., Zehnder, A. J. & van der Meer, J. R. **Low-Frequency Horizontal Transfer of an Element Containing the Chlorocatechol Degradation Genes from *Pseudomonas* sp. Strain B13 to *Pseudomonas putida* F1 and to Indigenous Bacteria in Laboratory-Scale Activated-Sludge Microcosms.** *Applied Environmental Microbiology* **64**, 2126-2132, doi: 10.1128/AEM.64.6.2126-2132.1998 (1998).
- 408 Gaillard, M., Vallaey, T., Vorhölter, F. J., Minoia, M., Werlen, C., Sentchilo, V., Pühler, A. & van der Meer, J. R. **The *clc* Element of *Pseudomonas* sp. Strain B13, a Genomic Island with Various Catabolic Properties.** *Journal of Bacteriology* **188**, 1999-2013, doi: 10.1128/JB.188.5.1999-2013.2006 (2006).
- 409 Reineke, W., Jeenes, D. J., Williams, P. A. & Knackmuss, H. J. **TOL Plasmid pWW0 in Constructed Halobenzoate-Degrading *Pseudomonas* Strains: Prevention of *meta* Pathway.** *Journal of Bacteriology* **150**, 195-201, doi: 10.1128/JB.150.1.195-201.1982 (1982).

- 410 Dorn, E., Hellwig, M., Reineke, W. & Knackmuss, H. J. **Isolation and Characterization of a 3-Chlorobenzoate Degrading Pseudomonad.** *Archives of Microbiology* **99**, 61-70, doi: 10.1007/BF00696222 (1974).
- 411 Ge, Y., Vaillancourt, F. H., Agar, N. Y. & Eltis, L. D. **Reactivity of Toluene Dioxygenase with Substituted Benzoates and Dioxygen.** *Journal of Bacteriology* **184**, 4096-4103, doi: 10.1128/jb.184.15.4096-4103.2002 (2002).
- 412 Reineke, W. & Knackmuss, H. J. **Chemical-Structure and Biodegradability of Halogenated Aromatic-Compounds - Substituent Effects on 1,2-Dioxygenation of Benzoic-Acid.** *Biochimica Et Biophysica Acta* **542**, 412-423, doi: 10.1016/0304-4165(78)90372-0 (1978).
- 413 Martínez-García, E., Aparicio, T., Goñi-Moreno, A., Fraile, S. & de Lorenzo, V. **SEVA 2.0: An Update of the Standard European Vector Architecture for De-/Re-Construction of Bacterial Functionalities.** *Nucleic Acids Research* **43**, D1183-D1189, doi: 10.1093/nar/gku1114 (2014).
- 414 Mutalik, V. K., Guimaraes, J. C., Cambray, G., Lam, C., Christoffersen, M. J., Mai, Q.-a., Tran, A. B., Paull, M., Keasling, J. D., Arkin, A. P. & Endy, D. **Precise and Reliable Gene Expression Via Standard Transcription and Translation Initiation Elements.** **10**, doi: 10.1038/nmeth.2404 (2013).
- 415 Schmidt, E., Remberg, G. & Knackmuss, H. J. **Chemical Structure and Biodegradability of Halogenated Aromatic Compounds - Halogenated Muconic Acids as Intermediates.** *Biochemical Journal* **192**, 331-337, doi: 10.1042/bj1920331 (1980).
- 416 Boersma, F. G., McRoberts, W. C., Cobb, S. L. & Murphy, C. D. **A ¹⁹F NMR Study of Fluorobenzoate Biodegradation by *Sphingomonas* sp. HB-1.** *FEMS Microbiology Letters* **237**, 355-361, doi: 10.1016/j.femsle.2004.06.052 (2004).
- 417 Bakke, I., Berg, L., Aune, T. E., Brautaset, T., Sletta, H., Tondervik, A. & Valla, S. **Random Mutagenesis of the *Pm* Promoter as a Powerful Strategy for Improvement of Recombinant-Gene Expression.** *Applied Environmental Microbiology* **75**, 2002-2011, doi: 10.1128/AEM.02315-08 (2009).
- 418 Ramos, J. L., Michan, C., Rojo, F., Dwyer, D. & Timmis, K. **Signal-Regulator Interactions, Genetic Analysis of the Effector Binding Site of XylS, the Benzoate-Activated Positive Regulator of *Pseudomonas* TOL Plasmid Meta-Cleavage Pathway Operon.** *Journal of Molecular Biology* **211**, 373-382, doi: 10.1016/0022-2836(90)90358-S (1990).

- 419 Cowles, C. E., Nichols, N. N. & Harwood, C. S. **BenR, a XylS Homologue, Regulates Three Different Pathways of Aromatic Acid Degradation in *Pseudomonas putida*.** *Journal of Bacteriology* **182**, 6339-6346, doi: 10.1128/jb.182.22.6339-6346.2000 (2000).
- 420 Kim, J., Oliveros, J. C., Nikel, P. I., de Lorenzo, V. & Silva-Rocha, R. **Transcriptomic Fingerprinting of *Pseudomonas putida* under Alternative Physiological Regimes.** *Environmental Microbiology Reports* **5**, 883-891, doi: 10.1111/1758-2229.12090 (2013).
- 421 Domínguez-Cuevas, P., Marín, P., Busby, S., Ramos, J. L. & Marqués, S. **Roles of Effectors in XylS-Dependent Transcription Activation: Intramolecular Domain Derepression and DNA Binding.** *Journal of Bacteriology* **190**, 3118-3128, doi: 10.1128/jb.01784-07 (2008).
- 422 Marqués, S., Manzanera, M., González-Pérez, M. M., Gallegos, M. T. & Ramos, J. L. **The XylS-Dependent *Pm* Promoter Is Transcribed in Vivo by RNA Polymerase with Sigma 32 or Sigma 38 Depending on the Growth Phase.** *Molecular Microbiology* **31**, 1105-1113, doi: 10.1046/j.1365-2958.1999.01249.x (1999).
- 423 Ramos, J. L., Michan, C., Rojo, F., Dwyer, D. & Timmis, K. **Signal-Regulator Interactions. Genetic Analysis of the Effector Binding Site of XylS, the Benzoate-Activated Positive Regulator of *Pseudomonas* TOL Plasmid Meta-Cleavage Pathway Operon.** *Journal of Molecular Biology* **211**, 373-382, doi: 10.1016/0022-2836(90)90358-S (1990).
- 424 Bojanovic, K., D'Arrigo, I. & Long, K. S. **Global Transcriptional Responses to Osmotic, Oxidative, and Imipenem Stress Conditions in *Pseudomonas putida*.** *Applied Environmental Microbiology* **83**, doi: 10.1128/AEM.03236-16 (2017).
- 425 Domínguez-Cuevas, P., González-Pastor, J. E., Marqués, S., Ramos, J. L. & de Lorenzo, V. **Transcriptional Tradeoff between Metabolic and Stress-Response Programs in *Pseudomonas putida* KT2440 Cells Exposed to Toluene.** *Journal of Biological Chemistry* **281**, 11981-11991, doi: 10.1074/jbc.M509848200 (2006).
- 426 Jahn, M., Vorpahl, C., Hübschmann, T., Harms, H. & Müller, S. **Copy Number Variability of Expression Plasmids Determined by Cell Sorting and Droplet Digital PCR.** *Microbial Cell Factories* **15**, 211, doi: 10.1186/s12934-016-0610-8 (2016).
- 427 Goñi-Moreno, Á., Benedetti, I., Kim, J. & Lorenzo, V. d. **Deconvolution of Gene Expression Noise into Physical Dynamics of Cognate Promoters.** *BioRxiv*, 019927, doi: 10.1101/019927 (2015).

- 428 Volke, D. C., Turlin, J., Mol, V. & Nikel, P. I. **Physical Decoupling of XylS/Pm Regulatory Elements and Conditional Proteolysis Enable Precise Control of Gene Expression in *Pseudomonas putida***. *Microb Biotechnol* **13**, 222-232, doi: 10.1111/1751-7915.13383 (2020).
- 429 Morales, G., Linares, J. F., Beloso, A., Albar, J. P., Martínez, J. L. & Rojo, F. **The *Pseudomonas putida* Crc Global Regulator Controls the Expression of Genes from Several Chromosomal Catabolic Pathways for Aromatic Compounds**. *Journal of Bacteriology* **186**, 1337-1344, doi: 10.1128/jb.186.5.1337-1344.2004 (2004).
- 430 Moreno, R. & Rojo, F. **The Target for the *Pseudomonas putida* Crc Global Regulator in the Benzoate Degradation Pathway Is the BenR Transcriptional Regulator**. *Journal of Bacteriology* **190**, 1539-1545, doi: 10.1128/jb.01604-07 (2008).
- 431 Putker, F., Tommassen-van Boxtel, R., Stork, M., Rodríguez-Herva, J. J., Koster, M. & Tommassen, J. **The Type II Secretion System (Xcp) of *Pseudomonas putida* Is Active and Involved in the Secretion of Phosphatases**. *Environmental Microbiology* **15**, 2658-2671, doi: 10.1111/1462-2920.12115 (2013).
- 432 Borraccino, R., Kharoune, M., Giot, R., Agathos, S. N., Nyns, E.-J., Naveau, H. P. & Pauss, A. **Abiotic Transformation of Catechol and 1-Naphthol in Aqueous Solution—Influence of Environmental Factors**. *Water Research* **35**, 3729-3737, doi: 10.1016/S0043-1354(01)00097-5 (2001).
- 433 Zobel, S., Benedetti, I., Eisenbach, L., De Lorenzo, V., Wierckx, N. & Blank, L. M. **Tn7-Based Device for Calibrated Heterologous Gene Expression in *Pseudomonas putida***. *ACS Synthetic Biology* **4**, 1341-1351, doi: 10.1021/acssynbio.5b00058 (2015).
- 434 Stolz, A., Busse, H.-J. & Kämpfer, P. ***Pseudomonas knackmussii* sp. nov.** *International Journal of Systematic and Evolutionary Microbiology* **57**, 572-576, doi: 10.1099/ijs.0.64761-0 (2007).
- 435 de Boer, H. A., Comstock, L. J. & Vasser, M. **The *tac* Promoter: A Functional Hybrid Derived from the *trp* and *lac* Promoters**. *Proceedings of the National Academy of Sciences USA* **80**, 21-25, doi: 10.1073/pnas.80.1.21 (1983).
- 436 Wirth, N. T., Kozaeva, E. & Nikel, P. I. **Accelerated Genome Engineering of *Pseudomonas putida* by I-SceI—Mediated Recombination and CRISPR-Cas9 Counterselection**. *Microbial Biotechnology* **0**, doi: 10.1111/1751-7915.13396 (2019).
- 437 van Duuren, J. B. J. H., Wijte, D., Karge, B., Martins dos Santos, V. A. P., Yang, Y., Mars, A. E. & Eggink, G. **ph-Stat Fed-Batch Process to Enhance the Production of *cis,cis*-Muconate from Benzoate by *Pseudomonas putida* KT2440-JD1**. *Biotechnology Progress* **28**, 85-92, doi: 10.1002/btpr.709 (2012).

- 438 Zhou, P., Zou, J., Tian, F. & Shang, Z. **Fluorine Bonding – How Does It Work in Protein–Ligand Interactions?** *Journal of Chemical Information and Modeling* **49**, 2344-2355, doi: 10.1021/ci9002393 (2009).
- 439 Olsen, J. A., Banner, D. W., Seiler, P., Wagner, B., Tschopp, T., Obst-Sander, U., Kansy, M., Müller, K. & Diederich, F. **Fluorine Interactions at the Thrombin Active Site: Protein Backbone Fragments H-C(α)-C=O Comprise a Favorable C-F Environment and Interactions of C-F with Electrophiles.** *ChemBioChem* **5**, 666-675, doi: 10.1002/cbic.200300907 (2004).
- 440 Burke, T. R., Ye, B., Yan, X., Wang, S., Jia, Z., Chen, L., Zhang, Z.-Y. & Barford, D. **Small Molecule Interactions with Protein–Tyrosine Phosphatase Ptp1b and Their Use in Inhibitor Design.** *Biochemistry* **35**, 15989-15996, doi: 10.1021/bi961256d (1996).
- 441 Paulini, R., Muller, K. & Diederich, F. **Orthogonal Multipolar Interactions in Structural Chemistry and Biology.** *Angewandte Chemie - International Edition* **44**, 1788-1805, doi: 10.1002/anie.200462213 (2005).
- 442 Tover, A., Ojangu, E.-L. & Kivisaar, M. **Growth Medium Composition-Determined Regulatory Mechanisms Are Superimposed on CatR-Mediated Transcription from the Pheba and Catbca Promoters in *Pseudomonas putida*.** *Microbiology* **147**, 2149-2156, doi: 10.1099/00221287-147-8-2149 (2001).
- 443 Jeffrey, W. H., Cuskey, S. M., Chapman, P. J., Resnick, S. & Olsen, R. H. **Characterization of *Pseudomonas putida* Mutants Unable to Catabolize Benzoate: Cloning and Characterization of *Pseudomonas* Genes Involved in Benzoate Catabolism and Isolation of a Chromosomal DNA Fragment Able to Substitute for XylS in Activation of the TOL Lower-Pathway Promoter.** *Journal of Bacteriology* **174**, 4986-4996, doi: 10.1128/jb.174.15.4986-4996.1992 (1992).
- 444 Rothmel, R. K., Shinabarger, D. L., Parsek, M. R., Aldrich, T. L. & Chakrabarty, A. M. **Functional Analysis of the *Pseudomonas putida* Regulatory Protein CatR: Transcriptional Studies and Determination of the CatR DNA-Binding Site by Hydroxyl-Radical Footprinting.** *Journal of Bacteriology* **173**, 4717-4724, doi: 10.1128/jb.173.15.4717-4724.1991 (1991).
- 445 Kukurugya, M. A., Mendonca, C. M., Solhtalab, M., Wilkes, R. A., Thannhauser, T. W. & Aristilde, L. **Multi-Omics Analysis Unravels a Segregated Metabolic Flux Network That Tunes Co-Utilization of Sugar and Aromatic Carbons in *Pseudomonas putida*.** *Journal of Biological Chemistry* **294**, 8464-8479, doi: 10.1074/jbc.RA119.007885 (2019).

- 446 Hester, K. L., Lehman, J., Najjar, F., Song, L., Roe, B. A., MacGregor, C. H., Hager, P. W., Phibbs, P. V., Jr. & Sokatch, J. R. **Crc Is Involved in Catabolite Repression Control of the Bkd Operons of *Pseudomonas putida* and *Pseudomonas aeruginosa*.** *Journal of Bacteriology* **182**, 1144-1149, doi: 10.1128/jb.182.4.1144-1149.2000 (2000).
- 447 del Castillo, T. & Ramos, J. L. **Simultaneous Catabolite Repression between Glucose and Toluene Metabolism in *Pseudomonas putida* Is Channeled through Different Signaling Pathways.** *Journal of Bacteriology* **189**, 6602-6610, doi: 10.1128/JB.00679-07 (2007).
- 448 Johnson, C. W., Abraham, P. E., Linger, J. G., Khanna, P., Hettich, R. L. & Beckham, G. T. **Eliminating a Global Regulator of Carbon Catabolite Repression Enhances the Conversion of Aromatic Lignin Monomers to Muconate in *Pseudomonas putida* KT2440.** *Metabolic Engineering Communications* **5**, 19-25, doi: 10.1016/j.meten.2017.05.002 (2017).
- 449 Friemann, R., Ivkovic-Jensen, M. M., Lessner, D. J., Yu, C.-L., Gibson, D. T., Parales, R. E., Eklund, H. & Ramaswamy, S. **Structural Insight into the Dioxygenation of Nitroarene Compounds: The Crystal Structure of Nitrobenzene Dioxygenase.** *Journal of Molecular Biology* **348**, 1139-1151, doi: 10.1016/j.jmb.2005.03.052 (2005).
- 450 Dong, X., Fushinobu, S., Fukuda, E., Terada, T., Nakamura, S., Shimizu, K., Nojiri, H., Omori, T., Shoun, H. & Wakagi, T. **Crystal Structure of the Terminal Oxygenase Component of Cumene Dioxygenase from *Pseudomonas fluorescens* Ip01.** *Journal of Bacteriology* **187**, 2483-2490, doi: 10.1128/jb.187.7.2483-2490.2005 (2005).
- 451 Mohamed, E. T., Werner, A. Z., Salvachúa, D., Singer, C. A., Szostkiewicz, K., Rafael Jiménez-Díaz, M., Eng, T., Radi, M. S., Simmons, B. A., Mukhopadhyay, A., Herrgård, M. J., Singer, S. W., Beckham, G. T. & Feist, A. M. **Adaptive Laboratory Evolution of *Pseudomonas putida* KT2440 Improves P-Coumaric and Ferulic Acid Catabolism and Tolerance.** *Metabolic Engineering Communications* **11**, e00143, doi: 10.1016/j.mec.2020.e00143 (2020).
- 452 Ferm, R. L. & VanderWerf, C. A. **Synthesis of Aromatic Fluorides through Diazotization in Anhydrous Hydrogen Fluoride.** *Journal of the American Chemical Society* **72**, 4809-4810, doi: 10.1021/ja01166a506 (1950).
- 453 Martínez-García, E., Aparicio, T., Goñi-Moreno, A., Fraile, S. & De Lorenzo, V. **SEVA 2.0: An Update of the Standard European Vector Architecture for De-/Re-Construction of Bacterial Functionalities.** *Nucleic Acids Research* **43**, D1183-1189, doi: 10.1093/nar/gku1114 (2015).

- 454 Zhao, C., Li, P., Deng, Z., Ou, H. Y., McGlinchey, R. P. & O'Hagan, D. **Insights into Fluorometabolite Biosynthesis in *Streptomyces cattleya* DSM46488 through Genome Sequence and Knockout Mutants.** *Bioorganic Chemistry* **44**, 1-7, doi: 10.1016/j.bioorg.2012.06.002 (2012).
- 455 Gilchrist, C. L. M. & Chooi, Y.-H. **Clinker & Clustermap.js: Automatic Generation of Gene Cluster Comparison Figures.** *Bioinformatics*, doi: 10.1093/bioinformatics/btab007 (2021).

Concluding remarks and future perspectives

P. putida epitomizes the journey of an environmental bacterium from its natural habitat into becoming a cell factory useful for contemporary biotechnology. After its discovery in 1960 in Japan, strain mt-2 was firstly studied for the biodegradation of a range of natural (subsequently, also xenobiotic) arenes. It was only later that researchers recognized that these outstanding metabolic capacities go hand-in-hand with physiological characteristics that underlie its potential as a hefty industrial cell factory. Examples of cellular and molecular features that distinguish *P. putida* from other microbial *chassis* are abundant, and some of these have been discussed in detail in **Chapter 2**. However, since the publication of the full genome sequence of strain KT2440 in 2002 and its reannotation in 2016, only 79% of all genes were associated with a (potential) function, many of which are only putative based on homologies with proteins whose function was identified in other organisms. One way or the other, the full metabolic potential of this host is yet to be fully exploited.

Traditionally, the identification of specific physiological aspects of a microbe relied on methods established within the fields of classical microbiology and biochemistry (valuable as they are, they include laborious and time-consuming experiments, studying one function at a time). The current progress in data sciences (with all varieties within the “omics” field) is taking these endeavors to a new level. A crucial element for the discovery of new genotype-phenotype relationships is accessing efficient molecular tools that allow the targeted manipulation of genomic sequences. The present work contributes to these efforts by providing a detailed operating manual and a versatile toolbox for the genetic engineering of pseudomonads (**Chapter 3**). One way to further improve the proposed strategy would be to transfer the self-curing ability of I-*SceI*-bearing plasmids to CRISPR/Cas9 vectors. The specific counter-selection against wild-type sequences could furthermore be combined with a double-crossover approach, in which the templates for homologous recombination are provided on a replicable plasmid. However, this requires the use of highly efficient guide RNAs to kill cells that retain the wild-type sequence effectively. For this approach to work reliably, further

studies need to clarify which sequence features characterize an efficient spacer sequence and automate the pipeline to select them.

The versatile network architecture of *P. putida* is composed by diverse metabolic reactions—the fluxes of which are controlled to a large degree at the metabolite level, in a driven-by-demand fashion. This property was exploited in the fundamental restructuring of central metabolism to establish a synthetic deficiency of acetyl-coenzyme A (Ac-CoA; **Chapter 4**). After the auxotrophy imposed was relieved by the implementation of an alternative glycolytic pathway, a metabolic conflict became evident, caused by the simultaneous activity of the extant Entner-Doudoroff pathway. To capitalize on the existing strain with carbon-conserving phosphoketolase pathway, glycolysis must be connected more efficiently to the TCA cycle to compensate for the removal of the main entry point Ac-CoA. This is particularly important when alternative, more peripheral biochemical pathways are used to provide Ac-CoA for cellular growth. By effectively linking the glycolytic flux of sugar substrates to the TCA cycle, only the C2 node of metabolism needs to be supplied by the production pathway that requires improvement through evolution (e.g., the fluorination pathway from *Streptomyces cattleya*). Furthermore, carboxylating the ‘excess’ pyruvate to oxaloacetate could provide a way to capture CO₂ in organic molecules. Notwithstanding, if the overflow production of 2-ketogluconate can be remediated, the current strain is highly suitable for the production of pyruvate or products thereof (e.g., lactate, branched-chain amino acids and isobutanol).

The second distinguishing feature of *P. putida* was exploited in **Chapter 5**—namely, its rich repertoire of biochemical functions acquired to utilize a large fraction of the carbon sources available in the environment. Building on its inherent capability to catabolize fluorinated benzoate derivatives, the *ortho*-cleavage pathway was repurposed for the production of 2-fluoro-*cis,cis*-muconate in a whole-cell bioconversion. This process provides access to a wealth of new fluorinated building blocks for the synthesis of novel polymers and bioactive compounds with medical and agricultural applications.

With a versatile genome engineering toolbox, a cell platform for the evolutionary engineering of various pathways, and a *chassis* for the production of novel fluorinated compounds, this thesis upgrades the biocatalytic potential of *P. putida*—and serves as a first-case example of production of novel molecules that are particularly difficult to produce by traditional chemistry.